Technische Universität München
Institut für Energietechnik

Professur für Thermofluiddynamik

Identification of Combustion Dynamics and Noise of Confined Turbulent Flames

Malte Tobias Merk

Vollständiger Abdruck der von der Fakultät für Maschinenwesen der Technischen Universität München zur Erlangung des akademischen Grades eines

DOKTOR – INGENIEURS

genehmigten Dissertation.

Vorsitzender:
Prof. Dr.-Ing. Volker Gümmer
Prüfer der Dissertation:
1. Prof. Wolfgang Polifke, Ph.D.
2. Prof. Dr. Nicolas Noiray, ETH Zürich

Die Dissertation wurde am 25.06.2018 bei der Technischen Universität München eingereicht und durch die Fakultät für Maschinenwesen am 04.10.2018 angenommen.

Abstract

Combustion noise is an undesirable but unavoidable by-product of every applied turbulent combustion device. Besides being harmful for those exposed to elevated noise levels, combustion noise may trigger thermoacoustic instabilities. The imperative of avoiding thermoacoustic instabilities, in turn, limits the operational conditions of a combustion device. In turbulent confined combustion systems, as they are found in most applied devices, the thermoacoustic stability and the noise levels reached are determined by an interplay of three main components: the combustion noise source, the flame dynamic response to acoustic perturbations and the cavity acoustics.

The present thesis deals with the thermoacoustic modeling of confined combustion systems. Large eddy simulation is combined with advanced system identification techniques to infer reduced order models for the flame dynamic response and the combustion noise source. By incorporating the identified models into a linear acoustic network model description of the combustor acoustics, predictions are achieved of linear stability margins, combustor dynamics and sound pressure distributions. An extensive comparison is conducted between the results obtained and experimental data provided from Laboratoire EM2C, Université Paris-Saclay.

Via a reactive compressible large eddy simulation the experimentally measured sound pressure spectra of a confined lab-scale combustor, which is located at Laboratoire EM2C, are precisely reproduced. Thereby, qualitative and quantitative agreement is found not only for thermoacoustically stable, but also for intermittent and fully unstable working conditions. The triggering of the instability is controlled solely by varying the length of the combustor exhaust tube, which is modeled in the compressible large eddy simulation through characteristic based state-space boundary conditions.

Advanced system identification techniques are investigated and evaluated, which allow to extend the established large eddy simulation / system identification approach: not only a model for the flame dynamic response is identified, but also an estimation of the combustion noise source is obtained from the same time series data. Surrogate data studies prove that compared with the established finite impulse response identification, a Box-Jenkins model yields unbiased estimates for the flame dynamic response in case of a closed-loop identification. Moreover, it is demonstrated that the additionally estimated noise model of the Box-Jenkins identification converges towards a reference solution, even if the reference noise model is of simpler structure.

Combining broadband time series data from the validated large eddy simulation and the investigated Box-Jenkins identification, models are identified for the flame dynamic response and the combustion noise source. Incorporation of these models into a linear acoustic network model of a confined combustor allows predictions of the combustor dynamics and its sound pressure distribution with reasonable computational effort. Satisfying agreement for the combustor scattering matrix is achieved between reduced order model predictions and measured data. The employment of the reduced order model yields additionally excellent agreement to experimental values of the sound spectra and allows an intuitive interpretation in terms of cavity resonances and acoustic-flame coupling. It is proven that the incorporation of

the flame dynamic response into the network model is mandatory for a correct sound pressure prediction.

In summary, a coherent framework is presented for the investigation of combustor dynamics and combustor noise: broadband data are generated by a compressible large eddy simulation, which is post-processed via advanced system identification techniques to infer simultaneously models for the flame dynamic response and the generation of combustion noise. In the present thesis these models are combined with a linear acoustic network model to obtain a reduced order model that allows predictions of combustor dynamics and combustor noise across a large parameter space with reasonable computational costs.

Kurzfassung

Verbrennungslärm ist ein unerwünschtes, dabei jedoch unvermeidbares Nebenprodukt eines jeden turbulenten Verbrennungssystems. Neben dem schädlichen Einfluss auf jene, die erhöhten Schalldruckpegeln ausgesetzt sind, kann Verbrennungslärm thermoakustische Instabilitäten auslösen. Das unabdingbare Vermeiden von thermoakustischen Instabilitäten wiederum begrenzt den Betriebsbereich des Verbrennungssystems. Für geschlossene Verbrennungssysteme, wie sie praktisch in den allermeisten Anwendungen zu finden sind, bestimmt sich der erreichte Schalldruckpegel sowie die thermoakustische Stabilität des Systems durch das Zusammenspiel von Verbrennungslärmquelle, dynamischer Flammenantwort auf akustische Störungen sowie akustischer Eigenmoden der Brennergeometrie.

Die vorliegende Arbeit beschäftigt sich mit der thermoakustischen Modellierung von geschlossenen Verbrennungssystemen. Dazu werden Modelle reduzierter Ordnung abgeschätzt über einen kombinierten Ansatz aus Grobstruktursimulation und fortgeschrittener Systemidentifikation. Durch Kopplung der identifizierten Modelle mit einem linear akustischen Netzwerkmodell der Brennergeometrie werden Vorhersagen getroffen über lineare Stabilitätsgrenzen, Verbrennungsdynamik und Schalldruckverteilung. Die erzielten Ergebnisse werden anschließend umfangreich validiert anhand experimenteller Daten, welche vom Laboratoire EM2C, Université Paris-Saclay, bereitgestellt werden.

Mittels einer kompressiblen Grobstruktursimulation werden zunächst experimentell gemessene Lärmspektren eines geschlossene Verbrennungsprüfstands präzise wiedergegeben. Dabei wird qualitative und quantitative Übereinstimmung nicht nur für thermoakustisch stabile Betriebsbedingungen erreicht, sondern auch für intermittierende und instabile Bedingungen. Das Auftreten thermoakustischer Instabilitäten wird dabei ausschließlich durch die Länge des Abgasrohrs bestimmt, welches in der kompressiblen Grobstruktursimulation durch charakteristische Zustandsraum-Randbedingungen modelliert wird.

Zudem werden fortgeschrittene Methoden der Systemidentifikation auf Basis von Ersatzdaten untersucht und ausgewertet. Die untersuchten Methoden stellen dabei eine Erweiterung der bisher etablierten Methoden dar: neben einer dynamischen Flammenantwort wird zusätzlich von der selben Zeitreihe ein Modell für die Verbrennungslärmquelle abgeschätzt. Untersuchungen zeigen, dass im Falle einer *'closed-loop'* Identifikation ein sogenanntes Box-Jenkins Modell keinen systematischen Fehler aufweist - im Gegensatz zu den bisher etablierten Modellen. Darüber hinaus wird demonstriert, dass das abgeschätzte Lärmquellenmodell der Box-Jenkins Identifikation gegen ein vorgegebenes Referenzmodell konvergiert, selbst wenn das Referenzmodell eine einfachere Struktur aufweist.

Durch Verknüpfung von breitbandig angeregten Zeitreihendaten, welche mittels der validierten Grobstruktursimulation erzeugt wurden, und der untersuchten Box-Jenkins Identifikation werden letztlich Modelle für die dynamische Flammenantwort *und* für die Verbrennungslärmquelle bestimmt. In Kombination mit einem linear akustischen Netzwerkmodell ergibt sich ein Modell reduzierter Ordnung, das sich durch geringen rechnerischen Aufwand auszeichnet und Vorhersagen über Verbrennungsdynamik und zu erwartende Lärmspektren erlaubt. Vorhergesagte und experimentell gemessene akustische Streumatrizen sind in guter Übereinstimmung. Desweiteren liefert das Modell reduzierter Ordnung her-

vorragende Übereinstimmung zu experimentell gemessenen Lärmspektren und ermöglicht darüber hinaus eine verständliche Interpretation der resultierenden Spektren bezüglich akustischer Resonanzen und Flammen-Akustik Interaktion. Die Berücksichtigung der dynamischen Flammenantwort im akustischen Netzwerkmodell ist dabei Grundvoraussetzung für eine korrekte Vorhersage des erreichten Schalldruckpegels.

Zusammengefasst wird in der vorliegenden Arbeit eine umfassende und in sich geschlossene Methode präsentiert, mit der sowohl die Verbrennungsdynamik als auch der Verbrennungslärm in geschlossen Verbrennungssystemen bestimmt werden kann: breitbandige Daten werden mittels einer kompressiblen Grobstruktursimulation generiert und anschließend anhand fortgeschrittener Systemidentifikationsmethoden ausgewertet. Dadurch lassen sich gleichermaßen Modelle für die dynamische Flammenantwort und die Verbrennungslärmquelle identifizieren. Durch Kombination mit einem akustische Netzwerkmodell wird ein Modell reduzierter Ordnung erlangt, welches Vorhersagen über einen weiten Parameterbereich erlaubt bei gleichzeitig vertretbarem Rechenaufwand.

Vorwort

Die vorliegende Arbeit entstand während meiner Zeit an der Professur für Thermofluiddynamik, TUM. Der größte Teil der Arbeit entstand im Rahmen des DFG geförderten *'NoiseDyn'* Projekts, welches durchgeführt wurde in Zusammenarbeit mit unseren französischen Kollegen am Laboratoire EM2C, Université Paris-Saclay. Natürlich gibt es im Rahmen der enstandenen Arbeit noch jede Menge Dank zu verteilen.

Meinem Doktorvater, Professor Wolfgang Polifke, danke ich herzlichst für die Möglichkeit in seiner Forschungsgruppe mitwirken zu können, was diese Arbeit überhaupt ermöglichte. Neben seinem exzellenten fachlichen Rat genoss ich stets das entgegengebrachte Vertrauen, die unkomplizierte und menschliche Zusammenarbeit sowie die 'lange Leine'. All dies ist keine Selbstverständlichkeit, gestaltete meine Zeit an der Professur aber umso angenehmer und trug dazu bei, dass es sich (meistens) nicht nach Arbeit anfühlte. Professor Nicolas Noiray danke ich für dessen prompte Übernahme des Korreferats und Professor Gümmer für dessen Prüfungsvorsitz.

Meinem französischen Kollegen, Renaud Gaudron, der für den experimentellen Teil des *NoiseDyn* Projekts verantwortlich war, danke ich für die reibungslose und produktive Zusammenarbeit. Die gute und enge Abstimmung war mitverantwortlich für den Erfolg dieser Arbeit. Professor Schuller danke ich für dessen stets wertvolle Anregungen und dessen Mitbetreuung meiner Arbeit.

Auch möchte ich mich bei all den Mitarbeitern von Professur und Lehrstuhl für die freundschaftliche Arbeitsatmosphäre bedanken. Stellvertretend danke ich: Stefan, Thomas, Carlo, Camilo und Armin für deren fachliche Unterstützung gerade zu Beginn meiner Arbeit, Kilian für die hervorragend Einführung in das Lehrstuhlleben und sämtliche organisatorischen Feinheiten, Helga für deren stetige organisatorische Unterstützung, Max und der gesamten Fußballtruppe für den wöchentlichen fußballerischen Hochgenuss und all den anderen Kollegen für die Ausrichtung von Ein- und Ausständen.

Ich danke selbstverständlich auch meiner Familie für deren Unterstützung, vor allem aber dafür, dass sie mich haben einfach machen lassen, stets begleitet von einem augenzwinkernden '*braucht's das alles?*'. Zu guter Letzt, der Dank an meine wunderbare Partnerin, Siona. Danke für deine Geduld, deine Unterstützung, dein Verständnis und die Leichtigkeit, die Du mir vermitteltest während meiner Promotion und dem Schreiben der Dissertation. Ich widme sie Dir.

Acknowledgment

The author gratefully acknowledges the financial support by the German Research Foundation DFG, project PO 710/16-1 and the Gauss Centre for Supercomputing e.V. for funding this project by providing computing time on the GCS Supercomputer SuperMUC at Leibniz Supercomputing Centre. The author thanks sincerely the Laboratoire EM2C, Université Paris-Saclay, and in particular R. Gaudron and T. Schuller for the fruitful collaboration and the constant support throughout the entire project. Moreover, the author is indebted to CERFACS, Toulouse, for making available the LES solver AVBP.

Contents

1 Introduction

This introductory chapter addresses the relevance and the motivation of the present thesis before discussing the scope of the work and its general structure.

1.1 Motivation

Modern combustion technologies are indispensable in the ubiquitous fields of power generation and transportation. The development towards renewable but unsteady power generation requires readily available back-up solutions, which should offer at the same time a distinct operational flexibility. Modern gas turbines engines meet both requirements. Likewise, the increasing number of flights per year [1] corroborates the need for advanced combustion technologies that allow the design of efficient aero-engines with low-emission of green-house gases, pollutants and noise.

The recent development of gas turbine and aero-engine manufacturers aims for lean combustion systems [2], which come with low emissions of unburnt hydrocarbons or oxides of nitrogen. Unfortunately, lean combustion systems are prone to thermoacoustic instabilities in which a self-amplifying feedback establishes between the unsteady heat release generated by the flame and the acoustic pressure fluctuations. This coupling between flame and acoustics may yield considerable oscillations of the flow variables. Pressure amplitudes reached during a thermoacoustic instability may cause severe damage to the engine such that the unconditional avoidance of thermoacoustic instabilities limits the operational flexibility of engines [3, 4].

The generation and emission of combustion noise is another challenge for the development of gas turbines and aero-engines [5, 6]. Combustion noise, which is also closely linked to the unsteady heat release rate generated by the flame, is an undesirable, but unavoidable by-product of every turbulent combustion process. Whereas the contribution of jet noise emitted by an aero-engine was reduced up to 10 dB over the last decades, the contribution of combustor noise has received less attention. Yet, combustion noise constitutes a significant contribution to the overall sound emission of an aircraft at approach and cutback conditions [7]. Besides harmful effects and annoyance to those being exposed to noise emissions, high levels of combustion noise may lead to structural excitations or even trigger thermoacoustic instabilities [8].

For confined turbulent flames, as they are found in most applied combustion systems, two contributions to the combustion generated sound can be distinguished: On the one hand, turbulent velocity fluctuations impinge upon the flame and generate broadband heat release rate fluctuations, which, in turn, act as a source of acoustic noise. On the other hand, acoustic waves perturb the flame. In response to the acoustic perturbations the flame generates additional heat release rate fluctuations. Thereby, the acoustic waves perturbing the flame depend strongly on the reflecting combustor confinement.

To optimize stability margins and noise emission of modern combustion devices, there is an increased interest in developing efficient and flexible prediction tools. In this context ‘flexible’ means that changes in the combustor confinement as well as changes in the noise source or the flame dynamics are quickly realizable. If this is given, estimates of the stability margins and the sound pressure level are possible

across a large range of parameters.

The main objective of the present thesis is to build and evaluate efficient and flexible prediction tools for combustor dynamics and noise levels. Key elements of such prediction tools are accurate models for the noise source *and* the flame dynamic response to acoustic perturbations. In the current thesis the simultaneous estimation of these models is achieved by combing Large Eddy Simulation (LES) with advanced System Identification (SI) techniques. The identified models for noise source and flame response are consequently incorporated into an acoustic low-order description of a confined combustor. The resulting reduced order model allows not only computationally affordable predictions of combustor dynamics and noise across a large range of parameters, but also helps to gain a deeper understanding of the thermoacoustic processes involved in a turbulent confined combustion system. Moreover, the reduced order model provides quantitative information on the uncertainty of the predictions in order to judge reliability and robustness of the obtained results.

1.2 Scope of the work

Large parts of the present thesis emerge from the joint *'NoiseDyn'* project between the Laboratoire EM2C, Université Paris-Saclay, and the Thermo-Fluid Dynamics Group at Technische Universität München. The NoiseDyn project is funded by the German Research Foundation (DFG PO 710/16-1) as well as by the Agence Nationale de la Recherche (ANR-14-CE35-0025-01) and deals with the flame dynamics and the combustion noise characteristics of a confined turbulent swirl combustor. The current thesis lays focus on the numerical modeling approach. Laboratoire EM2C commissioned the lab-scaled swirl combustor and provided experimental data to validate the results obtained from the numerical tools.

This thesis pursues the modeling strategy illustrated in Fig. 1.1. As mentioned in the preceding section, an LES/SI approach [9] is chosen to estimate models for the flame dynamic response and the combustion noise source. The main concept of the LES/SI approach is to post-process broadband input-output time series data extracted from LES via SI techniques. This 'black-box' approach permits to infer models for the flame response and the noise source from broadband time series data. Starting point of the LES/SI approach is the generation of broadband LES time series data, see first step in Fig. 1.1. Next, data-driven models are identified for the flame response and the combustion noise source. This is associated with the second step in Fig. 1.1. By combining the identified models with an acoustic description of a confined combustor, predictions of the combustor dynamics and the combustion noise level are achieved. This constitutes the final step in Fig. 1.1.

The main findings of the current thesis were presented at conferences and in journals. Major publications that summarize results of this dissertation are reproduced in the appendix. For a better readability throughout the manuscript the major publications are labeled. As shown in Fig. 1.1, each of these publications is related to one step of the modeling strategy. PAPER-LES focuses on the LES of the NoiseDyn combustor to obtain a validated LES setup for the time series data generation. PAPER-SI FTF and PAPER-SI NOISE propose an extension of the established LES/SI approach, which allows the simultaneous identification of flame response and noise source. Consequently, PAPER-SM, PAPER-2WAY, and PAPER-ROM combine the identified models with a linear network model of a confined combustor and compare the predicted combustor dynamics and noise distributions with experimental data.

The concept of this cumulative thesis is to guide through the major publications by summarizing only the most important results, highlighting the interconnection between the publications. Therefore, the following structure is chosen: to clarify what is required to describe correctly combustion dynamics and combustion noise, chapter 2 provides the essential physical background. As three of the major publications study the NoiseDyn test-rig, this test-rig is introduced in chapter 3 together with its operating con-

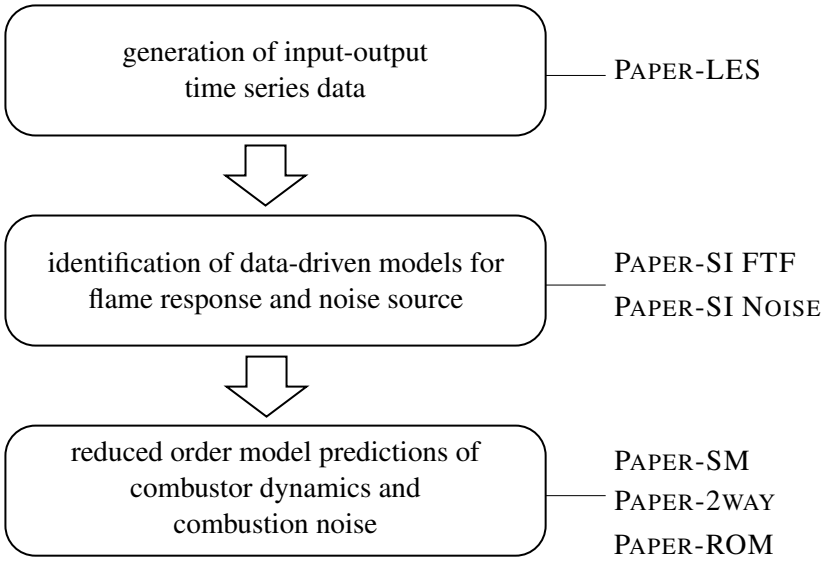

Figure 1.1: Modeling strategy chosen in the current thesis.

ditions (Sec. 3.2) and the diagnostic tools available (Sec. 3.3). The subsequent chapters follow roughly the structure of the modeling strategy shown in Fig. 1.1. Chapter 4 deals with the compressible LES performed. Therein, the main outcome of PAPER-LES is summarized in Sec. 4.3, the generation of broadband input-output data is covered in Sec. 4.4. The SI procedure is addressed in chapter 5, wherein the major findings from PAPER-SI FTF and PAPER-SI NOISE are described in Sec. 5.4. Chapter 6 elucidates the linear network model approach used. Section 6.3 and 6.4 discuss briefly the main results of PAPER-SM, PAPER-2WAY and PAPER-ROM. Chapter 7 gives a summary on the outcome of each publication and presents an extended version of Fig. 1.1 to pay attention in particular to the interconnection between the individual publications. Finally, chapter 8 concludes the thesis and provides an outlook on a potential continuation research project.

2 Physical Background

This chapter introduces the theoretical background and the essential concepts required for the overall understanding of the current thesis. Section 2.1 covers the basics of linear acoustics. Section 2.2 addresses the origin and generation of combustion noise whereas Sec. 2.3 deals with the response of a flame to acoustic perturbations, i.e. the flame dynamic response. In this context also the mechanism behind thermoacoustic instabilities is elucidated, since their origin is closely related to the flame dynamic response. As will become evident, combustion noise and flame dynamics are strongly linked and can hardly be examined separately. Hence, Sec. 2.4 considers the interplay between combustion noise and flame dynamics in a confined combustor configuration.

2.1 Linear acoustics

Acoustic waves are small perturbations in pressure and velocity, propagating in a gaseous medium. The pressure p and the velocity u may be may be formulated as functions of mean and fluctuating quantities

$$p = \bar{p} + p' \quad \text{and} \quad u = \bar{u} + u' \tag{2.1}$$

herein, $[\bar{\cdot}]$ denotes a reference quantity, $[\cdot]'$ describes a fluctuation around the reference value. The concept of *linear* acoustics is to limit the fluctuating parts to small amplitudes compared with the reference value. This allows to neglect higher-order products of acoustic perturbations p' and u' without a significant loss of generality. From the conservation equations of fluid dynamics a formulation can be derived that describes the propagation of acoustic perturbations in gaseous medium, i.e. the wave equation. Assuming 1-D acoustics, as it would be the case for a plane wave propagating in a duct with constant cross-section, the wave equation reads as

$$\frac{\partial^2 p'}{\partial t^2} - c^2 \frac{\partial^2 p'}{\partial x^2} = 0 \tag{2.2}$$

with c specifying the propagation speed of the acoustic perturbations, i.e. the speed of sound. For an ideal gas the speed of sound depends on the thermophysical properties of the gas and its temperature

$$c = \sqrt{\gamma \mathscr{R} T} \tag{2.3}$$

where γ and $\mathscr{R}$ describe the isentropic expansion factor and the specific gas constant, respectively. A solution of the hyperbolic partial differential equation shown in Eq. 2.2 is given by the characteristic waves, also known as Riemann Invariants f and g, which are defined as

$$f = \frac{1}{2}\left(\frac{p'}{\bar{\rho}\bar{c}} + u'\right) \quad \text{and} \quad g = \frac{1}{2}\left(\frac{p'}{\bar{\rho}\bar{c}} - u'\right) \tag{2.4}$$

herein, f and g represent acoustic waves traveling in opposite direction. Both characteristic waves propagate with the speed of sound c. From Eq. 2.4 the acoustic pressure and velocity fluctuations can be retrieved

$$u' = f - g \quad \text{and} \quad \frac{p'}{\bar{\rho}\bar{c}} = f + g\,. \tag{2.5}$$

Because the present thesis deals with acoustics in *confined* configurations, an acoustic characterization of the boundaries is essential. One possibility is to formulate a complex reflection coefficient R that describes modulus and phase between incident and reflected acoustic wave. Corresponding to the propagation direction of f and g, the upstream and downstream reflection coefficients are defined as

$$R_u = \frac{f}{g} \quad \text{and} \quad R_d = \frac{g}{f} \tag{2.6}$$

2.2 Combustion noise

For a turbulent flame one distinguishes between *direct* and *indirect* combustion noise. *Direct* combustion noise, on the one hand, originates from unsteady fluctuations of the heat release rate due to the incoming turbulent flow field. These heat release rate fluctuations, in turn, cause unsteady volumetric expansions of the gas across the reaction zone that finally result in acoustic pressure fluctuations. Thus, the generation of direct combustion noise is an inherent mechanism of turbulent flames and is unavoidable. Consequently, several studies suggest to consider a turbulent flame as a distributed acoustic monopole source [10–12]. *Indirect* combustion noise, on the other hand, is typical for technically premixed flames. Equivalence ratio fluctuations in the mixture upstream of the flame may generate entropy fluctuations in the burnt gas region. If these entropy fluctuations are accelerated, for example across a chocked nozzle at the combustor outlet, acoustic pressure fluctuations arise, which are referred to as indirect combustion noise [13]. In the present thesis, however, only perfectly premixed flames are studied, no mixture ratio fluctuations are present upstream of the flame. Therefore, the generation of direct combustion noise is the only noise source considered in the remainder of this thesis.

To characterize the spectral source distribution resulting from direct combustion noise, a multitude of studies were conducted. It is generally recognized that the source distribution is of broadband type, with a colored spectral distribution [14, 15]: the magnitude of the combustion noise source increases in the low-frequency region towards a peak frequency, before it rolls-off again in the high-frequency region [16]. This behavior is confirmed experimentally in [17, 18] by systematic measurements of unconfined jet-flames.

Yet, when considering the combustion generated sound of turbulent flames for *confined* systems, a distinct differentiation has to made compared with open systems. In open or unconfined configurations the acoustic pressure spectrum is strongly correlated with the source spectrum [7, 19–21]. In most engineering relevant applications, however, the flame is enclosed by a combustor cavity, which exhibits strong acoustic reflections at the boundaries. This adds an additional degree of complexity. The broadband acoustic pressure fluctuations emitted by the flame may excite an eigenmode of the surrounding cavity. This yields a resonant amplification at a given eigenfrequency, which is perceivable as a moderate peak in the resulting sound pressure distribution [22]. Consequently, the sound pressure distribution is no longer directly related to the source spectrum, but instead is modulated by the cavity acoustics.

Fig. 2.1(a) illustrates schematically a *resonating* system. The turbulent flame is represented as a noise source in terms of heat release rate fluctuations $\dot{Q}'$. It is placed in a closed acoustic cavity that has a certain acoustic characterization depending on its reflection coefficients upstream and downstream. Figure 2.1(b) represents a typical spectral distribution of the noise source and the resulting sound pressure. The broadband noise source $\dot{Q}'$ generates a broadband distribution of acoustic waves (dotted line). This broadband forcing may excite, in turn, some of the cavity modes (vertical lines). The resulting sound pressure spectrum (red line) consequently exhibits moderate resonant peaks at the frequencies of the cavity modes. Thus, the cavity acoustics modulate the initial pressure distribution of the noise source such that the resulting sound pressure distribution differs from the noise source distribution. This would

not be the case for an unconfined system.

The situation explained in regard to Fig. 2.1 is referred to as *one-way coupling*: the source excites the acoustics of the system, but the acoustic field does not have any impact on the excitation or the source itself. In the present thesis this is understood as *resonance*.

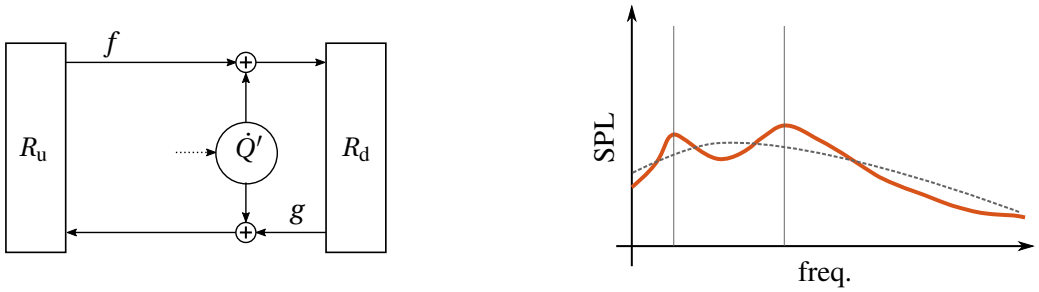

(a) system sketch

(b) sound pressure spectrum

Figure 2.1: Left: schematic of a resonating system. Right: spectral sound pressure distribution (red) resulting from an acoustic broadband source (dotted line) that goes in resonance with acoustic eigenmodes of the system (vertical lines).

2.3 Flame dynamic response and thermoacoustic instabilities

The flame dynamic response, also referred to as combustion dynamics, describe the response of the flame to upstream acoustic perturbations, i.e. the effect of the acoustic field on the generation of heat release rate fluctuations.

If the fuel/air mixture is perfectly premixed or the fuel injection is stiff and its distance to the flame is acoustically compact, the Flame Transfer Function (FTF) is sufficient to fully describe the flame response [23]. The FTF relates upstream velocity fluctuations at a given reference position to global heat release rate fluctuations by

$$G(\omega) = \frac{u'_{\mathrm{ref}}/\bar{u}}{\dot{Q}'/\bar{\dot{Q}}} \tag{2.7}$$

The FTF is a linear description that is valid only in the limit of small acoustic perturbations. If large amplitudes of acoustic perturbation are considered, the flame response becomes non-linear, requiring consequently a non-linear flame description such as the Flame Describing Function (FDF) [24, 25].

To describe the FTF, a wide range of models with varying complexity can be found in literature. A first simplistic modeling approach was proposed by Crocco [26], where the relation between u'_{ref} and $\dot{Q}'$ is characterized by a constant interaction index n and a constant time delay τ. Polifke [9] suggested the use of a Finite Impulse Response (FIR) model for a more detailed description of the flame response.

The coupling between flame and acoustics, which is described by the FTF, may lead to a thermoacoustic instability [1, 27]. If acoustic pressure fluctuations and heat release rate fluctuations are in phase, a self-amplifying feedback may establish between both contributions. This results usually in large oscillations of the flow variables, including strong pressure oscillations within the system. The flame dynamic response, i.e. the FTF, is essential in this context as it characterizes the link between acoustic fluctuations and heat release rate fluctuations.

Figure 2.2(a) illustrates the modeling conception for a *coupled* system. In opposite to the *resonant* system depicted in Fig. 2.1, the acoustic source $\dot{Q}'$ is now coupled to the acoustic field within the closed system. Note that this coupling is mandatory for a thermoacoustic instability to occur, but does not necessarily imply one. Fig. 2.2(b) shows a typical sound pressure distribution in case of an occurring thermoacoustic instability. Again, the broadband distribution of the acoustic noise source is indicated by the dotted line. Nevertheless, in case of thermoacoustic instability the resulting spectral sound pressure distribution is rather independent from the broadband source distribution. A sharp peak has to be expected at the fundamental oscillation frequency of the thermoacoustic instability. The resulting sound pressure spectrum is no longer 'noise dominated' compared with the case shown in Fig. 2.1. Instead, its peak frequency depends mainly on the flame dynamic response and the cavity acoustics. The amplitude of the sound pressure peak, in turn, is governed by effects of non-linear flame saturation. The successional peaks observable in the schematic sketch appear as higher harmonics, i.e. at integer multiples of the fundamental frequency, which is typical for non-linear systems. For completeness, however, it is remarked that the peaks occurring at the higher harmonics do not necessarily have be lower in amplitude as the peak at the fundamental frequency [28, 29].

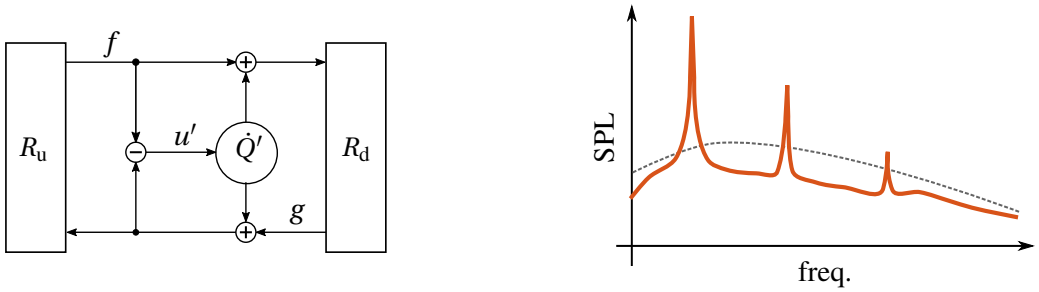

(a) system sketch

(b) sound pressure spectrum

Figure 2.2: Left: schematic of a coupled system. Right: resulting spectral sound pressure distribution (red). The broadband source (dashed line) only has a minor influence on the resulting sound pressure distribution.

The situation explained in regard to Fig. 2.2 is referred to as *two-way coupling*. Compared with the *one-way* coupling illustrated in Fig. 2.1, the acoustic source is now *coupled* to the acoustic field within the system. A mutual interaction between flame and acoustics is established.

2.4 Interplay of combustion noise, flame dynamics and cavity acoustics

As alluded in the introduction and in the preceding two sections, the combustion generated sound within a confined turbulent combustion system depends not exclusively on the combustion noise source itself, but instead also on the flame dynamic response. Thereby, the two contributions cannot always be separated clearly such that the two spectra shown in Fig. 2.1(b) and Fig. 2.2(b) must be considered as idealized showcases for the respective contributions. In applied combustion systems the actual sound pressure distribution may show features of both contributions. Therefore, the current section further elucidates the interplay between combustion noise source, flame response and cavity acoustics in a confined system.

Figure 2.3 illustrates schematically the interplay between combustion noise, flame response and combustor confinement. It can be considered as an extension of the previously shown figures 2.1(a) and 2.2(a). The gray box in Fig. 2.3 represents the flame. The total heat release rate fluctuations generated by the flame $\dot{Q}'_{\text{sum}}$ are described as the sum of two contributions: 1) a deterministic contribution $\dot{Q}'_c$ that origi-

nates from the flame response to upstream acoustic velocity fluctuations u'_{ref}. 2) a stochastic contribution $\dot{Q}'_s$ that depends mainly on the stochastic activity of the turbulent flow field. Whereas the flame response $\dot{Q}'_c$ is associated with the FTF, the second contribution $\dot{Q}'_s$ describes a broadband noise source (similar to the dotted line in Fig. 2.1 and Fig. 2.2). It is anticipated at this point that conceptually the modeling of $\dot{Q}'_{\mathrm{sum}}$ as the sum of $\dot{Q}'_c$ and $\dot{Q}'_s$ is essential for the identification of low-order models of the flame response and the noise source. The according identification procedure is described in detail in chapter 5.

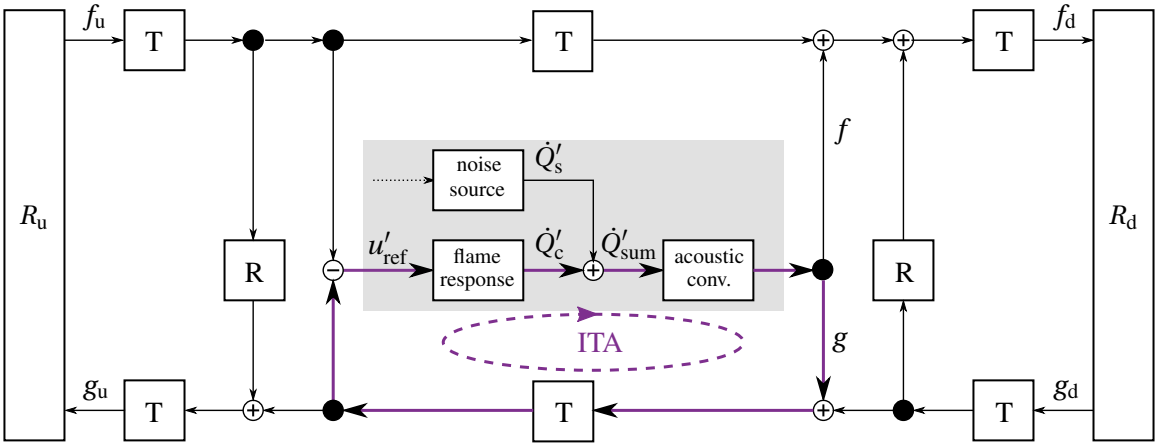

Figure 2.3: Schematic of interplay between combustion noise source, flame response and cavity acoustics.

The unsteady total heat release rate fluctuations $\dot{Q}'_{\mathrm{sum}}$ generate acoustic waves through an unsteady volumetric gas expansion across the flame such that the flame can be seen as a source of sound. The conversion from heat release rate fluctuations to acoustic waves is marked as 'acoustic conv.' in Fig. 2.3.

In many applications the frequencies considered are low and acoustic waves may be described in good approximation as plane acoustic waves. Accordingly, the acoustic waves generated by the turbulent flame propagate upstream (g) and downstream (f) within the combustion system. Depending on the combustor geometry, transmission and reflection of acoustic waves occur at the individual combustor elements (nozzles, area contractions, swirler element, ...). Figure 2.3 indicates transmission and reflection of acoustic waves by the boxes 'T' and 'R', respectively. When the acoustic waves f and g reach the boundaries of the confined setup, the acoustic waves do not leave the combustor. Instead, they are reflected back into the combustor depending on the reflection coefficients R_u and R_d. This closes the outer acoustic loop of the system.

In addition to the outer acoustic loop an internal feedback loop, the Intrinsic ThermoAcoustic (ITA) feedback loop [30–32], may be identified in Fig. 2.3, highlighted by the purple arrows. The chain of mechanisms within the ITA loop may be explained as follows: the unsteady heat release rate fluctuations $\dot{Q}'_{\mathrm{sum}}$ generate upstream and downstream traveling acoustic waves. The upstream traveling wave g is transmitted up to the reference position, where it causes acoustic velocity fluctuations u'_{ref}. The flame response relates the generated acoustic perturbations u'_{ref} again to heat release rate fluctuations $\dot{Q}'_c$, which contribute to $\dot{Q}'_{\mathrm{sum}}$ and close consequently the ITA loop. Figure 2.3 clarifies that the ITA loop is independent of the acoustic boundary conditions R_u and R_d. Instead, the ITA loop is characterized by the flame response and the transmission behavior of the combustor configuration between flame and reference position.

Note that ITA feedback is a flame inherent attribute and is thus *always* present. Yet, the strength of the ITA feedback may vary from case to case. In certain configurations this feedback causes a self-sustained thermoacoustic instability [28, 33, 34]. In other cases it does not necessarily cause an instability, but

instead manifests itself as a resonance peak in the spectral sound pressure distribution [35]. In [36] only a minor impact is found from ITA feedback.

The identified ITA feedback loop has also its implication for the publications of the current thesis. Due to the unavoidable internal feedback, the alluded identification of reduced order models for noise source and flame response results always in a closed-loop identification problem. The ramifications of a closed-loop identification are investigated in PAPER-SI FTF and PAPER-SI NOISE. In addition to the outer acoustic loop, which is characterized by the combustor confinement, the ITA loop has to be be considered as a contribution to the two-way coupling between flame and acoustics, see discussion in Sec. 2.3. This means, in turn, that two-way coupling needs always to be taken into account, even for non-reflecting boundary conditions. The effect of two-way coupling and in particular of ITA feedback on the sound pressure spectrum of a confined turbulent combustor is studied in PAPER-2WAY.

As mentioned in Sec. 1.1, the main objective of the current thesis is the formulation of a reduced order model that allows to determine the combustor dynamics and the sound pressure distribution within a confined turbulent combustor. Thereby, the current thesis aims for a *linear* model, which allows the investigation of linear stability margins and the prediction of the sound pressure distributions for thermoacoustically stable configurations. From the explanations given in this section it becomes evident that for this purpose accurate descriptions for three components are required: the flame response, the noise source and the cavity acoustics. All three components mutually interact such that none of them can be neglected.

3 Confined Swirl Combustion Test-Rig

In the framework of the NoiseDyn project an experimental test-rig of a confined premixed swirl combustor was constructed and commissioned at EM2C laboratoire, Université Paris-Saclay. Three of the publications reproduced in the appendix (PAPER-LES, PAPER-SM and PAPER-ROM) deal with this test-rig. In each of these publications, however, different test-rig configurations and measurement diagnostics are used and discussed. Therefore, this chapter provides an overview of the various test-rig configurations and the available diagnostic tools.

Section 3.1 introduces the test-rig setup before the operating conditions are further specified in Sec. 3.2. Section 3.3 summarizes the diagnostic tools available and their measurement purpose.

For a description of the experimental setup investigated in PAPER-2WAY the reader is referred to [37].

3.1 NoiseDyn test-rig

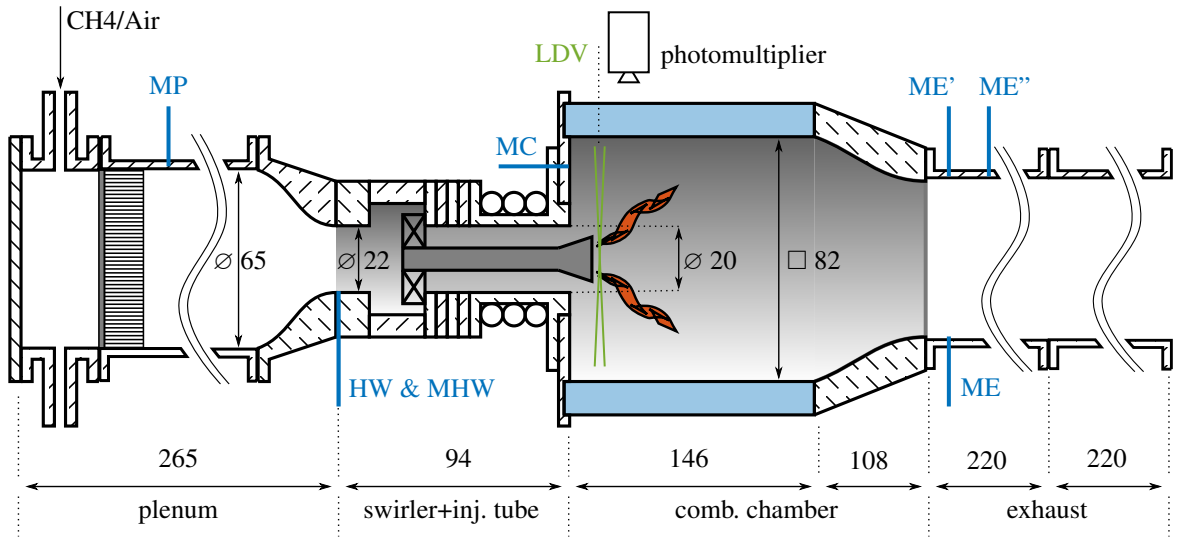

Figure 3.1: Sketch of NoiseDyn test-rig. The shaded area represents the part resolved within the LES domain. Dimensions are given in mm.

Figure 3.1 depicts a sketch of the NoiseDyn test-rig. A methane/air mixture is injected via a tranquillization box (not shown in Fig. 3.1) at the upstream end of the plenum. By passing a honeycomb structure within the plenum, the flow is laminarized before passing through a first convergent part (contraction ratio: 8.73). Next, the mixture passes a radial swirler and the adjacent injection tube before entering the combustion chamber. Figure 3.1 represents only insufficiently the complex radial swirler geometry with its six off-centered swirler vanes. Hence, Fig. 3.2 depicts separately a detailed sketch of the radial swirler. In the combustion chamber the turbulent V-shaped flame anchors at the central conical shaped bluff body tip and is stabilized by swirl. The combustion chamber confinement walls are made out of quartz glass, granting optical access to the flame. Burnt gases leave the combustion chamber through

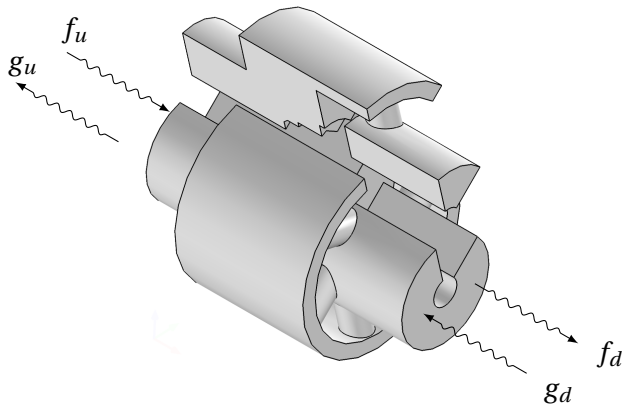

Figure 3.2: Detailed sketch of the radial swirler used in the NoiseDyn test-rig (reproduced from PAPER-SM).

a square-to-round convergent part with a relatively small contraction ratio of 2.03. After the square-to-round convergent part an exhaust tube of variable length may be added optionally.

The test-rig can be equipped with a loudspeaker at the bottom of the tranquillization box (not shown in Fig. 3.1). This allows to impose a monofrequent acoustic excitation of the flow from upstream.

3.2 Operating conditions

For the publications PAPER-LES, PAPER-SM and PAPER-ROM identical flow operating conditions were used. The perfectly premixed methane/air mixture has an equivalence ratio of $\phi = 0.82$. The mixture has a bulk flow velocity of $\bar{u}_b = 5.4$ m/s after the first convergent (HW in Fig. 3.1) and reaches consequently a bulk flow velocity of $\bar{u}_{\text{inj}} = 7.1$ m/s in the injection tube. With a diameter of $D = 22$ mm after the first convergent this yields a Reynolds number of approximately $\text{Re} = u_b D/\nu \approx 7000$. Nevertheless, measurements show that the flow remains laminar after the first convergent at the measurement position HW: a top-hat velocity profile forms with less than 2% relative velocity fluctuations in the boundary layer and much lower fluctuations within the core flow. The inlet temperature is equal to 300 K, whereas the thermal power for the given operating conditions amounts to $P_{\text{th}} = 5.5$ kW.

Regarding the acoustic boundary conditions, the combustor exit must not be considered as choked. The contraction ratio of the square-to-round convergent at the downstream end of the combustor is only small (2.03), yielding a mean combustor exit velocity of $\bar{u}_e = 2.8$ m/s and a corresponding Mach number of Ma= 0.0043. For the termination of the combustor two different configurations can be realized: the combustor is either open-ended or a perforated plate may be installed. The perforated plate has the same outer diameter as the square-to-round convergent and a square pattern of 12 holes of radius r = 2.5 mm with an inter-hole spacing d = 20 mm. At the upstream end the combustor is terminated by a rigid wall.

The length of the optional open-ended exhaust tube controls the thermoacoustic stability of the configuration. Without an exhaust tube the system is thermoacoustically stable and no distinct self-sustained coherent flame motion is detectable. The sound pressure level remains at moderate levels with a maximum value of 117 dB. If an exhaust tube of length L = 220 mm is appended, the system becomes intermittently unstable, having an oscillation frequency of $f = 205$ Hz that reaches a peak amplitude of 138 dB. Further extending the exhaust tube to a length of L = 440 mm provokes a pronounced thermoacoustic instability that reaches a stable limit cycle oscillation with an oscillation frequency of $f = 185$

Hz corresponding to a 3/4 λ wave of the combustor, which is predominantly active in the combustion chamber. The peak amplitude of the fully unstable case is equal to 148 dB.

Figure 3.3 shows the resulting sound pressure spectra within the combustion chamber. For the sound pressure spectrum of the stable configuration no distinct tone emerges and the spectrum is broadband with a moderate peak that stems from a resonant cavity mode. This observation is in agreement with the modeling conception shown in Fig. 2.1. For the fully unstable configuration, which is equipped with an exhaust tube of length $L = 440$ mm, the sound pressure spectrum is no longer broadband, but instead exhibits a distinct peak with smaller peaks at odd-numbered harmonics. Again, this is in accordance with the modeling conception introduced with Fig. 2.2. Note that if the exhaust is equipped with the perforated plate, all three configurations become stable.

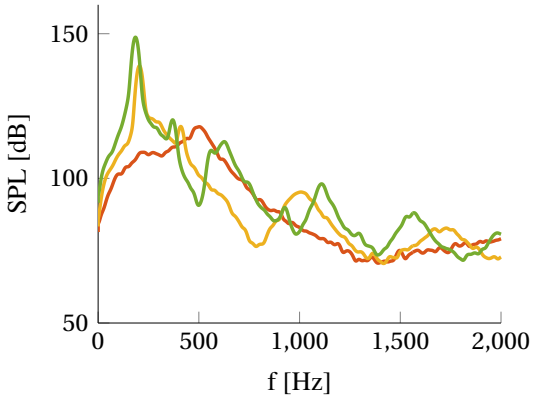

Figure 3.3: Experimentally measured sound pressure spectra for different open-ended exhaust tubes: no exhaust tube (——), exhaust tube of length $L = 220$ mm (——) and exhaust tube of length $L = 440$ mm (——).

3.3 Available diagnostics

The test-rig is equipped with various diagnostic tools. In the publications PAPER-LES, PAPER-SM and PAPER-ROM, however, different diagnostic tools are used and accordingly different measurement data are shown. For giving an overview, this section summarizes the diagnostic tools available and clarifies in which publication the respective experimental data are presented. For more detailed information on every diagnostic tool, the reader is referred to the individual publication reproduced in the appendix.

A Laser Doppler Velocimetry (LDV in Fig. 3.1) is available to measure the flow velocity at the combustion chamber entrance, 3 mm above the combustion chamber backplate. This provides an accurate local determination of the incoming flow field directly upstream of the turbulent swirl flame. The LDV measures mean as well as root-mean-squared velocity profiles of axial, radial and circumferential velocity. PAPER-LES contains the corresponding velocity profiles. From these velocity measurements a swirl number of $S \approx 0.8$ is determined.

A photomultiplier mounted with an interferometric filter measures OH* chemiluminescence, which is assumed to be proportional to the heat release rate for perfectly premixed flames. This allows to record OH* images of the averaged turbulent flame shape as well as phase-conditioned pictures of the flame when submitted to an external acoustic forcing via the upstream loudspeaker. PAPER-LES presents Abel deconvoluted images of both averaged and phase conditioned flame images.

A hot-wire probe for velocity measurements (HW in Fig. 3.1) is installed in between the first convergent and the radial swirler. The FTF can be determined by acoustically forcing the flow via the upstream loudspeaker and simultaneously recording the signals of velocity fluctuations at the hot-wire location and resulting OH* chemiluminescence fluctuations. FTF measurements are reproduced in PAPER-SM and PAPER-ROM.

Multiple microphones are installed across the test-rig (see Fig. 3.1: MP, MHW, MC, ME, ME', ME"). They are used to measure time traces of sound pressure fluctuations - and accordingly spectral sound pressure distributions - as shown in PAPER-LES and PAPER-ROM. The microphones ME, ME' and ME" at the downstream end of the combustor may additionally be used to reconstruct acoustic velocity fluctuations via the three-microphone method [38]. Together with the hot-wire probe HW and the microphone MHW (both installed upstream) this allows the assessment of the acoustic variables p' and u' during upstream acoustic forcing. Consequently, the acoustic transfer matrix of the combustor can be determined by employing the two-load method [39]. Since only upstream acoustic excitation is used in the test-rig, the two-load method is retained for determining the acoustic transfer matrix instead of the more frequently used two-source method [40–42]. PAPER-SM presents the experimental results for the non-reactive and the reactive combustor scattering matrix, which are directly deduced from the transfer matrix measurements through simple algebraic transformation.

The capability of the microphones ME, ME' and ME" to reconstruct acoustic velocity fluctuations is further exploited to measure gain and phase of the downstream reflection coefficient. PAPER-LES and PAPER-ROM contain measurements for both the open end and the perforated plate. The upstream reflection coefficient has not been determined experimentally. Yet, the upstream plenum is terminated by a rigid wall such that the upstream reflection coefficient may assumed to be equal to unity without any phase shift. Note that the studies [43–45], which investigated self-sustained combustion instabilities, used the same plenum configuration as shown in Fig. 3.1. In these studies the upstream reflection coefficient is also assumed to be fully reflective. Since the resulting model predictions in these works are in good agreement with measured data, it is concluded that the assumption of a fully reflective upstream end is valid.

With the sum of these diagnostics a comprehensive set of experimental data is obtained, where the flame response (i.e. the FTF), the spectral distribution of sound pressure within the combustor and the acoustic boundary conditions are accurately quantified. An acoustic characterization of a turbulent combustor in this entirety is rare in literature. As elaborated in Sec. 2.4, however, such a complete characterization is crucially necessary for a proper comparison between measurements and the numerical modeling approaches developed.

4 Large Eddy Simulation of a Premixed Combustor

Before models for the flame response and the noise source may be determined via SI techniques, input-output data need to be generated. This corresponds to the first step of the modeling strategy introduced in Fig. 1.1. In the current thesis a compressible reactive LES is chosen for the data generation step.

The general concept of LES is to resolve directly the large turbulent structures within the flow, which are often dependent on the specific geometry investigated. The small turbulent structures are more universal and hence not resolved directly, but instead modeled by a subgrid scale model. A *compressible* LES is particularly suited in the current study as it describes not only the turbulent reactive flow but also takes into account all relevant *acoustic* mechanisms involved: the two-way acoustic-flame interaction, the generation of combustion noise by resolved turbulent structures and the acoustic wave propagation in a complex geometry.

Section 4.1 describes the LES setup of the NoiseDyn test-rig that is used in the publications PAPER-LES, PAPER-SM and PAPER-ROM. Whereas in PAPER-LES the LES is used to reproduce directly experimental measurements, it serves in PAPER-SM and PAPER-ROM for the generation of broadband time series data that are consequently used for the SI procedure. Section 4.2 addresses briefly the benefit of coupling Characteristic Based State-space Boundary Conditions (CBSBC) with the LES since this is not only essential for the publications [46] and PAPER-LES, but is used also in PAPER-SM and PAPER-ROM. Section 4.3 addresses the direct assessment of sound pressure spectra via compressible LES. By comparing the resulting LES spectra against measured spectra, the descriptions of flame dynamics and generation of combustion noise are validated within the LES. The concluding section 4.4 illustrates the procedure for the generation of broadband input-output time series data via the compressible LES.

Note that for the publications PAPER-2WAY, PAPER-SI FTF and PAPER-SI NOISE the LES data used for the reference model identification were provided from [47].

4.1 NoiseDyn LES setup

The compressible reactive flow solver AVBP [48], developed by CERFACS, Toulouse, is used for the LES computations of the NoiseDyn test-rig. The fully compressible Navier-Stokes equations are solved on an unstructured grid [49, 50] by using the Lax-Wendroff scheme, which has a spatial and temporal accuracy of second order. Subgrid stresses are taken into account by the wall adapting linear eddy (WALE) model [51] without application of any wall-functions. The turbulence-flame interaction is modeled by the dynamically thickened flame model [52], ensuring that the laminar flame thickness is resolved by seven cells. The chemistry of the premixed methane/air flame is describe by the reduced two-step BFER [53] scheme.

Figure 3.1 indicates the extent of the LES domain. The LES resolves only the 'core' part of the combustion test-rig extending from upstream of the radial swirler to downstream of the combustion chamber. This delimitation of the computational LES domain saves computational costs and is applicable because

complex flow phenomena, which would need to be resolved via LES, are not expected in the upstream plenum or downstream of the combustion chamber. The acoustic impedances of the neglected combustor parts, however, need to be taken into account to guarantee a complete acoustic description of the test-rig. This is achieved by coupling the LES to CBSBC, as described in the subsequent section 4.2. The LES inlet coincides with the hot-wire probe location in experiments (denoted as HW in Fig. 3.1). As mentioned in Sec. 3.2, the flow at this position is laminar with a top-hat velocity profile. Thus, a laminar velocity block profile is imposed at the LES inlet with a bulk velocity of $\bar{u}_{\text{in}} = 5.4$ m/s. Atmospheric pressure of $\bar{p}_{\text{out}} = 1$ atm is set at the LES outlet.

The unstructured LES grid used consists of approximately 19 million tetrahedral cells. The mesh is refined in the reaction zone region with a maximum cell size of 0.6 mm. A maximum cell size of 0.8 mm is used within the complex burner geometry upstream of the flame, which contains the radial swirler and the injection tube. The radial swirler is fully described by the computational mesh, meaning that no geometrical simplification are applied. Each of the six radial swirler vanes has a diameter of 6 mm and is resolved by approximately 18 cells, which are refined towards the walls. To keep the computational effort on a reasonable level, the mesh resolution in the burnt gas region downstream of the flame is coarsened by allowing a maximum cell size of 1.4 mm. This coarsening is permissible since less complex flow dynamics are expected in the burn gas region due to the elevated viscosity and the relatively simple geometry.

As one objective of the compressible LES is to reproduce correctly the flame response and the generation of combustion noise, an obligatory test is the comparison between measured and computed velocity profiles directly upstream of the flame. The mean velocity field is essential for the mean flame shape, which has a direct impact on the flame response. The incoming turbulent velocity fluctuations that impinge on the flame front are strongly linked to the generation of combustion noise. A comparison between the LDV measurements described in Sec. 3.3 and the computed velocity profiles from LES for mean and fluctuating values exhibits an overall good agreement (see PAPER-LES). This comparison proves that the LES setup chosen is able to precisely describe the flow field directly upstream of the flame - a prerequisite for further investigations. In particular the generation of turbulence and swirl across the radial swirler, located in between LES inlet and combustion chamber entrance, are reproduced correctly by the LES.

Regarding subgrid scale modeling and wall treatment, it is worth mentioning that different combinations were tested. Thereby, it is found that the WALE model applied without any wall-functions provides overall the best agreement with experimental data. This observation is in accordance with [54]. When using wall-functions in combination with the WALE model, the fluctuating velocity components are overestimated.

After the validation of velocity profiles upstream of the flame, mesh independence in regard to the generation of combustion noise is affirmed. Compared to the reference mesh with its 19 million cells one coarser and one finer mesh are tested, which have approximately 11 million and 34 million cells, respectively. The mesh resolution in the burnt gas region is kept constant and the coarsening / refining is applied only on the reaction zone and the upstream region as they are assumed to be essential for the generation of combustion noise. It is found that for all three mesh resolutions the resulting sound pressure spectrum is comparable, see Fig. 4.1. Hence, the LES results for the sound pressure spectra are assumed to be mesh-independent. For a more detailed description of the mesh study performed the reader is referred to PAPER-LES.

One uncertainty in the LES setup arises from the wall temperatures, since experimental values are not available due their cumbersome accessibility. For the publications PAPER-LES, PAPER-SM and PAPER-ROM, which all deal with the NoiseDyn setup, a set of wall temperatures is used that yields the same global heat loss as the experimental configuration. This is validated by comparing the mean combustor

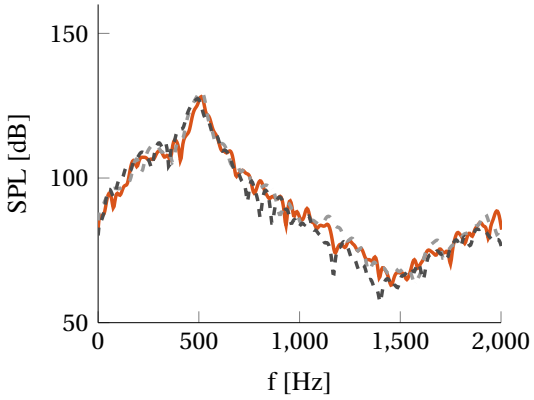

Figure 4.1: Sound pressure spectra from LES computed with different mesh resolutions: reference mesh with 19 million cells (——), coarse mesh with 11 million cells (- - -) and fine mesh with 34 million cells (- - -).

exit temperatures in experiment and LES. A detailed discussion of the effects of the respective wall temperatures, however, is not provided in any of the publications and is therefore given in the following.

For the injection tube and the swirler adiabatic walls are assumed because the inlet gas temperature is approximately equal to the ambient temperature. The lateral confinement walls of the combustion chamber and the square-to-round convergent part represent the biggest area portion in the burnt gas region. The heat loss across these boundaries has a major impact on the mean bulk flow temperature and hence the mean speed of sound in the burnt gas region. This, in turn, affects the eigenmodes of the combustor cavity. For the subsequent LES based prediction of sound pressure spectra within the combustion chamber this results in a shift of the peak frequency. In particular for an unstable working condition this may also have a significant impact on the limit cycle oscillation amplitude. In the present setup heat loss boundary conditions are used for the lateral combustion chamber walls. Together with a thermal resistance of the quartz walls, experimentally determined values of the *outside* wall temperature are imposed as reference temperature. This yields a spatially non-uniform wall temperature distribution that adapts to the internal temperature field.

Moreover, it is observed that the lateral wall temperatures have only a minor impact on the flame shape and hence on the flame dynamic response, i.e. the FTF. The wall temperatures of the combustor back plate and of the bluff body tip, however, are found to have a strong impact on the FTF. With increasing combustor back plate temperature the flame shape gradually changes from a V-shaped to a M-shaped flame. The M-shaped flame anchors additionally at the outer rim of the injection tube. As a result of this gradual change, the flame length is decreasing, which impacts primarily the phase of the resulting FTF: the shorter the flame length, the steeper the phase decay.

The bluff body tip temperature controls the stand-off distance between flame and bluff body and is important for the flame anchoring and the flame root behavior. It is found that a large bluff body tip temperature results in a short stand-off distance between bluff body tip and flame root. In this case the flame is well anchored. From these observations it is deemed that variations of the bluff body tip temperature have an impact on gain *and* phase of the FTF.

For numeric values of the respective wall temperatures in the LES setup the reader is referred to PAPER-LES.

4.2 Coupling of LES with characteristic based state-space boundary conditions

As argued in Sec. 2.4, the sound pressure spectrum in a confined combustor setup depends crucially on the acoustic characteristics of the surrounding cavity. A proper validation of computed sound pressure spectra is thus possible only if the cavity acoustics are fully taken into account in the LES. The most natural approach would be to resolve directly the complete combustor configuration within the LES domain, meaning from upstream plenum to downstream exhaust. Yet, Fig. 3.1 shows that the LES domain chosen resolves only the part from upstream swirler to downstream combustion chamber in order cut down computational costs. To ensure nonetheless a complete description of the acoustic cavity as it is found in experiments, the LES is coupled to CBSBC [55]. These boundary conditions allow to impose complex reflection coefficients at the boundaries to model acoustic systems adjacent to the LES domain. Figure 3.1 clarifies that the upstream plenum and the downstream exhaust tube are not resolved within the LES domain, hence they are modeled acoustically via CBSBC instead. For an extensive and complete description of the CBSBC the reader is referred to [55] or PAPER-LES.

Besides providing boundary impedances for an accurate description of the acoustics *within* the LES domain, CBSBC also make possible to reconstruct the sound pressure spectra at locations *outside* of the LES domain. The state-space model of the CBSBC retains spatial information. Accordingly, PAPER-LES assesses the sound pressure at the microphone locations MP or ME (see Fig. 3.1), although these locations do not lie within the LES domain. This is achieved by an additional post-processing step: the boundary state-space model is simulated forward in time with the characteristic wave leaving the LES domain as input signal. Note that the assessment of pressure fluctuation outside the LES domain would not be possible with other time domain impedance boundary conditions as used e.g. in [56, 57].

Compared with the formulation of the well established Navier-Stokes Characteristic Boundary Condition (NSCBC) [58], which exhibits acoustic reflections in the low frequency range [59, 60], the CBSBC are fully non-reflective, even in the low frequency limit. This is achieved by making use of a wave masking technique [60]. PAPER-SM and PAPER-ROM exploit this property to ensure fully non-reflective boundary conditions.

Note that in a prior study the CBSBC are applied to a laminar case [46]. Therein, the CBSBC are used to model an upstream plenum of variable length whereas the flame and its vicinity are resolved by a compressible CFD. The length of the plenum modeled controls the thermoacoustic stability of the laminar slit burner: the longer the plenum, the larger the occurring oscillation amplitudes. This study proves two essential aspects that are of importance for the sound pressure prediction of the NoiseDyn test-rig. First, a change of the impedance modeled by CBSBC may be enough to trigger thermoacoustic instabilities. Second, it is demonstrated that the acoustics can be treated linearly also in case of a strong non-linear thermoacoustic oscillation. Consequently, the non-linearity can be attributed to hydrodynamic effects and flame dynamics, which are both resolved via the compressible CFD.

4.3 Sound pressure prediction in the NoiseDyn test-rig

Section 4.1 illustrated that the LES reproduces correctly the velocity field upstream of the flame and that the resulting sound pressure spectra are mesh independent. Section 4.2 described how to model efficiently the unresolved acoustic parts upstream and downstream of the LES domain. Yet, it is still unclear if the computed sound pressure spectra are physically correct, i.e. if they are in agreement with experiments.

The successful validation of the LES against experimental data is essential for further investigations,

which are based on the compressible LES data. Therefore, PAPER-LES assesses the spectral sound pressure distribution in the NoiseDyn setup for stable and unstable working conditions and compares results with measurement data. This section presents only one of the main results from PAPER-LES. The focus is thereby laid on the implications of this result for the following investigations and publications. The fully reproduced publication can be found in the appendix of this thesis.

As explained in the preceding section 4.2, the CBSBC are used in PAPER-LES to model the acoustic impedance of the upstream plenum and of the part downstream from the square-to-round convergent. Whereas the upstream impedance model remain unchanged - a fully reflective end with a constant phase lag that is defined by the plenum length - different downstream impedances are studied. The exhaust tubes used are always open-ended but differ in their length. This means that the absolute value of the downstream reflection coefficient is in good approximation always equivalent to the analytically predicted values for an open unflanged tube [61]. The phase values, however, depend on the exhaust tube length and the speed of sound within the exhaust tube.

Recalling the explanations given in Sec. 3.2, without exhaust tube the configuration is stable, with an exhaust tube of L = 440 mm a fully developed limit cycle oscillation is obtained. When modeling the particular impedances via CBSBC, excellent agreement is found between LES and measurements, see figure 4.2.

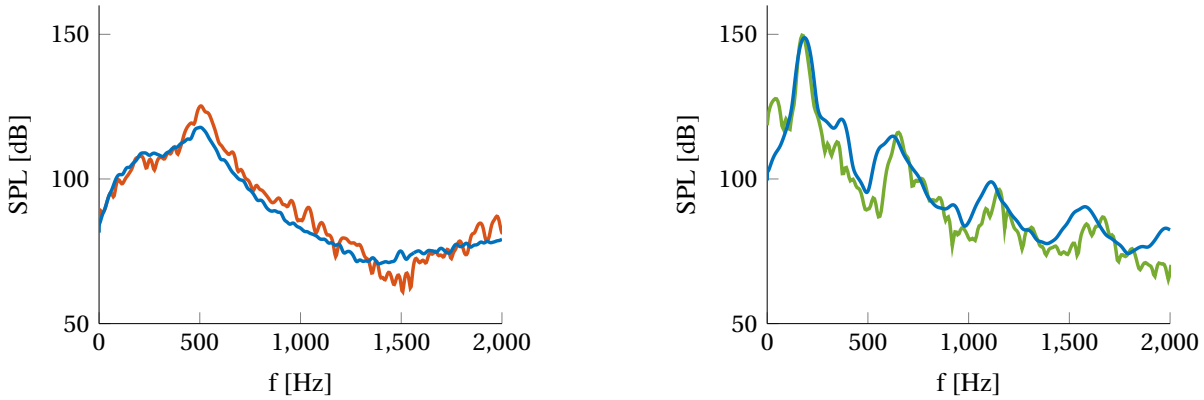

(a) stable

(b) fully unstable

Figure 4.2: Sound pressure measurements (—) and LES results for the stable (—) and the fully unstable (—) configuration (reproduced from PAPER-LES).

As argued previously in Sec. 2.2, the spectrum of the stable configuration has a rather broadband distribution. It is dominated by the combustion source characteristics, subsequently modulated by cavity resonances. A linear network model analysis conducted later in PAPER-ROM reveals that the moderate peak observable in this configuration stems from a resonant combustion chamber mode. The spectral sound pressure distribution for the unstable configuration, however, exhibits distinct peaks. This spectrum is influenced not only by the noise source, but instead depends strongly on the flame dynamics, which are the governing mechanism during a thermoacoustic instability. The peak in the sound pressure spectrum occurs at the oscillation frequency of the thermoacoustic instability. Non-linear saturation effects, which are accounted for in the LES, control the amplitude of the pressure peak.

The LES reproduces accurately both stable and unstable configurations. In turn, this suggests strongly that both aspects, i.e. the combustion noise source as well as the flame dynamics, are described precisely by the compressible LES. In the framework of the current thesis this is an important aspect. Because the LES/SI procedure yields *data-driven* models for the flame dynamic response and the combustion noise

source, physically correct models can only be estimated if the responsible mechanisms are correctly reproduced by the LES. If the SI procedure is fed with erroneous data from the LES, erroneous model estimations result. The successful validation of the LES against measurements of the sound pressure distribution ensures that the LES setup can be used for the generation of broadband input-output time series data. Subsequently, the broadband time series data from LES are post-processed via SI techniques to estimate reduced order models for the flame dynamic response and the combustion noise source.

4.4 Generation of broadband time series

The following section explains the procedure of generating input-output time series data via acoustic forcing of the LES. This corresponds to the first step of the modeling strategy introduced in Fig. 1.1. Focus is laid in this section on the LES relevant aspects in regard to acoustic forcing. For the implications of different forcing parameters on the SI procedure itself the reader is referred to Sec. 5.1.

The general concept is to impose an acoustic excitation signal at the LES domain boundaries. At the inlet a characteristic wave f_{in} is imposed, whereas at the outlet a characteristic wave g_{out} is applied. Thereby, for example an ingoing wave f_{in} should be regarded as an input signal that causes a certain system response, e.g. heat release rate fluctuations across the flame $\dot{Q}'$ or an outgoing characteristic wave f_{out}.

The system under study may be characterized from its response to the input signal. By using a mono-frequent excitation signal, as it is usually done in an experimental approach, the transfer behavior of a system at a given excitation frequency can be directly determined from its response at that same frequency. Instead of forcing the system mono-frequently, one may excite the system with a broadband forcing signal, which contains spectral energy not only at one discrete frequency, but instead across a specified frequency range. From the resulting broadband input-output time series data the transfer behavior of the system can be directly estimated across a complete frequency range via the use of SI techniques (see chapter 5). Compared to repeated mono-frequent excitation across a certain frequency range, the broadband forcing technique reduces the computationally effort significantly in LES and yields a transfer function that is valid in the complete complex plane ($\omega \in \mathbb{C}$). The determination of the transfer behavior of a system across a given frequency range via mono-frequent excitation would be rather expensive in LES, as for every excitation frequency multiple forcing cycles need to be computed.

Different signal types are possible for broadband excitation. The present thesis, in particular PAPER-SM and PAPER-ROM, use a broadband signal that is based on Daubechies wavelets [62]. This signal type offers certain advantages for the use in LES. First, the amplitude of the signal is bounded. Other than a random Gaussian White Noise signal, no amplitude values above a certain threshold value are present in the Daubechies wavelet signal. This ascertains that no non-linear flame response is triggered unintentionally by the input forcing. Second, its spectral energy content is constant up to a certain cut-off frequency above which the spectral energy content monotonically decreases. Third, the broadband signal used is continuous. Even though a Pseudo Random Binary Signal would also be bounded in amplitude, its discrete amplitude distribution causes numerical difficulties if applied in LES. Overshoots result in the actual input signal, which impede the subsequent identification.

Figure 4.3 depicts a typical time series generated by LES with applied broadband forcing. The input quantity u' causes in the LES a certain flame response in terms of $\dot{Q}'$, which is considered as output. By post-processing this input-output time series data set via advanced SI techniques, a causal relation between u' and $\dot{Q}'$ may be formulated, i.e. the FTF, as well as a model for the generation of combustion noise. This will be further explained in Sec. 5.5.

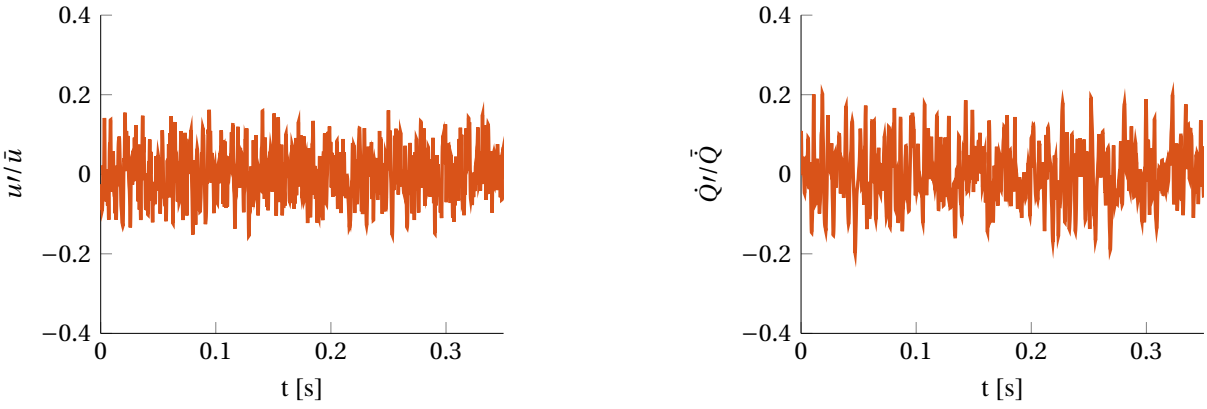

(a) input

(b) output

Figure 4.3: LES generated broadband input-output time series data. The normalized velocity fluctuations serve as input whereas the normalized global heat release rate fluctuations are considered as output.

5 System Identification in Thermoacoustics

The first step of the modeling strategy shown in Fig. 1.1 is carried out by generating broadband input-output time series data via a compressible LES. The subsequent step deals with the identification of data-driven models for flame response and noise source. Therefore, advanced SI techniques are applied in this thesis.

This chapter introduces the required background information on SI in general and explains the SI techniques used. After a short overview on SI, the three essential steps of the identification procedure are discussed: generation of broadband data (Sec. 5.1), choice of model structure (Sec. 5.2) and model coefficient estimation (Sec. 5.3). Therein, attention is paid on the comparison between the established FIR identification and the more advanced Box-Jenkins (BJ) identification. It is shown that the BJ identification is suited in particular in the framework of the current thesis as it allows the simultaneous identification of reduced order models for the flame response, i.e. the FTF, *and* the combustion noise source. Section 5.4 summarizes the main outcome of the two surrogate data studies performed in PAPER-SI FTF and PAPER-SI NOISE before in Sec. 5.5 the investigated SI techniques are applied on actual LES data of the NoiseDyn configuration.

Methods for SI originate from the field of control theory [63–65] and may be considered as a combination of different theories, such as estimation theory, signal processing and system theory. The overall objective of SI is described by Keesman as '*the construction of mathematical models of the system under study based on noisy time series*' [64]. The 'mathematical models' in this context are often referred to as transfer functions, which should precisely describe the input-output behavior of a given system.

From a system theory perspective the FTF may be seen as a linear transfer function that relates upstream velocity perturbations at a given reference position u'_{ref} to resulting heat release rate fluctuations $\dot{Q}'_c$. By recalling Fig. 2.3 and the underlying modeling principle of summing a deterministic contribution $\dot{Q}'_c$ and a stochastic contribution $\dot{Q}'_s$, the most general description of a linear time invariant system that describes the total heat release rate $\dot{Q}'(t)$ as an output is given by

$$\dot{Q}'(t) = \underbrace{G \cdot u'_{\mathrm{ref}}(t)}_{\dot{Q}'_c} + \underbrace{H \cdot e(t)}_{\dot{Q}'_s} \tag{5.1}$$

herein, the so-called *plant model* G may be associated with the FTF since it establishes a causal relation between the input signal $u'_{\mathrm{ref}}(t)$ and the heat release rate fluctuations $\dot{Q}'(t)$. It describes thus the deterministic contribution $\dot{Q}'_c$, which stems from upstream acoustic perturbations. The *noise model* H, with its generic Gaussian White Noise input term $e(t)$, describes the stochastic contribution $\dot{Q}'_s$ to the global heat release rate $\dot{Q}'(t)$. This contribution may be associated with the combustion noise contribution and is understood to be uncorrelated to any incoming acoustic perturbations.

Figure 5.1 represents graphically Eq. (5.1). Note that this representation corresponds clearly to the modeling principle of the flame contributions shown in Fig. 2.3. In an actual combustor colored turbulent velocity fluctuations cause a certain spectral distribution of $\dot{Q}'_s$. In the modeling approach of Fig. 5.1 this effect is mimicked by filtering a generic Gaussian White Noise input term $e(t)$ through the noise model H in order to obtain directly the same spectral distribution of $\dot{Q}'_s$, as it would have been caused by turbulent velocity fluctuations in an actual combustor. The noise model H contains thus physical information of the system.

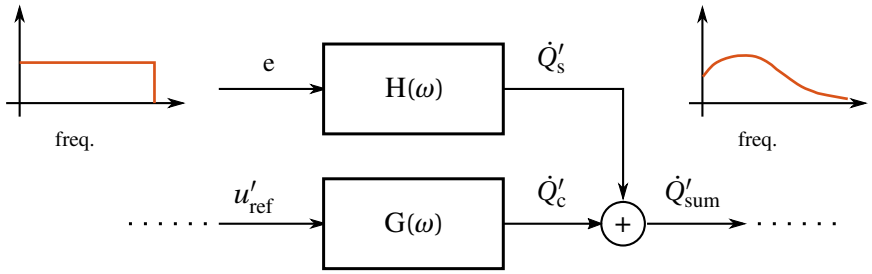

Figure 5.1: Modeling approach of total heat release rate fluctuations $\dot{Q}'_{sum}$.

Objective of the SI procedure is then to estimate descriptions of the plant model G and the noise model H. The necessary procedure may be divided into three main steps: 1) generation of broadband data 2) choice of model structure and 3) solution of an optimization problem to find the model coefficients, which describe best the input-output time series data. In the following three sections these steps are briefly covered.

5.1 Properties of broadband data

As described in Sec. 4.4, a compressible LES is used in the current thesis for the generation of broadband time series data. Whereas the aspects relevant for the LES were already described in Sec. 4.4, this section discusses the implications of different time series properties on the subsequent SI procedure.

The main properties of the broadband time series data are the cut-off frequency, the signal-to-noise ratio (SNR) and the time series length. The influence of the latter two is studied among other aspects in PAPER-SI FTF and PAPER-SI NOISE.

The cut-off frequency of the excitation signal determines up to which frequency the transfer behavior of the system may be inferred. Estimations for the frequency response of a system are only possible for frequencies that are contained in the excitation signal. Consequently, a large cut-off frequency yields a large validity range of the identified models. A large cut-off frequency of the broadband excitation signal, however, results also in a wide spread of spectral energy, which decreases the identification accuracy. Thus, as a best practice the cut-off frequency should be chosen as high as necessary, but not higher. Fortunately, flames usually exhibit a low-pass behavior [1] and combustion noise is known to be active predominantly in the low frequency region [14]. Consequently, the works PAPER-SM and PAPER-ROM use a maximal cut-off frequency of 1000 Hz.

The excitation signal amplitude determines the SNR of the time series data, since the noise source strength usually cannot be controlled. Generally, a high SNR results in accurate model estimations. Yet, a trade-off has to be made regarding the SNR. If the excitation amplitude is chosen too large, it may trigger a non-linear flame response, which cannot be handled by the *linear* identification techniques used. Therefore, in the publications PAPER-SM and PAPER-ROM a forcing amplitude equivalent to 10 % of the mean inflow velocity is chosen to achieve a favorable SNR by ensuring at the same time a linear flame response [66].

Regarding the identification error and the identification uncertainties, a strong dependence is recognized on the time series length available. Based on surrogate data PAPER-SI FTF and PAPER-SI NOISE demonstrate that the identification error and the identification uncertainty decrease with increasing time series length. Yet, LES computations for the time series generation are computationally demanding such that the time series length is usually limited. In PAPER-SM and PAPER-ROM an LES time series length

of 350 ms is used for the subsequent identification, which yields for the gain of the FTF a 95 % confidence interval that ranges approximately in between ±0.2. Phase values of the identified FTF exhibit usually significantly smaller confidence intervals. The impact of the identification uncertainty in the FTF on stability margins and growth rates of a thermoacoustic system is studied in [67].

5.2 Choice of model structure

After the input-output data are generated, a certain model structure needs to be chosen. By expanding in Eq. (5.1) the plant model G and the noise model H in terms of polynomial filters, the most general polynomial model structure reads as

$$A(q,\theta)\dot{Q}'(t,\theta) = \frac{B(q,\theta)}{F(q,\theta)}u'_{\mathrm{ref}}(t) + \frac{C(q,\theta)}{D(q,\theta)}e(t) \tag{5.2}$$

herein A, B, C, D and F are polynomials in time shift operator q^{-i} defined as

$$q^{-i}u'(t) = u'(t - i\Delta t) \tag{5.3}$$

Thus, the respective polynomial filters result in

$$\begin{aligned}
A(q) &= 1 + a_1 q^{-1} + a_2 q^{-2} \dots a_{n_a} q^{-n_a} \\
B(q) &= b_0 + b_1 q^{-1} + b_2 q^{-2} \dots b_{n_b} q^{-n_b} \\
C(q) &= 1 + c_1 q^{-1} + c_2 q^{-2} \dots c_{n_c} q^{-n_c} \\
D(q) &= 1 + d_1 q^{-1} + d_2 q^{-2} \dots d_{n_d} q^{-n_d} \\
F(q) &= 1 + f_1 q^{-1} + f_2 q^{-2} \dots f_{n_f} q^{-n_f}
\end{aligned}$$

The difference between $\left[B(q,\theta),\ C(q,\theta)\right]$ and $\left[D(q,\theta),\ F(q,\theta)\right]$ is that $\left[B(q,\theta),\ C(q,\theta)\right]$ relate prior *inputs* to the current output whereas $\left[D(q,\theta),\ F(q,\theta)\right]$ take prior *outputs* into account and can describe consequently possible auto-regressive behavior. The individual model coefficients in the parameter vector θ

$$\theta = \{a_1 \dots a_{n_a}, b_0 \dots b_{n_b}, c_1 \dots c_{n_c}, d_1 \dots d_{n_d}, f_1 \dots f_{n_f}\}$$

weight the relation between current as well as prior inputs and output samples. Therein, the respective model orders n_a, n_b, n_c, n_d and n_f specify the number of prior samples that are taken into consideration. Concluding, this means that the current output on the left-hand side of Eq. (5.2) is computed from a convolution of the polynomial model coefficients with prior inputs and outputs. The amount of prior time series samples that are taken into account is determined by the model order.

When comparing Eq. (5.1) and Eq. (5.2), it becomes evident that the polynomial filters $B(q,\theta)/F(q,\theta)$ describe the plant model G whereas $C(q,\theta)/D(q,\theta)$ specify the noise model H. By including or excluding some of the polynomial filters A,B,C,D and F, different model structures of varying complexity may be deduced from the general model structure shown in Eq. (5.2). The remainder of this section discusses in detail two specific model structures with respect to their capability of describing the plant model G and the noise model H. On the one hand, the well established FIR model structure is examined, which is applied on LES data in PAPER-SM and PAPER-2WAY. On the other hand, the more general BJ model structure is introduced, as it allows the additional identification of a model for the combustion noise source. PAPER-ROM applies a BJ model identification on broadband LES data from the NoiseDyn configuration.

The FIR model structure is retained from the general model structure shown in Eq. (5.2) by setting the polynomial filters A, C, D and F equal to unity

$$\dot{Q}'(t,\theta) = B(q,\theta)\,u'_{\mathrm{ref}}(t) + e(t)\ . \tag{5.4}$$

In this case, the output $\dot{Q}'$ is computed by a simple convolution of the model coefficients $\theta = \{b_0,\ b_2,\ ...,\ b_{n_b}\}$ with prior inputs $u'_{\mathrm{ref}}(t)$. The FIR is widely used to model the flame dynamic response [47, 68–78]. By setting $C(q,\theta) = D(q,\theta) = 1$, however, no noise model H is estimated. Consequently, the noise contribution is assumed to be Gaussian White Noise. For laminar flame configurations in which no turbulent combustion noise is present, this might be a valid assumption. Yet, a turbulent flame, as it is studied in the framework of the current thesis, exhibits turbulent combustion noise, which is known to be colored [14, 15]. Deploying a FIR model structure for the identification of a turbulent flame does not provide any estimates of the colored noise contribution. Moreover, assuming erroneously a colored noise contribution to be white, introduces a bias into the plant model identification, see PAPER-SI FTF and PAPER-SI NOISE.

The more general BJ model structure may be considered as an extension of the FIR model structure and is retained from Eq. (5.2) by setting only $A(q,\theta)$ equal to unity

$$\dot{Q}'(t,\theta) = \frac{B(q,\theta)}{F(q,\theta)}\,u'_{\mathrm{ref}}(t) + \frac{C(q,\theta)}{D(q,\theta)}\,e(t)\ . \tag{5.5}$$

Compared with the FIR model structure, the BJ model structure includes also the polynomial filters $C(q,\theta)$ and $D(q,\theta)$ and provides thus a description for the noise model H. Consequently, it allows to model a colored noise contribution $\dot{Q}'_s$. The BJ model structure identification was already applied successfully in the field of aeroacoustics [79]. Therein, the BJ model structure was deployed in an LES/SI approach to identify the scattering matrix and a respective aeroacoustic noise model of an orifice configuration with mean flow. Excellent agreement to experimental data was found. In the field of thermoacoustics, however, only an exploratory study on laminar flames was conducted yet [80]. Therein, stochastic combustion noise was mimicked by imposing an 'unknown' equivalence ratio fluctuation.

For completeness it is mentioned that also other model structures such as an Autoregressive model with eXogenous input (ARX) or an Output-Error (OE) model may be deduced from the general model structure shown in Eq. (5.2). Yet, only the FIR model and the BJ model are applied on LES data in the current thesis (PAPER-SM, PAPER-2WAY and PAPER-ROM). The behavior of the ARX model is explored on the basis of surrogate data in PAPER-SI FTF and PAPER-SI NOISE and is found to be inferior to the BJ model for the present application.

5.3 Model coefficient estimation

After a certain model structure is chosen, the polynomial model coefficients contained in θ need to be estimated. This is achieved by a solving a least-squares optimization problem of the form

$$\min_{\theta} J(\theta) \equiv \min_{\theta} \frac{1}{N} \sum_{i=0}^{N-1} \left(\dot{Q}'(i\Delta t,\theta) - \dot{\mathscr{Q}}'(i\Delta t)\right)^2 \tag{5.6}$$

herein, the cost function $J(\theta)$ is minimized by reducing the squared error between the *modeled* output $\dot{Q}'(i\Delta t,\theta)$ and the *actual* output $\dot{\mathscr{Q}}'(i\Delta t)$ of the time series used. The set of model coefficients that describes best the input-output behavior yields the lowest value of the cost function $J(\theta)$. Depending on the chosen model structure, the optimization problem may become non-linear. Also a regularization of the optimization problem may be applied, which reduces the variance of the estimated coefficients at

the cost of model flexibility. Yet, for details on both of these aspects the reader is referred to PAPER-SI NOISE.

It is emphasized at this point that the estimated models result from a mere 'black-box' approach: the identified model is *not* determined by analytical derivation from the underlying governing equations of the problem. Instead, its input-output transfer behavior is deduced solely from an error minimization between modeled and actual output. Hence, for the identification of the purely data-driven models no prior knowledge of the system itself is necessary. Even though data-driven models crucially require accurate input-output time series data, this property may also be regarded as an advantage. Compared to noise models that are based on a Strouhal number scaling [17, 18] or a temporal correlation analysis [81], data-driven models are more general: they do not rely on any physical modeling assumptions such as the definition of a characteristic flame length and are not limited to a certain flame shape or similar.

5.4 Surrogate data study

Before applying the SI techniques directly on actual LES data, a better understanding of their behavior and their applicability would be helpful. In particular for the BJ model identification and the corresponding combustion noise model estimation only limited experience is available. Therefore, two studies based on surrogate data were conducted in PAPER-SI FTF and PAPER-SI NOISE to investigate the behavior of different model structures in a thermoacoustic context. These two studies should be regarded as an intermediate step before applying the SI techniques on actual LES data and may be associated with the second step of the modeling strategy shown in Fig. 1.1.

The surrogate data in PAPER-SI FTF an PAPER-SI NOISE are generated by a model, which simulates a linear acoustic network in the time domain. Using surrogate data instead of actual LES data, exhibits two considerable advantages for the investigations conducted in PAPER-SI FTF and PAPER-SI NOISE. First, the generation of time series data is computationally very efficient and affordable. This allows to cover a wide range of varying time series properties (such as SNR or time series length) and to perform a Monte Carlo simulation. Second, the *true* plant model and the *true* noise model are known and can be used as reference models, since they are used to generate the surrogate data in the first place. Consequently, the error made by the re-identified models may be quantified accurately by comparing the re-identified models with the *true* solution. For a detailed discussion of the surrogate data approach and its limitations, the reader is referred to PAPER-SI FTF and PAPER-SI NOISE.

PAPER-SI FTF focuses on the identifiability of the FTF under the aspect of a closed-loop identification problem. Due to the flame inherent ITA feedback loop explained in Sec. 2.3, the thermoacoustic system is always a closed-loop, yielding a closed-loop identification problem. Taking this into consideration, PAPER-SI FTF compares the FTF models resulting from a BJ identification approach with the ones from a regularized and a standard FIR identification procedure. The study demonstrates that a FIR identification yields biased estimates for closed-loop systems even in the limit of infinitely long time series. Conversely, the BJ model structure yields superior estimates in case of a closed-loop problem, see Fig. 5.2. Yet, Fig. 5.2 also demonstrates that for short time series length no significant improvement is observable for the BJ identification approach. In this case the identification error originating from using a finite time series length dominates the bias introduced by the closed-loop identification.

Note that in PAPER-SI FTF advanced SI techniques are already used but no attention is paid to the identified noise model itself. Only the improvement of the FTF estimation is studied when taking into account a colored noise contribution. Conversely, PAPER-SI NOISE focuses on the identification accuracy of the noise model. Similarly to the outcome of PAPER-SI FTF it is demonstrated that the BJ identification is superior to simpler model structures when it comes to the noise model identification. Due to its gen-

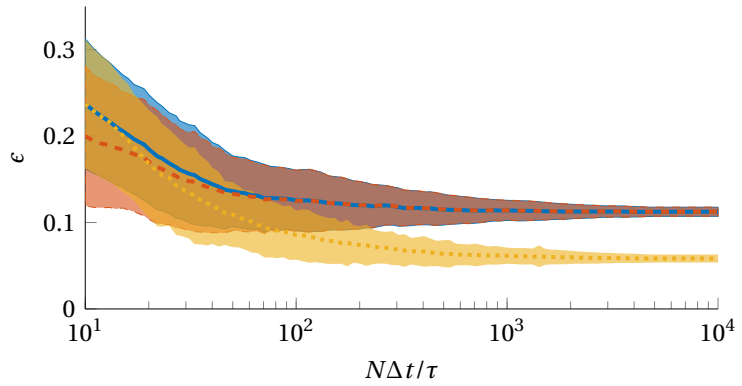

Figure 5.2: Identification error for the FTF depending on the time series data length. Different model structures are compared: FIR (——), regularized FIR (- - -) and BJ (·····). The BJ identification yields superior estimates for longer time series (reproduced from PAPER-SI FTF).

eral model structure, the BJ model identification also yields accurate estimates if the noise source is of simpler structure. This is an important finding. Whereas for the plant model part the choice of model structure and order is physically motivated (no auto-regression and the model order depends on the convective time delay [82]), the most suitable model structure and order of the noise model is not evident. Therefore, the general BJ model structure is preferable as it introduces no restrictions on the noise model structure.

In this context PAPER-SI NOISE demonstrates the combined use of Akaike Information Criterion [83] and a model residual analysis to estimate the most suitable model order. A representative result of a model residual analysis is shown in Fig. 5.3. If the identified model exhibits a significant auto-correlation within its residuals, the so-called 'Test of Whiteness' is failed. This means that there are predictable dynamics in the noise contribution, which are not yet resolved by the noise model. Accordingly, the noise model order needs to be increased. Similarly, if a significant cross-correlation between input and output signal is found, the deterministic part is under-resolved. The 'Independence Test' fails. In combination with Akaike Information Criterion, which judges the trade-off between model accuracy and model uncertainty, the residual analysis provides a purely data-driven indication of the most suitable model order.

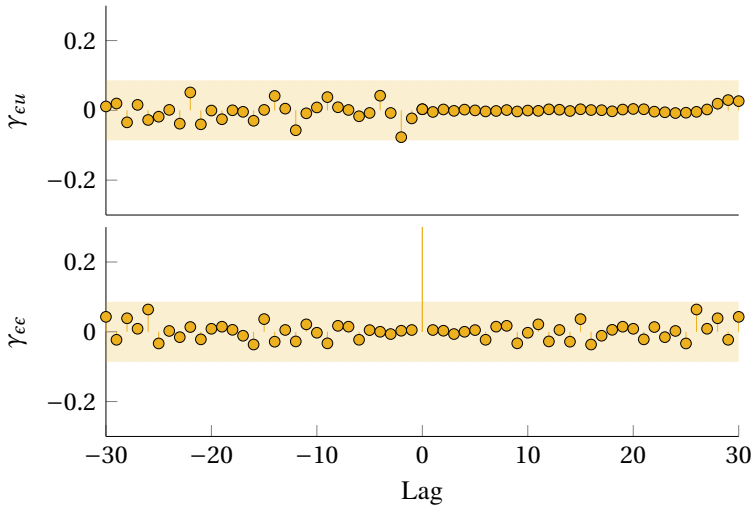

Figure 5.3: Residual analysis of an identified model that passes successfully the Test of Whiteness (bottom) and the Independence Test (top) (reproduced from PAPER-SI NOISE).

In summary, PAPER-SI FTF and PAPER-SI NOISE suggest that a BJ model structure is the most suitable one to apply for the simultaneously identification of flame response and combustion noise model of a turbulent flame.

5.5 Application on NoiseDyn LES data

After PAPER-SI FTF and PAPER-SI NOISE investigated the BJ model identification on the basis of surrogate data, it is applied now on *actual* broadband LES data of the NoiseDyn case, which are shown in Fig. 4.3. By choosing a BJ model order of $n_b = 30$, $n_c = 6$, $n_d = 6$ and $n_f = 1$, a plant model, i.e. an FTF, and a noise model are identified from the same broadband time series data.

Figure 5.4 shows the identified plant model part G as well as the experimentally measured FTF, which was determined via subsequent mono-frequent excitation at different frequencies. The gain of the identified FTF is in satisfactory agreement with the measured FTF. Phase values are in excellent agreement.

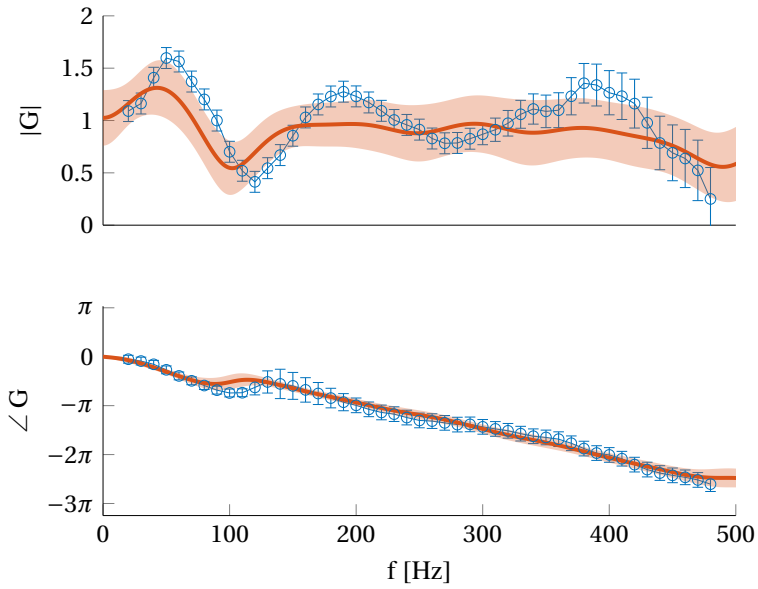

Figure 5.4: Measured FTF (○) with corresponding error bars (I) compared with the FTF (——) obtained from the LES/SI approach via BJ identification (Reproduced from PAPER-ROM).

Figure 5.5 depicts the identified noise model H. The amplitude of H has to be interpreted as normalized heat release rate fluctuations $\dot{Q}'_s$, meaning that at 200 Hz the noise source amplitude amounts to approximately 13 % of the mean heat release rate. In accordance with Strouhal number based noise models [17, 18, 81] the noise source amplitude increases towards a peak frequency and rolls off to higher frequencies.

Generally, the BJ identification could be applied to any signal including experimentally generated broadband time series data. The excitation with a broadband signal, however, is not available in the test-rig facility - a one-to-one validation of the identified model, as it is shown for the FTF, is not possible. Nonetheless, to validate the identified noise model to some extent, it is compared with the spectral distribution of heat release rate fluctuation extracted from an *unforced* LES with non-reflective boundary conditions. Although non-reflective boundary conditions are applied, it is emphasized that the spectrum

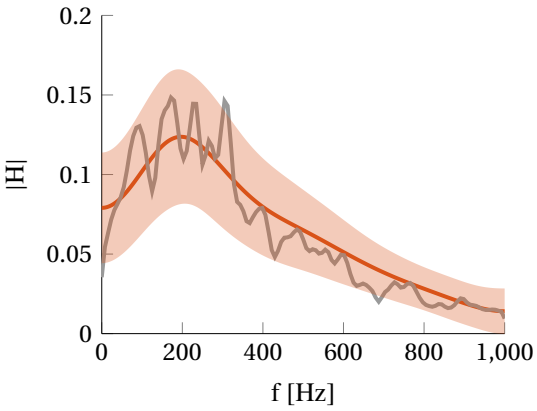

Figure 5.5: Noise model from LES/SI approach via BJ identification (——) compared with spectral distribution of heat release rate from an unforced LES with non-reflective boundary conditions (——).

extracted from LES cannot be considered as a pure source term $\dot{Q}'_s$. Instead, it comprises additionally feedback effects from the two-way coupling between flame and acoustics, see explanations given in Sec. 2.3. Since the two-way coupling is inherently resolved within the compressible LES, a separation is not readily possible between the source contribution and the contribution from coupling effects. Nevertheless, Fig. 5.5 shows that the spectrum of heat release rate fluctuations extracted from LES is in good agreement with the identified noise model H. This does not necessarily imply that the identified model is *physically* correct. If the LES data used for the identification would not describe the involved processes *physically* correct, an erroneous noise model would result. The level of agreement shown by results in Fig. 5.5, however, confirm at least that the identification procedure itself does not introduce significant deviations.

The data-driven identification of models for the flame dynamic response and the combustion noise source corresponds to the second step of the modeling strategy introduced in Fig. 1.1. The remaining step is now to incorporate the identified models into an acoustic low-order model description of the combustor in order to predict the combustor dynamics and the sound pressure level within the combustor.

6 Reduced Order Model Based Predictions

One possibility to study the thermoacoustic behavior of a combustion system is to regard the combustor as an assembly of acoustic elements, wherein each element relates the upstream and downstream acoustic field through simple algebraic relations. By connecting the individual elements, a linear acoustic network model can be composed, which provides an acoustic description of the combustor. If additionally a flame model is incorporated into the network model, a *reduced order model* results, providing a thermoacoustic description of the combustor.

Via a linear acoustic network model that contains an FTF model a thermoacoustic stability analysis may be conducted [84–91]. This yields frequencies, growth rates and mode shapes of the combustor eigenmodes. Taking additionally a model for the combustion noise source into account, the network model allows also to predict the sound pressure distribution reached at a given location within the combustor [35, 36, 92, 93], given that the model used is thermoacoustically stable. Quantitative sound pressure estimations for cases that undergo a thermoacoustic instability require a model formulation that takes non-linear flame behavior into account [29, 94]. Regarding the validity range of a network model and the interpretation of its results, the reader finds a detailed discussion in PAPER-2WAY.

The capabilities, namely the simple formulation and the straightforward incorporation of the identified models from LES/SI, make the acoustic network model approach the natural choice for the *'reduced order model predictions of combustor dynamics and noise'*. This is the third and final step of the modeling strategy shown in Fig. 1.1. Note that for the use of more complex acoustic descriptions, such as e.g. a Helmholtz solver or a solver using linearized flow equations, the incorporation of the identified models would not imply additional effort. The identical model formulation of plant model and noise model could be used and their coupling into the acoustic solver would be realized similarly to the network model approach. Yet, due to its flexibility and computational efficiency, a linear acoustic network model has the potential to predict the combustor dynamics and the sound pressure spectra within a combustor configuration across a large range of parameters. In addition, the model provides valuable insight into the interplay between flame dynamics, noise source and cavity acoustics within a confined combustor.

In the present thesis a reduced order model approach is used in PAPER-SM to reproduce the non-reactive and the reactive combustor scattering matrix of the NoiseDyn configuration. In PAPER-2WAY and PAPER-ROM the spectral sound pressure distributions within two different turbulent combustor test-rigs are predicted via a reduced order model.

The structure of this chapter is the following: Sec. 6.1 introduces the transfer and scattering matrix notations. These notations are essential for the formulation of the linear network model itself and are needed for a correct interpretation of the results shown in PAPER-SM. After Sec. 6.2 explains the network model used for the NoiseDyn test-rig, the sections 6.3 and 6.4 refer to the reduced model order predictions of combustor dynamics and sound pressure spectra, respectively.

6.1 Transfer and scattering matrix notation

Transfer matrix and scattering matrix are interchangeable notations for describing the acoustic relations across a single or an assembly of acoustic elements. The transfer matrix relates the acoustic field upstream and downstream of an element either in terms of the primitive acoustic variables u' and p'

$$\begin{bmatrix} \frac{p'_d}{\bar{\rho}\bar{c}} \\ u'_d \end{bmatrix} = \begin{bmatrix} T_{11} & T_{12} \\ T_{21} & T_{22} \end{bmatrix} \begin{bmatrix} \frac{p'_u}{\bar{\rho}\bar{c}} \\ u'_u \end{bmatrix} \tag{6.1}$$

or in terms of the characteristic waves f and g

$$\begin{bmatrix} f_d \\ g_d \end{bmatrix} = \begin{bmatrix} T_{11}^{fg} & T_{12}^{fg} \\ T_{21}^{fg} & T_{22}^{fg} \end{bmatrix} \begin{bmatrix} f_u \\ g_u \end{bmatrix} \tag{6.2}$$

The scattering matrix, in turn, relates the outgoing characteristic waves f_d and g_u to their incoming counterparts f_u and g_d

$$\begin{bmatrix} f_d \\ g_u \end{bmatrix} = \begin{bmatrix} S_{11} & S_{12} \\ S_{21} & S_{22} \end{bmatrix} \begin{bmatrix} f_u \\ g_d \end{bmatrix} = \begin{bmatrix} T_{ud} & R_{dd} \\ R_{uu} & T_{du} \end{bmatrix} \begin{bmatrix} f_u \\ g_d \end{bmatrix} \tag{6.3}$$

All three notations can be converted into one another by simple algebraic transformations. Each notation, however, exhibits certain advantages. On the one hand, the transfer matrix notation often allows a fluid dynamical interpretation of its individual coefficients. If a reactive combustor is described by a transfer matrix, the thermoacoustic interaction is mainly characterized by its T_{22} coefficient [42]. On the other hand, the scattering matrix notation makes possible a clear distinction between input and output signals. The characteristic waves f_u and g_d are considered as inputs signals, whereas f_d and g_u can be seen as the response of the system to the given input signals. Hence, the scattering matrix respects causality as it represents a causal relation between ingoing and outgoing signals. Accordingly, the coefficients S_{11} and S_{22} may be interpreted as transmission coefficients, whereas the coefficients S_{12} and S_{21} describe the reflection of ingoing characteristic waves, see Eq. (6.3).

From an LES/SI perspective the scattering matrix is suited better for identification. The respected causality of the scattering matrix notation implies that the current output signals depend only on *prior* inputs and outputs. For the identification a *causal* FIR model may be used, which convolutes the model coefficients with prior inputs only. This would not hold for a non-causal system such as the transfer matrix notation. For the transfer matrix a clear separation between input and response is not possible and the current output signal depends therefore on *future* inputs and outputs. Thus, non-causal SI techniques are necessary for the direct identification of the transfer matrix coefficients [95].

6.2 Reduced order model of NoiseDyn combustor

In this section the reduced order model of the NoiseDyn combustor is explained as it is used in the publications PAPER-SM and PAPER-ROM. Figure 6.1 shows a sketch of the model. In accordance with the experimental test-rig shown in Fig. 3.1 it can be divided into four main components: plenum, swirler + injection tube, combustion chamber and exhaust.

The network model is implemented in the open-source acoustic network tool taX [96]. Therein, network elements are characterized by transfer matrices that are formulated in terms of characteristic waves, see Eq. (6.2). This notation has the advantage that an assembly of multiple elements can be realized by simple concatenation of the individual elements, represented mathematically by a multiplication of the

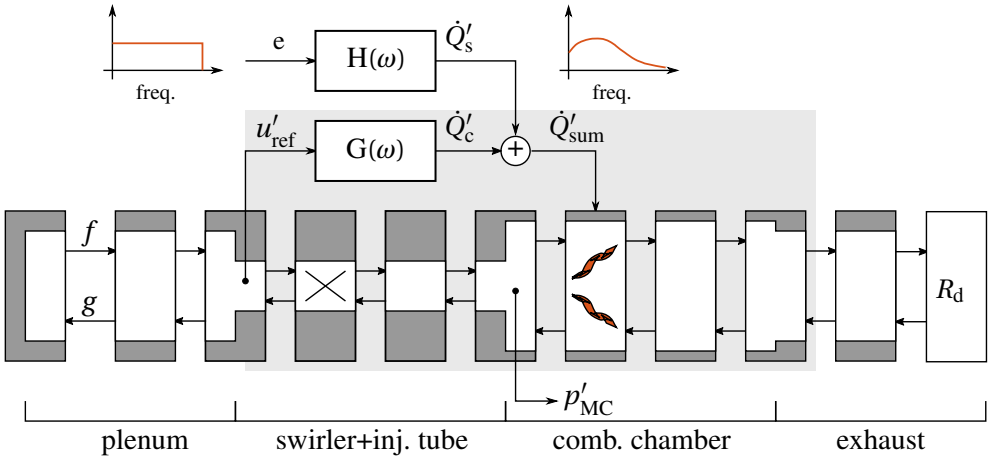

Figure 6.1: Reduced order model used for the NoiseDyn test-rig.

individual transfer matrices. Duct sections are modeled loss free and introduce only a time lag between ingoing and outgoing acoustic wave

$$\begin{bmatrix} f_d \\ g_d \end{bmatrix} = \begin{bmatrix} e^{-\mathrm{i}\omega l/\bar{c}} & 0 \\ 0 & e^{\mathrm{i}\omega l/\bar{c}} \end{bmatrix} \begin{bmatrix} f_u \\ g_u \end{bmatrix} \tag{6.4}$$

with ω, l and $\bar{c}$ denoting the angular frequency, the duct length and the mean speed of sound, respectively. To avoid uncertain modeling parameters, the formulation for an area jump does not include any loss coefficients or end corrections. It reads simply as

$$\begin{bmatrix} f_d \\ g_d \end{bmatrix} = \begin{bmatrix} 1 + A_u/A_d & 1 - A_u/A_d \\ 1 - A_u/A_d & 1 + A_u/A_d \end{bmatrix} \begin{bmatrix} f_u \\ g_u \end{bmatrix} \tag{6.5}$$

where A_u/A_d describes the area ratio from upstream to downstream. The complex radial swirler geometry shown in Fig. 3.2 and indicated by the cross in Fig. 6.1 is described only insufficiently by duct sections and area jumps. Therefore, its acoustic transfer behavior is determined separately via LES/SI. The according procedure is as follows: The flow in an LES domain, which comprises only the radial swirler geometry, is excited sequentially from upstream and downstream with an acoustic broadband signal. From the upstream forced data set the characteristic waves f_d and g_u are used as output signals for the identification of the coefficients S_{11} and S_{21}. The remaining two coefficients of the scattering matrix are estimated analogously from the downstream forced data set. As an additional cross-validation of the obtained swirler scattering matrix, the scattering matrix was also determined via a multiple-input multiple-output identification: a broadband excitation was applied simultaneously upstream and downstream and all 4 scattering matrix coefficients were identified from the resulting time series data set. The scattering matrices for both approaches were in excellent agreement. For the swirler scattering matrix identification a standard FIR model structure is applied since no feedback or colored noise contribution is expected in this non-reactive LES computation.

Figure 6.2 shows the identified scattering matrix. The swirler is not completely transparent for acoustic waves, but instead exhibits increasing acoustic reflection with increasing frequencies. Experimental data for the validation of the swirler scattering matrix are not available, however, the correctness of the identified swirler scattering matrix is corroborated by two different studies. First, PAPER-SM shows that the identified swirler scattering matrix improves the accuracy of the network model compared with a simplified modeling of the swirler. Second, the identified swirler scattering matrix is cross-validated in [97] against results obtained from linearized compressible flow equations. Therein, very good agreement is found.

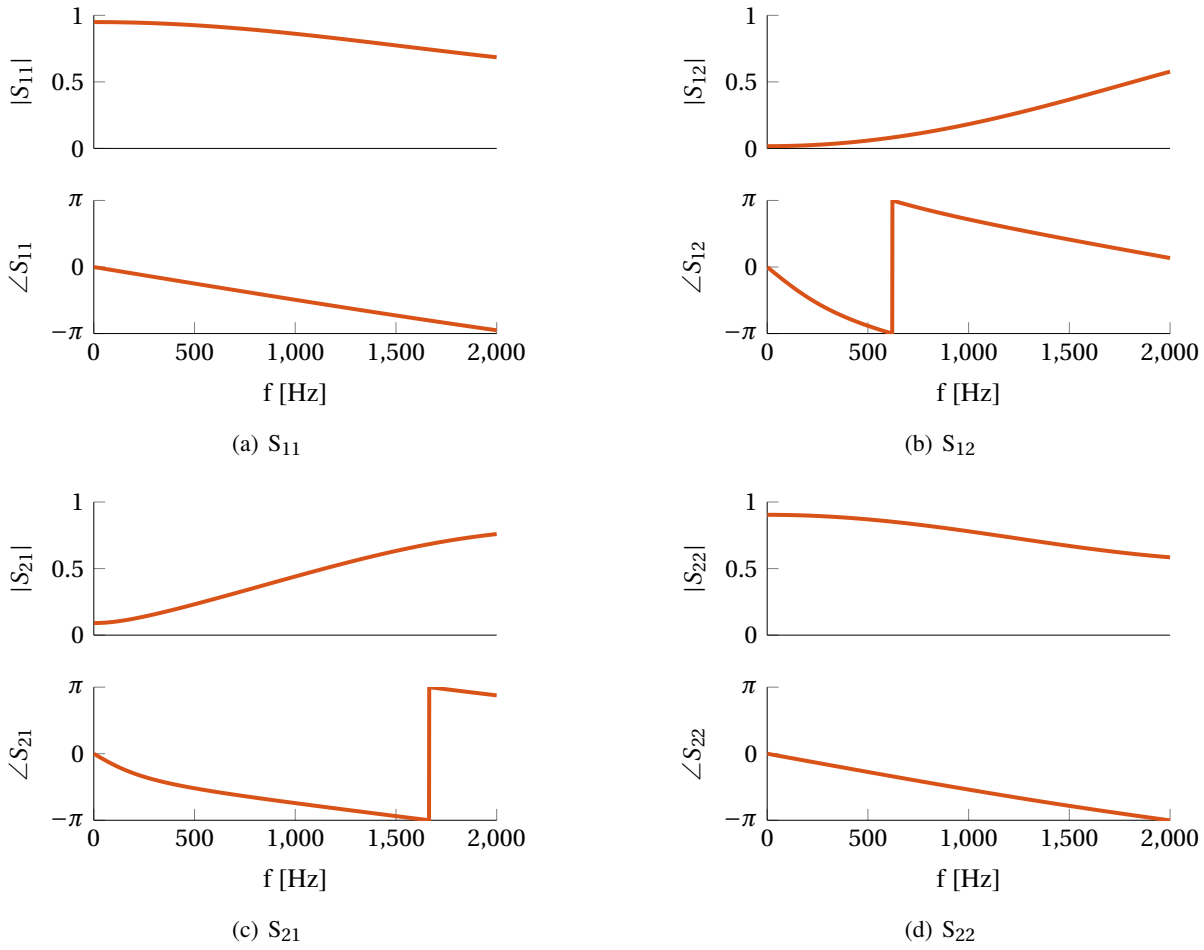

(a) S_{11} (b) S_{12}

(c) S_{21} (d) S_{22}

Figure 6.2: Acoustic scattering matrix of the radial NoiseDyn swirler identified via LES/SI (——).

At the downstream end of the network model shown in Fig. 6.1 the acoustic reflection is described by

$$\begin{bmatrix} f_d \\ g_d \end{bmatrix} = \begin{bmatrix} 0 & 0 \\ -R_\mathrm{d}(\omega) & 1 \end{bmatrix} \begin{bmatrix} f_u \\ g_u \end{bmatrix} \tag{6.6}$$

Depending on the outlet condition studied, open-ended or equipped with a perforated plate, the reflection coefficient $R_\mathrm{d}(\omega)$ is adapted. At the upstream end the combustor is assumed to be fully reflecting, yielding a constant reflection coefficient equal to unity.

By using the analytical formulations above, the *passive* acoustics are fully described within the combustor. A validation of the passive acoustics is included in PAPER-SM and PAPER-ROM. PAPER-SM compares successfully the measured and the predicted scattering matrix for the non-reactive combustor. This validates the transmission and reflection of acoustic waves within the network model. PAPER-ROM proves that the eigenfrequencies found in experiment for the non-reactive configuration are in accordance with the predicted ones from the network model, which validates additionally the acoustic cavity description of the network model.

For describing the reactive or *active* setup, the effect of the flame is taken into account in the linear network model via the heat release rate fluctuations $\dot{Q}'$, see Fig. 6.1. Thereby, the flame modeling strategy of two separate contributions $\dot{Q}'_s$ and $\dot{Q}'_c$ corresponds exactly to the modeling strategy described in Fig. 2.3 and to the model structure chosen in the identification procedure, see Fig. 5.1. Hence, for the plant model $G(\omega)$ and the noise model $H(\omega)$ the models identified in Sec. 5.5 are used directly.

The remaining step is to establish a link between the total heat release rate fluctuations $\dot{Q}'_{\text{sum}}$ and the thereof generated acoustic variables f and g. Fig. 2.3 denotes this step as *'acoustic conversion'* of heat release rate fluctuations into acoustic waves. The conversion is realized through the linearized Rankine-Hugoniot equations [86, 98], which describe the jump conditions across a thin reaction zone in the limit of low Mach numbers. Formulated in terms of primitive variables the Rankine-Hugoniot equations read as:

$$\begin{bmatrix} \frac{p'_d}{(\bar{\rho}\bar{c})}{}_d \\ u'_d \end{bmatrix} = \begin{bmatrix} \xi & 0 \\ 0 & 1 \end{bmatrix} \begin{bmatrix} \frac{p'_u}{(\bar{\rho}\bar{c})}{}_u \\ u'_u \end{bmatrix} + \begin{bmatrix} 0 \\ \Theta \bar{u}_u \end{bmatrix} \dot{Q}'_{\text{sum}} \tag{6.7}$$

herein, the indices 'u' and 'd' specify quantities upstream and downstream of the flame, respectively, $\xi = (\bar{\rho}\bar{c})_u)/(\bar{\rho}\bar{c})_d)$ describes the specific acoustic impedance and $\Theta = T_d/T_u - 1$ denotes the temperature jump across the flame. Equation (6.7) states that the acoustic pressure fluctuations across the compact reaction zone, i.e. the flame, remain constant and only the acoustic velocity fluctuations are modulated across the flame. Using the definitions of f and g, see Eq. (2.4), one may reformulate Eq. (6.7) as

$$\begin{bmatrix} f_d \\ g_d \end{bmatrix} = \frac{1}{2} \begin{bmatrix} \xi+1 & \xi-1 & \Theta\bar{u}_u \\ \xi-1 & \xi+1 & -\Theta\bar{u}_u \end{bmatrix} \begin{bmatrix} f_u \\ g_u \\ \dot{Q}'_{\text{sum}} \end{bmatrix} \tag{6.8}$$

Recalling Eq. (5.1) from the general SI model approach and assuming that $\dot{Q}'_{\text{sum}} = \dot{Q}'_c + \dot{Q}'_s$, one finds

$$\begin{bmatrix} f_d \\ g_d \end{bmatrix} = \frac{1}{2} \begin{bmatrix} \xi+1 & \xi-1 \\ \xi-1 & \xi+1 \end{bmatrix} \begin{bmatrix} f_u \\ g_u \end{bmatrix} + \Theta\bar{u}_u \left(G(\omega) u'_{\text{ref}} + H(\omega) e \right) \begin{bmatrix} 1 \\ -1 \end{bmatrix} \tag{6.9}$$

herein, u'_{ref} is already normalized with the mean reference velocity $\bar{u}_{\text{ref}}$, which can be related to $\bar{u}_u$ via the area ratio between reference position and upstream flame position

$$\bar{u}_{\text{ref}} = \bar{u}_u \frac{A_u}{A_{\text{ref}}} \tag{6.10}$$

With Eq. (6.9) this yields

$$\begin{aligned} \begin{bmatrix} f_d \\ g_d \end{bmatrix} = & \underbrace{\frac{1}{2} \begin{bmatrix} \xi+1 & \xi-1 \\ \xi-1 & \xi+1 \end{bmatrix} \begin{bmatrix} f_u \\ g_u \end{bmatrix}}_{\text{passive flame}} \\ & + \underbrace{\frac{1}{2} \frac{A_{\text{ref}}}{A_u} \Theta G(\omega) \begin{bmatrix} 1 & -1 \\ -1 & 1 \end{bmatrix} \begin{bmatrix} f_{\text{ref}} \\ g_{\text{ref}} \end{bmatrix}}_{\text{active flame}} \\ & + \underbrace{\frac{1}{2} \frac{A_{\text{ref}}}{A_u} \bar{u}_{ref} \Theta H(\omega)\ e \begin{bmatrix} 1 \\ -1 \end{bmatrix}}_{\text{noise source}} \end{aligned} \tag{6.11}$$

The three terms on the right-hand side of Eq. 6.11 should be interpreted as follows. The first term specifies scattering of acoustic waves by the change in impedance across the *passive flame* (steady heat release), i.e. the temperature discontinuity. The second term describes the *active flame* part (unsteady heat release) as the flame response resulting from acoustic perturbations at the reference position. The third term defines the contribution of the stochastic *noise source*.

Equation (6.11), however, is only valid and applicable if certain constraints are respected: 1) The reaction zone has to be compact with respect to the smallest wavelength considered. 2) The influence of pressure fluctuations on the flame must be negligible such that the flame reacts predominantly to upstream velocity perturbations. 3) Heat loss across the boundaries has to be negligible in the reaction zone. In the

NoiseDyn configuration all three constraints are respected. Acoustic compactness is usually assumed if the Helmholtz number is small, i.e. He $\ll 1$. For the working conditions explained in Sec. 3.2 the characteristic flame length amounts to about $l_f \approx 0.04$ m. In PAPER-ROM the network model is evaluated up to a maximum frequency of 1000 Hz. With the given flame length this corresponds to a Helmholtz number of He < 0.1. Next, the flame studied is perfectly premixed. For perfectly premixed flames velocity sensitivity is a valid assumption [32]. Regarding the heat loss across the reaction zone, the combustion chamber walls are made out of quartz glass walls without any active cooling applied. Accordingly, no significant heat loss is expected across the boundaries in the compact reaction zone.

The finally resulting reduced order model is a *linear* model, which is capable of predicting the linear stability limits and the sound pressure distribution for thermoacoustically stable configurations. Yet, the validity range of the reduced order model is restricted to the *linear* regime. An FTF is used in the model formulation that provides only a valid flame description in the limit of small perturbations and thus for linear flame behavior. This allows indeed to predict frequency and instability margin of linearly unstable eigenmodes (see PAPER-2WAY), but the estimation of the saturation amplitude for a limit cycle oscillation is not possible. The flame response saturation for increasing perturbation amplitudes and consequently the limit cycle amplitude is governed by non-linear effects, which are not accounted for in the FTF. A non-linear flame description would be necessary in this case for predictions of the oscillation amplitude [29, 94].

6.3 Prediction of combustor dynamics

The combustor scattering matrix is a valuable tool for characterizing the combustor dynamics as it allows to set up an acoustic energy balance, which in turns determines the amplification or damping across the scattering object [99]. In addition, possible feedback mechanisms may be revealed by an analysis of the combustor scattering matrix [100].

In PAPER-SM the scattering matrix from upstream of the swirler to downstream of the combustion chamber, indicated by the gray box in Fig. 6.1, is determined by three different approaches: 1) experimentally by applying an upstream forcing for two different acoustic loads, 2) numerically by identifying the scattering matrix directly via LES/SI from the corresponding input and output signals, 3) by using a reduced order model that contains only the parts within the gray box shown in Fig. 6.1. This means that in the third approach only the identified FTF, see Fig. 5.4, is taken into account, but not yet the noise source model and the acoustic boundaries.

The attractiveness of the third approach is twofold. One the one hand, it offers large flexibility at reduced computational cost. Modifications in the combustor geometry and their effects on the scattering matrix may easily be studied by adapting and re-evaluating the reduced order model in the frequency domain. In experiments or a standalone LES approach, this would imply considerable effort. On the other hand, PAPER-SM shows that the network model provides intuitive physical insight into the chain of mechanisms involved by including or excluding individual terms in the analysis. A possibility that is not readily available in experiments or a mere LES approach.

One objective of PAPER-SM is to investigate up to which extend the reduced order model yields satisfactory results for the combustor scattering matrix, compared to the other two approaches. The simplifications made in the network model such as 1-D acoustics, loss-free area contractions, geometry simplifications or constant mean temperature in the burnt gas region may introduce errors, however, their significance is unknown. Note that a one-to-one comparison between the three approaches is still missing in literature for a turbulent combustor scattering matrix. A successful comparison between these methods would validate among other things the Rankine-Hugoniot coupling applied in the reduced order model.

Figure 6.3 depicts exemplarily the results for the S_{11} coefficient of the combustor scattering matrix. Overall, good agreement is found between the three methods. Consequently, it is reasoned that the com-

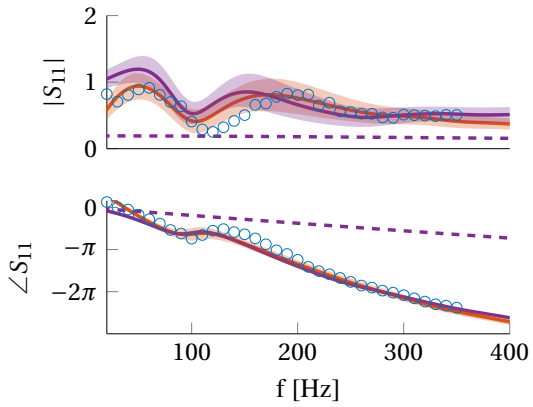

Figure 6.3: Gain and phase of S_{11} coefficient of reactive combustor scattering matrix. Experimental values (○) are in excellent agreement with results obtained from LES/SI (——) and the reduced order model approach (——). A strong modulation of the passive flame case (- - -) is found in the S_{11} coefficient (reproduced from PAPER-SM).

bustor dynamics are described satisfyingly by the reduced order model, the errors introduced due to simplifications made are only of minor significance. Only the S_{12} coefficient (not shown here) exhibits a noticeable discrepancy. Although the two independent numerical approaches yield agreeing results, a deviation from measured values is observed. For a detailed discussion on this aspect the reader is referred to PAPER-SM. In addition to the active scattering matrix in PAPER-SM the combustor scattering matrix is evaluated for a passive flame, see (- - -) in Fig. 6.3. In the passive flame case the temperature jump across the flame is taken into account but *not* the flame response. Thus, in Eq. 6.11 not only the source term is set to zero, but also the second term on the right-hand side. Note that such a study is possible only with the reduced order model at hand. The comparison between active and passive flame case highlights the influence of the flame response. It is found that the impact of the active flame manifests itself mainly in the S_{11} coefficient of the scattering matrix. In PAPER-SM an intuitive explanation of this behavior is given based on the travel path of the acoustic waves.

To summarize PAPER-SM, the validation of the reduced order model puts the subsequent prediction of sound pressure spectra on a solid basis. It justifies the use of the Rankine-Hugoniot equations for the '*acoustic conversion*' from heat release rate fluctuations to acoustic fluctuations, see Fig. 2.3.

6.4 Prediction of sound pressure distribution

The last section in this chapter deals with the prediction of the sound pressure level within a confined combustor. Together with the results of the preceding section this covers the last step of the modeling strategy shown in Fig. 1.1. For the sound pressure prediction the full model shown in Fig. 6.1 is retained, including the noise model part H and the acoustic boundaries. In case of thermoacoustically stable configurations this allows quantitative estimates of the sound pressure distribution within the combustor.

For sound pressure predictions the reduced order model represents an immensely flexible approach. The effect of changes in the boundary impedance or in the confinement geometry that do not have an impact on the flame characteristic may be investigated by simply adapting the respective network model element. Even if the flame characteristics are varied, i.e. the combustor operating point changes, only a

single additional LES run is necessary to re-identify the FTF and the corresponding noise model.

By using a reduced order model, PAPER-2WAY investigates the implications of one-way coupling and two-way coupling on the resulting sound pressure distribution. Compared to the subsequently discussed investigations in PAPER-ROM, two important aspects need to be clarified. First, the test-rig studied in PAPER-2WAY is *not* the NoiseDyn combustor, but instead a turbulent swirl combustor located at the Technische Universität München [37]. Thus, a different network model as well as different models for the FTF and the noise source are used. Second, in PAPER-2WAY a standard FIR identification is applied for the estimation of the FTF. As the FIR model structure does not include any estimation of the noise contribution *during* the identification step, see Eq. (5.4), a rough estimation of the noise contribution is achieved by an additional post-processing step, which is preformed *after* the FTF identification. PAPER-SI NOISE demonstrates, however, that this procedure yields inferior estimates of the noise contribution since any bias in the FTF model propagates directly into the noise source estimation. Yet, PAPER-2WAY focuses mainly on the implications of ITA feedback on the sound pressure distribution within the combustor. Therefore, a simplified estimation of the noise source is enough to meet the requirements for that study.

Incorporation of the FTF into the linear network model resolves inherently the two-way coupling between flame and acoustic field. Other than in experiments or a mere LES approach, the network model allows also to retain a one-way coupling situation by neglecting the response of the flame to upstream velocity perturbations, i.e. by neglecting the FTF. Consequently, the second term on the right-hand side of Eq. (6.11) vanishes. A setup as shown schematically in Fig. 2.1 results. An isolated acoustic source is placed in a resonant cavity. PAPER-2WAY demonstrates that the sound pressure distribution in a confined combustor is only predicted correctly if the prediction method accounts for the two-way coupling between flame and acoustic field within the combustor. Placing solely a noise source in a resonant cavity yields reasonable results, but it may not be enough to capture the full characteristics of the resulting spectral sound pressure distribution. Hence, for reduced order model based predictions of sound pressure the consideration of the flame response is mandatory - an aspect not always recognized.

In PAPER-ROM it is the first time that the BJ identification is applied on actual LES time series data of a turbulent swirl combustor. The FTF and the noise model shown in Fig. 5.4 and Fig. (5.5) are identified simultaneously from the *same* broadband LES time series. By using the identified models consequently in the reduced order model shown in Fig. 6.1, sound pressure spectra in the NoiseDyn combustor are predicted for two different outlet boundary conditions. Results are compared with measurements at the microphone location MC. Note that a proper and extensive comparison to experimental results is only possible because the flame dynamics (i.e. the FTF), the spectral distribution of sound pressure and the acoustic boundary conditions are quantified accurately in experiments.

Figure 6.4 exhibits an excellent quantitative agreement between measured and predicted values of the sound pressure for the open-ended combustor configuration. An evaluation of the combustor eigenmodes via the network model shows that the moderate peak observable in Fig. 6.4 results from a resonant $3/4\ \lambda$ mode, which is predominantly active in the combustion chamber. In PAPER-ROM pressure spectra for the configuration equipped with the perforated plate are also compared successfully (not shown here). The result for the configuration with perforated plate is therein achieved by a simple re-evaluation of the linear network model with the *same* FTF and the *same* noise model. Only R_d is adapted according to the measured values of the reflection coefficient of the perforated plate.

So having a validated network model at hand, the influence on the resulting sound pressure spectrum of modifications in combustor geometry or reflection conditions may be studied across a large range of parameters at reasonable computational costs. This would allow to optimize the combustor in terms of sound pressure levels reached already in the design stage of a device.

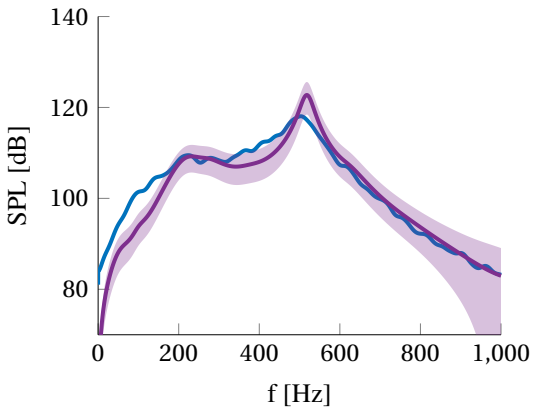

Figure 6.4: Measured sound pressure distribution (——) and corresponding reduced order model prediction (——) for the open-ended NoiseDyn combustor (reproduced from PAPER-ROM).

7 Summary and Discussion of Papers

This chapter serves as a summary to highlight compactly the interconnection between the major publications discussed in the current thesis. Figure 7.1 is an extension of the initially depicted modeling strategy shown in Fig. 1.1. It illustrates how each individual publication contributes to the overall framework developed.

In PAPER-LES the capability of the compressible LES setup is ascertained to reproduce qualitatively and quantitatively measured sound pressure distributions for stable as well as unstable working conditions. From today's standpoint this has not yet been achieved with the same level of quantitative agreement and may therefore be considered as a novelty. Conversely, the overall good agreement corroborates that the flame dynamics as well as the generation of combustion noise are well described within the LES. This is a prerequisite for the subsequent application of SI techniques. If the SI routines are fed with erroneous input-output data from LES, incorrect data-driven models would result. Consequently, the validated LES setup from PAPER-LES is used for the generation of input-output time series data, which constitutes the first step in Fig. 7.1. This step builds the basis for the simultaneous identification of flame dynamics and combustion noise source for the NoiseDyn combustor via the LES/SI approach.

Based on surrogate data PAPER-SI FTF and PAPER-SI NOISE evaluate and investigate in detail advanced SI techniques. These studies provide a theoretical framework and represent an exploratory study before the application of advanced SI techniques on actual LES data. Therein, the BJ model investigated may be seen as an extension of the established FIR identification, which does not provide any estimation of a combustion noise model. The BJ model yields not only unbiased estimates of the FTF under closed-loop conditions, but also allows from one set of time series data the simultaneous identification of models for the flame dynamic response *and* the combustion noise source. This extends considerably the scope of applications of the established LES/SI approach. The exploratory studies in PAPER-SI FTF and PAPER-SI NOISE provide a detailed understanding of the advanced SI methods used and demonstrate that the BJ model structure is superior compared with simpler model structures. It is thus deemed to be the most suitable model structure to be applied on input-output time series, which are generated in the preceding step via compressible LES. Data-driven models for the flame response and the noise source result that are associated with the second step shown in Fig. 7.1.

The identified models of flame response and noise source are consequently incorporated into a linear acoustic network model. A reduced order model is obtained that allows the prediction of combustor dynamics and noise. In a first step, PAPER-SM couples only the flame response model into the linear acoustic network model of the NoiseDyn combustor. Thereof, the scattering matrix of the combustor is deduced for non-reactive and reactive conditions. The successful one-to-one comparison of the predicted combustor dynamics against the results from LES/SI and experiment proves the applicability of the Rankine-Hugoniot equations and validates the acoustic network model description. Accordingly, PAPER-SM may be seen as an intermediate step before coupling additionally the combustion noise source into the acoustic network model via the Rankine-Hugoniot equations, as it is done in PAPER-2WAY and PAPER-ROM

Therein, reduced order predictions are made for the sound pressure distribution within confined combustors. PAPER-2WAY investigates the effect of two-way coupling and in particular of ITA feedback on the

resulting sound pressure spectrum. The comparison of the computed spectra against measurement data demonstrates that the sound pressure spectrum is correctly reproduced only if the full two-way coupling approach is retained, i.e. not only the noise model but also the FTF is coupled into the linear acoustic network model. In PAPER-ROM the BJ identification is applied for the first time to actual LES data in order to identify simultaneously the FTF and a noise model. Spectral sound pressure distributions are predicted for two different combustor cavities and satisfactory agreement with experimental data is found for both configurations. A validation with measurement data is merely possible since an accurate and complete experimental characterization of the test-rig is available in terms of flame response, pressure spectra and acoustic boundary reflections. PAPER-SM, PAPER-2WAY and PAPER-ROM synthesize the findings and outcome of the preceding three publications to predict the combustor dynamics and noise via a reduced order model. This covers the last step shown in Fig. 7.1.

By having a validated reduced order model at hand, an intuitive physical interpretation of the resulting sound spectra is possible. Moreover, the sound pressure spectra for a variety of combustor configurations would be possible to predict with reasonable computational effort. In turn, this allows the optimization of the combustor geometry in terms of reducing the combustion noise level already in the design phase of a device.

In summary, the present thesis covers the whole procedure explained in Fig. 7.1: from broadband data generation via compressible LES over to the concurrent identification of models for flame response and noise source to the point of combining the identified models with a linear network model. Thus, a closed framework is developed, presented and validated in the current thesis that allows to determine combustion noise and combustion dynamics of a confined turbulent combustor.

The main outcome of the present work was published in several papers. In the following sections only the publications that contributed essentially to the present thesis are summarized with respect to their main findings and their relevance for the thesis. Moreover, the contribution of the present author to the individual publications is clearly addressed. The respective papers are fully reproduced in the appendix.

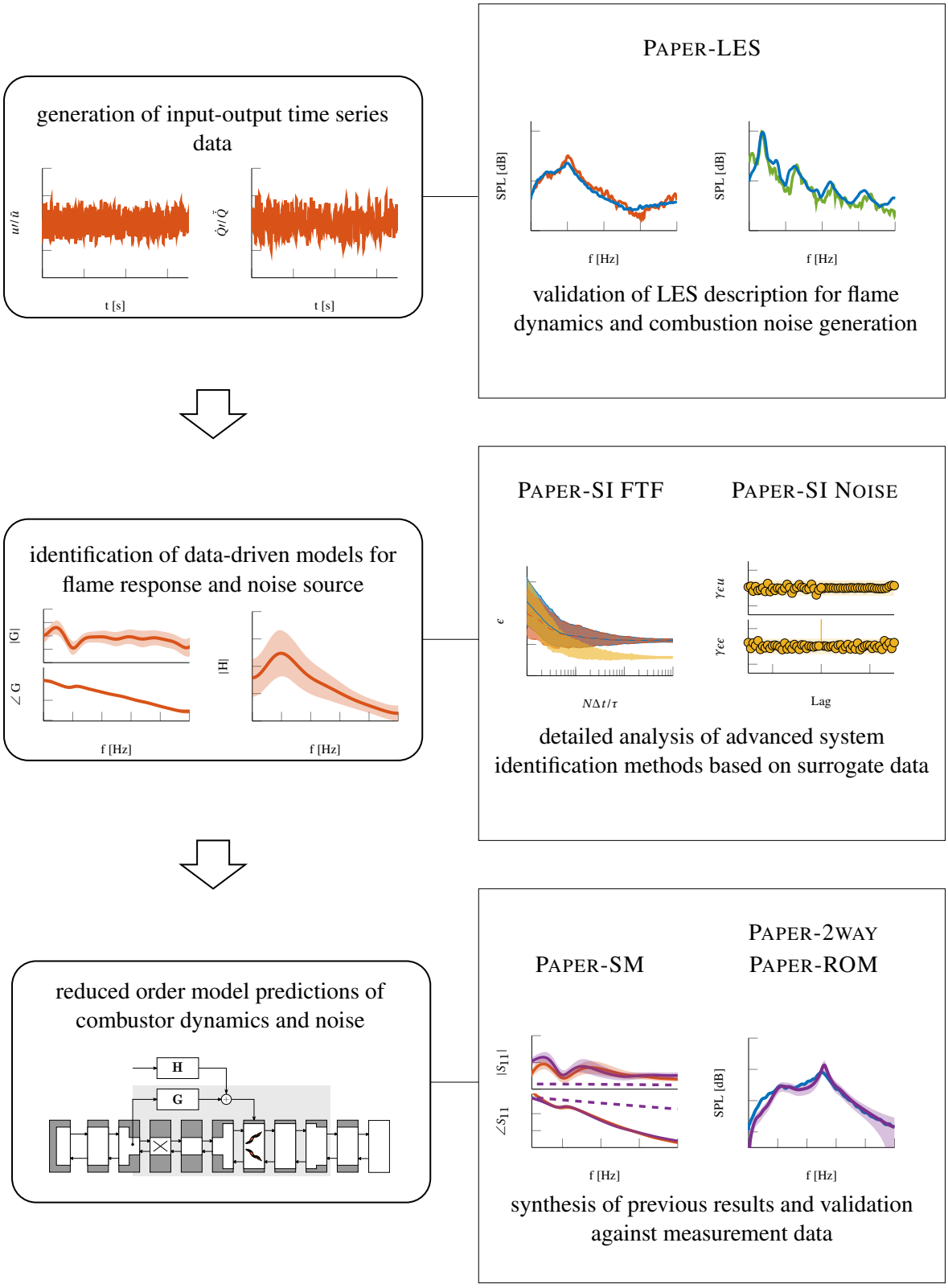

Figure 7.1: Summary on how the respective publications contributed to the current thesis.

7.1 Measurement and Simulation of Combustion Noise and Dynamics of a Confined Swirl Flame

Label: PAPER-LES

Outcome: The compressible LES of turbulent reactive flow is capable of reproducing qualitatively and quantitatively the sound pressure distribution within a confined turbulent swirl combustor. The excellent agreement of sound pressure spectra from LES and experiment, for both stable and unstable working conditions, was not achieved previously and may be considered as a novelty. The agreeing results prove that not only the generation of combustion noise, but also the flame response and the two-way interaction between flame and acoustics are accurately described within the LES.

Relevance for the thesis: In this publication the basis is provided for the following publications. An accurate LES description of flame response and noise generation is prerequisite for the generation of broadband time series data via LES used for the subsequent identification of FTF and noise model.

Contribution: The research objective was formulated jointly by the Thermo-Fluid Dynamics group at TUM and the laboratoire EM2C, Paris. The structure and scope of the work was defined by the present author. The LES and the post-processing of the computational raw data were conducted by the present author. Experimental measurements were carried out by R. Gaudron, M. Gatti and C. Mirat at EM2C, Université Paris-Saclay. Except of the experimental description, the manuscript was composed and written by the lead author. T. Schuller and W. Polifke contributed critical revision. The rebuttal to the comments / remarks of the reviewers and their implementation into the manuscript were taken care of by the present author.

Status: Published in *AIAA Journal*.

Review process: Peer-reviewed.

Reference: M. Merk, R. Gaudron, M. Gatti, C. Mirat, T. Schuller, and W. Polifke. Measurement and Simulation of Combustion Noise and Dynamics of a Confined Swirl Flame. *AIAA Journal*, 56(5):1930–1942, 2018. doi:10.2514/1.J056502, reproduced on p. 67ff.

Comment: A first version of this publication was published in the proceedings of the *53rd AIAA/SAE/ASEE Joint Propulsion Conference, AIAA Propulsion and Energy Forum* [102].

7.2 Identification of flame transfer functions in the presence of intrinsic thermoacoustic feedback and noise

Label: PAPER-SI FTF

Outcome: Due to ITA feedback, the identification of the FTF from a compressible LES is always a closed-loop problem. The conducted surrogate data study shows that in this case the widely used FIR model yields biased estimates for the FTF, even in the limit of infinitely long time series data. This bias can be avoided by using advanced SI techniques such as the BJ model identification. Moreover, it is demonstrated that non-reflective boundary conditions are not essentially necessary for an accurate identification of the FTF, which extends the applicability of the LES/SI approach.

Relevance for the thesis: The BJ identification is introduced into the thermoacoustic framework and its potential of identifying an unbiased FTF under closed-loop conditions is highlighted. This publication, however, focuses only on the identification of the FTF. The added value of identifying additionally a noise model from the same time series data is not yet discussed in detail.

Contribution: The research objective was identified by S. Jaensch. The present author contributed significantly to the study execution as well as to the acquisition and post-processing of data. T. Emmert was mainly responsible for the 1-D acoustic network tool that was used for the surrogate data model formulation. Supplementary analysis of the data and critical revision was provided by W. Polifke. A first draft of the manuscript was prepared by S. Jaensch, which was revised, improved and extended by the present author before the first submission. The rebuttal (major revision) as well as the revision of the manuscript were handled by the present author.

Status: Published in *Combustion Theory and Modelling*.

Review process: Peer-reviewed.

Reference: S. Jaensch, M. Merk, T. Emmert, and W. Polifke. Identification of flame transfer functions in the presence of intrinsic thermoacoustic feedback and noise. *Combustion Theory and Modelling*, 22 (3):613–634, 2018. doi:10.1080/13647830.2018.1443517, reproduced on p. 81ff.

7.3 Simultaneous Identification of Transfer Functions and Combustion Noise of a Turbulent Flame

Label: PAPER-SI NOISE

Outcome: Advanced SI methods are used for the simultaneous identification of an FTF and a combustion noise model. Based on surrogate data the performance of SI methods in regard to the noise model identification is tested systematically for different time series properties. It is demonstrated that the BJ model structure is superior to the widely used FIR model as it allows an accurate and unbiased identification of the combustion noise source, even if the reference noise model is of simpler structure. Moreover, it is shown how the combined use of Akaike Information Criterion and a model residual analysis allows an estimation of the most suitable model order of FTF and noise model. The additional identification of a noise source model extends considerably the scope of applications of the LES/SI approach in the field of thermoacoustics.

Relevance for the thesis: This work exploits the capability of advanced SI methods to identify not only the FTF but also a model for the combustion noise source from the same time series data. As limited experience is available for the noise model identification, methods are investigated that provide data-driven estimates of the most suitable model order. Together with PAPER-SI FTF this work builds a solid theoretical basis for the application of advanced SI techniques on actual broadband LES data of a turbulent combustor.

Contribution: The research objective was formulated by W. Polifke and C. Silva in the NoiseDyn project proposal. The study concept and the scope of the paper were defined by the present author, who is also responsible for the acquisition, analysis and interpretation of the data. S. Jaensch, C. Silva and W. Polifke contributed critical revision and significant suggestions for study improvements. The present author composed and wrote the manuscript, took care of the rebuttal and implemented the changes requested by the reviewers.

Status: Published in *Journal of Sound and Vibration*.

Review process: Peer-reviewed.

Reference: M. Merk, S. Jaensch, C. Silva, and W. Polifke. Simultaneous identification of transfer functions and combustion noise of a turbulent flame. *Journal of Sound and Vibration*, 422:432–452, 2018. doi:10.1016/j.jsv.2018.02.040, reproduced on p. 103ff.

7.4 Direct Assessment of the Acoustic Scattering Matrix of a Turbulent Swirl Combustor by Combining System Identification, Large Eddy Simulation and Analytical Approaches

Label: PAPER-SM

Outcome: It is shown for the first time that the scattering matrix of a turbulent combustor under reactive conditions may be derived directly via an LES/SI approach. As long as the constraints of the Rankine-Hugoniot jump equations are respected, the scattering matrix may also be derived from a flexible and computationally more efficient reduced order model, which is composed from a coupling between FTF and passive acoustic network model.

Relevance for the thesis: The satisfying agreement between the composed approach and the direct LES/SI approach validates the acoustic network model and the use of the Rankine-Hugoniot jump equations in the current setup. In turn, this is of importance for the publications PAPER-2WAY and PAPER-ROM. Therein, the combustion noise model used is formulated in terms of stochastic heat release rate fluctuations, which are coupled into the linear network model via the Rankine-Hugoniot jump equations.

Contribution: The research objective was formulated jointly by the Thermo-Fluid Dynamics group at TUM and the laboratoire EM2C, Paris. The study concept and the scope of the work were defined by the author. The results for the direct LES/SI approach and the composed approach were generated by the present author. The corresponding measurements and the post-processing of experimental data were conducted by R. Gaudron, M. Gatti and C. Mirat at EM2C, Université Paris-Saclay. C. Silva contributed to the analysis and interpretation of the data. Most of the manuscript and the rebuttal were written by the lead author. W. Polifke and T. Schuller contributed by revising critically the results and the manuscript.

Status: Published in *Journal of Engineering for Gas Turbines and Power*.

Review process: Peer-reviewed.

Reference: M. Merk, R. Gaudron, C. Silva, M. Gatti, C. Mirat, T. Schuller, and W. Polifke. Direct Assessment of the Acoustic Scattering Matrix of a Turbulent Swirl Combustor by Combining System Identification, Large Eddy Simulation and Analytical Approaches. *Journal of Engineering for Gas Turbines and Power*, 2018. doi:10.1115/1.4040731, reproduced on p. 125ff.

Comment: A first version of this publication was published in the proceedings of the *ASME Turbo Expo 2018: Turbomachinery Technical Conference & Exposition* [106].

7.5 The contribution of intrinsic thermoacoustic feedback to combustion noise and resonances of a confined turbulent premixed flame

Label: PAPER-2WAY

Outcome: The sound pressure distribution in a confined turbulent combustor is predicted via a linear acoustic network model that includes a combustion noise model. Overall good agreement to experimental measurements is achieved. Peaks in the sound pressure spectrum are found that are not related to any acoustic cavity modes. A thorough network model analysis shows that these peaks can only be reproduced if the full two-way coupling between flame and acoustics is taken into account in the network model formulation. This is ensured by incorporating not only a noise source into the linear network model but also the FTF. Consequently, this publication highlights the importance of retaining the full two-way coupling for sound pressure predictions.

Relevance for the thesis: The need of retaining the full two-way coupling requires models for both the combustion noise source as well as for the flame response, i.e. the FTF. With regard to the SI procedure this outcome stresses the necessity of an identification procedure that provides both of these models. As shown in PAPER-SI FTF and PAPER-SI NOISE, the BJ model identification is capable of providing these models. Note that in PAPER-2WAY the FTF is estimated via an FIR and the noise model is only a simplistic estimation that stems from an additional post-processing step.

Contribution: C. Silva and W. Polifke were responsible for the study concept and design. The present author contributed significantly to the study execution by conducting the linear network model analysis, generating the data and drafting the results shown in the publication. T. Komarek provided the experimental data. C. Silva wrote most of the manuscript, whereas the present author only wrote a small part. Interpretation of the results as well as critical revision was contributed by the present author and W. Polifke.

Status: Published in *Combustion and Flame*.

Review process: Peer-reviewed.

Reference: C. F. Silva, M. Merk, T. Komarek, and W. Polifke. The Contribution of Intrinsic Thermoacoustic Feedback to Combustion Noise and Resonances of a Confined Turbulent Premixed Flame. *Combustion and Flame*, 182:269–278, 2017. doi:10.1016/j.combustflame.2017.04.015, reproduced on p. 135ff.

Comment: A first version of this publication was published in the proceedings of the *International Symposium: Thermoacoustic Instabilities in Gas Turbines and Rocket Engines* [107].

7.6 Prediction of Combustion Noise of an Enclosed Flame by Simultaneous Identification of Noise Source and Flame Dynamics

Label: PAPER-ROM

Outcome: In this publication a BJ model identification is applied for the first time on actual LES broadband data of a turbulent combustor. Thereby, not only the FTF but also a combustion noise source model is identified from a single LES time series. By incorporating both models into a linear acoustic network model via the Rankine-Hugoniot jump equations, the sound pressure spectrum of a confined turbulent swirl combustor is predicted. Excellent agreement to experimental sound pressure spectra is found for two different combustor configurations. Thereby, the use of the linear acoustic network model allows an intuitive physical interpretation of the resulting sound pressure spectra in terms of resonating cavity acoustics and flame-acoustic interaction.

Relevance for the thesis: In this work the outcome and findings of the preceding studies are synthesized. The LES setup of PAPER-LES is used for generating a broadband time series. By using the BJ identification technique, which is investigated on the basis of surrogate data in PAPER-SI FTF and PAPER-SI NOISE, an FTF and a combustion noise model are identified from the same broadband time series. These models are incorporated into a linear network model via the Rankine-Hugoniot jump equations, whose validity for the setup used is demonstrated in PAPER-SM.

Contribution: The research objective and question was raised by W. Polifke and T. Schuller in the NoiseDyn project proposal. The scope of the work and the study design were defined by the present author. The generation of broadband LES data, the subsequent SI and the linear acoustic network analysis were also conducted by the present author. Measurement data shown in this work were provided by R. Gaudron, M. Gatti and C. Mirat from EM2C, Université Paris-Saclay. C. Silva assisted in the analysis and interpretation of the data, whereas critical revision and further suggestions were contributed by T. Schuller and W. Polifke. The manuscript was drafted by the present author as well as the revised version of the manuscript.

Status: Published in *Proceedings of the Combustion Institute, 37*.

Review process: Peer-reviewed.

Reference: M. Merk, R. Gaudron, C. Silva, M. Gatti, C. Mirat, T. Schuller, and W. Polifke. Prediction of Combustion Noise of an Enclosed Flame by Simultaneous Identification of Noise Source and Flame Dynamics. *Proceedings of the Combustion Institute*, 37, 2018. doi:10.1016/j.proci.2018.05.124, reproduced on p.145ff.

8 Conclusion and Outlook

In this final chapter a few concluding remarks on the thesis are given followed by an outlook on a potential continuative research project.

8.1 Conclusion

The overall motivation of the current work was to gain a better and deeper understanding of the thermoacoustic processes responsible for the combustion generated sound in a confined turbulent swirl combustor. The thereof resulting objective was then to formulate a reduced order model that allows the prediction of combustor dynamics and combustion noise in a confined setup. Key elements for this purpose are accurate models for the generation of combustion noise and for the flame dynamics, i.e. the flame response to acoustic perturbations. To deduce these models a compressible LES was combined with advanced SI techniques, which can be seen as an extension of the established and widely used LES/SI approach [9, 47, 68–78]. The identified models were consequently incorporated into a linear acoustic network model yielding a closed reduced order formulation, which allowed predictions on the combustor dynamics and the noise level within a confined combustor setup. Results of the reduced order model and its individual parts were compared extensively with experimental measurement data.

By means of the obtained reduced order model it is demonstrated that the sound pressure spectrum within a confined combustor configuration is shaped by the spectral distribution of the noise source *and* resonances. Thereby, the resonance might arise either from acoustic eigenmodes of the confining cavity or from an excitation of the intrinsic thermoacoustic feedback loop [30–32]. To capture the latter resonance effect, it is proven that the consideration of the flame dynamic response in the reduced order model is a prerequisite to recover the two-way coupling [35] between flame and acoustic field.

Indeed, one may find in literature more thorough analysis of the flame dynamics of swirling flames [37, 66, 70, 71, 108, 109], but with a fairly rough treatment of the acoustics at the system boundaries and more often without any analysis of the sound pressure spectrum within the confined system. Conversely, one may also find a detailed analysis of the combustion noise source [14, 17, 18, 22, 81, 110, 111] and the acoustic field within the system [56, 92, 112, 113], but with only limited comparisons of the associated flow and flame dynamics. Therefore, it is believed that the current work is among the first, where all of these aspects were taken into account with the same concern of analysis.

8.2 Outlook

The current thesis investigates only *perfectly* premixed flames. Consequently, two mechanisms of combustion noise generation may be neglected. First, no contribution from upstream equivalence ratio fluctuations to the generation of direct combustion noise has to be expected [114, 115]. Second, indirect combustion noise does not play any role in the studied setups since perfectly premixed flames do not generate any entropy fluctuations across flame [13]. This does not hold for *technically* premixed flames, where equivalence ratio fluctuations upstream of the flame cause both a contribution to the direct noise

generation as well as entropy fluctuations in the downstream burnt gas region [12, 116]. Even though it is unclear how strong the contribution of equivalence ratio fluctuations is on the generation of direct combustion noise, it is recognized that the generation of indirect combustion noise through the acceleration of entropy inhomogeneities at the outlet may be significant [7]. A potential continuation research project may aim for an extension of the herein developed methods for technically premixed flames to include additionally the effect of upstream equivalence ratio fluctuations.

Whereas the additional contribution to the generation of direct combustion noise through upstream equivalence ratio fluctuations would be inherently resolved within a compressible LES, the consideration of indirect combustion requires further work. In the CBSBC formulation [55] used in PAPER-LES, the outgoing entropy waves ($\mathscr{L}_2$ in LODI formulation [58]) are already extracted from the LES. Hence, these entropy waves may be considered as an additional input of the state-space boundary model. By adding a relation in the state-space model that provides a link between ingoing entropy waves and generated acoustic waves across a chocked outlet [6], the output of the boundary state-space model could be reformulated as a superposition of the reflected acoustic wave and the acoustic wave originating from indirect combustion noise. Similarly to the study in PAPER-LES, this would allow a direct assessment of the resulting sound pressure spectrum of a technically premixed combustor. Compared for example to the works [113, 117], the contribution of indirect noise could be taken into account without resolving in LES the computationally demanding chocked outflow.

After having assured that the LES correctly describes the generation of direct combustion noise and entropy waves, the LES setup could be used again for the generation of input-output time series data. From the resulting broadband data set a Multiple-Input Multiple-Output (MIMO) transfer function could be identified. Upstream velocity fluctuations u'_{ref} and upstream equivalence ratio fluctuations ϕ' would serve as inputs, whereas the outputs of the MIMO transfer function would be described by the global heat release rate fluctuations $\dot{Q}'$ and the entropy fluctuations s'. Challenges in this step would be probably the accurate extraction of entropy fluctuations from the LES and the development of a SI procedure, which is suitable for the MIMO identification. If the input signals are correlated this might impede the model estimation [63, 65]. Yet, another project within the Thermo-Fluid Dynamics group of Technische Universität München deals with the Multiple-Input Single-Output (MISO) transfer function identification of technically premixed flames ($u'_{\mathrm{ref}}, \phi' \rightarrow \dot{Q}'$). The insight gained in this project could be used for the additional identification of the missing 'entropy transfer function' ($\phi' \rightarrow s'$). The assessment of a entropy transfer function for a laminar flame via SI was already studied in [118] . Results for the identified entropy transfer function could be compared additionally with the analytical formulation derived in [119].

In a last step the network model approach could be extended to take also the *convective* transport of ϕ' and s' into account. Corresponding formulations are proposed for example in [119–121]. Together with the previously identified MIMO transfer function system a reduced order model would be obtained, which is valid for technically premixed flames. Based on this model a stability analysis and a sound pressure prediction would be possible, which also take the additional feedback of indirect combustion noise into account.

Bibliography

[1] T. Poinsot and D. Veynante. Flame-acoustics interactions. In *Theoretical and Numerical Combustion*, pages 375–431. R.T. Edwards, Inc., Philadelphia, PA, USA, 2nd edition, 2005. ISBN 978-1-930217-10-2.

[2] A. H. Lefebvre. *Gas Turbine Combustion*. Taylor & Francis, Philadelphia, PA, USA, 2nd edition, 1999. ISBN 978-1-56032-673-1.

[3] T. Lieuwen and V. Yang, editors. *Combustion Instabilities in Gas Turbine Engines: Operational Experience, Fundamental Mechanisms, and Modeling*, volume 210 of *Progress in Astronautics and Aeronautics*. AIAA, 2005. ISBN 1-56347-669-X.

[4] E. Giacomazzi. The importance of operational flexibility in gas turbine power plants. *Energia, Ambiente e Innovazione*, (6):58–63, 2014. doi:10.12910/EAI2013-35.

[5] Y. Liu, A. P. Dowling, N. Swaminathan, R. Morvant, M. A. Macquisten, and L. F. Caracciolo. Prediction of Combustion Noise for an Aeroengine Combustor. *Journal of Propulsion and Power*, 30(1):114–122, 2013. doi:10.2514/1.B34857.

[6] I. Duran and S. Moreau. Solution of the quasi-one-dimensional linearized Euler equations using flow invariants and the Magnus expansion. *Journal of Fluid Mechanics*, 723:190–231, 2013. doi:10.1017/jfm.2013.118.

[7] A. P. Dowling and Y. Mahmoudi. Combustion Noise. *Proceedings of the Combustion Institute*, 35(1):65–100, 2015. doi:10.1016/j.proci.2014.08.016.

[8] V. S. Burnley and F. E. Culick. Influence of Random Excitations on Acoustic Instabilities in Combustion Chambers. *AIAA Journal*, 38(8):1403–1410, 2000. doi:10.2514/2.1116.

[9] W. Polifke. Black-Box System Identification for Reduced Order Model Construction. *Annals of Nuclear Energy*, 67C:109–128, 2014. doi:10.1016/j.anucene.2013.10.037.

[10] W. C. Strahle. On Combustion Generated Noise. *Journal of Fluid Mechanics*, 49(2):399–414, 1971. doi:10.1017/S0022112071002167.

[11] S. Candel, D. Durox, S. Ducruix, A.-L. Birbaud, N. Noiray, and T. Schuller. Flame Dynamics and Combustion Noise: Progress and Challenges. *International Journal of Aeroacoustics*, 8(1):1–56, 2009. doi:10.1260/147547209786234984.

[12] M. Ihme. Combustion and Engine-Core Noise. *Annual Review of Fluid Mechanics*, 49(1):277–310, 2017. doi:10.1146/annurev-fluid-122414-034542.

[13] F. E. Marble and S. M. Candel. Acoustic Disturbance from Gas Non-Uniformities Convected Through a Nozzle. *Journal of Sound and Vibration*, 55(2):225–243, 1977. doi:10.1016/0022-460X(77)90596-X.

[14] H. A. Hassan. Scaling of combustion-generated noise. *Journal of Fluid Mechanics*, 66(03):445–453, 1974. doi:10.1017/S0022112074000292.

[15] S. Kotake and K. Takamoto. Combustion noise: Effects of the shape and size of burner nozzle. *Journal of Sound and Vibration*, 112(2):345–354, 1987. doi:10.1016/S0022-460X(87)80201-8.

[16] P. Clavin and E. D. Siggia. Turbulent Premixed Flames and Sound Generation. *Combustion Science and Technology*, 78(1-3):147–155, 1991. doi:10.1080/00102209108951745.

[17] C. Hirsch, J. Wäsle, A. Winkler, and T. Sattelmayer. A spectral model for the sound pressure from turbulent premixed combustion. *Proceedings of the Combustion Institute*, 31(1):1435–1441, 2007. doi:10.1016/j.proci.2006.07.154.

[18] R. Rajaram and T. Lieuwen. Acoustic radiation from turbulent premixed flames. *Journal of Fluid Mechanics*, 637:357–385, 2009. doi:10.1017/S0022112009990681.

[19] W. C. Strahle. Combustion Noise. *Progress in Energy and Combustion Science*, 4(3):157–176, 1978. doi:10.1016/0360-1285(78)90002-3.

[20] T. Schuller, D. Durox, and S. Candel. Dynamics of and noise radiated by a perturbed impinging premixed jet flame. *Combustion and Flame*, 128(1-2):88–110, 2002. doi:10.1016/S0010-2180(01)00334-0.

[21] S. Schlimpert, S. Koh, K. Pausch, M. Meinke, and W. Schröder. Analysis of Combustion Noise of a Turbulent Premixed Slot Jet Flame. *Combustion and Flame*, 175:292–306, 2017. doi:10.1016/j.combustflame.2016.08.001.

[22] J. R. Mahan and A. Karchmer. Aeroacoustics of Flight Vehicles: Theory and Practice. Volume 1: Noise Sources. In *Chapter 9 : Combustion and Core Noise*, volume 1, pages 483–517. NASA, Langley Research Center, 1991. ISBN NASA RP-1258.

[23] A. Huber and W. Polifke. Impact of Fuel Supply Impedance on Combustion Stability of Gas Turbines. In *ASME Turbo Expo 2008: Power for Land, Sea, and Air*, GT2008-51193, Berlin, Germany, 2008. ASME. doi:10.1115/GT2008-51193.

[24] A. P. Dowling. A Kinematic Model of a Ducted Flame. *Journal of Fluid Mechanics*, 394:51–72, 1999. doi:10.1017/S0022112099005686.

[25] N. Noiray, D. Durox, T. Schuller, and S. Candel. A unified framework for nonlinear combustion instability analysis based on the flame describing function. *Journal of Fluid Mechanics*, 615: 139–167, 2008. doi:10.1017/S0022112008003613.

[26] L. Crocco. Aspects of Combustion Stability in Liquid Propellant Rocket Motors Part1: Fundamentals. Low frequency instability with monopropellants. *Journal of the American Rocket Society*, 21 (6):163–178, 1951. doi:10.2514/8.4393.

[27] T. C. Lieuwen. *Unsteady Combustor Physics*. Cambridge University Press, New York, N.Y., USA, 2012. ISBN 978-1-107-01599-9.

[28] A. Albayrak, T. Steinbacher, T. Komarek, and W. Polifke. Convective Scaling of Intrinsic Thermo-Acoustic Eigenfrequencies of a Premixed Swirl Combustor. *Journal of Engineering for Gas Turbines and Power*, 140(4):041510–041510–9, 2018. doi:10.1115/1.4038083.

[29] M. Häringer, M. Merk, and W. Polifke. Inclusion of higher Harmonics in the Flame Describing Function for Predicting Limit Cycles of self-excited Combustion Instabilitites. *Proceedings of the Combustion Institute*, 37, 2018. doi:10.1016/j.proci.2018.06.150.

[30] M. Hoeijmakers, V. Kornilov, I. Lopez Arteaga, P. de Goey, and H. Nijmeijer. Intrinsic Instability of Flame-Acoustic Coupling. *Combustion and Flame*, 161(11):2860–2867, 2014. doi:10.1016/j.combustflame.2014.05.009.

[31] E. Courtine, L. Selle, and T. Poinsot. DNS of Intrinsic Thermoacoustic Modes in Laminar Premixed Flames. *Combustion and Flame*, 162(11):4331–4341, 2015. doi:10.1016/j.combustflame.2015.07.002.

[32] S. Bomberg, T. Emmert, and W. Polifke. Thermal Versus Acoustic Response of Velocity Sensitive Premixed Flames. *Proceedings of the Combustion Institute*, 35(3):3185–3192, 2015. doi:10.1016/j.proci.2014.07.032.

[33] C. F. Silva, T. Emmert, S. Jaensch, and W. Polifke. Numerical Study on Intrinsic Thermoacoustic Instability of a Laminar Premixed Flame. *Combustion and Flame*, 162(9):3370 – 3378, 2015. doi:10.1016/j.combustflame.2015.06.003.

[34] T. Emmert, S. Bomberg, S. Jaensch, and W. Polifke. Acoustic and Intrinsic Thermoacoustic Modes of a Premixed Combustor. *Proceedings of the Combustion Institute*, 36(3):3835–3842, 2017. doi:10.1016/j.proci.2016.08.002.

[35] C. F. Silva, M. Merk, T. Komarek, and W. Polifke. The Contribution of Intrinsic Thermoacoustic Feedback to Combustion Noise and Resonances of a Confined Turbulent Premixed Flame. *Combustion and Flame*, 182:269–278, 2017. doi:10.1016/j.combustflame.2017.04.015.

[36] M. Merk, R. Gaudron, C. Silva, M. Gatti, C. Mirat, T. Schuller, and W. Polifke. Prediction of Combustion Noise of an Enclosed Flame by Simultaneous Identification of Noise Source and Flame Dynamics. *Proceedings of the Combustion Institute*, 37, 2018. doi:10.1016/j.proci.2018.05.124.

[37] T. Komarek and W. Polifke. Impact of Swirl Fluctuations on the Flame Response of a Perfectly Premixed Swirl Burner. *Journal of Engineering for Gas Turbines and Power*, 132(6):061503, 2010. doi:10.1115/1.4000127.

[38] J. Y. Chung and D. A. Blaser. Transfer function method of measuring in-duct acoustic properties. II. Experiment. *The Journal of the Acoustical Society of America*, 68(3):914–921, 1980. doi:10.1121/1.384779.

[39] M. Guedra, G. Penelet, P. Lotton, and J. Dalmont. Theoretical prediction of the onset of thermoacoustic instability from the experimental transfer matrix of a thermoacoustic core. *The Journal of the Acoustical Society of America*, 130(1):145–152, 2011. doi:10.1121/1.3592227.

[40] C. O. Paschereit and W. Polifke. Investigation of the Thermo-Acoustic Characteristics of a Lean Premixed Gas Turbine Burner. In *Int'l Gas Turbine and Aeroengine Congress & Exposition*, ASME 98-GT-582, Stockholm, Sweden, 1998. ASME. doi:10.1115/98-GT-582.

[41] C. O. Paschereit, B. Schuermans, W. Polifke, and O. Mattson. Measurement of Transfer Matrices and Source Terms of Premixed Flames. *Journal of Engineering for Gas Turbines and Power*, 124 (2):239–247, 2002. doi:10.1115/1.1383255.

[42] P. R. Alemela, Fanaca D., Ettner F., Hirsch C., Sattelmayer T., and B. Schuermans. Flame Transfer Matrices of a Premixed Flame and a Global Check with Modelling and Experiments. In *ASME Turbo Expo 2008: Power for Land, Sea, and Air Technical Conference and Exposition*, GT2008-50111, Berlin, Germany, 2008. ASME. doi:10.1115/GT2008-50111.

[43] D. Durox, T. Schuller, and S. Candel. Self-induced instability of a premixed jet flame impinging on a plate. *Proceedings of the Combustion Institute*, 29(1):69–75, 2002. doi:10.1016/S1540-7489(02)80013-X.

[44] T. Schuller, D. Durox, and S. Candel. Self-induced combustion oscillations of laminar premixed flames stabilized on annular burners. *Combustion and Flame*, 135(4):525–537, 2003. doi:10.1016/j.combustflame.2003.08.007.

[45] D. Durox, T. Schuller, N. Noiray, A. L. Birbaud, and S. Candel. Rayleigh criterion and acoustic energy balance in unconfined self-sustained oscillating flames. *Combustion and Flame*, 156(1): 106 – 119, 2009. doi:10.1016/j.combustflame.2008.07.016.

[46] S. Jaensch, M. Merk, E. Gopalakrishnan, S. Bomberg, T. Emmert, R. Sujith, and W. Polifke. Hybrid CFD/Low-Order Modeling of Nonlinear Thermoacoustic Oscillations. *Proceedings of the Combustion Institute*, 36(3):3827–3834, 2017. doi:10.1016/j.proci.2016.08.006.

[47] L. Tay-Wo-Chong, S. Bomberg, A. Ulhaq, T. Komarek, and W. Polifke. Comparative Validation Study on Identification of Premixed Flame Transfer Function. *Journal of Engineering for Gas Turbines and Power*, 134(2):021502–1–8, 2012. doi:10.1115/1.4004183.

[48] Centre Européen de Recherche et de Formation Avancée en Calcul Scientific. *The AVBP Hand-Book*. CERFACS, Toulouse, France, 2008.

[49] L. Selle, G. Lartigue, T. Poinsot, R. Koch, K.-U. Schildmacher, W. Krebs, B. Prade, P. Kaufmann, and D. Veynante. Compressible Large Eddy Simulation of Turbulent Combustion in Complex Geometry on Unstructured Meshes. *Combustion and Flame*, 137(4):489–505, 2004. doi:10.1016/j.combustflame.2004.03.008.

[50] L. Y. M. Gicquel, G. Staffelbach, and T. Poinsot. Large Eddy Simulations of gaseous flames in gas turbine combustion chambers. *Progress in Energy and Combustion Science*, 38(6):782 – 817, 2012. doi:10.1016/j.pecs.2012.04.004.

[51] F. Nicoud and F. Ducros. Subgrid-Scale Stress Modelling Based on the Square of the Velocity Gradient Tensor. *Flow Turbulence and Combustion*, 62(3):183–200, 1999. doi:10.1023/A:1009995426001.

[52] O. Colin, F. Ducros, D. Veynante, and T. Poinsot. A Thickenend Flame Model for Large Eddy Simulation of Turbulent Premixed Combustion. *Physics of Fluids*, 12(7):1843–1863, 2000. doi:10.1063/1.870436.

[53] B. Franzelli, E. Riber, M. Sanjosé, and T. Poinsot. A two-step chemical scheme for kerosene–air premixed flames. *Combustion and Flame*, 157(7):1364–1373, 2010. doi:10.1016/j.combustflame.2010.03.014.

[54] F. Jaegle, O. Cabrit, S. Mendez, and T. Poinsot. Implementation Methods of Wall Functions in Cell-vertex Numerical Solvers. *Flow, Turbulence and Combustion*, 85(2):245–272, 2010. doi:10.1007/s10494-010-9276-1.

[55] S. Jaensch, C. Sovardi, and W. Polifke. On the Robust, Flexible and Consistent Implementation of Time Domain Impedance Boundary Conditions for Compressible Flow Simulations. *Journal of Computational Physics*, 314:145–159, 2016. doi:10.1016/j.jcp.2016.03.010.

[56] J.-M. Lourier, M. Stöhr, B. Noll, S. Werner, and A. Fiolitakis. Scale Adaptive Simulation of a thermoacoustic instability in a partially premixed lean swirl combustor. *Combustion and Flame*, 183:343–357, 2017. doi:10.1016/j.combustflame.2017.02.024.

[57] Q. Douasbin, C. Scalo, L. Selle, and T. Poinsot. Modeling Approach for Delayed Time Domain Impedance Boundary Condition. In *23rd AIAA/CEAS Aeroacoustics Conference*, Denver, CO, USA, 2017. AIAA/CEAS. doi:10.2514/6.2017-3506.

[58] T. Poinsot and S. K. Lele. Boundary Conditions for Direct Simulation of Compressible Viscous Flows. *Journal of Computational Physics*, 101(1):104–129, 1992. doi:10.1016/0021-9991(92)90046-2.

[59] L. Selle, F. Nicoud, and T. Poinsot. Actual Impedance of Nonreflecting Boundary Conditions: Implications for Computation of Resonators. *AIAA Journal*, 42(5):958–964, 2004. doi:10.2514/1.1883.

[60] W. Polifke, C. Wall, and P. Moin. Partially reflecting and non-reflecting boundary conditions for simulation of compressible viscous flow. *Journal of Computational Physics*, 213:437–449, 2006. doi:doi:10.1016/j.jcp.2005.08.016.

[61] H. Levine and J. Schwinger. On the Radiation of Sound from an Unflanged Circular Pipe. *Physical review*, 73(4):383–405, 1948. doi:10.1103/PhysRev.73.383.

[62] S. Föller and W. Polifke. Advances in Identification Techniques for Aero-Acoustic Scattering Coefficients from Large Eddy Simulation. In *18th International Congress on Sound and Vibration (ICSV18)*, volume 4, pages 3122–3129, Rio de Janeiro, Brazil, 2011.

[63] L. Ljung. System Identification. In *Signal Analysis and Prediction*, pages 163–173. Birkhäuser Boston, Boston, MA, USA, 1998. ISBN 978-1-4612-7273-1.

[64] K. J. Keesman. Time-invariant System Identification. In *System Identification*, Advanced Textbooks in Control and Signal Processing, pages 59–167. Springer London, London, UK, 2011. ISBN 978-0-85729-521-7.

[65] A. K. Tangirala. *Principles of System Identification: Theory and Practice*. CRC Press, Boca Raton, FL, USA, 2014. ISBN 978-1-4398-9602-0.

[66] R. Gaudron, M. Gatti, C. Mirat, and T. Schuller. Flame describing functions of a confined premixed swirled combustor with upstream and downstream forcing. *Journal of Engineering for Gas Turbines and Power*, 2018. doi:10.1115/1.4041000.

[67] S. Guo, C. F. Silva, A. Ghani, and W. Polifke. Quantification and Propagation of Uncertainties in Identification of Flame Impulse Response for Thermoacoustic Stability Analysis. In *ASME Turbo Expo 2018: Turbomachinery Technical Conference & Exposition*, GT2018-75644, Lillestrom, Norway, 2018. ASME.

[68] A. Gentemann, C. Hirsch, K. Kunze, F. Kiesewetter, T. Sattelmayer, and W. Polifke. Validation of Flame Transfer Function Reconstruction for Perfectly Premixed Swirl Flames. In *ASME Turbo Expo 2004: Power for Land, Sea, and Air*, GT2004-53776, Vienna, Austria, 2004. ASME. doi:10.1115/GT2004-53776.

[69] M. Zhu, A. P. Dowling, and K. N. C. Bray. Transfer Function Calculations for Aeroengine Combustion Oscillations. *Journal of Engineering for Gas Turbines and Power*, 127(1):18–26, 2005. doi:10.1115/1.1806451.

[70] B. Schuermans, H. Luebcke, D. Bajusz, and P. Flohr. Thermoacoustic analysis of gas turbine combustion systems using unsteady CFD. In *ASME Turbo Expo 2005: Power for Land, Sea, and Air*, GT2005-68393, Reno, NV, USA, 2005. ASME. doi:10.1115/GT2005-68393.

[71] K. Kostrzewa, J. Lepers, B. Noll, W. Krebs, M. Aigner, B. Prade, and M. Huth. Validation of Advanced Computational Methods for Determining Flame Transfer Functions in Gas Turbine Combustion Systems. In *ASME Turbo Expo 2007: Power for Land, Sea, and Air*, GT2007-27267, Montreal, Canada, 2007. ASME. doi:10.1115/GT2007-27267.

[72] A. Giauque, T. Poinsot, and F. Nicoud. Validation of a Flame Transfer Function Reconstruction Method for Complex Turbulent Configurations. In *14th AIAA/CEAS Aeroacoustics Conference (29th AIAA Aeroacoustics Conference)*, Vancouver, Canada, 2008. AIAA/CEAS. doi:10.2514/6.2008-2943.

[73] A. Huber and W. Polifke. Dynamics of Practical Premix Flames, Part II: Identification and Interpretation of CFD Data. *International Journal of Spray and Combustion Dynamics*, 1:229–250, 2009. doi:10.1260/175682709788707440.

[74] L. Tay-Wo-Chong and W. Polifke. Large Eddy Simulation-Based Study of the Influence of Thermal Boundary Condition and Combustor Confinement on Premix Flame Transfer Functions. *Journal of Engineering for Gas Turbines and Power*, 135:021502, 2013. doi:10.1115/1.4007734.

[75] A. Innocenti, A. Andreini, and B. Facchini. Numerical Identification of a Premixed Flame Transfer Function and Stability Analysis of a Lean Burn Combustor. *Energy Procedia*, 82:358–365, 2015. doi:https://doi.org/10.1016/j.egypro.2015.11.803.

[76] Y. Yang, N. Noiray, A. Scarpato, O. Schulz, K. M. Düsing, and M. Bothien. Numerical Analysis of the Dynamic Flame Response in Alstom Reheat Combustion Systems. In *ASME Turbo Expo 2015: Turbine Technical Conference and Exposition*, GT2015-42622, Montreal, Quebec, Canada, 2015. ASME. doi:10.1115/GT2015-42622.

[77] F. Biagioli, A. Scarpato, and K. J. Syed. Dynamic Response of Swirl Stabilized Turbulent Premixed Flames Based on the Helmholtz-Hodge Velocity Decomposition. *Flow, Turbulence and Combustion*, 96(4):1005–1022, 2016. doi:10.1007/s10494-016-9736-3.

[78] A. Innocenti, A. Andreini, B. Facchini, and A. Peschiulli. Numerical analysis of the dynamic flame response of a spray flame for aero-engine applications. *International Journal of Spray and Combustion Dynamics*, 9(4):310–329, 2017. doi:10.1177/1756827717703577.

[79] C. Sovardi, S. Jaensch, and W. Polifke. Concurrent Identification of Aero-acoustic Scattering and Noise Sources at a Flow Duct Singularity in low Mach Number Flow. *Journal of Sound and Vibration*, 377:90–105, 2016. doi:10.1016/j.jsv.2016.05.025.

[80] C. F. Silva, W. Polifke, J. O'Brien, and M. Ihme. Towards concurrent identification of flame dynamics and combustion noise of enclosed flames. In *Proceedings of the Summer Program*, page 179, Stanford, USA, 2014. Center for Turbulence Research, Stanford University.

[81] Y. Liu. Two-time correlation of heat release rate and spectrum of combustion noise from turbulent premixed flames. *Journal of Sound and Vibration*, 353:119–134, 2015. doi:10.1016/j.jsv.2015.05.027.

[82] C. F. Silva, M. Merk, S. Jaensch, and W. Polifke. The intrinsic thermoacoustic feedback loop and its role on the acoustic scattering matrix. *Combustion theory and modeling*, submitted, 2018.

[83] H. Akaike. Modern development of statistical methods. In *Trends and Progress in System Identification*, pages 169–184. Elsevier Science Limited, 1981. ISBN 978-0-08-025683-2.

[84] D. Bohn and E. Deucker. An acoustical model to predict combustion driven oscillations. In *20th Int'l Congress on Combustion Engines*, 20th International Congress on Combustion Engines, London, UK, 1993. CIMAC.

[85] A. P. Dowling. The Calculation of Thermoacoustic Oscillation. *Journal of Sound and Vibration*, 180(4):557–581, 1995. doi:10.1006/jsvi.1995.0100.

[86] J. J. Keller. Thermoacoustic Oscillations in Combustion Chambers of Gas Turbines. *AIAA Journal*, 33(12):2280–2287, 1995. doi:10.2514/3.12980.

[87] A. P. Dowling and S. R. Stow. Acoustic Analysis of Gas Turbine Combustors. *Journal of Propulsion and Power*, 19(5):751–764, 2003. doi:10.2514/2.6192.

[88] B. Schuermans, V. Bellucci, and C. O. Paschereit. Thermoacoustic Modeling and Control of Multi-Burner Combustion Systems. In *ASME Turbo Expo 2003, Collocated with the 2003 International Joint Power Generation Conference*, GT2003-38688, pages 509–519, Atlanta, GA, USA, 2003. ASME. doi:10.1115/GT2003-38688.

[89] M. Bothien, J. Moeck, A. Lacarelle, and C. O. Paschereit. Time Domain Modelling and Stability Analysis of Complex Thermoacoustic Systems. *Proceedings of the Institution of Mechanical Engineers, Part A: Journal of Power and Energy*, 221(5):657–668, 2007. doi:10.1243/09576509JPE384.

[90] J. Li and A. S. Morgans. Time Domain Simulations of Nonlinear Thermoacoustic Behaviour in a Simple Combustor Using a Wave-Based Approach. *Journal of Sound and Vibration*, 346:345–360, 2015. doi:10.1016/j.jsv.2015.01.032.

[91] T. Emmert, M. Meindl, S. Jaensch, and W. Polifke. Linear State Space Interconnect Modeling of Acoustic Systems. *Acta Acustica united with Acustica*, 102(5):824–833, 2016. doi:10.3813/AAA.918997.

[92] F. Weyermann, C. Hirsch, and T. Sattelmayer. Influence of boundary conditions on the noise emission of turbulent premixed swirl flames. In J. Janicka and A. Schwarz, editors, *Combustion Noise*, pages 161–188. Springer Verlag, Berlin, Germany, 2009. ISBN 978-3-642-02037-7.

[93] W. C. Ullrich, Y. Mahmoudi, K. Lackhove, A. Fischer, C. Hirsch, T. Sattelmayer, A. P. Dowling, N. Swaminathan, A. Sadiki, and M. Staufer. Prediction of Combustion Noise in a Model Combustor Using a Network Model and a LNSE Approach. *Journal of Engineering for Gas Turbines and Power*, 140(4):041501, 2017. doi:10.1115/1.4038026.

[94] N. Noiray, D. Durox, T. Schuller, and S. Candel. A method for estimating the noise level of unstable combustion based on the flame describing function. *International Journal of Aeroacoustics, 8*, 1(2):157–176, 2009. doi:10.1260/147547209786234957.

[95] M. Bothien, D. Lauper, Y. Yang, and A. Scarpato. Reconstruction and Analysis of the Acoustic Transfer Matrix of a Reheat Flame From Large-Eddy Simulations. In *ASME Turbo Expo 2017: Turbine Technical Conference and Exposition*, GT2017-64188, Charlotte, NC, USA, 2017. ASME. doi:10.1115/GT2017-64188.

[96] T. Emmert, S. Jaensch, C. Sovardi, and W. Polifke. taX - a Flexible Tool for Low-Order Duct Acoustic Simulation in Time and Frequency Domain. In *7th Forum Acusticum*, Krakow, 2014. DEGA.

[97] M. Meindl, M. Merk, F. Fritz, and W. Polifke. Determination of acoustic scattering matrices from linearized compressible flow equations. *Journal of Theoretical and Computational Acoustics*, 26 (0):1850027–1 – 1850027–27, 2018. doi:10.1142/S2591728518500275.

[98] B. T. Chu. On the Generation of Pressure Waves at a Plane Flame Front. In *4th Symposium (International) on Combustion*, volume 4, pages 603–612, Cambridge, MA, USA, 1953. Combustion Institute. doi:10.1016/S0082-0784(53)80081-0.

[99] D. Laera, A. Gentile, S. M. Camporeale, E. Bertolotto, L. Rofi, and F. Bonzani. Numerical and Experimental Investigation of Thermo–Acoustic Combustion Instability in a Longitudinal Combustion Chamber: Influence of the Geometry of the Plenum. In *ASME Turbo Expo 2015: Turbine Technical Conference and Exposition*, GT2015-42322, Montreal, Quebec, Canada, 2015. ASME. doi:10.1115/GT2015-42322.

[100] A. Gentemann and W. Polifke. Scattering and generation of acoustic energy by a premix swirl burner. In *ASME Turbo Expo 2007: Power for Land, Sea, and Air*, GT2007-27238, Montreal, Quebec, Canada, 2007. ASME. doi:10.1115/GT2007-27238.

[101] M. Merk, R. Gaudron, M. Gatti, C. Mirat, T. Schuller, and W. Polifke. Measurement and Simulation of Combustion Noise and Dynamics of a Confined Swirl Flame. *AIAA Journal*, 56(5): 1930–1942, 2018. doi:10.2514/1.J056502.

[102] M. Merk, R. Gaudron, M. Gatti, C. Mirat, W. Polifke, and T. Schuller. Quantitative Comparisons Between LES Predictions and Experimental Measurements of Sound Pressure Spectra in a Confined Swirl Combustor. In *53rd AIAA/SAE/ASEE Joint Propulsion Conference, AIAA Propulsion and Energy Forum*, Atlanta, GA, USA, 2017. American Institute of Aeronautics and Astronautics. doi:10.2514/6.2017-4687.

[103] S. Jaensch, M. Merk, T. Emmert, and W. Polifke. Identification of flame transfer functions in the presence of intrinsic thermoacoustic feedback and noise. *Combustion Theory and Modelling*, 22 (3):613–634, 2018. doi:10.1080/13647830.2018.1443517.

[104] M. Merk, S. Jaensch, C. Silva, and W. Polifke. Simultaneous identification of transfer functions and combustion noise of a turbulent flame. *Journal of Sound and Vibration*, 422:432–452, 2018. doi:10.1016/j.jsv.2018.02.040.

[105] M. Merk, R. Gaudron, C. Silva, M. Gatti, C. Mirat, T. Schuller, and W. Polifke. Direct Assessment of the Acoustic Scattering Matrix of a Turbulent Swirl Combustor by Combining System Identification, Large Eddy Simulation and Analytical Approaches. *Journal of Engineering for Gas Turbines and Power*, 2018. doi:10.1115/1.4040731.

[106] M. Merk, R. Gaudron, C. Silva, M. Gatti, C. Mirat, T. Schuller, and W. Polifke. Direct assessment of the acoustic scattering matrix of a turbulent swirl combustor by combining system identification, large eddy simulation and analytical approaches. In *ASME Turbo Expo 2018: Turbomachinery Technical Conference and Exposition*, GT2018-75529, Lillestrom, Norway, 2018. ASME. doi:10.1115/GT2018-75529.

[107] C. F. Silva, M. Merk, T. Komarek, and W. Polifke. The Contribution of Intrinsic Thermoacoustic Feedback to Combustion Noise and Resonances of a Confined Turbulent Premixed Flame. In *International Symposium: Thermoacoustic Instabilities in Gas Turbines and Rocket Engines*, Garching, Germany, 2016.

[108] S. Candel, D. Durox, T. Schuller, J. F. Bourgouin, and J. P. Moeck. Dynamics of Swirling Flames. *Annual Review of Fluid Mechanics*, 46(1):147–173, 2014. doi:10.1146/annurev-fluid-010313-141300.

[109] M. Gatti, R. Gaudron, C. Mirat, and T. Schuller. Effects of the Injector Design on the Transfer Function of Premixed Swirling Flames. In *ASME Turbo Expo 2017: Turbomachinery Technical Conference and Exposition*, Charlotte, NC, USA, 2017. ASME. doi:10.1115/GT2017-63874.

[110] J. Wäsle, A. Winkler, F. Weyermann, C. Hirsch, and T. Sattelmayer. A Model for Turbulent Combustion Noise. *Acta Acustica united with Acustica*, 95(3):391–401, 2009. doi:10.3813/AAA.918163.

[111] C. Bailly, C. Bogey, and S. Candel. Modelling of Sound Generation by Turbulent Reacting Flows. *International Journal of Aeroacoustics*, 9(4-5):461–489, 2010. doi:10.1260/1475-472X.9.4-5.461.

[112] C. F. Silva, M. Leyko, F. Nicoud, and S. Moreau. Assessment of combustion noise in a premixed swirled combustor via Large-Eddy Simulation. *Computers & Fluids*, 78:1–9, 2013. doi:10.1016/j.compfluid.2010.09.034.

[113] M. Huet, F. Vuillot, N. Bertier, M. Mazur, N. Kings, W. Tao, P. Scouflaire, F. Richecoeur, S. Ducruix, C. Lapeyre, and T. Poinsot. Recent Improvements in Combustion Noise Investigation: From the Combustion Chamber to Nozzle Flow. *Journal AerospaceLab*, (11), 2016. doi:10.12762/2016.AL11-10.

[114] M. Ihme, H. Pitsch, and D. Bodony. Radiation of noise in turbulent non-premixed flames. *Proceedings of the Combustion Institute*, 32(1):1545–1553, 2009. doi:10.1016/j.proci.2008.06.137.

[115] M. Ihme and H. Pitsch. On the generation of direct combustion noise in turbulent non-premixed flames. *International Journal of Aeroacoustics*, 11(1):25–78, 2012. doi:10.1260/1475-472X.11.1.25.

[116] M. Muthukrishnan, W. C. Strahle, and D. H. Neale. Separation of Hydrodynamic, Entropy, and Combustion Noise in a Gas Turbine Combustor. *AIAA Journal*, 16(4):320–327, 1978. doi:10.2514/3.60895.

[117] N. Kings, W. Tao, P. Scouflaire, F. Richecoeur, and S. Ducruix. Experimental and Numerical Investigation of direct and Indirect Combustion Noise Contributions in a Lean Premixed Laboratory Swirled Combustor. In *ASME Turbo Expo 2016: Turbomachinery Technical Conference and Exposition*, GT2016-57848, Seoul, Korea, 2016. ASME. doi:10.1115/GT2016-57848.

[118] L. Strobio Chen, T. Steinbacher, C. Silva, and W. Polifke. On Generation of Entropy Waves Across a Premixed Flame. In *Proceedings of ASME 2016 Turbo Expo: Turbomachinery Technical Conference & Exposition*, GT2016-57026, Seoul, Korea, 2016. doi:10.1115/GT2016-57026.

[119] T. Steinbacher, M. Meindl, and W. Polifke. Modeling the Generation of Temperature Inhomogeneities by a Premixed Flame. *International Journal of Spray and Combustion Dynamics*, 10(2): 111–130, 2018. doi:10.1177/1756827717738139.

[120] T. Sattelmayer. Influence of the Combustor Aerodynamics on Combustion Instabilities From Equivalence Ratio Fluctuations. *Journal of Engineering for Gas Turbines and Power*, 125(1): 11–19, 2003. doi:10.1115/1.1365159.

[121] A. Giusti, N. A. Worth, E. Mastorakos, and A. P. Dowling. Experimental and Numerical Investigation into the Propagation of Entropy Waves. *AIAA Journal*, 55(2):446–458, 2017. doi:10.2514/1.J055199.

[122] M. Merk, S. Jaensch, and W. Polifke. On Hydrodynamic Effects During Self-Excited Thermoacoustic Oscillations. In *24th ICTAM Conference*, Montreal, Canada, 2016.

[123] M. Merk, R. Gaudron, C. Mirat, M. Gatti, T. Schuller, and W. Polifke. Numerical and experimental investigation of the noise level in a confined premixed swirl-stabilized combustor. In *CDCN2 - Second Colloquium on Combustion Dynamics and Combustion Noise*, Menaggio, Italy, 2016.

[124] M. Merk, S. Jaensch, and W. Polifke. Concurrent identification of flame dynamics and combustion noise for turbulent flames. In *CDCN2 - Second Colloquium on Combustion Dynamics and Combustion Noise*, Menaggio, Italy, 2016.

Appendices

A Reproduction of Papers

The major publications that summarize results of this dissertation are reproduced in the following appendix. Preliminary results of the reproduced publications were presented at the *International Symposium: Thermoacoustic Instabilities in Gas Turbines and Rocket Engines 2016, Garching, Germany* [107], at the *24th ICTAM conference 2016, Montreal, Canada* [122], at the *Second Colloquium on Combustion Dynamics and Combustion Noise 2016, Menaggio, Italy* [123, 124], at the *53rd AIAA/SAE/ASEE Joint Propulsion Conference, AIAA Propulsion and Energy Forum 2017, Atlanta, Georgia, USA* [102] and at the *ASME Turbo Expo 2018: Turbomachinery Technical Conference & Exposition, Oslo, Norway* [106].

Moreover, the present author contributed additionally as a second author to three peer-reviewed publications, which are briefly summarized in the following.

In [46] two hybrid non-linear time-domain models are proposed and compared for predicting self-excited thermoacoustic oscillations of laminar premixed flames. The first model uses a low Mach number simulation that is coupled to a linear acoustic network model via fluctuations of reference velocity and global heat release rate. The second model is based on a fully compressible simulation, which is coupled to CBSBC [55] in order to model the acoustics in the unresolved upstream plenum part. Both models yield complex non-linear oscillations, which are in good agreement. Therefore, it is concluded that the non-linearities that occur during thermoacoustic oscillations may be attributed only to hydrodynamic effects and flame dynamics. The acoustics remain linear. The present author was responsible for the generation of results for the compressible approach.

In [97] the swirler scattering matrix shown in Fig. 6.2 is reproduced by linearized flow equations. It is shown that the linearized Navier-Stokes equations describe accurately the scattering of acoustic waves across the swirler. The swirler scattering matrix deduced from LES serves as a benchmark in this study. The present author provided the mean fields for the linearized flow equations and the benchmark result for the scattering matrix.

In [29] the standard Flame Describing Function (FDF) is extended to include not only the fundamental frequency but also higher harmonics. With the extended FDF it is possible to predict precisely the amplitudes and frequencies of the thermoacoustic oscillations computed in [46], even if the first higher harmonic mode dominates the thermoacoustic oscillation. A case in which the standard FDF formulation fails. This publication originated within the scope of the Master Thesis of M. Häringer, which the present author supervised.

As these publications have only limited relevance for the topic of the present thesis, they are not reproduced in the following.

AIAA JOURNAL
Vol. 56, No. 5, May 2018

Measurement and Simulation of Combustion Noise and Dynamics of a Confined Swirl Flame

Malte Merk* and Wolfgang Polifke†
Technical University of Munich, 85747 Garching, Germany
and
Renaud Gaudron,‡ Marco Gatti,‡ Clément Mirat,§ and Thierry Schuller¶
University of Paris-Saclay, 92295 Châtenay-Malabry, France

DOI: 10.2514/1.J056502

The combustion noise produced by a confined, turbulent, premixed swirl burner is predicted with large-eddy simulation of compressible, reacting flow. Characteristics-based state-space boundary conditions are coupled to the large-eddy simulation to impose precisely and independently from each other magnitude and phase of the acoustic reflection coefficients at the boundaries of the computational domain. The coupling approach proves to be accurate and flexible in regard to the estimation of sound pressure spectra in a confined swirl combustor for different operating conditions. The predicted sound pressure levels and its spectral distributions are compared to measurements. Excellent qualitative and quantitative agreement is achieved not only for a stable configuration but also for configurations that exhibit a thermoacoustic instability. This indicates that the flow and flame dynamics are reasonably well reproduced by the simulations.

Downloaded by BIBLIOTHEK DER TU MUENCHEN on June 19, 2018 | http://arc.aiaa.org | DOI: 10.2514/1.J056502

Nomenclature

A, B, C, D	=	system matrices
$\bar{c}$	=	mean speed of sound, m/s
f, g	=	characteristic waves
p'	=	pressure fluctuation, Pa
SPL	=	sound pressure level, dB
St	=	Strouhal number
u'	=	velocity fluctuation, m/s
$\boldsymbol{x}$	=	state vector
$\bar{\rho}$	=	mean density, kg/m^3

Subscripts

ax	=	axial
d	=	downstream
in	=	inlet
out	=	outlet
u	=	upstream
r	=	radial
θ	=	circumferential

I. Introduction

COMBUSTION noise is an undesirable but unavoidable byproduct of turbulent combustion. In many industrial applications such as aeronautical engines or stationary gas turbines, high levels of combustion noise are reached (e.g., for aeronautical engines, combustion noise constitutes a significant contribution to the overall sound emission from a plane at approach and cutback conditions [1]). Besides harmful effects and annoyance to those being exposed to noise emissions, high levels of combustion noise may lead to structural excitations or even trigger thermoacoustic instabilities [2]. As a consequence, combustion noise is an ongoing research topic.

One distinguishes direct from indirect combustion noise. Direct combustion noise is generated by fluctuations of heat release rate in turbulent flow. These heat release rate fluctuations in turn cause unsteady expansion of the gases across the flame brush that generates acoustic pressure fluctuations. The generation of direct combustion noise is hence an inherent mechanism of turbulent flames, which should thus be regarded as a distributed monopole source [3–5]. Indirect combustion noise refers to the generation of acoustic pressure fluctuations due to an acceleration of entropy inhomogeneities in the flowfield (e.g., at a choked outlet of a gas turbine combustor [6]). The present study only focuses on direct combustion noise and the sound pressure spectra arising thereof.

When it comes to the estimation of the spectral sound pressure distribution resulting from a turbulent flame, there are characteristic differences between open and confined configurations. In open configurations, which have been widely studied [1,3,5,7], the sound pressure spectrum is strongly correlated with the spectrum of the combustion noise source of the flame [8,9]. Analytical studies suggest that, in the low-frequency region, the magnitude of the combustion noise source spectrum increases toward a peak frequency and then decays in the high-frequency region. Accordingly, the sound pressure distributions of unconfined flames show similar behavior and do not exhibit pronounced peaks. This is confirmed by systematic measurements for unconfined jet flames [10,11] and slit flames [12]. The sound pressure spectra measured therein are of broadband nature with a peak frequency that scales linearly with the flame length and with the inverse of the injection velocity. Rajaram and Lieuwen [10] formulate in their work a Strouhal number scaling of the peak frequency based on the mean upstream convective velocity and the characteristic flame length, which is defined as "the distance between the axial locations where the transversely integrated intensity of the variance image crosses 25% of the maximum value" [10]. Winkler et al. [13] propose the distance between the burner exit plane and the maximum heat release as characteristic flame length.

The decrease of magnitude in the combustion noise source spectrum at higher frequencies was derived analytically by Clavin and Siggia [14]. Based on a Kolmogorov turbulence spectrum, a decay rate proportional to $f^{-2.5}$ is predicted.

Received 6 July 2017; revision received 4 December 2017; accepted for publication 13 December 2017; published online 29 January 2018. Copyright © 2018 by Malte Merk. Published by the American Institute of Aeronautics and Astronautics, Inc., with permission. All requests for copying and permission to reprint should be submitted to CCC at www.copyright.com; employ the ISSN 0001-1452 (print) or 1533-385X (online) to initiate your request. See also AIAA Rights and Permissions www.aiaa.org/randp.

*Ph.D. Student, Department of Mechanical Engineering, Boltzmannstraße 15; merk@tfd.mw.tum.de.

†Professor, Department of Mechanical Engineering, Boltzmannstraße 15, 85747 Garching.

‡Ph.D. Student, Laboratoire EM2C, CNRS, CentraleSupélec, 3, rue Joliot Curie, 91192 Gif-sur-Yvette cedex, France.

§Research Engineer, Laboratoire EM2C, CNRS, CentraleSupélec, 3, rue Joliot Curie, 91192 Gif-sur-Yvette cedex, France.

¶Professor, Laboratoire EM2C, CNRS, CentraleSupélec, 3, rue Joliot Curie, 91192 Gif- sur-Yvette cedex, France; currently Professor at Institut de Mécanique des Fluides de Toulouse, Université de Toulouse, CNRS, INPT, UPS, Toulouse, France.

Downloaded by BIBLIOTHEK DER TU MUENCHEN on June 19, 2018 | http://arc.aiaa.org | DOI: 10.2514/1.J056502

In most engineering applications, however, combustion takes place in a cavity with highly reflecting boundaries. In confined setups, the broadband acoustic pressure fluctuations emitted by the flame may excite the acoustic modes of the combustor. Resonant amplification may lead to distinct tonal peaks in the spectral sound pressure distribution [15–17]. Enhanced coupling between the unsteady heat release of the flame and the acoustic field may even lead to a self-amplifying feedback resulting in the occurrence of a thermoacoustic instability [4]. Therefore, an increasing number of studies was conducted on confined setups recently [15,18–25].

Because unsteadiness due to turbulence needs to be taken into account, large-eddy simulation (LES) appears as the natural tool to model combustion noise from first principles. LES may be used either in an LES/computational aeroacoustics (CAA) approach or in a direct approach. In the LES/CAA approach, the noise source is computed via LES, but propagation and reflection of acoustic of waves within the numerical domain are evaluated by an acoustic solver using an acoustic analogy. Effectively, the noise source is decoupled from the acoustic propagation. For unconfined setups, this methodology is successfully demonstrated by, for example, Flemming et al. [26] and Bui et al. [27], whereas Silva et al. [23] computed the sound pressure spectrum within a confined swirl combustor by means of a LES/CAA approach. In the compressible LES of the source region, the intrinsic thermoacoustic feedback [28–30] is inherently taken into account, meaning that effects of acoustic waves on the upstream flowfield and thus on the combustion dynamics are captured. This is not the case in an incompressible LES. However, any effects on the source region from outside the source region (i.e., the part resolved from the acoustic solver) are not modeled. Indeed, Silva et al. [23] found that their LES/CAA approach fails as soon as the interaction between flame and cavity acoustics is strong. The absence of source coupling also prohibits the use of a LES/CAA approach for describing thermoacoustic instabilities. The two-way coupling between flame dynamics and cavity acoustics, which cannot be captured by an LES/CAA approach, is necessary for the correct prediction of a self-excited instability [31].

For situations in which a significant coupling between flame and acoustics needs to be considered, the direct approach may be preferred. It resolves the combustion noise generation as well as the acoustic propagation within the LES, such that the respective acoustic pressure fluctuations may be extracted directly from the LES. By means of this approach, the mutual influence of flame and acoustics is resolved inherently. Using a direct approach, Silva et al. [23] and Kings et al. [24] achieved a qualitative agreement with experimental data for the sound pressure spectra in confined swirling flames, wherein only stable working conditions were considered. However, in both studies, the amplitude level in the numerically computed sound pressure spectra are overpredicted compared to acoustic pressure measurements made on the combustion chamber walls. Lourier et al. [32] simulated the sound pressure spectrum of a laboratory swirl combustor featuring a thermoacoustic instability. The peak frequency of the sound pressure spectrum is accurately reproduced, but the measured sound pressure level amplitudes are also overpredicted in these simulations. Tran et al. [33,34] showed that the sound pressure field of a confined swirling flame is very sensitive to the reflection coefficient of the premixer, and this may in turn be used to control the fluctuating pressure distribution.

The main objective of the current study is to determine the sound pressure spectra of a confined laboratory swirl combustor by means of LES with a direct approach. Because of the newly introduced coupling of the LES to characteristics-based state-space boundary conditions (CBSBCs), the analysis can easily be conducted for stable and unstable working conditions. The sound pressure spectra of one stable, one intermittently unstable, and one fully unstable working condition are investigated. The triggering of the thermoacoustic instability is reproduced only by according changes in the boundary conditions. Simulation results are compared to sound pressure spectra measured at the three operating conditions.

The instrumented experimental setup, the operating conditions, and the acoustic boundary conditions of the system are described in the next section. The corresponding numerical model is then presented in Sec. III. Focus is put on the modeling approach of the acoustic boundary conditions. It is shown that the boundary conditions have a significant influence on the predicted sound pressure field in the configurations investigated. The validity of the numerical model is then challenged in Sec. IV. Velocity profiles are compared between simulations and measurements as well as mean and phase-averaged images of the mean reaction zone submitted to a harmonic flow modulation. Additionally, the generated sound pressure spectrum for a nonreflective LES setup is tested against the analytical prediction of Clavin and Siggia [14]. Last, the numerically computed sound pressure spectra for the three configurations investigated are compared to measured sound pressure spectra.

II. Experimental Setup

The investigated test rig is a confined premixed swirl combustor sketched in Fig. 1 and located at EM2C laboratory. The shaded pink area indicates the domain resolved by the LES. Additionally, the microphone locations (MP, MC, ME, ME', ME''), the position of the hot-wire probe (HW), and the associated microphone (MHW) are shown.

A methane/air mixture is well premixed before it is injected in a tranquilization box, upstream of the plenum. The flow is then laminarized by a perforated plate followed by a honeycomb structure. It then passes through a first convergent (contraction ratio: 8.73) that generates a top-hat velocity profile at the inlet of the LES domain. Up to this position, the upstream parts including the plenum and the contraction have an acoustic equivalent length of 265 mm. A hot-wire probe is used to measure the velocity at the outlet of the convergent, where the diameter is 22 mm. The flow in this section is laminar with a top-hat axial velocity profile. After being pushed through a radial swirler, the fuel/air mixture enters the combustion chamber, which has a square cross section of 82 mm. The resulting turbulent, swirled-stabilized flame is V-shaped, anchored at a cylindrical bluff body that is topped by a cone. The combustion products are exhausted through a water-cooled convergent (contraction ratio: 2.03) with a square-to-round cross section, and an exhaust tube of variable length can be added optionally. The numerical LES domain, highlighted in red in Fig. 1, ends at the outlet of the exhaust convergent.

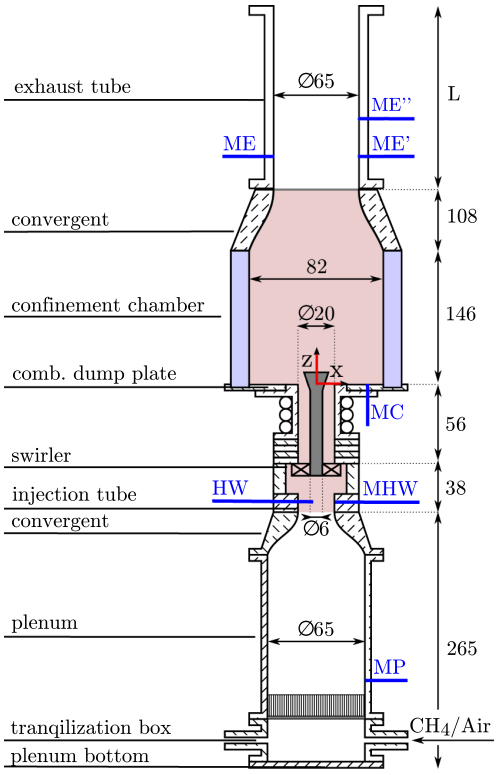

Fig. 1 Sketch of the EM2C turbulent swirl combustor for configuration B. Dimensions are given in millimeters.

Downloaded by BIBLIOTHEK DER TU MUENCHEN on June 19, 2018 | http://arc.aiaa.org | DOI: 10.2514/1.J056502

A. Operating Conditions

Experiments are all presented for the same flow operating condition. A perfectly premixed methane/air mixture with an equivalence ratio of $\phi = 0.82$ and a thermal power of $P_{\text{th}} = 5.5$ kW is considered. In the injection tube of diameter $D = 22$ mm, the resulting bulk flow velocity is $u_b = 5.4$ m/s, yielding a Reynolds number of approximately $Re = u_b D/\nu \simeq 7000$. Note that the flow remains laminar in this section. Relative fluctuations of the velocity are less than 2% in the boundary layer and much lower within the core flow. The flow temperature in this section is equal to 300 K. The mean combustor exit velocity and Mach Number are $u_e = 2.8$ m/s and $Ma = 0.0043$, respectively. The thermoacoustic state of the combustor is modified by varying the exhaust tube length shown in Fig. 1. Three configurations are investigated and are designated by A, B, and C in the remainder of this study.

Without any exhaust tube (configuration A), the system is stable, and no distinct tone emerges from the pressure spectrum. The flame features in this case turbulent fluctuations without any detectable low-frequency self-sustained coherent motion.

Adding an exhaust tube of $L = 220$ mm length on top of the exhaust convergent provokes a mild thermoacoustic instability with intermittent bursts and synchronized pressure oscillations at a frequency $f = 205$ Hz (configuration B). The temperature of the gases in the exhaust tube is on average approximately $T = 1080$ K. If the exhaust tube length is further increased to $L = 440$ mm, the instability grows in amplitude and reaches a stable limit cycle with a fixed oscillation amplitude $p' = 840$ Pa in the combustion chamber and an oscillation frequency equal to $f = 185$ Hz (configuration *C*). In this case, the average temperature of the gases within the exhaust tube drops to approximately $T = 1000$ K due to the larger heat transfer to the surrounding. A summary of the three configurations investigated is given in Table 1.

The instability at $f = 185$ Hz is coupled to the 3/4 wave mode of the system. Figure 2 shows that the signal recorded by the microphone located in the plenum (MP, blue) is almost out of phase with respect to the signals measured by the microphones located in the confinement chamber (MC, green) and in the exhaust tube (ME, purple). Simulations carried out with a low-order thermoacoustic model of the combustor yields the same frequency and structure of the acoustic field.

B. Diagnostics

The thermoacoustic state of the combustor is characterized by the hot-wire probe HW and the microphone MHW placed in front of the hot wire, as sketched in the Fig. 1. The hot wire measures the velocity signal in the tube of 22 mm diameter before the swirler, where the flow is laminar with a top-hat velocity profile. A microphone MP is flush-mounted, before the convergent. A second microphone MC is mounted on a water-cooled wave guide that is itself connected to the backplate of the combustion chamber. Three additional microphones, which are also mounted on water-cooled wave guides, can be inserted on the exhaust tube to measure the combustor outlet reflection coefficient R_{out} using the three-microphone method [35]. All the microphones are connected to preamplifiers (Brüel & Kjaer Type 4938-A-011) and then connected to a conditioning amplifier (Brüel & Kjaer Type 2690). All microphones are first calibrated with a known sound source (94 dB, 1000 Hz).

All signals are sampled at a frequency $f_s = 8192$ Hz and recorded for a duration of 4 s. This corresponds to around 1000 natural instability cycles for configuration C, of which a few are illustrated in Fig. 2.

Optical access in the confinement chamber is granted through the use of quartz walls, which are transparent for both the visible and close ultraviolet wavelengths. OH* images of the average turbulent flame structure and phase-conditioned images of the flame submitted to external acoustic forcing are recorded with an intensified charge-coupled device (ICCD) camera mounted with an interferometric filter centered on 310 nm with a 10 nm bandwidth. Abel deconvolutions are then performed on these images. Laser Doppler velocimetry is also used to analyze the flow at the swirling injector outlet in the absence of combustion. The three velocity components (axial, radial, and circumferential) velocities are measured by seeding the flow with small oil droplets of 2 μm in diameter. Velocity measurements are made 3 mm above the combustion chamber backplate.

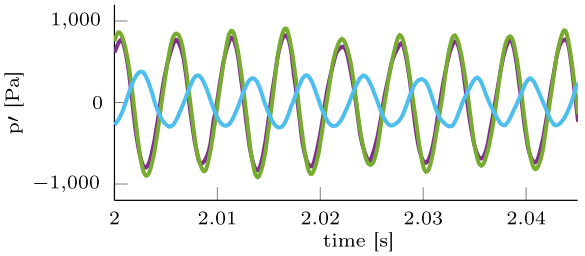

Fig. 2 Pressure measurements at limit cycle of the instability at $f = 185$ Hz in configuration C. Plenum microphone (MP, blue), combustion chamber microphone (MC, green), and exhaust tube microphone (ME, purple).

C. Acoustic Boundary Conditions

Reflection of acoustic waves at the upstream and downstream terminations of the combustor needs to be considered to determine the sound pressure level (SPL) and the spectral content of the acoustic pressure field. At the bottom of the plenum, the test rig is terminated by a metallic thick rigid wall. This boundary is accordingly assumed to be fully reflective without any phase shift and the reflection coefficient is $R_{\text{in}} = 1$. The same plenum system with the same components up to the injection tube before the hot-wire probe (HW) was already used in previous analysis of self-sustained combustion instabilities [36–38]. In these studies, it was also assumed that the bottom of the burner was a perfectly reflecting rigid plate and that the grid and honeycomb structure were transparent to sound waves. The excellent match in these references between model predictions and measurements for the different acoustic pressure and velocity signals strongly suggests that these assumptions are correct.

On the downstream side, the combustor exhaust is open to the atmosphere, and a fraction of the sound is radiated out of the combustor. The reflection coefficient R_{out} at the downstream end is determined with three microphones mounted on water-cooled wave guides that are introduced on the exhaust tube shown in Fig. 1. The three-microphone method along with coherence functions and the switching method from Chung and Blaser [35] are used to determine R_{out} between 20 and 500 Hz. These measurements shown in Fig. 3 are carried out for the combustor operating at the nominal condition $\phi = 0.82$ and $u_b = 5.4$ m/s. It is found that reflection is well reproduced by the Levine and Schwinger [39] model for an open-ended unflanged pipe.

III. Numerical Setup

The LES code AVBP [40] from CERFACS is used to assess the spectral sound distribution of the given setup. The fully compressible Navier–Stokes equations are solved on an unstructured grid [41,42]

Table 1 Summary of configurations studied

Configuration	Exhaust tube length, mm	Thermoacoustic state	Frequency, Hz	Amplitude	Color
A	0	Stable	— —	— —	Orange
B	220	Intermittent instability	205	$u'/\bar{u} = 0.2$	Yellow
C	440	Instability at limit cycle	185	$u'/\bar{u} = 0.7$	Green

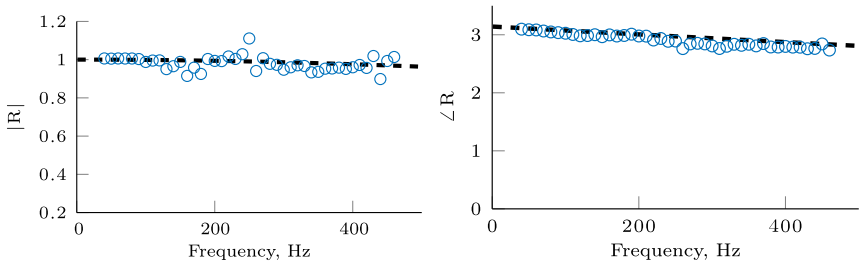

a) Modulus of R_{out} **b) Phase of R_{out}**

Fig. 3 Comparison between measured reflection coefficient (circles) and model of Levine and Schwinger [39] for an open-ended unflanged pipe (dashed line).

Downloaded by BIBLIOTHEK DER TU MUENCHEN on June 19, 2018 | http://arc.aiaa.org | DOI: 10.2514/1.J056502

by using the Lax–Wendroff scheme, which is of second-order accuracy in space and time. To reduce the computational effort, the LES domain is limited to the region downstream of the plenum contraction and upstream of the exhaust tube; see Fig. 1.

The unstructured grid consists of approximately 19 million tetrahedral cells with a maximum cell size of 0.6 mm in the flame region and 0.8 mm in the burner flow region, which consists of the swirler and the injection tube. The geometrical details of the swirler are fully modeled. The six radial swirler vanes, which have a diameter of 6 mm, are resolved by approximately 18 cells in the diameter that are refined toward the walls. In total, the swirler part is resolved by about 4 million cells.

Mesh independence of the results has been affirmed by testing one coarser and one finer mesh, compared to the reference mesh denoted as M_{ref}. The different mesh resolutions result from a local refinement in the flame region and the upstream flow region. The finer mesh M3 has a maximum cell size of 0.4 mm in the flame region and 0.6 mm in the upstream flow region, respectively, yielding a total cell number of approximately 34 million cells. For the coarser configuration M1, the mesh resolution was decreased in the flame region and the upstream flow region to 0.8 and 1.0 mm, respectively. This numerical configuration has a total cell number of approximately 11 million cells. The mesh resolution of the downstream flow region is kept constant with a cell size of 1.4 mm for two reasons.

1) The upstream flow region is of more relevance for the incoming flowfield of the flame and thus for the flame characteristics.

2) Less complex flow dynamics is expected in the downstream region due to the simpler geometry and the elevated viscosity in the burned gas region.

Table 2 summarizes the given values of the three meshes.

Results of the velocity profiles at the combustion chamber inlet (nonreacting flow) as well as noise spectra (reacting flow) were compared for the three different meshes. Whereas the mean velocity profiles in axial, radial, and circumferential directions are almost identical for all three meshes, the fluctuating components deviate slightly for the coarsest mesh M1 compared to M_{ref} and M3. For the reactive case, however, the resulting pressure spectra agree fairly well for all three meshes, even for the coarsest one. It is thus concluded that the results obtained for M_{ref} are mesh independent.

Subgrid stresses are handled by the wall adapting linear eddy (WALE) model [43], whereas interactions between the turbulent flowfield and the flame are described via the dynamically thickened flame model [44], resolving the laminar flame thickness within seven cells. The reduced two-step BFER scheme [45] is used to reproduce the chemistry of the premixed methane/air flame.

All parts upstream of the combustion chamber are assumed to be adiabatic. For the bluff body tip, a temperature of 1000 K is applied, which is in agreement to measured values. For the combustion chamber walls, which are made out of quartz glass, a heat loss boundary condition is used. For that, the experimentally measured temperature at the outside of the quartz wall is imposed at the LES boundaries as a reference temperature and an according thermal resistance is defined. This allows the wall temperature in LES to have a spatially nonuniform temperature distribution and to adapt to the internal temperature field. The metallic combustor dump plate is assumed to have an isothermal temperature of 823 K. With these imposed wall temperatures and the respective heat losses, the exhaust gas temperature at the LES domain outlet is in good accordance with the measured mean exhaust gas temperature of configuration A of approximately 1150 K. Reproducing the temperatures and thus the speed of sound accurately in LES is of importance to correctly predict the frequencies of the thermoacoustically unstable modes and the resulting sound pressure spectra in general.

Table 2 Summary of tested mesh resolutions

Mesh	Burner region cell size, mm	Flame region cell size, mm	Total number of cells
M1	1	0.8	11.06 million
M_{ref}	0.8	0.6	19.08 million
M3	0.6	0.4	34.15 million

To correctly model the acoustic transmission and reflection of the up- and downstream components of the test rig that are not included in the numerical domain, the LES domain is coupled to characteristics-based state-space boundary conditions (CBSBCs) [46], which are described later in this section.

A. Extracting Acoustic Pressure Fluctuations

It has been proposed to combine incompressible LES with a source model based on the spatiotemporal variations of heat release fluctuations to predict combustion noise [47–49]. Alternatively, a fully compressible formulation of the Navier–Stokes equations allows to assess combustion noise directly and without the need of a source model. However, the pressure signal in a compressible LES is a superposition of the acoustic and hydrodynamic pressure fluctuations, which may make the separation of the two contributions challenging. Turbulent and acoustic fluctuations cover the same range of amplitudes and frequencies or are at least in the same order of magnitude. In the present study, the method of characteristics-based filtering (CBF) [50] is used to extract the acoustic pressure fluctuations from the LES pressure field. This method exploits the difference in propagation speed between turbulent and acoustic fluctuations and allows to identify acoustic waves in turbulent compressible flows.

B. Modeling of Acoustic Boundaries

As already mentioned, correct acoustic modeling at boundaries of the numerical domain is crucial for predicting the sound pressure field inside the system as well as its thermoacoustic stability. Acoustic reflections at the boundaries may cause, for example, peaks in the sound pressure spectrum due to resonant amplification of acoustic eigenmodes or may couple with the flame dynamics to provoke a thermoacoustic instability. The acoustic characteristics of all components upstream and downstream of the numerical domain that are present in the test rig but are not resolved directly by LES and need to be modeled in an appropriate manner (see Fig. 4). This is achieved in the present study by using the characteristics-based state-space boundary conditions (CBSBCs) proposed by Jaensch et al. [46], which are a variant of time-domain impedance boundary conditions (TDIBC) [32,51–53].

Downloaded by BIBLIOTHEK DER TU MUENCHEN on June 19, 2018 | http://arc.aiaa.org | DOI: 10.2514/1.J056502

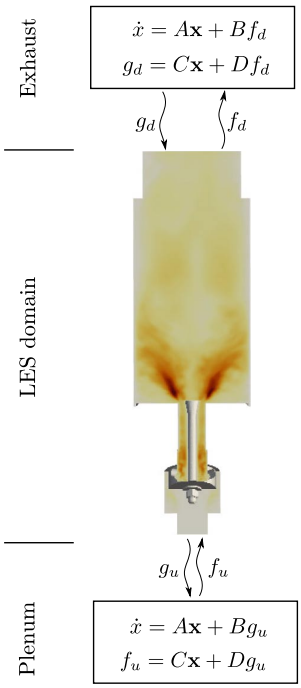

Fig. 4 LES domain coupled to CBSBCs via the characteristic waves f and g. Impedances of plenum and exhaust tube are modeled by CBSBCs.

In the simplest case, CBSBCs may be regarded as a fully nonreflective extension of the well known Navier–Stokes characteristic boundary conditions (NSCBCs) [54]. Like the NSCBCs, the CBSBCs avoid a drift of the mean flow variables. But whereas the NSCBCs yield a reflection coefficient of a first-order low-pass filter [55,56], the CBSBCs make use of plane wave masking [56] yielding a fully nonreflective behavior also at low frequencies. This behavior is achieved by an extension of the linear relaxation term of the NSCBCs that explicitly eliminates outgoing wave contributions from the linear relaxation term [56]. To identify accurately the outgoing wave contributions from the turbulent compressible flowfield, the CBF method is again applied.

In the present context, the main benefit of the CBSBCs is that they allow also to impose an ingoing wave, which effectively emulates a time-domain impedance with complete control over the phase and magnitude of the reflection coefficient. This is not feasible with the standard NSCBC formulation. This flexible and individual control of magnitude and phase allows to set complex reflection coefficients to the numerical domain. An exact description of the reflection conditions at the LES domain boundaries is achieved by imposing the measured impedances.

Because of the impact of the CBSBCs on the resulting sound pressure spectra, the coupling of the LES to the state-space model of the acoustic subsystem is explained in more detail. This is exemplarily done for the inlet boundary condition that describes the acoustic propagation within the plenum tube and the fully reflective plenum bottom. First, the upstream traveling characteristic wave

$$g_u = \frac{1}{2}\left(\frac{p'_a}{\bar{\rho}\,\bar{c}} - u'_a\right)_u \tag{1}$$

which is leaving the LES domain, is extracted by the CBF method. Herein, p'_a and u'_a represent the acoustic pressure and velocity fluctuation, respectively, whereas $\bar{\rho}$ and $\bar{c}$ refer to the mean values of density and speed of sound. The CBF filtering allows a proper separation between acoustic and turbulent fluctuations by exploiting their different propagation speeds. Whereas the acoustic perturbations propagate with the speed of sound, turbulent fluctuations are transported with the convective velocity.

In a next step, the extracted characteristic wave g_u serves as an input for the state-space model, which describes the acoustic processes downstream of the LES domain:

$$\dot{x} = A\boldsymbol{x} + Bg_u \tag{2a}$$

$$f_u = C\boldsymbol{x} + Dg_u \tag{2b}$$

Herein, $\boldsymbol{x}$ denotes the state-vector of the boundary model. The model itself depends on the system matrices A, B, C, and D, which describe the acoustic properties of the state-space model. As demonstrated by Jaensch et al. [46], there are different approaches to determine the system matrices A, B, C, and D (e.g., from a set of partial differential equations, from a polynomial fit of measured reflection conditions at discrete frequencies, or even from an acoustic network model).

To help the reader to develop a better physical understanding of the state-space model in Eq. (2), the state-space model used for the inlet boundary condition is constructed in the following from a set of partial differential equations. The linearized Euler equations describe the plane wave acoustics within the plenum and read as

$$\frac{\partial f}{\partial t} + (\bar{u} + \bar{c})\frac{\partial f}{\partial x} = 0 \tag{3a}$$

$$\frac{\partial g}{\partial t} + (\bar{u} - \bar{c})\frac{\partial g}{\partial x} = 0 \tag{3b}$$

with $\bar{u}$ denoting the mean convective velocity within the plenum. Following the notation introduced in Fig. 5, the partial differential equation system is closed by the boundary conditions

$$g(x = 0, t) = g_1 = g_u \tag{4a}$$

$$f(x = L, t) = f_N = R_{\text{in}} \cdot g(x = L, t) \tag{4b}$$

The boundary condition at $x = 0$ provides the characteristic wave g_u, which is extracted from the LES, as input to the boundary state-space model. At $x = L$, the reflected wave f_N is described in terms of the imposed reflection coefficient R_{in}. After applying a spatial discretization of the plenum (e.g., a linear upwind finite difference scheme), Eqs. (3a) and (3b) yield

$$\frac{\partial f_i}{\partial t} = -(\bar{u} + \bar{c})\frac{f_{i+1} - f_i}{\Delta x} \quad \text{for } i = 1, \ldots, N-1 \tag{5a}$$

$$\frac{\partial g_i}{\partial t} = -(\bar{u} - \bar{c})\frac{g_i - g_{i-1}}{\Delta x} \quad \text{for } i = 2, \ldots, N \tag{5b}$$

Combined with the boundary conditions of Eqs. (4a) and (4b), it follows for g_2 and f_{N-1}

$$\frac{\partial g_2}{\partial t} = -(\bar{u} - \bar{c})\frac{g_2 - g_d}{\Delta x} \tag{6a}$$

$$\frac{\partial f_{N-1}}{\partial t} = -(\bar{u} + \bar{c})\frac{R_{\text{in}} \cdot g_N - f_{N-1}}{\Delta x} \tag{6b}$$

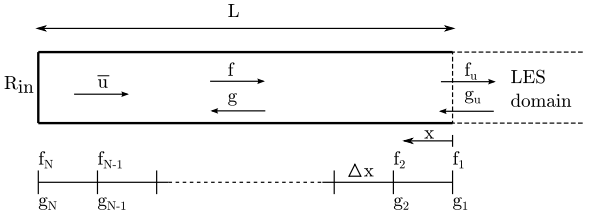

Fig. 5 Sketch of inlet plenum discretization.

From Eqs. (4–6), the state-space model can now be constructed as

$$\underbrace{\frac{\partial}{\partial t}\begin{bmatrix} g_2 \\ \vdots \\ g_N \\ f_1 \\ \vdots \\ f_{N-1} \end{bmatrix}}_{\dot{x}} = \underbrace{\begin{bmatrix} -\alpha_- & 0 & & & & & & \\ & \ddots & \ddots & & & & & \\ & & +\alpha_- & -\alpha_- & & & & \\ & & & & +\alpha_+ & -\alpha_+ & & \\ & & & & & \ddots & \ddots & \\ & & & -R_{in}\alpha_+ & & & 0 & \alpha_+ \end{bmatrix}}_{A} \underbrace{\begin{bmatrix} g_2 \\ \vdots \\ g_N \\ f_1 \\ \vdots \\ f_{N-1} \end{bmatrix}}_{x} + \underbrace{\begin{bmatrix} \alpha_- \\ 0 \\ \vdots \\ 0 \\ 0 \end{bmatrix}}_{B} \underbrace{[g_u]}_{u}$$

$$\underbrace{f_u}_{y} = f_1 = \underbrace{[0 \quad \cdots \quad 0 \quad 1 \quad \cdots \quad 0]}_{C}\boldsymbol{x} + \underbrace{[0]}_{D}\boldsymbol{u} \tag{7}$$

where $\alpha_+ = (\bar{u} + \bar{c})/\Delta x$, and $\alpha_- = (\bar{u} - \bar{c})/\Delta x$. The interpretation of the constructed state-space model is the following. The state vector $\boldsymbol{x}$ contains the values of f and g at the discrete locations. The state matrix $\boldsymbol{A}$ is mainly determined by the discretization scheme and describes the wave propagation along the characteristics on its main diagonals. However, the off-diagonal element relates the values f_{N-1} and g_N in terms of the prescribed reflection coefficient R_{in}. The vector $\boldsymbol{B}$ denotes the input vector and describes the influence of the input quantity g_u on the system. The output vector $\boldsymbol{C}$ defines which values of the state vector $\boldsymbol{x}$ serve as outputs and are consequently fed back into the LES. In the present case, only the value corresponding to $f_1 = f_u$ is nonzero, meaning that, at the LES inlet, an acoustic wave is imposed with

$$f_u = \frac{1}{2}\left(\frac{p'_a}{\bar{\rho}\,\bar{c}} + u'_a\right)_u \tag{8}$$

Here, f_u is the time-lagged reflection of the acoustic wave g_u. The time lag depends on the length of the plenum L and the speed of sound c. Because no additional external excitation is imposed at the LES inlet, the feedthrough vector $\boldsymbol{D}$ is a null vector.

The coupling between LES and CBSBC at the outlet of the numerical domain is established in an analogous manner. However, the respective state-space model is constructed from a polynomial function, representing the Levine–Schwinger conditions for an open unflanged pipe [39]. For the details of this alternative approach and further information on the CBSBC formulation, the reader is referred to the publication of Jaensch et al. [46]. Note that the coupling of a compressible LES to CBSBC was already used successfully by Jaensch et al. [57] and Tudisco et al. [58].

C. Acoustic Boundary Conditions of the Numerical Domain

The three configurations A, B, and C feature different reflection coefficients at the boundaries of the numerical domain. All three configurations share the same acoustic impedance at the numerical domain inlet, which is characterized by the reflection coefficient R_{in} shown in Fig. 6. This boundary condition models the acoustic impedance of the plenum terminated by a rigid wall. According to the hard wall at the upstream end of the plenum (see Sec. II.C), the absolute value of the reflection coefficient remains constant and equal to unity across all frequencies $|R_{\text{in}}| = 1$. The plenum itself introduces a frequency-dependent phase lag that only depends on the plenum length and the speed of sound within the plenum. For the given plenum, the acoustic equivalent length of $l = 265$ mm, and the speed of sound of $c = 340$ m/s, a phase lag as shown in Fig. 6b results.

The outlet reflection coefficient R_{out}, however, changes between the three configurations studied and has a major impact upon the resulting sound pressure spectra in the combustion chamber. Because all three configurations are open-ended, the magnitude of R_{out} is thus the same for all three configurations. The Levine–Schwinger condition [39] for an open-ended unflanged pipe is applied as shown in Fig. 7a. Even though experimental data are only available up to 500 Hz, the analytical expression allows a reliable definition of the reflection coefficient in the LES up to higher frequencies. But for a better readability, only the frequency range [0–1000 Hz] is depicted in Fig. 7. The reflection coefficient R_{out} at the numerical domain outlet is fully reflective in the low-frequency limit and introduces a slight decrease of the reflection magnitude with increasing frequencies. The decay rate of $\angle R_{\text{out}}$ is a function of the exhaust tube length, diameter, and speed of sound. For configuration A, the Levine–Schwinger condition can directly be used for R_{out}, as shown by Fig. 7b (orange). However, for configurations B and C, an additional phase lag has to be taken into account due to the additional length of the exhaust tube. This phase lag increases linearly with the exhaust tube length. For both configurations, a mean speed of sound of $c = 634$ m/s was assumed, corresponding to a mean exhaust gas temperature of $T_{\text{out}} = 1000$ K. Figure 7b also shows the phase of the reflection coefficient for configurations B (orange) and C (green).

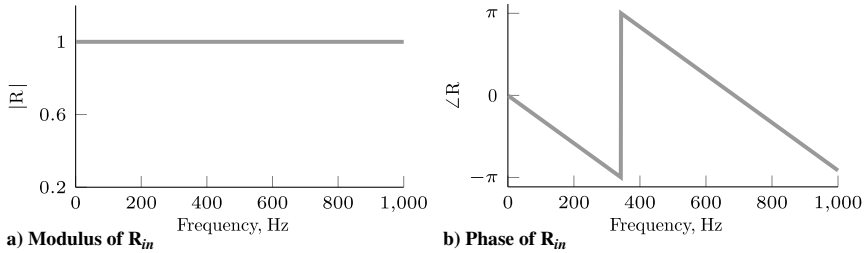

a) Modulus of R_{in} **b) Phase of R_{in}**

Fig. 6 Complex inlet reflection coefficient R_{in} used in numerical model for the three configurations A, B, and C.

Downloaded by BIBLIOTHEK DER TU MUENCHEN on June 19, 2018 | http://arc.aiaa.org | DOI: 10.2514/1.J056502

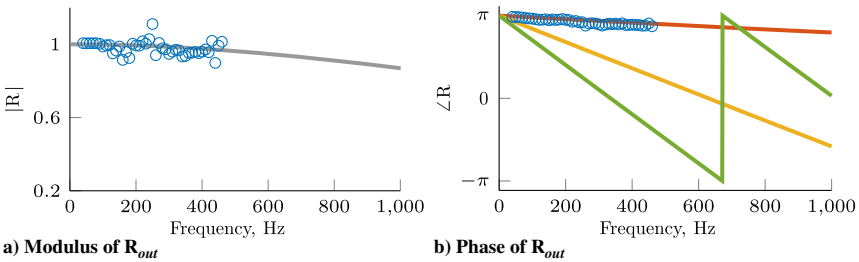

a) Modulus of R_{out} **b) Phase of R_{out}**

Fig. 7 Complex outlet reflection coefficient used in the numerical model. Left: modulus for configurations A, B, and C. Right: phase for configuration A (orange), B (yellow), and C (green).

IV. Results

An overview of the LES carried out for the different cases explored is given in Table 1 together with the dynamic state of the system observed in the experiments. Note that the plenum and exhaust tubes could also be modeled directly by the LES, similar to the setup of Franzelli et al. [59], but this would significantly increase the numerical domain size and thus the computational effort. Moreover, a remeshing would be necessary for every configuration investigated. The chosen coupling of LES and CBSBC allows to analyze changes in acoustic impedance at the numerical domain boundaries by a simple reformulation of the state-space model. Practically, this means that the LES numerical domain remains the same for all three configurations, and the resulting instability only arises due to the reformulation of the boundary state-space model at the numerical domain outlet.

A. Velocity Profiles

The velocities measured by LDV in the experiments are first compared to the numerical results under cold flow operation for a bulk velocity of $u_b = 5.4$ m/s at the numerical domain inlet. In LES, the averaging time amounts to 240 ms and corresponds thus to approximately 16 flow trough times. The velocity profiles are compared 3 mm above the combustion chamber dump plate.

Figures 8a–8c show an excellent agreement for all three velocity components between measurements and LES computations. In this figure, the radial distance x to the burner axis is normalized by the injector outlet radius $R = 10$ mm. The radial location of the velocity peaks and their associated amplitudes are correctly predicted by the numerical results.

The measured rms values are slightly less well reproduced by the simulations. The rms values of the axial velocity are still in fairly in good agreement in Fig. 8d between experiments and LES, whereas the rms velocity profiles of the radial and circumferential velocity profile show some discrepancy in Figs. 8e and 8f. Even though the respective total values are in the same range of magnitude, the values downstream the bluff body close to $x/R = 0$ and in the outer shear layer $x/R \pm 1$ differ slightly.

One possible reason might be that the relatively short time in the LES over which averages were made is not long enough to converge toward the correct average values that were found to be statistically independent of the number of samples in the experiments. The LDV measurements are also averaged over the collection volume probed by the laser beams. This might also introduce a small bias in the measurements, especially in the regions of high shear due to the large gradients. The overall comparison between mean and rms velocity profiles for the three velocity components, however, yields satisfying agreement for the cold flow condition explored.

B. Shape of Mean Reaction Zone

Because velocity measurements are only available for cold flow conditions, as a first step, the comparison with simulations is further investigated in reacting conditions by examining the mean reaction zone shape.

The mean shape taken by the flame in configuration A, when the combustor is stable, is shown in Fig. 9 in the midlongitudinal plane of

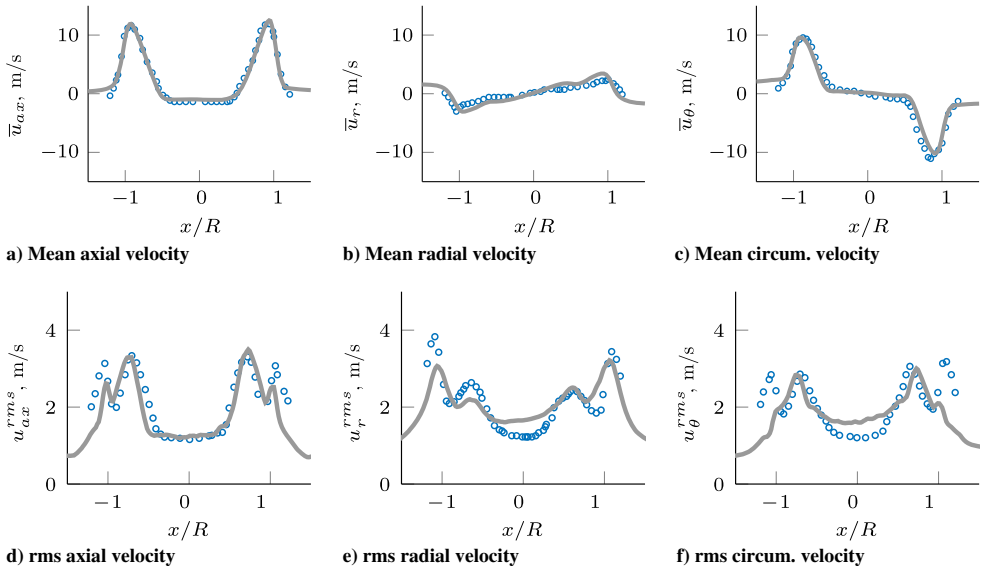

a) Mean axial velocity **b) Mean radial velocity** **c) Mean circum. velocity**

d) rms axial velocity **e) rms radial velocity** **f) rms circum. velocity**

Fig. 8 Cold flow velocity fields (axial, radial, circumferential) measured by LDV (circles) and LES results (solid line). Top: mean values. Bottom: rms values.

Downloaded by BIBLIOTHEK DER TU MUENCHEN on June 19, 2018 | http://arc.aiaa.org | DOI: 10.2514/1.J056502

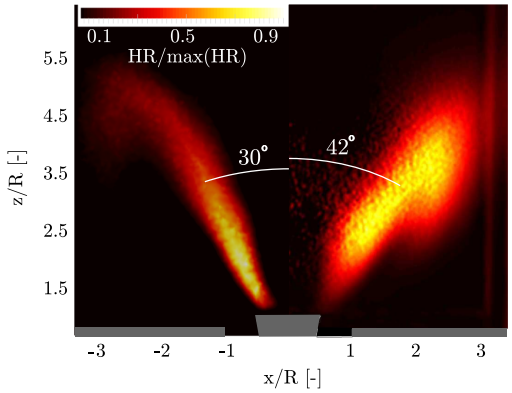

Fig. 9 Mean reaction zone shape for stable configuration A. Left: LES results temporally averaged over 120 ms. Right: Abel deconvolution of the OH* signal averaged over 100 frames.

the combustion chamber. The combustor dump plate and the central bluff body are sketched in gray. The flow is directed from bottom to top. On the left-hand side, the distribution of the volumetric heat release rate calculated by LES is depicted. Results are normalized by the maximum value found in the simulation and averaged over data accumulated over 120 ms. The right-hand side of Fig. 9 shows the Abel transform of the OH* experimental signal recorded over 100 frames with an exposure time of 20 ms for each snapshot. Five frames were taken each second, which amounts to a total integration time of 20 s. At this point, it is emphasized that the measured mean reaction zone shape and the one resulting from LES can only be compared to a certain extent. The measured Abel transformed images depict the OH* chemiluminescence distribution, whereas LES results represent the mean reaction zone in terms of heat release rate. The global two-step reaction scheme of the LES cannot be used to infer the OH* distribution.

Figure 9 indicates that the simulated mean reaction zone shape is in reasonable agreement with that observed in experiments. Even though the flame angle at the injector outlet differs by about 12 deg, the positions of the flame leading edge and the flame height are fairly well reproduced by the LES. The flame length is an essential feature that governs the cutoff frequency of the flame transfer function [60] and has also be shown to be an important parameter that governs the peak frequency of the broadband combustion noise radiated by unconfined flames [10]. A reasonable reproduction of the flame length is thus compulsory to reproduce the sound pressure spectra.

In configuration C, the system is unstable, and the oscillation reaches a limit cycle with a frequency of 185 Hz. This is also what is observed in the numerical simulation of this configuration. A comparison is made of phase-averaged flame images in Fig. 10. These pictures shed additional light on the flame dynamics and the flame motion during one oscillation cycle.

The images recorded in the experiments, on the right-hand side in Fig. 10, show OH* phase-averaged and Abel transformed images. In this case, each frame corresponds to an exposure time of 40 μs, and results are averaged over 100 frames. These images are synchronized with respect to the velocity signal measured by the hot-wire probe HW in the injection tube, shown in Fig. 11. The mean reaction zone shapes from LES, shown on the left-hand side in Fig. 10, are represented by a heat release rate isocontour averaged over 20 frames at the same phase angles in the oscillation cycle as in the experiments. The time covered by the 20 LES frames adds up to approximately 110 ms. Every LES flowfield is sliced along the *x* axis, the *y* axis, and the two bisectors, yielding in total eight flame halves to average across per frame. In the LES, the sampling frequency is set constant and equal to a sixth of the oscillation frequency of the instability. Because of small cycle-to-cycle variations caused by the acoustic velocity fluctuations induced by the flame, the phase angle of the respective snapshots (×) is slightly varying in respect to the inlet velocity signal. The time instants at which the ICCD camera is triggered in the experiment is marked by the dashed vertical lines and

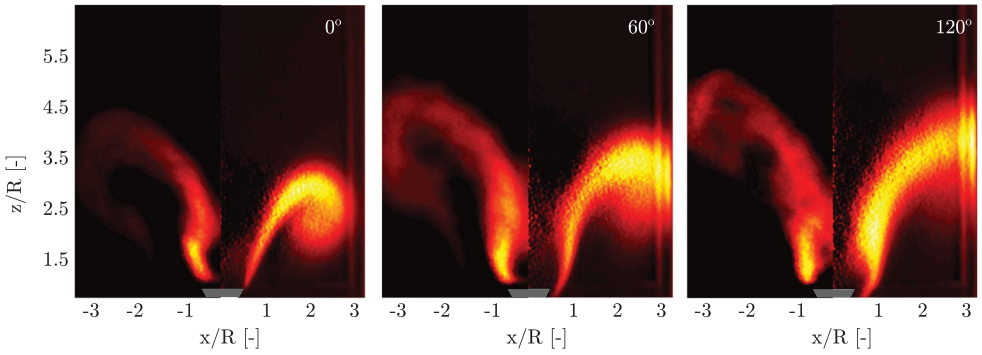

a) Phase angles 0°-120°

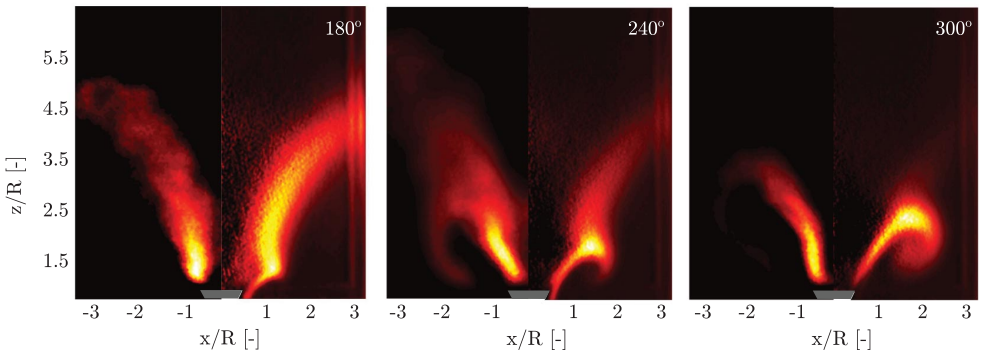

b) Phase angles 180°-300°

Fig. 10 Phase-averaged flame images over one oscillation at limit cycle for configuration C. Left: LES. Right: experiment. The coordinates are normalized with the injection tube radius $R = 10$ mm.

Downloaded by BIBLIOTHEK DER TU MUENCHEN on June 19, 2018 | http://arc.aiaa.org | DOI: 10.2514/1.J056502

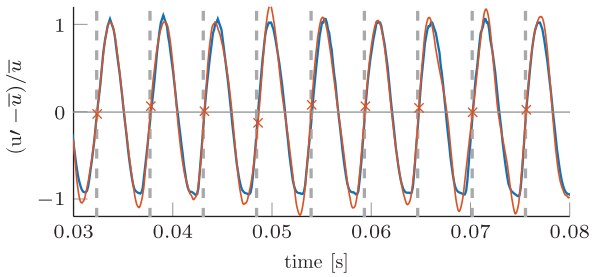

Fig. 11 Velocity signals used for the synchronization: measured at MHW (blue), LES inlet velocity (orange), triggering of ICCD camera (dashed line), snapshot in the LES (×).

is controlled by the phase angle of the velocity signal in the injection tube.

The general flame motion during the oscillation cycle is satisfyingly described by the compressible LES in Fig. 10. The position of the largest structures of the flame and the respective flame length are fairly well reproduced by the LES at each phase of the oscillation cycle. Flame length increase per phase increase is captured by the simulation as well as the radial flame extension observed in the experiments. Despite the limitations of this qualitative comparison, such as the slightly varying phase angle of the respective snapshots or the comparison between OH* chemiluminescence and heat release rate, it can be concluded that the compressible LES is capable of describing the main important features of the flame motion during a limit-cycle oscillation.

C. Sound Pressure Spectra

The acoustic pressure time series recorded in the experiments are statistically averaged by the use of Welch's power spectral estimate because a direct use of the fast Fourier transform has no meaning for noisy signals over a finite duration of time. Thirty-two Blackman–Harris windows are used with an overlap of 50% over the 4-s-long experimental time series. The numerical time series are postprocessed with only three Blackman–Harris windows because they have a length of only 360 ms. The sound pressure level (SPL) is defined here as

$$\mathrm{SPL} = 20 \times \log_{10}\left(\frac{p'_{\mathrm{rms}}}{p_{\mathrm{ref}}}\right) \tag{9}$$

with a reference pressure $p_{\mathrm{ref}} = 2. \times 10^{-5}$ Pa. Sound pressure signatures are compared between experiments and simulations for the microphone MC set in the combustion chamber (see Fig. 1).

A first calculation is made by imposing perfectly nonreflective boundary conditions at the inlet and outlet of the numerical domain. This situation mimics an open flame radiating noise as long as the acoustic wavelength is significantly larger than the characteristic transverse dimensions of the combustor. The power spectral density of the SPL signal is here compared to the theoretical spectrum from Clavin and Siggia [14]. Their analytical scaling law is based on the assumption of a Kolmogorov turbulence spectrum and predicts that the power spectral density of the noise radiated by an unconfined turbulent flame features a decay proportional to $f^{-2.5}$, where f is the frequency.

Figure 12 shows the computed sound pressure spectrum for nonreflective boundary conditions at the inlet and outlet (gray). By determining from LES the bulk flow velocity at the combustion chamber inlet u_{ave} and the distance between the maximum heat release and the burner exit plane L_f, the Strouhal number scaling proposed by Winkler et al. [13] can be applied:

$$St = \frac{f_{\mathrm{peak}} L_f}{u_{\mathrm{ave}}} \simeq 1 \tag{10}$$

From LES, the values of $u_{\mathrm{ave}} = 7.1$ m/s and $L_f \simeq 0.028$ m are found, resulting in an estimated peak frequency of $f_{\mathrm{peak}} \simeq 250$ Hz.

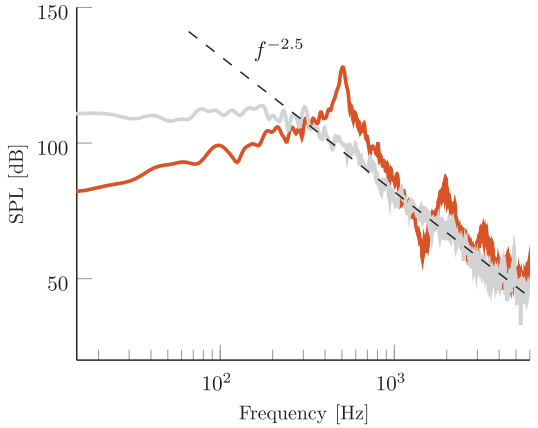

Fig. 12 Spectral sound pressure distribution from LES with nonreflective boundary conditions (gray), with partially reflecting conditions of configuration A (orange) and prediction of spectral decay by [14] (dashed line).

The spectral decay rate above the peak frequency is well reproduced by the decaying scaling law of Clavin and Siggia [14] (dashed line). One may conclude that all relevant mechanisms responsible for the generation and propagation of acoustic waves in the turbulent combustion process are described qualitatively correct by the LES.

Additionally, the sound pressure spectrum of the nonreflective case is overlaid with the sound pressure spectrum that results from applying the fully reflective boundary conditions of configuration A (orange). Even though the spectrum for configuration A is discussed in more detail in the next section, two aspects are already worth emphasizing at this point. First, compared to the reflecting conditions of configuration A, no distinct peaks emerge from the pressure spectrum if nonreflective boundary conditions are applied. Second, the general spectral shape of the case with nonreflecting boundary conditions is preserved in the spectrum of configuration A. Especially the spectral rolloff at higher frequencies is also visible for configuration A, although distinct peaks resulting from cavity resonances are observable.

Figure 13 shows on the left 100 ms of the computed pressure time series (orange) for configuration A when the system is stable with respect to thermoacoustic instabilities but features reflection at its inlet and outlet. The exhibited pressure fluctuations of the time series remain small. On the right-hand side, the measured (green) and computed (orange) sound pressure power spectral distributions are depicted. One observes a remarkable agreement between the measured and simulated values. In the low-frequency limit, the slope of the pressure spectral distribution and its level are in overall good agreement. The level at the peak frequency at around 500 Hz is slightly overpredicted by 7 dB in the LES. This slight difference between measurements and the LES is mainly attributed to the differences in the mean reaction zone shape, observed in Fig. 9. This is believed to be the main origin of discrepancies in the low-frequency region and at the peak frequency. The subsequent measured decay of the SPL is well reproduced by LES coupled to CBSBCs. The slight difference between measurements and the LES prediction in the region of the local minimum around 1500 Hz can be mainly attributed to the uncertainties in the thermal boundaries. Inaccuracies in the temperature field yield to a shift of frequencies in the LES, especially in the higher-frequency regions.

According to theory and the spectral distribution of the nonreflective configuration shown in Fig. 12, the combustion noise source in Fig. 13 is mainly active in the midfrequency region up to 300 Hz and rolls off to higher frequencies. However, the spectral sound pressure distribution is no longer completely flat over the whole frequency range. The appearance of the peak at 500 Hz with an amplitude of approximately 120 dB may be seen as the combustor resonance. The broadband noise emitted by the flame goes in resonance with the system cavities. Depending on the cavity

Downloaded by BIBLIOTHEK DER TU MUENCHEN on June 19, 2018 | http://arc.aiaa.org | DOI: 10.2514/1.J056502

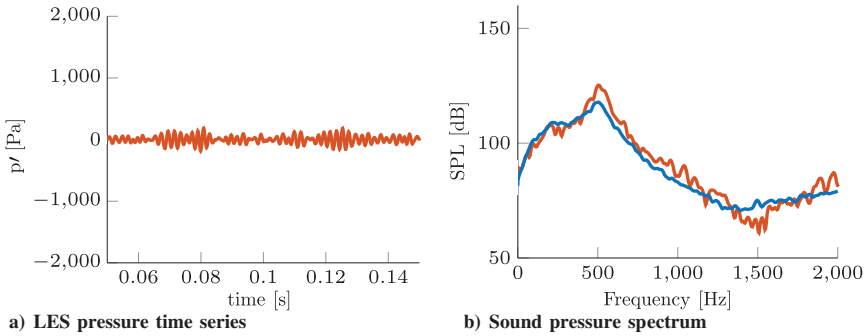

a) LES pressure time series b) Sound pressure spectrum

Fig. 13 LES pressure time series and sound pressure spectrum of the stable configuration A. SPL measurements (blue) and LES results (orange) for microphone MC.

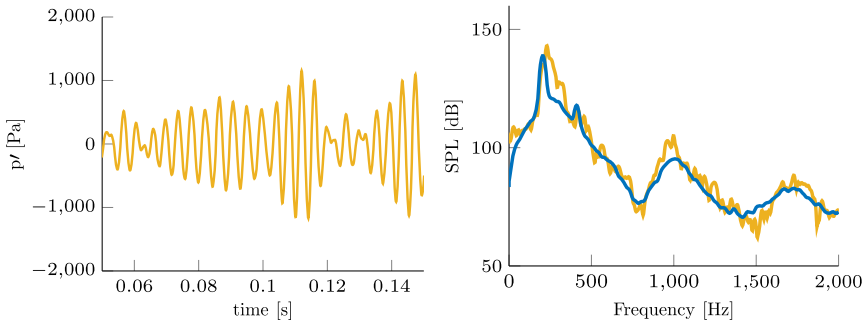

a) LES pressure time series b) Sound pressure spectrum

Fig. 14 LES pressure time series and sound pressure spectrum of the intermittent unstable configuration B. SPL measurements (blue) and LES results (yellow) for microphone MC.

Downloaded by BIBLIOTHEK DER TU MUENCHEN on June 19, 2018 | http://arc.aiaa.org | DOI: 10.2514/1.J056502

geometry, certain frequencies are damped, and others are amplified, resulting in the formation of peaks in the spectral sound pressure distribution. By using a linear acoustic network model of the combustor [61], the resonant peak in the sound pressure spectrum of configuration A can be identified as the $3/4\lambda$ wave mode of the system that is resonating. Nonetheless, the combustion remains stable, and the overall SPL magnitude remains at a moderate level.

Figure 14 shows the results obtained for configuration B featuring an intermittent thermoacoustic instability at an oscillation of approximately 205 Hz. The computed time series shown in Fig. 14a demonstrates the intermittent behavior that manifests in the pressure signal. A distinct oscillating frequency is observable that grows in amplitude. At a certain amplitude level, the oscillation breaks down and starts to grow again. With respect to the time series shown in Fig. 13a, larger pressure fluctuations are reached. Compared to the pressure spectrum shown in Fig. 13b for the stable configuration A, an elevated SPL is reached in Fig. 14 with a peak amplitude of approximately 140 dB. The resulting SPL peak amplitude measured in the experiments is correctly reproduced by LES, with a difference of less than 5 dB. The rest of the spectral sound pressure distribution is also well reproduced by the simulation with a broad hump around 1000 Hz and a second smaller one at about 1750 Hz.

Using LES to simulate the spectral distribution of the sound pressure in presence of a thermoacoustic instability is a challenging task. The peak frequency and the peak amplitude significantly depend on the nonlinear coupling between acoustics and flame dynamics. In the respective sound pressure spectrum, this manifests by a peak at the frequency of the instability. The fully compressible LES strategy coupled with CBSBC is, however, capable of resolving directly both contributions and consequently also their nonlinear interaction. The main difference observed in configuration B is the spread of spectral energy around the peak frequency, which is much larger in the simulation than in the experiment. This might be due to the slight difference in the mean reaction zone shape already noticed in Fig. 9. But it is also worth recalling that regime B is unstable by intermittence, meaning that the system does not reach a well defined limit cycle at a constant oscillation frequency and amplitude. The lock on of the instability frequency with the combustor resonant frequency is only achieved intermittently. This is a challenging configuration, in which subtle changes of the flow alter the thermoacoustic state of the system. Differences in turbulence might be the origin of the broader peak observed in the simulation.

The reader is reminded that this simulation is carried out by modifying only the reflection coefficient at the numerical domain outlet with the model shown in Fig. 7 (orange). This change is enough to reproduce the thermoacoustic instability in the LES with yet a reasonable match with experiments of the spectral content below 2000 Hz.

In addition to the pressure signal measured by microphone MC located in the combustion chamber, the signals measured by the microphones MP in the plenum and ME in the exhaust tube (see Fig. 1) are also compared to the computed data for configuration B. Note that the LES domain does not comprise the locations of MP and ME. The pressure signals needed for computing the respective sound pressure spectra cannot be extracted directly from the LES. Instead, the pressure time series are reconstructed from the state-space model used within the CBSBC. Therefore, the characteristic acoustic waves leaving the LES domain are stored during the computation. In an additional postprocessing step, these signals are used as input signals to simulate the boundary state-space model forward in time and thus compute the pressure signal at a given location. The resulting spectra are shown in Fig. 15. The sound pressure spectrum measured by microphone MP located in the plenum exhibits smaller pressure amplitudes over all frequencies compared to the signal measured by microphone MC in the combustion chamber. This is correctly predicted by the reconstructed numerical spectrum in Fig. 15a, even though certain differences are observed for frequencies higher than 1000 Hz. The reconstruction of the signal in the exhaust tube at the microphone location ME is in very good agreement with the measured spectrum in Fig. 15b. The reconstructed peak amplitude

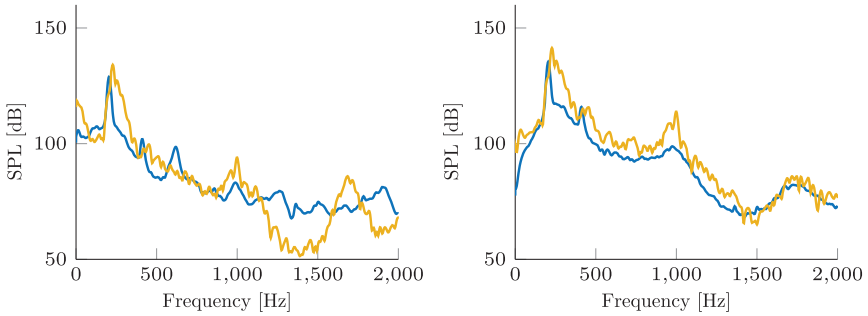

a) Plenum microphone MP b) Exhaust tube microphone ME

Fig. 15 Sound pressure spectrum of the intermittent unstable configuration B in a) the plenum, and b) the exhaust tube. SPL measurements (blue) and CBSBC reconstruction (yellow).

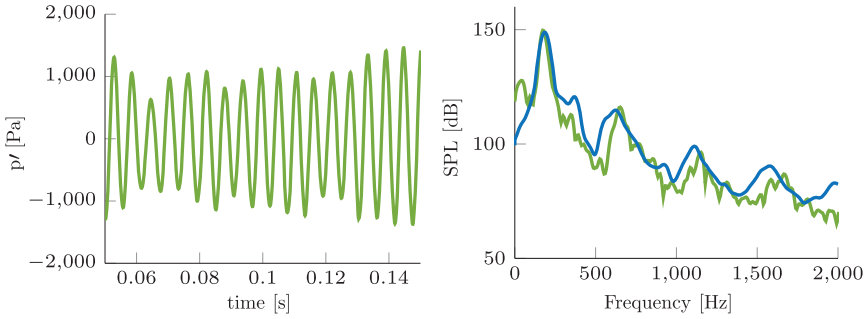

a) LES pressure time series b) Sound pressure spectrum

Fig. 16 LES pressure time series and sound pressure spectrum at the limit cycle of the unstable configuration C. SPL measurements (blue) and LES results (green) for microphone MC.

Downloaded by BIBLIOTHEK DER TU MUENCHEN on June 19, 2018 | http://arc.aiaa.org | DOI: 10.2514/1.J056502

differs by about 4 dB from the measured one. The secondary bumps at around 1000 and 1600 Hz are well captured by the reconstructed spectrum. As already mentioned for the pressure spectra shown in Fig. 14, the main differences between the measured and reconstructed spectra in the plenum and exhaust tube are the width of the pressure peak of the thermoacoustic instability.

It is emphasized that the explained reconstruction procedure would not be applicable for TDIBC like they are used, for example, by Lourier et al. [32], in which the acoustic boundary impedances are modeled globally. Yet the used CBSBC describes duct sections within the state-space model as spatially discretized elements on which an advection equation is solved numerically. The according state variables may be assessed at every discretized element. Therefore, the CBSBC provides also spatial information of the state variables within the boundary model. However, the reconstructed pressure time series directly depend on the input time series (i.e., the extracted characteristic waves at the LES domain boundary). Errors made in the LES propagate directly into the reconstructed time series. Nevertheless, the overall good agreement between measured and reconstructed sound pressure spectrum proves that the CBSBC allows to reconstruct the main features of the measured signals even out of the LES numerical domain.

Last, the sound pressure spectrum obtained from LES (green) is compared to the measured one (blue) in configuration C at the limit cycle of the instability in Fig. 16. The thermoacoustic instability has a peak frequency of 185 Hz where the SPL reaches 150 dB in the combustion chamber. The LES now well reproduces not only the correct peak value of the pressure oscillation but also the same shape of the power spectral distribution around this frequency. The self-sustained oscillation reaches in this case a much larger oscillation amplitude of $u'/\bar{u} = 0.7$ at the hot-wire location in the injection tube. Compared to the intermittent configuration B, a well-defined limit cycle is reached in configuration C. In this case, reproducing turbulent fluctuations is of less importance for the determination of the exact thermoacoustic state around the instability frequency. This may explain why the shape of the spectral distribution is better reproduced in configuration C compared to the intermittent state B. However, in the region above 500 Hz, a slight shift of the LES results to higher frequencies is observable. Again, this is probably due to the uncertainties regarding the temperatures in the exhaust tube region. If the mean gas temperature in the CBSCB model is overestimated, a shift to higher frequencies results.

Compared to the stable configuration A without exhaust tube ($L = 0$) and a peak frequency around 500 Hz, the distinctively lower value of the peak frequency in configuration C is explained by the elongated cavity ($L = 440$ mm) that shifts the acoustic modes to lower frequencies. As for configuration B, the instability in the LES is only provoked through a change of the outlet reflection condition of the numerical domain according to the model shown in Fig. 7 (green). Also for configuration C, in which the thermoacoustic instability is even more pronounced than in configuration B, the compressible LES coupled to CBSBC reproduces accurately the measured data for the sound pressure spectral distribution.

V. Conclusions

In the present study, the spectral sound pressure distribution of a confined lab-scale swirl combustor has been investigated by combining experiments and simulations. The flowfield and the mean reaction zone shape have been characterized as well as the acoustic fields for thermoacoustic stable, intermittently unstable, and unstable states of the test rig. The burner is operated with a methane/air mixture of constant flow injection conditions; the stability is only varied by changing the exhaust tube length. The turbulent flowfield, the flame, and the acoustics are resolved by performing fully compressible large-eddy simulation (LES) computations. It has been shown that the correct description of the complex acoustic boundary conditions from the test rig in the numerical approach is of crucial importance to correctly predict the resulting sound pressure spectrum and the sound level. The CBSBC formulation has proven itself to be very convenient for the description of the acoustic boundaries in the computational approach. They allow the correct modeling of the

different experimental configurations investigated without resolving all parts of the test rig within the LES numerical domain. Consequently, the thermoacoustically stable as well as the unstable combustion regimes could be well reproduced by a simple reformulation of the boundary inherent state-space model. The acoustic pressure fluctuations are extracted via a characteristics-based filter from the compressible LES. Accordingly, computed sound pressure spectra have been compared to the measured spectra. Excellent qualitative and quantitative agreement of resulting sound pressure spectra has been achieved for stable and unstable working conditions. Slight differences were identified for the intermittent unstable regime, probably due to difficulties in reproducing the same turbulent flow and reacting fields in the LES. But even in this case, the developed strategy could reproduce the main spectral features of the measured data with a fairly good fidelity. This holds not only for the combustion chamber that is comprised in the LES domain. Also the sound pressure spectra within the plenum and exhaust tube, which are located outside the numerical domain, could be reconstructed from the boundary state-space model.

Downloaded by BIBLIOTHEK DER TU MUENCHEN on June 19, 2018 | http://arc.aiaa.org | DOI: 10.2514/1.J056502

Acknowledgments

The authors acknowledge financial support by the German Research Foundation, project PO 710/16-1, and by the Agence Nationale de la Recherche, NOISEDYN project (ANR-14-CE35-0025-01). This project also has received funding from the European Union's Horizon 2020 Research and Innovation Programme under the Marie Sklodowska-Curie grant agreement number 643134. Moreover, the authors gratefully acknowledge the Gauss Centre for Supercomputing (GCS) for funding this project by providing computing time on the GCS Supercomputer SuperMUC at Leibniz Supercomputing Centre. The authors would also like to acknowledge Christian Kraus from Institut de Mécanique des Fluides de Toulouse for pointing out the incompatibility of the Wall Adapting Linear Eddy (WALE) model model and wall functions.

References

[1] Dowling, A. P., and Mahmoudi, Y., "Combustion Noise," *Proceedings of the Combustion Institute*, Vol. 35, No. 1, 2015, pp. 65–100. doi:10.1016/j.proci.2014.08.016

[2] Burnley, V. S., and Culick, F. E., "Influence of Random Excitations on Acoustic Instabilities in Combustion Chambers," *AIAA Journal*, Vol. 38, No. 8, 2000, pp. 1403–1410. doi:10.2514/2.1116

[3] Strahle, W. C., "Combustion Noise," *Progress in Energy and Combustion Science*, Vol. 4, No. 3, 1978, pp. 157–176. doi:10.1016/0360-1285(78)90002-3

[4] Candel, S., Durox, D., Ducruix, S., Birbaud, A.-L., Noiray, N., and Schuller, T., "Flame Dynamics and Combustion Noise: Progress and Challenges," *International Journal of Aeroacoustics*, Vol. 8, No. 1, 2009, pp. 1–56. doi:10.1260/147547209786234984

[5] Ihme, M., "Combustion and Engine-Core Noise," *Annual Review of Fluid Mechanics*, Vol. 49, Jan. 2017, pp. 277–310. doi:10.1146/annurev-fluid-122414-034542

[6] Marble, F. E., and Candel, S. M., "Acoustic Disturbance from Gas Non-Uniformities Convected Through a Nozzle," *Journal of Sound and Vibration*, Vol. 55, No. 2, 1977, pp. 225–243. doi:10.1016/0022-460X(77)90596-X

[7] Schuller, T., Durox, D., and Candel, S., "Dynamics of and Noise Radiated by a Perturbed Impinging Premixed Jet Flame," *Combustion and Flame*, Vol. 128, Nos. 1–2, 2002, pp. 88–110. doi:10.1016/S0010-2180(01)00334-0

[8] Strahle, W. C., "On Combustion Generated Noise," *Journal of Fluid Mechanics*, Vol. 49, No. 2, 1971, pp. 399–414. doi:10.1017/S0022112071002167

[9] Ihme, M., Pitsch, H., and Bodony, D., "Radiation of Noise in Turbulent Non-Premixed Flames," *Proceedings of the Combustion Institute*, Vol. 32, No. 1, 2009, pp. 1545–1553. doi:10.1016/j.proci.2008.06.137

[10] Rajaram, R., and Lieuwen, T., "Acoustic Radiation from Turbulent Premixed Flames," *Journal of Fluid Mechanics*, Vol. 637, Oct. 2009, pp. 357–385. doi:10.1017/S0022112009990681

[11] Hirsch, C., Wäsle, J., Winkler, A., and Sattelmayer, T., "A Spectral Model for the Sound Pressure from Turbulent Premixed Combustion," *Proceedings of the Combustion Institute*, Vol. 31, No. 1, 2007, pp. 1435–1441. doi:10.1016/j.proci.2006.07.154

[12] Schlimpert, S., Koh, S., Pausch, K., Meinke, M., and Schröder, W., "Analysis of Combustion Noise of a Turbulent Premixed Slot Jet Flame," *Combustion and Flame*, Vol. 175, Jan. 2017, pp. 292–306. doi:10.1016/j.combustflame.2016.08.001

[13] Winkler, A., Wäsle, J., Hirsch, C., and Sattelmayer, T., "Peak Frequency Scaling of Combustion Noise From Premixed Flames," *Proceedings of the 13th International Congress on Sound and Vibration*, The International Inst. of Acoustics and Vibration (IIAV), Auburn, AL, 2006.

[14] Clavin, P., and Siggia, E. D., "Turbulent Premixed Flames and Sound Generation," *Combustion Science and Technology*, Vol. 78, Nos. 1–3, 1991, pp. 147–155. doi:10.1080/00102209108951745

[15] Mahan, J. R., and Karchmer, A., "Combustion and Core Noise," *Noise Sources*, Vol. 1, Aeroacoustics of Flight Vehicles: Theory and Practice, NASA, 1991, pp. 483–517.

[16] Bellucci, V., Schuermans, B., Nowak, D., Flohr, P., and Paschereit, C. O., "Thermoacoustic Modeling of a Gas Turbine Combustor Equipped with Acoustic Dampers," *Journal of Turbomachinery*, Vol. 127, No. 2, 2005, pp. 372–379. doi:10.1115/1.1791284

[17] Weyermann, F., Hirsch, C., and Sattelmayer, T., "Influence of Boundary Conditions on the Noise Emission of Turbulent Premixed Swirl Flames," *Combustion Noise*, edited by J. Janicka, and A. Schwarz, Springer–Verlag, Berlin, 2009, pp. 161–188.

[18] Muthukrishnan, M., Strahle, W. C., and Neale, D. H., "Separation of Hydrodynamic, Entropy, and Combustion Noise in a Gas Turbine Combustor," *AIAA Journal*, Vol. 16, No. 4, 1978, pp. 320–327. doi:10.2514/3.60895

[19] Habisreuther, P., Bender, C., Petsch, O., Büchner, H., and Bockhorn, H., "Prediction of Pressure Oscillations in a Premixed Swirl Combustor Flow and Comparison to Measurements," *Flow, Turbulence and Combustion*, Vol. 77, Nos. 1–4, 2006, pp. 147–160. doi:10.1007/s10494-006-9041-7

[20] Lamraoui, A., Richecoeur, F., Schuller, T., and Ducruix, S., "A Methodology for on the Fly Acoustic Characterization of the Feeding Line Impedances in a Turbulent Swirled Combustor," *Journal of Engineering for Gas Turbines and Power*, Vol. 133, No. 1, 2011, Paper 011504. doi:10.1115/1.4001987

[21] Grimm, F., Ewert, R., Dierke, J., Reichling, G., Noll, B., and Aigner, M., "Efficient Combustion Noise Simulation of a Gas Turbine Model Combustor Based on Stochastic Sound Sources," American Soc. of Mechanical Engineers Paper GT2015-42390, New York, 2015. doi:10.1115/GT2015-42390

[22] Zhang, F., Habisreuther, P., Bockhorn, H., Nawroth, H., and Paschereit, C. O., "On Prediction of Combustion Generated Noise with the Turbulent Heat Release Rate," *Acta Acustica United with Acustica*, Vol. 99, No. 6, 2013, pp. 940–951. doi:10.3813/AAA.918673

[23] Silva, C. F., Leyko, M., Nicoud, F., and Moreau, S., "Assessment of Combustion Noise in a Premixed Swirled Combustor via Large-Eddy Simulation," *Computers & Fluids*, Vol. 78, April 2013, pp. 1–9. doi:10.1016/j.compfluid.2010.09.034

[24] Kings, N., Tao, W., Scouflaire, P., Richecoeur, F., and Ducruix, S., "Experimental and Numerical Investigation of Direct and Indirect Combustion Noise Contributions in a Lean Premixed Laboratory Swirled Combustor," *Proceedings of the ASME Turbo Expo 2016: Turbomachinery Technical Conference and Exposition*, American Soc. of Mechanical Engineers Paper GT2016-57848, New York, 2016. doi:10.1115/GT2016-57848

[25] Lourier, J. M., Stöhr, M., Noll, B., Werner, S., and Fiolitakis, A., "Scale Adaptive Simulation of a Thermoacoustic Instability in a Partially Premixed Lean Swirl Combustor," *Combustion and Flame*, Vol. 183, Sept. 2017, pp. 343–357. doi:10.1016/j.combustflame.2017.02.024

[26] Flemming, F., Sadiki, A., and Janicka, J., "Investigation of Combustion Noise Using a LES/CAA Hybrid Approach," *Proceedings of the Combustion Institute*, Vol. 31, No. 2, 2007, pp. 3189–3196. doi:10.1016/j.proci.2006.07.060

[27] Bui, T., Schröder, W., and Meinke, M., "Numerical Analysis of the Acoustic Field of Reacting Flows via Acoustic Perturbation Equations," *Computers & Fluids*, Vol. 37, No. 9, 2008, pp. 1157–1169. doi:10.1016/j.compfluid.2007.10.014

[28] Hoeijmakers, M., Kornilov, V., Lopez Arteaga, I., de Goey, P., and Nijmeijer, H., "Intrinsic Instability of Flame-Acoustic Coupling,"

Combustion and Flame, Vol. 161, No. 11, 2014, pp. 2860–2867. doi:10.1016/j.combustflame.2014.05.009

[29] Bomberg, S., Emmert, T., and Polifke, W., "Thermal Versus Acoustic Response of Velocity Sensitive Premixed Flames," *Proceedings of the 35th Symposium on Combustion*, Vol. 35, Combustion Inst., Pittsburgh, PA, 2014. doi:10.1016/j.proci.2014.07.032

[30] Courtine, E., Selle, L., and Poinsot, T., "DNS of Intrinsic Thermoacoustic Modes in Laminar Premixed Flames," *Combustion and Flame*, Vol. 162, No. 11, 2015, pp. 4331–4341. doi:10.1016/j.combustflame.2015.07.002

[31] Silva, C. F., Merk, M., Komarek, T., and Polifke, W., "The Contribution of Intrinsic Thermoacoustic Feedback to Combustion Noise and Resonances of a Confined Turbulent Premixed Flame," *Combustion and Flame*, Vol. 182, Aug. 2017, pp. 269–278. doi:10.1016/j.combustflame.2017.04.015

[32] Lourier, J.-M., Noll, B., and Aigner, M., "Large Eddy Simulation of a Thermoacoustic Instability Within a Swirl-Stabilized Burner Using Impedance Boundary Conditions," *Proceedings of the ASME Turbo Expo 2014: Turbine Technical Conference and Exposition*, American Soc. of Mechanical Engineers Paper GT2014-26200, New York, 2014.

[33] Tran, N., Ducruix, S., and Schuller, T., "Damping Combustion Instabilities with Perforates at the Premixer Inlet of a Swirled Burner," *Proceedings of the Combustion Institute*, Vol. 32, No. 2, 2009, pp. 2917–2924. doi:10.1016/j.proci.2008.06.123

[34] Tran, N., Ducruix, S., and Schuller, T., "Passive Control of the Inlet Acoustic Boundary of a Swirled Burner at High Amplitude Combustion Instabilities," *Journal of Engineering for Gas Turbines and Power*, Vol. 131, No. 5, 2009, Paper 051502. doi:10.1115/1.3078206

[35] Chung, J. Y., and Blaser, D. A., "Transfer Function Method of Measuring In-Duct Acoustic Properties. 2. Experiment," *Journal of the Acoustical Society of America*, Vol. 68, No. 3, 1980, pp. 914–921. doi:10.1121/1.384779

[36] Durox, D., Schuller, T., and Gandel, S., "Self-Induced Instability of a Premixed Jet Flame Impinging on a Plate," *Proceedings of the Combustion Institute*, Vol. 29, No. 1, 2002, pp. 69–75. doi:10.1016/S1540-7489(02)80013-X

[37] Schuller, T., Durox, D., and Candel, S., "Self-Induced Combustion Oscillations of Laminar Premixed Flames Stabilized on Annular Burners," *Combustion and Flame*, Vol. 135, No. 4, 2003, pp. 525–537. doi:10.1016/j.combustflame.2003.08.007

[38] Durox, D., Schuller, T., Noiray, N., Birbaud, A. L., and Candel, S., "Rayleigh Criterion and Acoustic Energy Balance in Unconfined Self-Sustained Oscillating Flames," *Combustion and Flame*, Vol. 156, No. 1, 2009, pp. 106–119. doi:10.1016/j.combustflame.2008.07.016

[39] Levine, H., and Schwinger, J., "On the Radiation of Sound from an Unflanged Circular Pipe," *Physical review*, Vol. 73, No. 4, 1948, pp. 383–406. doi:10.1103/PhysRev.73.383

[40] *The AVBP HandBook*, Centre Européen de Recherche et de Formation Avancée en Calcul Scientifique, and IMFT, Toulouse, France, 2008, http://www.cerfacs.fr/ [retrieved 16 Jan. 2018].

[41] Selle, L., Lartigue, G., Poinsot, T., Koch, R., Schildmacher, K.-U., Krebs, W., Prade, B., Kaufmann, P., and Veynante, D., "Compressible Large Eddy Simulation of Turbulent Combustion in Complex Geometry on Unstructured Meshes," *Combustion and Flame*, Vol. 137, No. 4, 2004, pp. 489–505. doi:10.1016/j.combustflame.2004.03.008

[42] Gicquel, L. Y. M., Staffelbach, G., and Poinsot, T., "Large Eddy Simulations of Gaseous Flames in Gas Turbine Combustion Chambers," *Progress in Energy and Combustion Science*, Vol. 38, No. 6, 2012, pp. 782–817. doi:10.1016/j.pecs.2012.04.004

[43] Nicoud, F., and Ducros, F., "Subgrid-Scale Stress Modelling Based on the Square of the Velocity Gradient Tensor," *Flow, Turbulence and Combustion*, Vol. 62, No. 3, 1999, pp. 183–200. doi:10.1023/A:1009995426001

[44] Colin, O., Ducros, F., Veynante, D., and Poinsot, T., "A Thickened Flame Model for Large Eddy Simulation of Turbulent Premixed Combustion," *Physics of Fluids A*, Vol. 12, No. 7, 2000, pp. 1843–1863. doi:10.1063/1.870436

[45] Franzelli, B., Riber, E., Sanjosé, M., and Poinsot, T., "A Two-Step Chemical Scheme for Kerosene–Air Premixed Flames," *Combustion and Flame*, Vol. 157, No. 7, 2010, pp. 1364–1373. doi:10.1016/j.combustflame.2010.03.014

[46] Jaensch, S., Sovardi, C., and Polifke, W., "On the Robust, Flexible and Consistent Implementation of Time Domain Impedance Boundary Conditions for Compressible Flow Simulations," *Journal of Computational Physics*, Vol. 314, 2016, pp. 145–159. doi:10.1016/j.jcp.2016.03.010

[47] Langella, I., Mahmoudi-Larimi, Y., Swaminathan, N., and Dowling, A., "Combustion Noise Analysis of Open Flames Using Incompressible LES," *22nd AIAA/CEAS Aeroacoustics Conference*, AIAA Paper 2016-2827, 2016. doi:10.2514/6.2016-2827

[48] Bailly, C., Bogey, C., and Candel, S., "Modelling of Sound Generation by Turbulent Reacting Flows," *International Journal of Aeroacoustics*, Vol. 9, Nos. 4–5, 2010, pp. 461–489. doi:10.1260/1475-472X.9.4-5.461

[49] Schwarz, A., and Janicka, J., *Combustion Noise*, Vol. 102, Fluid Mechanics and Its Applications, Springer, Dordrecht, 2009, pp. 147–174.

[50] Kopitz, J., Bröcker, E., and Polifke, W., "Characteristics-Based Filter for Identification of Acoustic Waves in Numerical Simulation of Turbulent Compressible Flow," *Proceedings of the 12th International Congress on Sound and Vibration*, Vol. 389, The International Inst. of Acoustics and Vibration (IIAV), Auburn, AL, July 2005, 00004.

[51] Fung, K.-Y., and Ju, H., "Time-Domain Impedance Boundary Conditions for Computational Acoustics and Aeroacoustics," *International Journal of Computational Fluid Dynamics*, Vol. 18, No. 6, 2004, pp. 503–511. doi:10.1080/10618560410001673515

[52] Schuermans, B., Luebcke, H., Bajusz, D., and Flohr, P., "Thermoacoustic Analysis of Gas Turbine Combustion Systems Using Unsteady CFD," *Proceedings of the ASME Turbo Expo*, American Soc. of Mechanical Engineers Paper GT2005-68393, New York, 2005. doi:10.1115/GT2005-68393

[53] Kaess, R., Huber, A., and Polifke, W., "A Time-Domain Impedance Boundary Condition for Compressible Turbulent Flows," *14th AIAA/CEAS Aeroacoustics Conference*, AIAA Paper 2008-2921, 2008. doi:10.2514/6.2008-2921

[54] Poinsot, T., and Lele, S. K., "Boundary Conditions for Direct Simulation of Compressible Viscous Flows," *Journal of Computational Physics*, Vol. 101, No. 1, 1992, pp. 104–129. doi:10.1016/0021-9991(92)90046-2

[55] Selle, L., Nicoud, F., and Poinsot, T., "Actual Impedance of Nonreflecting Boundary Conditions: Implications for Computation of Resonators," *AIAA Journal*, Vol. 42, No. 5, 2004, pp. 958–964. doi:10.2514/1.1883

[56] Polifke, W., Wall, C., and Moin, P., "Partially Reflecting and Non-Reflecting Boundary Conditions for Simulation of Compressible Viscous Flow," *Journal of Computational Physics*, Vol. 213, No. 1, 2006, pp. 437–449. doi:10.1016/j.jcp.2005.08.016

[57] Jaensch, S., Merk, M., Gopalakrishnan, E., Bomberg, S., Emmert, T., Sujith, R., and Polifke, W., "Hybrid CFD/Low-Order Modeling of Nonlinear Thermoacoustic Oscillations," *Proceedings of the Combustion Institute*, Vol. 36, No. 3, 2017, pp. 3827–3834. doi:10.1016/j.proci.2016.08.006

[58] Tudisco, P., Ranjan, R., Menon, S., Jaensch, S., and Polifke, W., "Application of the Time-Domain Admittance Boundary Condition to Large-Eddy Simulation of Combustion Instability in a Shear-Coaxial, High Pressure Combustor," *Flow, Turbulence and Combustion*, Vol. 99, No. 1, 2017, pp. 185–207. doi:10.1007/s10494-017-9804-3

[59] Franzelli, B., Riber, E., Gicquel, L. Y. M., and Poinsot, T., "Large Eddy Simulation of Combustion Instabilities in a Lean Partially Premixed Swirled Flame," *Combustion and Flame*, Vol. 159, No. 2, 2012, pp. 621–637. doi:10.1016/j.combustflame.2011.08.004

[60] Schuller, T., Durox, D., and Candel, S., "A Unified Model for the Prediction of Laminar Flame Transfer Functions: Comparisons Between Conical and V-Flame Dynamics," *Combustion and Flame*, Vol. 134, Nos. 1–2, 2003, pp. 21–34. doi:10.1016/S0010-2180(03)00042-7

[61] Emmert, T., Jaensch, S., Sovardi, C., and Polifke, W., "taX—A Flexible Tool for Low-Order Duct Acoustic Simulation in Time and Frequency Domain," *Proceedings of the 7th Forum Acusticum*, Deutsche Gesellschaft für Akustik (DEGA), Berlin, 2014.

C. Bailly
Associate Editor

Downloaded by BIBLIOTHEK DER TU MUENCHEN on June 19, 2018 | http://arc.aiaa.org | DOI: 10.2514/1.J056502

Combustion Theory and Modelling, 2018
Vol. 22, No. 3, 613–634, https://doi.org/10.1080/13647830.2018.1443517

Taylor & Francis
Taylor & Francis Group

Check for updates

Identification of flame transfer functions in the presence of intrinsic thermoacoustic feedback and noise

Stefan Jaensch, Malte Merk*, Thomas Emmert and Wolfgang Polifke

Fakultät für Maschinenwesen, Technische Universität München, Garching, Germany

(*Received 31 May 2017; accepted 9 February 2018*)

The Large Eddy Simulation/System Identification (LES/SI) approach is a general and efficient numerical method for deducing a Flame Transfer Function (FTF) from the LES of turbulent reacting flow. The method may be summarised as follows: a simulated flame is forced with a broadband excitation signal. The resulting fluctuations of the reference velocity and of the global heat release rate are post-processed via SI techniques in order to estimate a low-order model of the flame dynamics. The FTF is readily deduced from the low-order model. The SI method most frequently applied in aero- and thermo-acoustics has been Wiener–Hopf Inversion (WHI). This method is known to yield biased estimates in situations with feedback, thus it was assumed that non-reflective boundary conditions are required to generate accurate results with the LES/SI approach. Recent research has shown that the FTF is part of the so-called Intrinsic ThermoAcoustic (ITA) feedback loop. Hence, identifying an FTF from a compressible LES is always a closed-loop problem, and consequently one should expect that the WHI would yield biased results. However, several studies proved that WHI results compare favourably with validation data. To resolve this apparent contradiction, a variety of identification methods are compared against each other, including models designed for closed-loop identification. In agreement with theory, we show that the estimate given by WHI does not converge to the *actual* FTF. Fortunately, the error made is small if excitation amplitudes can be set such that the signal-to-noise ratio is large, but not large enough to trigger nonlinear flame dynamics. Furthermore, we conclude that non-reflective boundary conditions are not essentially necessary to apply the LES/SI approach.

Keywords: system identification; network models; thermoacoustics; flame transfer function; Box–Jenkins model

1. Introduction

The development of low-emission gas turbine combustion technology for propulsion or power generation is often hampered by the occurrence of thermoacoustic instabilities. A self-amplifying feedback between the unsteady heat release of the flame and the acoustic field can result in large oscillations of the flow variables. These oscillations can cause serious damage to an engine.

Thermoacoustic network models have proven themselves as a useful tool for predicting frequencies, growth rates, and mode shapes of thermoacoustic instabilities at negligible computational cost [1–6]. Finite-element based models of acoustics are advantageous for more complex combustor geometries or higher frequencies [7–9]. Hybrid formulations combine advantages of both methods [10]. All these approaches require information on the flame dynamics as model input. In the low-amplitude, low-frequency regime, such

*Corresponding author: merk@tfd.mw.tum.de

© 2018 Informa UK Limited, trading as Taylor & Francis Group

This is the authors accepted manuscript of an article published as the version of record in Combustion Theory and Modelling © Taylor & Francis https://doi.org/10.1080/13647830.2018.1443517

information is represented via a Flame Transfer Function (FTF), which relates fluctuations of flow variables upstream of the flame to the resulting fluctuations of the global heat release rate.

If the fuel injection is acoustically 'stiff' and located only a short distance, i.e. a fraction of pertinent acoustic wavelengths, upstream of the flame, an FTF that relates upstream flow velocity to heat release is sufficient to describe the relevant flame dynamics fully [11]. Such an FTF, which is mandatory to predict thermoacoustic stability, can be determined experimentally by forcing a flame with a harmonic signal at several distinct frequencies. The resulting fluctuations of velocity at a reference position upstream of the flame and of global heat release rate are measured. Finally, gain and phase of the FTF at the forcing frequencies are calculated via a Fourier transform.

In principle, the very same procedure can be applied to a numerical simulation of a flame, but necessitates a large number of compute runs, i.e. one simulation per frequency. For configurations of applied interest, the accurate numerical computation of a turbulent flame requires Large Eddy Simulation (LES), which is computationally demanding. It follows that the frequency-by-frequency determination of an FTF from LES data is prohibitively expensive for many applications.

Polifke [12] proposed forcing the flame simulation with a broadband signal and to use tools from System Identification (SI) [13–15] in order to determine the FTF from the time series data. This approach allows a reduced-order model to be determined for the FTF from a single simulation run, with significant savings in computational costs. In the majority of applications to date, SI of flame dynamics relied on correlation analysis, and in particular inversion of the Wiener–Hopf equation, which relates auto- and cross-correlation of input and output signals to each other via the impulse response [16–26].

This procedure is based on the minimisation of the correlation between input signal and noise contribution and yields an accurate and unbiased estimate of the FTF as long as the input signal and the noise contribution are uncorrelated in the system under study. This is for example the case for an open-loop system. However, if a feedback mechanism is present, as for example under closed-loop conditions, a correlation between input signal and noise contribution results. It is known from literature on SI that in this case the Wiener–Hopf Inversion (WHI) yields incorrect results [13–15]. In order to avoid possible feedback and thus closed-loop conditions, non-reflective Boundary Conditions (BCs) were deemed necessary in LES to generate accurate results via the WHI procedure [12,18,27,28].

Recently, Bomberg, Emmert, and Polifke [29] have shown that the FTF is part of the ITA feedback loop, which is illustrated and explained in Figure 1. Consequences of ITA feedback, such as unstable thermoacoustic modes in an anechoic environment, thermoacoustic modes that are not related to acoustic cavity modes, convective scaling of

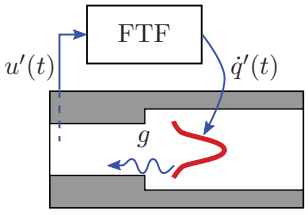

Figure 1. ITA feedback: a velocity fluctuation $u'(t)$ causes a fluctuation of the global heat release rate $\dot{q}'(t)$. The fluctuation of the heat release rate generates an acoustic wave g travelling in the upstream direction, where it modulates the velocity at the reference location, thereby closing the feedback loop.

This is the authors accepted manuscript of an article published as the version of record in Combustion Theory and Modelling © Taylor & Francis https://doi.org/10.1080/13647830.2018.1443517

thermoacoustic frequencies, and large instability potentiality as well as singularities of the flame scattering matrix have been explored in a series of papers [30–37]. Note that the ITA feedback loop does not rely on reflection of acoustic waves at the domain boundaries. It is inevitably present in thermoacoustic systems with a velocity-sensitive flame and is inherently resolved by a fully compressible flow simulation of a flame. Non-reflecting acoustic boundary conditions do not eliminate ITA feedback, but may on the contrary render a stable ITA mode unstable [36,37]. Hence, identifying the FTF from a compressible LES is unavoidably a closed-loop problem. To conclude, the literature on SI suggests that WHI should not be capable of accurately estimating the FTF from a compressible LES due to the inherent and unavoidable ITA feedback.

Furthermore, LES of a turbulent flame explicitly resolves large-scale turbulent fluctuations, which manifest themselves as noise, i.e. a broadband contribution to the output signal that is uncorrelated with the excitation signal. One should expect that noise will worsen the accuracy of SI, in particular if the signal-to-noise ratio (SNR) is small, and indeed Biagioli, Scarpato, and Syed [24] observed this problem in their LES/SI study of a turbulent swirling flame. An increase of the excitation amplitude will increase the SNR and thus can alleviate this problem. However, if the excitation is too strong, the flame response will exhibit nonlinear effects, which should be avoided in linear identification [12–15]. Again one might conclude that the LES/SI approach based on WHI should not be capable of providing accurate low-order models of flame dynamics. On the other hand, validation of WHI results against FTFs determined frequency-by-frequency (in experiment as well as in simulation) have repeatedly delivered very satisfactory agreement [18,22,33].

In the present work we investigate these apparent contradictions with a surrogate data model that simulates a thermoacoustic network model in the time domain. For generating surrogate time series data, a certain reference FTF is assumed *a priori*. The knowledge on the reference or *actual* FTF can be used in the following to assess directly the quality of the models that are identified from the surrogate time series data. A perfectly identified model would coincide exactly with the *actual* FTF, which is the *true* solution, as it is used for generating the surrogate data in the first place. Note that the *true* solution is usually unknown when LES data is used. So the advantage of the surrogate data approach is that the *actual* FTF of the model is known and can be used as reference. In consistence with the theory [15] we demonstrate that results of the WHI do not converge to the actual FTF even for very long time series. On the other hand, if the system identification is based on the so-called Box–Jenkins (BJ) model, the error decays for long time series, even in the presence of feedback. We will demonstrate that the error made by the WHI depends on the amplitude of the excitation signal relative to the noise level. If the SNR is sufficiently large, the error is small – which is why the WHI did repeatedly provide satisfactory results when applied to real data. This resolves the paradox noted above. Our results also indicate that acoustic reflection at the system boundaries does not introduce additional errors. Therefore, any boundary condition that stabilises the simulation can be used for the LES/SI approach. This extends significantly the range of configurations where the LES/SI approach can be applied.

The paper is organised as follows: in the next section, we discuss the thermoacoustic network model used to generate the surrogate data in detail. The theory behind SI is addressed in Section 3. In Section 4 the results are illustrated by means of numerical examples.

This is the authors accepted manuscript of an article published as the version of record in Combustion Theory and Modelling © Taylor & Francis https://doi.org/10.1080/13647830.2018.1443517

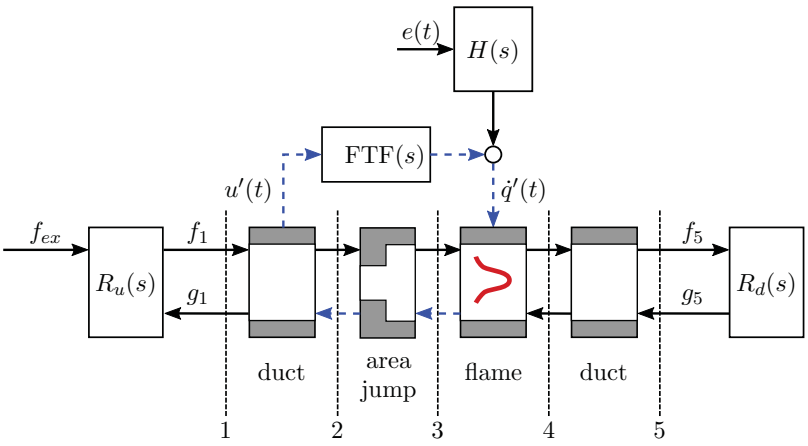

Figure 2. Thermoacoustic network model investigated. The ITA feedback is highlighted with the dashed arrows.

2. Low-order modelling of thermoacoustic systems

As discussed above, the present study is based on surrogate data. The surrogate data is generated with a network model mimicking an LES configuration that is set up to generate time series data for SI. The surrogate model used in this study represents a turbulent swirl burner that was designed and investigated by Komarek and Polifke [38]. This burner is particularly suited for the present investigation, because ITA feedback plays an important role in its dynamics and thermoacoustic stability [29,36,37].

The surrogate network model was originally formulated by Silva, Merk, Komarek, and Polifke [37] and may divided into two main parts (see Figure 2): (1) a model for the flame dynamics, represented by the FTF; and (2) a model for the acoustics. In the context of the present study, the most significant advantage of a surrogate data approach is that the *actual* FTF is known precisely and can serve as reference for the *estimation* of the FTF from time series generated with the surrogate model. Furthermore, the computational cost for generating even very long time series is negligible, such that one can explore the asymptotic behaviour of various system identification strategies.

2.1. *Modelling of the flame dynamics*

We model the flame response using a Finite Impulse Response (FIR) model

$$\dot{q}'_{u'}(t) = \sum_{i=0}^{n_b} b_i u'(t - i\Delta t), \tag{1}$$

with the n_b impulse response coefficients b_i, the model time step Δt, and $\dot{q}'_{u'}(t)$ as the fluctuation of the global heat release rate induced by the velocity fluctuation $u'(t)$ upstream of the flame.

The FIR model accounts for the physical effects that dominate the flame response. Compact, perfectly premixed flames are known to be *velocity sensitive*, i.e. the flame responds predominantly to axial velocity fluctuations upstream of the flame (see e.g. [29,33]). The FIR model accounts for this as the fluctuation of the global heat release is deduced from the fluctuation of the reference velocity.

This is the authors accepted manuscript of an article published as the version of record in Combustion Theory and Modelling © Taylor & Francis https://doi.org/10.1080/13647830.2018.1443517

The lagged velocity signal used by the FIR model accounts for the convective nature of the flame response. In order to understand the physics behind the flame response it is convenient to consider an impulse velocity fluctuation imposed on the flame, as proposed by Blumenthal, Subramanian, Sujith, and Polifke [39].

A velocity perturbation at the flame foot causes a distortion of the flame at the anchoring point. The distortion is convected along the flame front and causes a fluctuation of the global heat release rate. Simultaneously, as discussed in [39], starting from the anchoring point the unperturbed flame position and shape are restored. The restoration process is also a convective effect. Once the perturbative and the restorative effects are convected through the flame, the fluctuation of the global heat release rate vanishes. Therefore, the response of the flame to a velocity impulse is *finite* and can be modelled with a *finite* impulse response model. The length of the impulse response is given as

$$\tau = n_b \Delta t. \tag{2}$$

This allows the number of coefficients n_b of the FIR model to be determined:

$$n_b = \frac{\tau}{\Delta t}. \tag{3}$$

Therefore, the use of an FIR model is on a profound, physically motivated basis as the model design corresponds to the convective nature of the effects that govern the dynamic response of the flame. Note that the length τ of the impulse response describes the 'memory' of the FIR model. If it is chosen shorter than the physical time delay of the flame impulse response τ, the FTF is said to be under-resolved and the flame response is insufficiently described. If the flame response time is chosen too long, the impulse response coefficients b_i start to describe stochastic perturbations if noise is present. From LES the physical time delay of the flame impulse response is known as $\tau = 0.15$ s. The LES time series data is down-sampled to $\Delta t = 5 \times 10^{-4}$ s yielding a filter length $n_b = 30$.

The coefficients b_i of the FIR model used by the network model were determined via SI with WHI, based on LES data of the turbulent swirl burner generated by L. Tay-Wo-Chong [22]. In Figure 3, the corresponding FTF is shown and compared against experimental measurements.

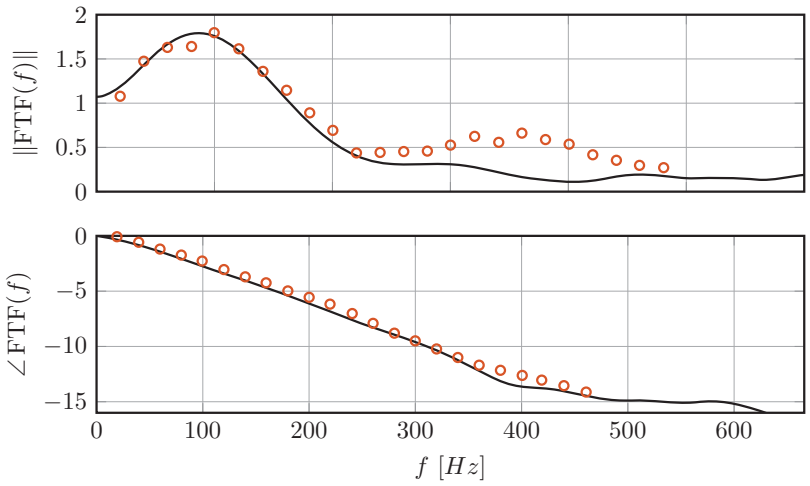

Figure 3. Gain (top) and phase (bottom) of the FTF. o: experimentally determined FTF [22]; ——: identified FTF used to generate the surrogated time series.

This is the authors accepted manuscript of an article published as the version of record in Combustion Theory and Modelling © Taylor & Francis https://doi.org/10.1080/13647830.2018.1443517

The purpose of this figure is to demonstrate that the identified FTF is qualitatively correct (overall low-pass, but with excess gain) and quantitatively accurate in the frequency range where instabilities were observed (around 100 Hz). At this point it is emphasised that deviations or biases between the identified FIR and the flame dynamics in experiment are quite irrelevant in the following. In the framework of the surrogate data model, the identified FIR is the *true* solution that needs to be recovered. An FIR model of realistic order, however, ensures values of, for example, time series length or SNR that are comparable to values that could be found when the methods are applied on LES data.

For turbulent flames, unsteady fluctuations of the global heat release rate $\dot{q}'_{\text{turb}}(t)$ result from turbulent fluctuations in the vicinity of the flame front, unrelated to any excitation signal. These fluctuations generate direct combustion noise [37,40,41]. We model this effect in the present work using an FIR filter with a white noise input $e(t)$

$$\dot{q}'_{\text{turb}}(t) = \sum_{i=0}^{n_c} c_i e(t - i\,\Delta t), \tag{4}$$

with the n_c impulse response coefficients of the noise model c_i. Again, the coefficients of the model used to generate the surrogate data time series were determined by SI based on the LES data generated by Luis Tay-Wo-Chong [22]. From LES data the power spectral density of the combustion noise contribution is depicted in Figure 4. The peak frequency of the spectrum is at around 150 Hz, which is in agreement with the estimation of the source spectrum of the turbulent swirl burner by Weyermann [42], who employed the model of Hirsch *et al.* [43]. The spectral distribution shown is fitted by the model coefficients c_i in the time domain, the reference noise filter order is set to $n_c = 15$. For further details on the determination of the noise model and its validation, the reader is referred to [37].

Please note, in contrast to the FIR model used for the flame dynamics, i.e. the FTF, at the current state of understanding there is no fundamental justification for the use of an FIR model for the noise term. Further studies are needed to build a better understanding of the nature of turbulent combustion noise that is based on flow and combustion physics. This is beyond the scope of the present study. The only necessary requirement to obtain the results shown in Section 4 is that the noise signal is coloured. As shown in Figure 4, this requirement is fulfilled by the model used.

Altogether, in the network model used to generate the surrogate data the global heat release is modelled as

$$\begin{aligned}\dot{q}'(t) &= \dot{q}'_{u'}(t) + \dot{q}'_{\text{turb}}(t) \\ &= \sum_{i=0}^{n_b} b_i u'(t - i\,\Delta t) + \sum_{i=0}^{n_c} c_i e(t - i\,\Delta t).\end{aligned} \tag{5}$$

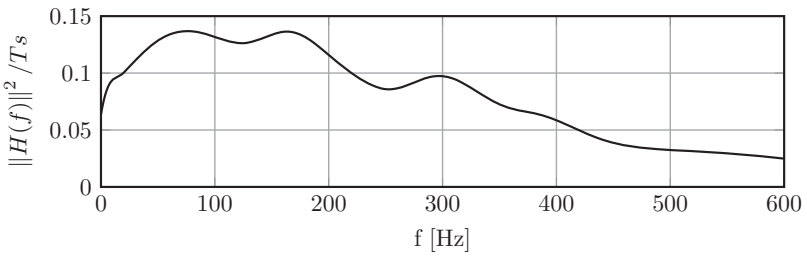

Figure 4. Power spectral density of the noise model used.

This is the authors accepted manuscript of an article published as the version of record in Combustion Theory and Modelling © Taylor & Francis https://doi.org/10.1080/13647830.2018.1443517

2.2. *Modelling of the acoustics*

The thermoacoustic network model employed in the present study to generate surrogate data is shown in Figure 2. The model is to represent an LES model of the burner test rig as one would use it to generate time series data for subsequent SI.

Acoustic waves are assumed to be plane, as the minimal acoustic wavelength observed is much larger then the cross-sectional length of the geometry. The waves are described in terms of the characteristic wave amplitudes

$$f = \frac{1}{2}\left(\frac{p'_A}{\bar{\rho}\bar{c}} + u'_A\right) \quad \text{and} \quad g = \frac{1}{2}\left(\frac{p'_A}{\bar{\rho}\bar{c}} - u'_A\right). \tag{6}$$

Here, p'_A and u'_A are the pressure and velocity fluctuations, respectively, $\bar{\rho}$ is the mean density, and $\bar{c}$ is the mean speed of sound. The mean flow properties vary in order to account for the different cross-sectional areas and flow temperature.

The area jump is assumed to be lossless and given as

$$\begin{bmatrix} g_2 \\ f_3 \end{bmatrix} = \begin{bmatrix} \dfrac{\alpha-1}{\alpha+1} & \dfrac{2}{\alpha+1} \\ \dfrac{2\alpha}{\alpha+1} & \dfrac{\alpha-1}{\alpha+1} \end{bmatrix} \begin{bmatrix} f_2 \\ g_3 \end{bmatrix} \tag{7}$$

with the area ratio $\alpha = A_2/A_3 = 0.13$. The indices refer to the interfaces between the elements of the network model and are defined in Figure 2.

The duct sections shown in Figure 2 represent a part of the annular flow section downstream of the swirler, and a part of the combustion chamber, respectively. Their length is much shorter than the minimal acoustic wavelengths considered in this investigation. Therefore, all duct sections are assumed to be acoustically compact, i.e. the phase change associated with wave propagation along the duct sections is neglected. Note that, owing to the neglected duct length in the surrogate data model, the acoustic eigenfrequencies are shifted to very high values. This has the benefit of avoiding possible linear instability at low frequencies caused by cavity acoustic modes. The *linear* model used to generate the surrogate data does not allow any conclusion on the identifiability of the FTF in the presence of a thermoacoustic instability. The behaviour and saturation of thermoacoustic instabilities is mainly governed by nonlinear mechanisms, which are not accounted for in the *linear* surrogate data model.

LES models for subsequent SI often impose non-reflective BCs [44]. Thus the boundaries of the surrogate model are assumed non-reflective, with the exception of Section 4.5, where the influence of the reflection coefficient on the accuracy of SI results is explored. At the inlet, the (broadband) excitation signal is imposed as characteristic wave f_{ex}.

The coupling of the flame dynamics and the acoustics is implemented using the Rankine–Hugoniot equations, i.e. the linearised one-dimensional momentum and energy equations evaluated over the flame

$$\begin{bmatrix} g_3 \\ f_4 \end{bmatrix} = \frac{1}{\zeta+1}\begin{bmatrix} 1-\zeta & 2 & \theta\bar{u}_3 \\ 2\zeta & \zeta-1 & \theta\zeta\bar{u}_3 \end{bmatrix} \begin{bmatrix} f_3 \\ g_4 \\ \dot{q}' \end{bmatrix}, \tag{8}$$

with $\zeta = \bar{\rho}_3\bar{c}_3/\bar{\rho}_4\bar{c}_4 = 2.57$ and $\theta = \bar{T}_4/\bar{T}_1 - 1 = 5.59$. $\bar{T}$ is the mean temperature.

This is the authors accepted manuscript of an article published as the version of record in Combustion Theory and Modelling © Taylor & Francis https://doi.org/10.1080/13647830.2018.1443517

Please note that by using the Rankine–Hugoniot equations to couple flame dynamics and acoustics, one includes the ITA feedback in the network model, as discussed in [29,33]. The ITA feedback loop is highlighted with the dashed arrows in Figure 2.

In the test rig, fuel is injected such that the equivalence ratio at the flame is assumed homogeneous and insensitive to acoustic fluctuations. Under such conditions, the generation of entropy waves by a premixed flame is of first order in the Mach number [45], which is quite small. Furthermore, entropy waves couple with acoustics only in regions of strong mean flow acceleration [40], which are absent downstream of the flame. It follows that one may neglect the influence of entropy waves on the thermoacoustics of the test rig.

3. System identification

The network model discussed in the previous section is used in Section 4 to investigate the influence of ITA feedback on the results of the identification. In the present section we introduce and discuss the SI methodology in detail.

The general objective of SI methods discussed is to deduce quantitatively accurate low-order models of the frequency dependent input–output behaviour of the system under study from (broadband) time series. The input–output behaviour of a system can be characterised with the transfer function, e.g. the FTF. In this particular case the input signal is the fluctuation of the reference velocity and the output signal is the fluctuation of the global heat release rate. SI allows the FTF to be deduced over a wide range of frequencies from data generated with a single simulation run.

The SI procedure comprises the following three steps.

(1) Generation of broadband time series. When identifying an FTF from an LES, this means imposing a broadband excitation on the simulation and recording the resulting fluctuations of the reference velocity u' and of the global heat release rate $\dot{q}'$. In the present study, we generate the broadband signal by running the thermoacoustic surrogate network model, described in the previous section, in the time domain.
(2) Selection of model structure with (unknown) parameters Θ. Although SI relies on a 'black box' approach, more accurate identification results are achieved in practice if the model structure corresponds to the physics of the system investigated. As discussed in Section 2.1, an FIR model is well suited to describe the flame dynamics, which is dominated by convective processes.
(3) Determination of the free parameters of the model by solving an optimisation problem.

The reminder of this section discusses steps (2) and (3) in detail. Step (1) is discussed later, in Section 4.

3.1. *Wiener–Hopf inversion*

As discussed in Section 2.1, an FIR model accounts in a natural manner for convective effects. Therefore, an FIR model structure is a plausible candidate for the identification of flame dynamics. It is given as

$$\hat{\tilde{q}}'(t, \mathbf{b}) = \sum_{i=0}^{\tilde{n}_b} \tilde{b}_i \tilde{u}'(t - i\,\Delta t) = \tilde{\boldsymbol{\phi}}(t)^{\mathrm{T}} \tilde{\mathbf{b}} \tag{9}$$

This is the authors accepted manuscript of an article published as the version of record in Combustion Theory and Modelling © Taylor & Francis https://doi.org/10.1080/13647830.2018.1443517

with

$$\tilde{\phi}(t) = \left[\tilde{u}'(t)\,\tilde{u}'(t-\Delta t)\,\cdots\,\tilde{u}'(t-\tilde{n}_b\Delta t)\right]^{\mathrm{T}} \tag{10}$$

$$\tilde{\mathbf{b}} = \left[\tilde{b}_0\,\tilde{b}_1\,\cdots\,\tilde{b}_{\tilde{n}_b}\right]^{\mathrm{T}}. \tag{11}$$

Here, $\tilde{n}_b$ is the number of model parameters $\tilde{b}_i$, and $\hat{\dot{q}}'$ is the fluctuation of the global heat release rate in response to the excitation as predicted by the model. This prediction depends on the parameter vector $\tilde{\mathbf{b}}$ and on the fluctuations of the reference velocity $\tilde{u}'$ resulting from the imposed excitation signal f_{ex}. Using the model (9) with an identified parameter vector, one can predict the fluctuation of the global heat release rate to an arbitrary velocity fluctuation. In order to determine the parameter vector $\tilde{\mathbf{b}}$, the fluctuations of the reference velocity $\tilde{u}'(t)$ imposed on the model are chosen to be identical to the measured fluctuations of the reference velocity $u'(t)$. In this case, the fluctuation of the global heat release rate $\hat{\dot{q}}'(t)$ predicted by the model should be close to the measured fluctuation of the global heat release rate $\dot{q}'(t)$. Formulated as a least squares optimisation problem, this yields

$$\min_{\mathbf{b}} J_{\mathrm{WHI}}(\mathbf{b}) = \min_{\mathbf{b}} \frac{1}{N}\sum_{i=0}^{N-1}\left(\hat{\dot{q}}'(i\,\Delta t,\mathbf{b}) - \dot{q}'(i\,\Delta t)\right)^2, \tag{12}$$

with the cost function $J_{\mathrm{WHI}}(\mathbf{b})$.

The solution of this optimisation problem, known as Wiener–Hopf inversion (WHI), is given as

$$\hat{\mathbf{b}} = \left(\Phi^{\mathrm{T}}\Phi\right)^{-1}\Phi^{\mathrm{T}}\mathbf{Y}, \tag{13}$$

with

$$\phi(t) = \left[u'(t)\,u'(t-\Delta t)\,\cdots\,u'(t-\tilde{n}_b\Delta t)\right]^{\mathrm{T}} \tag{14}$$

$$\Phi = \left[\phi(0)\,\phi(\Delta t)\,\cdots\,\phi(N\Delta t)\right]^{\mathrm{T}} \tag{15}$$

$$Y = \left[\dot{q}'(0)\,\dot{q}'(\Delta t)\,\cdots\,\dot{q}'(N\Delta t)\right]^{\mathrm{T}}. \tag{16}$$

Please note that the number of parameters $\tilde{n}_b$ has also to be determined. When identifying the FTF, as in the present study, the length can be calculated via the physical time delay of the flame impulse response τ according to Equation (3). Therefore, we choose $\tilde{n}_b = n_b = 30$.

$\Phi^{\mathrm{T}}\Phi$ is the auto-correlation matrix of the input signal, i.e. the fluctuation of the reference velocity in the present case. As this matrix has to be inverted, it has to have full rank. This can be ensured by choosing an uncorrelated input signal. In the present study this requirement is fulfilled, as the input signal is a white noise signal. Föller and Polifke [46] proposed a general method for generating input signals for the LES/SI approach.

In order to assess the properties of the WHI, we now assume that the time series used for the identification were generated with an FIR model. This FIR model has a set of *actual* parameters $\mathbf{b}^*$. Consequently, it is assumed that the measured fluctuation of the global heat release rate $\dot{q}'(t)$ is given as

$$\dot{q}'(t) = \hat{\dot{q}}'(t,\mathbf{b}^*) + \nu(t) = \phi(t)\mathbf{b}^* + \nu(t). \tag{17}$$

This is the authors accepted manuscript of an article published as the version of record in Combustion Theory and Modelling © Taylor & Francis https://doi.org/10.1080/13647830.2018.1443517

Here, $\nu(t)$ accounts for the influence of the turbulent combustion noise. Evaluating this equation for each time instant of sampled data yields

$$\underbrace{\begin{bmatrix} \dot{q}'(0) \\ \dot{q}'(\Delta t) \\ \vdots \\ \dot{q}'(N\Delta t) \end{bmatrix}}_{\mathbf{Y}} = \underbrace{\begin{bmatrix} \phi(0) \\ \phi(\Delta t) \\ \vdots \\ \phi(N\Delta t) \end{bmatrix}}_{\Phi} \mathbf{b}^* + \underbrace{\begin{bmatrix} \nu(0) \\ \nu(\Delta t) \\ \vdots \\ \nu(N\Delta t) \end{bmatrix}}_{\Xi} \tag{18}$$

with $N\Delta t$ being the length of the time series measured. The WHI is a good estimator if the estimated parameter vector $\hat{\mathbf{b}}$ is close to the vector $\mathbf{b}^*$ of *actual* parameters. The error made can be calculated according to

$$\begin{aligned} \hat{\mathbf{b}} - \mathbf{b}^* &= \left(\Phi^{\mathrm{T}}\Phi\right)^{-1} \Phi^{\mathrm{T}} \underbrace{(\Phi\mathbf{b}^* + \Xi)}_{=Y} - \mathbf{b}^* \\ &= \left(\Phi^{\mathrm{T}}\Phi\right)^{-1} \Phi^{\mathrm{T}}\Xi, \end{aligned} \tag{19}$$

where $\Phi^{\mathrm{T}}\Xi$ is the cross-correlation matrix between the input and noise signals. The parameter vector identified $\hat{\mathbf{b}}$ is a good estimate to the *actual* parameter vector $\mathbf{b}^*$ as long as

$$\Phi^{\mathrm{T}}\Xi \approx 0. \tag{20}$$

holds.

Under open-loop conditions, the input and noise signals are uncorrelated and this requirement is fulfilled. In closed-loop conditions, however, the feedback results in a correlation between input and noise. The term $\Phi^{\mathrm{T}}\Xi$ will thus not vanish – even in the case of infinitely long time series. In this case, WHI will give a biased estimate of $\mathbf{b}$, which depends on both the kind of feedback and the properties of the noise. Note that this shortcoming of the WHI method is crucial in the context of the present study.

Please recall that, when deducing an FTF from compressible LES, two feedback mechanisms are present: (1) feedback due to reflections at the boundary conditions; and (2) ITA feedback. The former can be avoided via non-reflective BCs (see [44]). The ITA feedback, however, cannot be avoided. As a consequence of this feedback the combustion noise creates fluctuations of the reference velocity. These fluctuations can be considered as additional input signal. Hence, the input signal is correlated with the noise signal and the term $\Phi^{\mathrm{T}}\Xi$ will not vanish. Therefore, the WHI will always yield a biased estimate of the FTF. The question remaining is how large this bias is. This will be discussed in Section 4. But first, we introduce an advanced SI method based on the BJ model structure. This method yields unbiased estimates even if feedback is present.

3.2. *From Wiener–Hopf inversion to Box–Jenkins identification*

WHI uses an FIR model to describe the flame dynamics. As discussed in Section 2.1, this accounts for the physical effects dominating the response of the flame to a fluctuation of the reference velocity. However, the influence of the turbulent combustion noise is neglected. In contrast to the FIR model, a BJ model can account for this effect. As we will demonstrate in Section 4, this allows an unbiased estimate of the FTF to be obtained, even in the presence of feedback. Additionally, one obtains a model for the turbulent combustion noise.

This is the authors accepted manuscript of an article published as the version of record in Combustion Theory and Modelling © Taylor & Francis https://doi.org/10.1080/13647830.2018.1443517

The general BJ model structure is given as

$$\hat{q}'(t,\Theta) = \frac{B(z)}{F(z)}u'(t) + \frac{C(z)}{D(z)}e(t) \tag{21}$$

with

$$B(z) = b_0 + b_1 z^{-1} + \cdots + b_{\tilde{n}_b} z^{-\tilde{n}_b} \tag{22a}$$

$$F(z) = f_0 + f_1 z^{-1} + \cdots + f_{\tilde{n}_f} z^{-\tilde{n}_f} \tag{22b}$$

$$C(z) = c_0 + c_1 z^{-1} + \cdots + c_{\tilde{n}_c} z^{-\tilde{n}_c} \tag{22c}$$

$$D(z) = d_0 + d_1 z^{-1} + \cdots + d_{\tilde{n}_b} z^{-\tilde{n}_d}, \tag{22d}$$

where z is the time-shift operator defined as $u'(t)z^{-i} = u'(t - i\Delta t)$; b_i, f_i, c_i, and d_i are the (unknown) parameters of the model, which are lumped together in the parameter vector Θ. The polynomials $B(z)$, $F(z)$, $C(z)$, and $D(z)$ are also called filters.

The fundamental difference between the filters is that $B(z)$ and $C(z)$ relate prior inputs ($u'(t)z^{-1}$) and prior disturbances ($e(t)z^{-1}$) to the current estimated output ($\hat{q}'(t)$), whereas the filters $F(z)$ and $D(z)$ relate prior *outputs* ($\hat{q}'(t)z^{-i}$) to the current output and thus describe possible auto-regressive system behaviour.

The BJ model is the most general linear model. If the orders $\tilde{n}_b$, $\tilde{n}_f$, $\tilde{n}_c$, and $\tilde{n}_d$ of the filters are sufficiently large, it can represent any linear model. The limiting factor, besides numerical issues, is that high filter orders yield a large number of parameters. Consequently, long time series are necessary to identify these parameters accurately. The results of the identification can be significantly improved by a proper choice of the filter orders. Comparing the BJ model structure shown in (21) and the model structure of the reference model (5), it becomes evident that the general BJ structure is more complex than the reference model describing the flame dynamics inside the network model. The reference model structure does not contain the auto-regressive filters $F(z)$ and $D(z)$. Thus, in this study the general BJ model structure can be simplified, before estimating the parameter vector Θ by choosing

$$F(z) = D(z) = 1, \tag{23}$$

which yields

$$\hat{q}'(t) = B(z)u'(t) + C(z)e(t). \tag{24}$$

Now, the model structure is equivalent to the model describing the flame dynamics (5) and includes a model for the turbulent combustion noise. As for the WHI, the order $\tilde{n}_b$ of the filter $B(z)$ is determined via Equation (3) using the convective time lags describing the flame dynamics. As discussed in Section 2.1, within the current state of the art, relations for determining the filter orders of the noise model analytically are not known. However, there exist general methods like residual analysis, cross validation, or Akaike's information criterion (AIC) [47] for deducing the model structure from the time series (see e.g. [13,48]). These methods allow the order $\tilde{n}_c$ of the filter $C(z)$ to be determined in a general way. For the purpose of the present work we choose $\tilde{n}_c = n_c$.

After having determined a suitable model structure, the next step within the SI methodology is to determine the entries of the vector of unknown parameters Θ. Again, the key idea

This is the authors accepted manuscript of an article published as the version of record in Combustion Theory and Modelling © Taylor & Francis https://doi.org/10.1080/13647830.2018.1443517

is to formulate a least squares optimisation problem that minimises the difference between the output of the model identified and the time series data used for the identification. For the BJ model, additional difficulty arises when estimating the noise. The problem is that the noise input $e(t)$ is not known. One possible solution to this problem is the use of so-called one-step-ahead prediction:

$$\hat{\dot{q}}(t|t-\Delta t,\Theta)=\frac{D(z)}{C(z)}\frac{B(z)}{F(z)}u'(t)+\frac{C(z)-D(z)}{C(z)}\dot{q}'(t) \tag{25}$$

or with (23)

$$\hat{\dot{q}}(t|t-\Delta t,\Theta)=\frac{B(z)}{C(z)}u'(t)+\frac{C(z)-1}{C(z)}\dot{q}'(t), \tag{26}$$

where $u'(t)$ and $\dot{q}'(t)$ are the measured fluctuations of the velocity and of the global heat release rate, respectively. It is emphasised that the output of the one-step-ahead prediction $\hat{\dot{q}}'(t|t-\Delta t,\Theta)$ is now also dependent on the output time series $\dot{q}'(t)$. This means that the output of the BJ model has been calculated based on all information that was available at the previous time step $t-\Delta t$. The one-step-ahead predictor exploits the noise model to improve the prediction of the model output at the next time step. Please note that for $C(z)=1$ the BJ model (24) reduces to an FIR model. In this case, the corresponding one-step-ahead predictor (26) becomes also an FIR model and the prediction cannot be improved by this means. This is because the noise considered by an FIR model is uncorrelated. The essential difference between an FIR model estimation and, for example, a BJ model estimation, is that as soon as $C(z)\neq 1$ or $D(z)\neq 1$ the noise contribution $v(t)=C(z)/D(z)\,e(t)$ is coloured and is no longer Gaussian white noise. Consequently, it does not correlate out and has to be taken into account, which needs an estimation of the coloured noise term $v(t)$. This is not the case for an FIR model estimation. The one-step-ahead predictor exploits the correlation of the noise. A BJ model describes this correlation via the noise model.

Using (26), the output of the model can be determined as both input signals $u'(t)$ and $\dot{q}'(t)$ are known. Therefore, we can formulate an optimisation problem for determining the unknown parameters Θ of both the FTF and the noise model of the BJ structure:

$$\min_{\Theta} J_{\mathrm{PEM}}(\Theta)=\min_{\Theta}\frac{1}{N}\sum_{i=0}^{N-1}\left(\hat{\dot{q}}'(i\Delta t|(i-1)\Delta t,\Theta)-\dot{q}'(i\Delta t)\right)^2. \tag{27}$$

In contrast to WHI, this optimisation problem is nonlinear. In [49], Wills and Ninness discuss efficient algorithms for this problem.

The method for determining the unknown parameters of a BJ model described in the present section is known as the Prediction Error Method (PEM). It can be shown that the method yields an unbiased estimate [15]. This means that, if the data were generated with an *actual* BJ model, the parameters predicted via the PEM converge to the parameters of the *actual* model for long time series lengths. This holds as long as the noise is modelled correctly, which can always be fulfilled by using a noise model with a high number of parameters. However, a high number of parameters can only be identified accurately with long time series and consequently long LES runs. Therefore, one should try to find the minimal number of parameters necessary to obtain a good model. Here again, techniques like residual analysis, cross-validation, or Akaike's information criterion (AIC) [47] can be used [13,48].

This is the authors accepted manuscript of an article published as the version of record in Combustion Theory and Modelling © Taylor & Francis https://doi.org/10.1080/13647830.2018.1443517

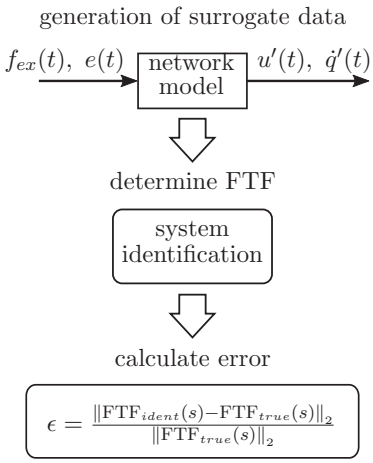

Figure 5. In order to evaluate the quality of the identified models, we first generate surrogate data using a network model. Afterwards, SI is performed and the FTF identified is compared against the FTF used in the network model.

3.3. *Regularisation of the identification*

As LES is computationally expensive, the lengths of the time series used for the LES/SI approach are typically very short. If only short time series are available, SI is prone to over-fitting, which results in a poor estimate of the FTF. Regularisation can be used to prevent over-fitting and to improve the results for short time series. The idea is to add constraints by modifying the cost function of the optimisation problem:

$$J_{\mathrm{reg}}(\Theta) = J(\Theta) + \lambda \Theta^{\mathrm{T}} R \Theta. \tag{28}$$

In general, the function $J(\Theta)$ can be $J_{\mathrm{WHI}}(\Theta)$ or $J_{\mathrm{PEM}}(\Theta)$. Within the scope of the present case study, we investigate only the regularised WHI, i.e. $J(\Theta) = J_{\mathrm{WHI}}(\Theta)$. R is the regularisation matrix and λ the regularisation parameter. In the literature, λR is often called the 'kernel'. A suitable choice of these variables allows additional information to be used for the identification. This allows an accurate estimation of the FTF to be obtained, even if only short time series are available. The key idea is to assume that the impulse response should be smooth and decay exponentially [50]. In Section 4, the so-called Tuned and Correlated (TC) kernel is used. For a detailed discussion on how the regularisation parameters can be determined, we refer the reader to [50–52].

4. Numerical examples

In the present section, we analyse how the intrinsic feedback influences the identification of the FTF. The general procedure is shown in Figure 5. First, surrogate data is generated by simulating the network model described in Section 2 in the time domain. Thereafter, the FTF is identified with the methods discussed in Section 3. Finally, the FTF identified is compared to the *actual* FTF used to generate the data.

4.1. *Generation of surrogate data and Monte Carlo simulation*

In order to generate the surrogate data, the network model is simulated in the time domain. Therefore, all elements of the network model as discussed in Sections 2.1 and 2.2 are

This is the authors accepted manuscript of an article published as the version of record in Combustion Theory and Modelling © Taylor & Francis https://doi.org/10.1080/13647830.2018.1443517

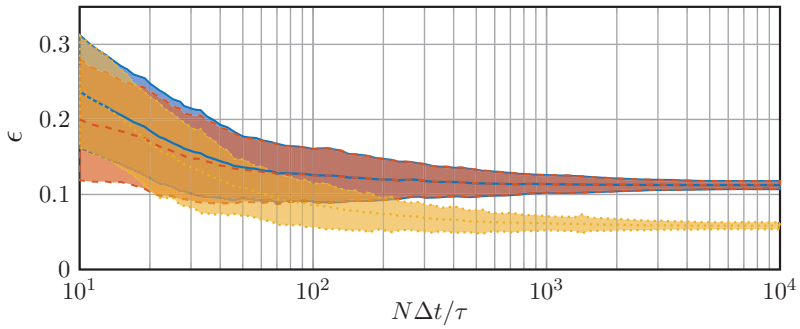

Figure 6. Error of the identified FTF compared to the actual FTF for different data lengths. ——: Wiener–Hopf inversion; - - - : regularised Wiener–Hopf inversion; ..... : Box–Jenkins identification.

formulated in state-space form (see e.g. [4,6]). This results in a state-space model describing the whole network model:

$$\mathbf{x}_{k+1} = \mathbf{A}\mathbf{x}_k + \mathbf{B}\begin{bmatrix} f_{\mathrm{ex}}(k\Delta t) \\ e(k\Delta t) \end{bmatrix} \tag{29a}$$

$$\begin{bmatrix} u'(k\Delta t) \\ \dot{q}'(k\Delta t) \end{bmatrix} = \mathbf{C}\mathbf{x}_k + \mathbf{D}\begin{bmatrix} f_{\mathrm{ex}}(k\Delta t) \\ e(k\Delta t) \end{bmatrix}, \tag{29b}$$

with time step Δt and time increment k. The matrices $\mathbf{A}$, $\mathbf{B}$, $\mathbf{C}$, and $\mathbf{D}$ are the state-space matrices. These matrices were obtained with the thermoacoustic network code taX [6,53] developed at the Technical University of Munich. The vector $\mathbf{x}_k$ is the state vector. The fluctuation of the reference velocity u' and of the global heat release rate $\dot{q}'$ are the output signals of the network model.

As shown in Figure 2, f_{ex} is the ingoing wave at the inlet of the domain. It represents the external forcing. This signal is a pseudo random binary signal. The signal $e(t)$ models the turbulent noise source. Hence, $e(t)$ is modelled as a *random* Gaussian distributed white noise signal. Owing to this random signal, several evaluations of the network model yield different output time series. This is also an essential characteristic of an LES: owing to turbulence, multiple LES runs with slightly different initial conditions will always yield different time series. The results of the LES/SI approach are affected by this randomness. By chance, one can get a better or a worse model. In the present study we quantify this uncertainty using a Monte Carlo simulation. Therefore, for each set of parameters investigated, the network model is evaluated several times. Owing to the random signal $e(t)$, each evaluation yields different time series, and hence a different FTF is identified. In Figures 6, 8, and 10, the results of the Monte Carlo simulation are shown in terms of mean values and standard deviation. For these plots, the network model was evaluated 100 times.

4.2. *Calculation of the error*

The advantage of using surrogate data is that the actual FTF is known and can be used as reference. In the present study, the error is calculated according to

$$\epsilon = \frac{\left\| \hat{\mathrm{FTF}}(j\omega) - \mathrm{FTF}^*(j\omega) \right\|_{\mathcal{H}_2}}{\| |\,\mathrm{FTF}^*(j\omega)\|_{\mathcal{H}_2}} \tag{30}$$

This is the authors accepted manuscript of an article published as the version of record in Combustion Theory and Modelling © Taylor & Francis https://doi.org/10.1080/13647830.2018.1443517

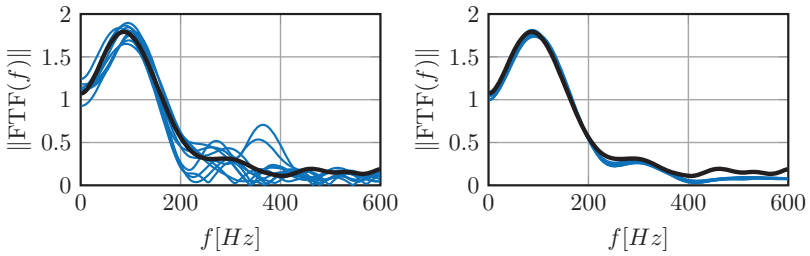

Figure 7. Comparison of identified FTFs against *actual* FTFs for different data lengths. ——: 10 random samples of Wiener–Hopf inversion; ——: *actual* FTFs. Left: time series length of $20N\Delta t/\tau$; right: time series length of $2000N\Delta t/\tau$.

with the angular frequency ω; $\|\cdot\|_{\mathcal{H}_2}$ denotes the $\mathcal{H}_2$-norm given as

$$\|\mathrm{FTF}(s)\|_{\mathcal{H}_2} = \sqrt{\frac{1}{2\pi}\int_{-\pi}^{\pi} \mathrm{FTF}\,(j\omega)^{\mathrm{H}}\,\mathrm{FTF}\,(j\omega)\;\mathrm{d}\omega} \tag{31}$$

with the imaginary unit j. The exponent 'H' denotes the complex conjugate. This error definition measures the error in the frequency domain. All frequencies are equally weighted. This error measure should be interpreted qualitatively. The absolute error made by the different SI methods is discussed in Section 4.6.

4.3. *Identification in the limit of infinite time series length*

As discussed in Section 3, under closed-loop conditions WHI, in contrast to the PEM with a BJ model, yields a biased estimate of the FTF. This means the FTF identified does not converge towards the *actual* FTF even in the limit of infinite time series length. In Figure 6, the error (see Equation 30) is plotted over the length of the time series used for the identification. The latter is normalised by the impulse response length as defined in Equation (2). The excitation amplitude was fixed to $A = 10\%$. Indeed, for very long time series the error made by the BJ identification is significantly smaller compared to the error made by WHI and the regularised WHI. However, when LES data is analysed the length of the time series available is typically smaller than 30τ. In this data range the confidence intervals of all methods overlap and hence, by chance any of the methods can yield the best estimate of the FTF. On average, the regularised WHI yields the best estimate. This is expected as the method is designed for short time series. The BJ identification becomes better than the regularised WHI estimate for time series longer than about 20τ. The classical WHI is inferior for any time series length, and hence should be avoided.

In order to provide a better understanding of the overall error shown in Figure 6 and to give an idea of the accuracy of the identified FTF, Figure 7 depicts a few samples of the Monte Carlo set of identified FTFs. Ten exemplary results from the WHI identification are shown and compared against the *actual* FTFs for different data lengths. It can be observed that, for the shorter data set lengths, the spread of the respectively identified models is rather large even if the general trend of the *actual* FTFs is still matched. In the case of a distinctively longer time series, the identified models converge to a single, but slightly biased, solution.

This is the authors accepted manuscript of an article published as the version of record in Combustion Theory and Modelling © Taylor & Francis https://doi.org/10.1080/13647830.2018.1443517

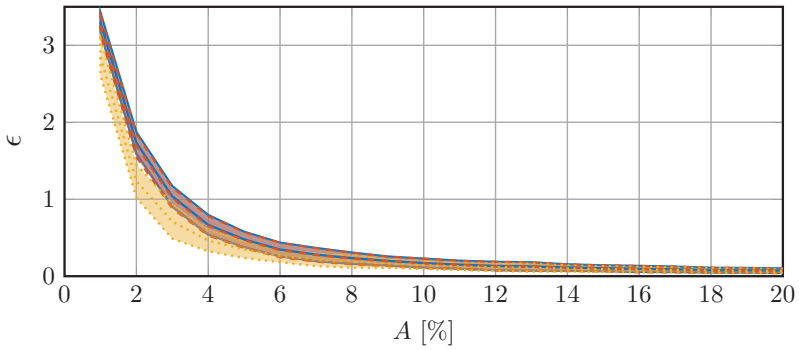

Figure 8. Error of the identified FTFs compared to the actual FTFs for different excitation amplitudes. ——: Wiener–Hopf inversion; - - -: regularised Wiener–Hopf inversion; .....: Box–Jenkins identification.

4.4. *Dependency on signal-to-noise-ratio and excitation amplitude*

The dependence of models identified with a certain excitation amplitude A is shown in Figure 8. Here, the excitation amplitude A is the amplitude of the wave f_{ex}. The time series for this plot were 30τ, which corresponds to the amount of data typically available for the LES/SI approach.

For all identification methods, the error decays with the amplitude. This strong decay of ϵ with increasing forcing amplitude may be attributed to the decreasing influence of the noise contribution, which impedes an accurate identification. Note that an increased SNR does not necessarily reduce the bias in the WHI method caused by the closed-loop ITA feedback. Hence, when applying the LES/SI approach to real data, the forcing amplitude should be chosen as high as possible. The limiting factor is the triggering of nonlinear effects by high excitation amplitudes. As the network model used in the present study is linear, it does not account for this limit. If data is generated via LES, the flame responds linearly for amplitudes lower than about 10%. At this amplitude level, the error made by all methods investigated is comparable. The BJ identification is superior for very low amplitudes. Thus, this method should be used for flames that are prone to nonlinearities or flames that exhibit a strong noise contribution.

A better understanding of this behaviour of the LES/SI approach can be obtained by looking at the SNR. It is defined as

$$\mathrm{SNR} = \frac{\mathrm{RMS}(\dot{q}'_{u'})}{\mathrm{RMS}(\dot{q}'_{\mathrm{turb}})}. \tag{32}$$

Here, $\dot{q}'_{u'}$ describes the heat release rate fluctuations resulting purely from the acoustic forcing. It is determined by simulating the network model in the time domain with a noise signal equal to zero. $\dot{q}'_{\mathrm{turb}}$ is equal to the variance of pure noise. In Figure 9, dependency of the SNR on the forcing amplitude is shown. It becomes evident that a small increase in the excitation amplitude increases SNR over-proportionally. This yields the significant decrease of the error made by the identification when the forcing amplitude is increased.

This is the authors accepted manuscript of an article published as the version of record in Combustion Theory and Modelling © Taylor & Francis https://doi.org/10.1080/13647830.2018.1443517

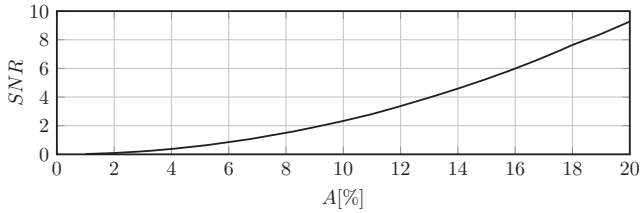

Figure 9. Dependence of the SNR on the excitation amplitude.

4.5. *The influence of reflections at the boundaries*

As discussed above, in a compressible LES the following two acoustic feedback mechanisms can be present.

(1) The intrinsic thermoacoustic feedback (see Figure 1). This feedback is always present and cannot be avoided.
(2) Feedback due to reflections at the BCs. Non-reflective BCs, as proposed by Polifke, Wall, and Moin [44], can suppress this feedback.

In many LES codes, however, only Navier–Stokes characteristic boundary conditions (NSCBCs) [54] are available. These BCs reflect acoustic waves according to a low-pass filter

$$R(\omega) = \frac{\hat{g}_d}{\hat{f}_d} = \frac{-1}{1 + i\omega\frac{2}{\sigma}} = \frac{-1}{1 + i\omega\frac{1}{f_c}}, \tag{33}$$

with the angular frequency ω and the cut-off frequency f_c. The hat ($\hat{\cdot}$) labels variables in the frequency domain. σ is the relaxation parameter. A relaxation parameter equal to zero yields perfectly non-reflective boundary conditions. However, this choice results in a drift of the mean flow variables. Thus, it is necessary to choose $\sigma > 0$ for practical applications. This avoids the drift at the cost of reflections according to Equation (33).

In order to investigate the influence of these reflections on the LES/SI approach, the network model shown in Figure 2 was modified. Instead of the non-reflective inflow and outflow BCs, used for the studies discussed in the previous sections, a low-pass filter according to Equation (33) was applied. In Figure 10, the dependency of the results of the LES/SI approach on the cut-off frequency f_c of this filter is shown. A high cut-off frequency corresponds to a large value of the relaxation parameter. Up to a cut-off frequency of 750 Hz, only a small influence of the relaxation parameter on the model identified is observed. For a cut-off frequency of 750 Hz and above (not shown here) the error suddenly increases. For these values the thermoacoustic network model is linearly unstable. This means that the amplitude of the instability grows infinitely in the generated time series as amplitude saturation is governed by nonlinear mechanisms, which are not captured by the *linear* surrogate data model. The linear unstable mode here can be attributed to the ITA mode of the BRS burner [36,37], which is independent of the duct length used and is thus not suppressed by using compact duct sections in the surrogate data model. An accurate identification from the surrogate data model is not possible any more.

In the range of stable working conditions (up to a cut-off frequency of 750 Hz), reflecting boundary conditions enhance the flame's inherent intrinsic feedback-loop feedback.

This is the authors accepted manuscript of an article published as the version of record in Combustion Theory and Modelling © Taylor & Francis https://doi.org/10.1080/13647830.2018.1443517

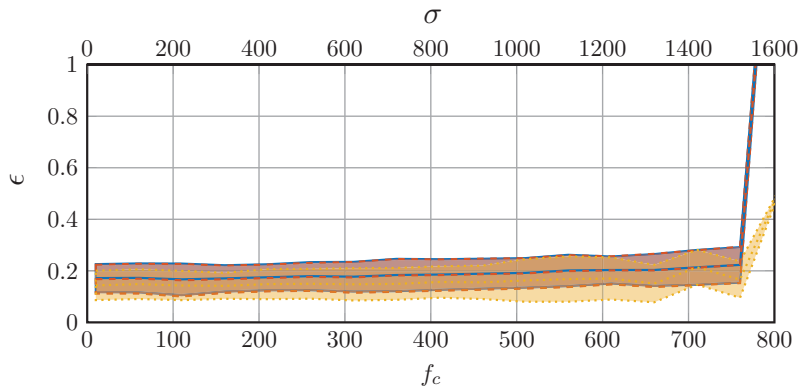

Figure 10. Error of the identified FTFs compared to the actual FTFs for different cut-off frequencies of the inlet and outlet BC. ——: Wiener–Hopf inversion; - - - : regularised Wiener–Hopf inversion; ..... : Box–Jenkins identification.

This enhanced coupling manifests itself in an amplification of the ITA frequency within the generated time series. Meaning that although the external forcing signal f_{ex} is a pure broadband signal (a pseudo random binary signal), the input (u') and output ($\dot{q}'$) signals exhibit a dominant frequency, which is equal to the ITA frequency. Nonetheless, the error ϵ hardly increases with an increasing reflection at the boundaries and is thus comparably small. Therefore, we conclude that the reason why non-reflective BCs are helpful for the identification is that they promote the thermoacoustic stability of the LES. As long as the simulation stays thermoacoustically stable the LES/SI approach works also with NSCBC. This simplifies the application of the LES/SI approach significantly.

4.6. *Application to LES data*

The $\mathcal{H}_2$-norm used in the previous sections, see Equation (30), allows only a statement on the global error made by the identified models, i.e. a summary over all frequencies. Moreover, the magnitude of the absolute value of the error made is difficult to interpret in terms of agreement to the *true* solution. Therefore, in this section the identified models are compared over the frequency range in order to provide a more immediate insight into the accuracy of the identified models.

For this we apply the methods to the LES data discussed in [22]. The intention of using actual LES data here instead of a surrogate dataset is that, for LES generated data, certain restrictions are given. For example the time series length affordable is limited or the SNR cannot be increased arbitrarily in order to avoid a nonlinear flame response. Moreover, the surrogate data relies on certain assumptions such as a pre-defined noise distribution or the acoustic compactness of the enclosing cavity. These assumptions may be dropped when using actual LES data and the performance of the different identification methods can be compared for a real application.

The results are shown in Figure 11. Please note that the FTF from WHI identification is identical to the one shown in Figure 3, since the same LES data set was used for the identification. The difference between the methods is negligible. As it turns out, even if theoretically the BJ model provides unbiased estimations for the FTF in the case of very long time series, the identification error introduced by the *finite* LES time series length dominates. Therefore, all three methods yield similar results. Thus, although the WHI

This is the authors accepted manuscript of an article published as the version of record in Combustion Theory and Modelling © Taylor & Francis https://doi.org/10.1080/13647830.2018.1443517

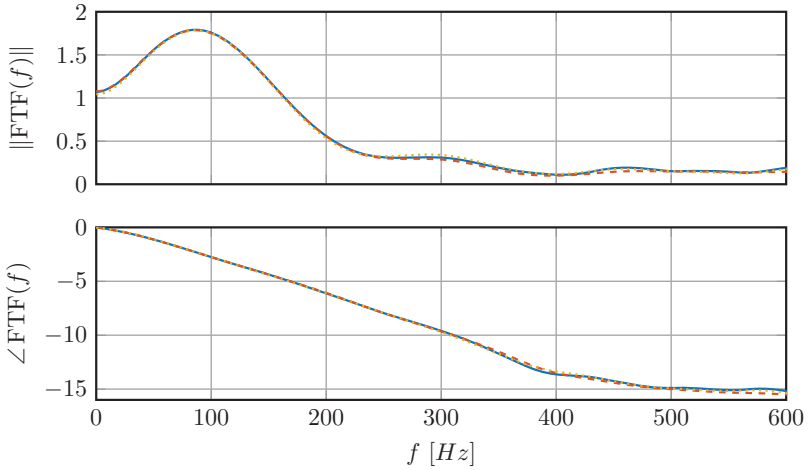

Figure 11. FTFs identified based on LES data using different identification methods. ——: Wiener–Hopf inversion; - - - : regularised Wiener–Hopf inversion; ……: Box–Jenkins identification.

yields biased estimates of the FTF, the error made can be neglected in many practical applications.

5. Conclusion

The Large Eddy Simulation/System Identification (LES/SI) approach is an efficient method for determining a flame transfer function (FTF) numerically. We have demonstrated that, due to Intrinsic ThermoAcoustic (ITA) feedback, Wiener–Hopf Inversion (WHI), which is the SI method most frequently applied, yields a biased estimate of the FTF. Fortunately, the bias error becomes small for medium excitation amplitudes. This is the reason why the WHI works well in many applications.

Furthermore, our analyses have shown that the model identified is influenced by reflections at the boundary conditions, but the error introduced by the enhanced coupling due to reflective boundary conditions is comparably small. Hence, non-reflective boundary conditions are not essentially needed for the LES/SI approach. This increases the applicability of the approach significantly, as it allows the method to be applied independently of the LES solvers used.

Acknowledgements

The authors wish to thank Dr. L. Tay-Wo-Chong for providing the LES data that was used to determine the FTF of the network model and formed the basis for Section 4.6.

Disclosure statement

No potential conflict of interest was reported by the authors.

Funding

This work was supported by the Research Association for Combustion Engines (Forschungsvereinigung Verbrennungskraftmaschinen e.V. – FVV) [Grant 6011150]; the Deutsche Forschungsgemeinschaft (DFG) [Grant PO 710/16-1].

This is the authors accepted manuscript of an article published as the version of record in Combustion Theory and Modelling © Taylor & Francis https://doi.org/10.1080/13647830.2018.1443517

References

[1] D. Bohn and E. Deucker, *An acoustical model to predict combustion driven oscillations*, 20th International Congress on Combustion Engines (CIMAC), London, UK, 1993.

[2] A.P. Dowling, *The calculation of thermoacoustic oscillation*, J. Sound Vibration 180 (1995), pp. 557–581. Available at https://dx.doi.org/10.1006/jsvi.1995.0100.

[3] J.J. Keller, *Thermoacoustic oscillations in combustion chambers of gas turbines*, AIAA J. 33 (1995), pp. 2280–2287. Available at https://dx.doi.org/10.2514/3.12980.

[4] B. Schuermans, V. Bellucci, and C.O. Paschereit, *Thermoacoustic modeling and control of multi-burner combustion systems*, in *International Gas Turbine and Aeroengine Congress & Exposition*, Atlanta, GA, ASME Paper GT2003-38688, 2003, pp. 509–519. Available at https://dx.doi.org/10.1115/GT2003-38688.

[5] M. Bothien, J. Moeck, A. Lacarelle, and C.O. Paschereit, *Time Domain modelling and stability analysis of complex thermoacoustic systems*, Proc. Inst. Mech. Engrs, Pt A: J. Power & Energy 221 (2007), pp. 657–668. Available at https://dx.doi.org/10.1243/09576509JPE384.

[6] T. Emmert, M. Meindl, S. Jaensch, and W. Polifke, *Linear state space interconnect modeling of acoustic systems*, Acta Acustica united with Acustica 102 (2016), pp. 824–833. Available at https://dx.doi.org/10.3813/AAA.918997.

[7] F. Nicoud, L. Benoit, C. Sensiau, and T. Poinsot, *Acoustic modes in combustors with complex impedances and multidimensional active flames*, AIAA J. 45 (2007), pp. 426–441. Available at https://dx.doi.org/10.2514/1.24933.

[8] F. Ni, M. Miguel-Brebion, F. Nicoud, and T. Poinsot, *Accounting for acoustic damping in a Helmholtz solver*, AIAA J. 55 (2017), pp. 1205–1220. Available at https://dx.doi.org/10.2514/1.J055248.

[9] T. Hummel, C. Temmler, B. Schuermans, and T. Sattelmayer, *Reduced-order modeling of aeroacoustic systems for stability analyses of thermoacoustically noncompact gas turbine combustors*, J. Engng Gas Turbines Power 138 (2015), Article ID 051502. Available at https://dx.doi.org/10.1115/1.4031542.

[10] G. Campa and S.M. Camporeale, *Prediction of the thermoacoustic combustion instabilities in practical annular combustors*, J. Engng Gas Turbines Power 136 (2014), Article ID 091504. Available at https://dx.doi.org/10.1115/1.4027067.

[11] A. Huber and W. Polifke, *Impact of fuel supply impedance on combustion stability of gas turbines*, in *International Gas Turbine and Aeroengine Congress & Exposition*, Berlin, ASME Paper GT2008-51193, 2008.

[12] W. Polifke, *Black-box system identification for reduced order model construction*, Ann. Nucl. Energy 67C (2014), pp. 109–128. Available at https://dx.doi.org/10.1016/j.anucene.2013.10.037.

[13] R. Isermann and M. Münchhof, *Identification of Dynamical Systems: An Introduction with Applications*, Advanced Textbooks in Control and Signal Processing, Springer-Verlag, Berlin, 2010.

[14] M. Verhaegen and V. Verdult, *Filtering and System Identification: A Least Squares Approach*, Cambridge University Press, New York, 2012.

[15] L. Ljung, *System Identification: Theory for the User*, 2nd ed. , Prentice Hall, Upper Saddle River, NJ, 1999.

[16] A. Gentemann, C. Hirsch, K. Kunze, F. Kiesewetter, T. Sattelmayer, and W. Polifke, *Validation of flame transfer function reconstruction for perfectly premixed swirl flames*, in *ASME Turbo Expo 2004: Power for Land, Sea, and Air*, Vienna, Austria, ASME Paper GT2004-53776.

[17] M. Zhu, A.P. Dowling, and K.N.C. Bray, *Transfer function calculations for aeroengine combustion oscillations*, J. Engng Gas Turbines Power 127 (2005), pp. 18–26.

[18] B. Schuermans, H. Luebcke, D. Bajusz, and P. Flohr, *Thermoacoustic analysis of gas turbine combustion systems using unsteady CFD*, in *ASME Turbo Expo 2005*, Reno, NV, ASME Paper GT2005-68393. Available at https://dx.doi.org/10.1115/GT2005-68393.

[19] K. Kostrzewa, J. Lepers, B. Noll, W. Krebs, M. Aigner, B. Prade, and M. Huth, *Validation of advanced computational methods for determining flame transfer functions in gas turbine combustion systems*, in *ASME Turbo Expo 2007: International Gas Turbine and Aeroengine Congress & Exposition*, Montreal, Canada, ASME Paper GT2007-27267.

[20] A. Giauque, T. Poinsot, and F. Nicoud, *Validation of a flame transfer function reconstruction method for complex turbulent configurations*, in *14th AIAA/CEAS Aeroacoustics Conference*

This is the authors accepted manuscript of an article published as the version of record in Combustion Theory and Modelling © Taylor & Francis https://doi.org/10.1080/13647830.2018.1443517

(29th AIAA Aeroacoustics Conference), AIAA/CEAS 2008, Vancouver, Canada. Available at https://dx.doi.org/10.2514/6.2008-2943.

[21] A. Huber and W. Polifke, *Dynamics of practical premix flames, Part II: Identification and interpretation of CFD data*, Int. J. Spray Combust. Dynam. 1 (2009), pp. 229–250. Available at https://dx.doi.org/10.1260/175682709788707440.

[22] L. Tay-Wo-Chong, S. Bomberg, A. Ulhaq, T. Komarek, and W. Polifke, *Comparative validation study on identification of premixed flame transfer function*, J. Engng Gas Turbines Power 134 (2012), 021502, 8pp. Available at https://dx.doi.org/10.1115/1.4004183.

[23] L. Tay-Wo-Chong and W. Polifke, *Large eddy simulation-based study of the influence of thermal boundary condition and combustor confinement on premix flame transfer functions*, J. Engng Gas Turbines Power 135 (2013), 021502, 9pp. Available at https://dx.doi.org/10.1115/1.4007734.

[24] F. Biagioli, A. Scarpato, and K.J. Syed, *Dynamic response of swirl stabilized turbulent premixed flames based on the Helmholtz–Hodge velocity decomposition*, Flow Turbul. Combust. 96 (2016), pp. 1005–1022. Available at https://dx.doi.org/10.1007/s10494-016-9736-3.

[25] A. Innocenti, A. Andreini, B. Facchini, and A. Peschiulli, *Numerical analysis of the dynamic flame response of a spray flame for aero-engine applications*, Int. J. Spray Combust. Dynam. 9 (2017), pp. 310–329. Available at https://dx.doi.org/10.1177/1756827717703577.

[26] Y. Yang, N. Noiray, A. Scarpato, O. Schulz, K.M. Düsing, and M. Bothien, *Numerical analysis of the dynamic flame response in Alstom reheat combustion systems*, in *ASME Turbo Expo 2015: International Gas Turbine Technical Conference and Exposition*, Montreal, Quebec, Canada, ASME Paper GT2015-42622.

[27] S.W. Yuen, A.M.G. Gentemann, and W. Polifke, *Influence of Boundary Reflection Coefficient on the System Identifiability of Acoustic Two-Ports*, in *ICSV 11*, Saint-Petersburg, Russia. IIAV, 2004, pp. 3501–3508.

[28] K. Kostrzewa, A. Widenhorn, B. Noll, M. Aigner, W. Krebs, M. Huth, and P. Kaufmann, *Impact of Boundary Conditions on the Reconstructed Flame Transfer Function for Gas Turbine Combustion Systems*, in *ASME Turbo Expo 2008: Power for Land, Sea, and Air*, Berlin, Germany, pp. 353–365.

[29] S. Bomberg, T. Emmert, and W. Polifke, *Thermal versus acoustic response of velocity sensitive premixed flames*, Proc. Combust. Inst. 35 (2015), pp. 3185–3192. Available at https://dx.doi.org/10.1016/j.proci.2014.07.032.

[30] M. Hoeijmakers, V. Kornilov, I. Lopez Arteaga, P. de Goey, and H. Nijmeijer, *Intrinsic instability of flame–acoustic coupling*, Combust. Flame 161 (2014), pp. 2860–2867. Available at https://dx.doi.org/10.1016/j.combustame.2014.05.009.

[31] M. Hoeijmakers, V. Kornilov, I.L. Arteaga, P. de Goey, and H. Nijmeijer, *Flames in context of thermo-acoustic stability bounds*, Proc. Combust. Inst. 35 (2015), pp. 1073–1078. Available at https://dx.doi.org/10.1016/j.proci.2014.06.059.

[32] T. Emmert, S. Bomberg, and W. Polifke, *Intrinsic thermoacoustic instability of premixed flames*, Combust. Flame 162 (2015), pp. 75–85. Available at https://dx.doi.org/10.1016/j.combustame.2014.06.008.

[33] C.F. Silva, T. Emmert, S. Jaensch, and W. Polifke, *Numerical study on intrinsic thermoacoustic instability of a laminar premixed flame*, Combust. Flame 162 (2015), pp. 3370–3378. Available at https://dx.doi.org/10.1016/j.combustame.2015.06.003.

[34] E. Courtine, L. Selle, and T. Poinsot, *DNS of intrinsic thermoacoustic modes in laminar premixed flames*, Combust. Flame 162 (2015), pp. 4331–4341. Available at https://dx.doi.org/10.1016/j.combustame.2015.07.002.

[35] C.F. Silva, S. Jaensch, T. Emmert, and W. Polifke, *On the autoregressive behavior of the intrinsic thermoacoustic feedback loop observed in premixed flames*, in *22nd International Congress on Sound and Vibration (ICSV22)*, Florence, Italy, 2015.

[36] T. Emmert, S. Bomberg, S. Jaensch, and W. Polifke, *Acoustic and intrinsic thermoacoustic modes of a premixed combustor*, Proc. Combust. Inst. 36 (2017), pp. 3835–3842. Available at https://dx.doi.org/10.1016/j.proci.2016.08.002.

[37] C.F. Silva, M. Merk, T. Komarek, and W. Polifke, *The contribution of intrinsic thermoacoustic feedback to combustion noise and resonances of a confined turbulent premixed flame*, Combust. Flame 182 (2017), pp. 269–278. Available at https://dx.doi.org/10.1016/j.combustame.2017.04.015.

This is the authors accepted manuscript of an article published as the version of record in Combustion Theory and Modelling © Taylor & Francis `https://doi.org/10.1080/13647830.2018.1443517`

[38] T. Komarek and W. Polifke, *Impact of swirl fluctuations on the flame response of a perfectly premixed swirl burner*, J. Engng Gas Turbines Power 132 (2010), 061503, 7pp. Available at https://dx.doi.org/10.1115/1.4000127.
[39] R.S. Blumenthal, P. Subramanian, R. Sujith, and W. Polifke, *Novel perspectives on the dynamics of premixed flames*, Combust. Flame 160 (2013), pp. 1215–1224. Available at https://dx.doi.org/10.1016/j.combustame.2013.02.005.
[40] A.P. Dowling and Y. Mahmoudi, *Combustion noise*, Proc. Combust. Inst. 35 (2015), pp. 65–100. Available at https://dx.doi.org/10.1016/j.proci.2014.08.016.
[41] M. Ihme, *Combustion and engine-core noise*, Annu. Rev. Fluid Mech. 49 (2017), pp. 277–310. Available at https://doi.org/10.1146/annurev-fluid-122414-034542.
[42] F. Weyermann, *Numerische Berechnung der Emission Verbrennungsinduzierten Lärms Automobiler Zusatzheizungen*, Ph.D. diss., TU München, 2010.
[43] C. Hirsch, J. Wäsle, A. Winkler, and T. Sattelmayer, *A spectral model for the sound pressure from turbulent premixed combustion*, Proc. Combust. Inst. 31 (2007), pp. 1435–1441.
[44] W. Polifke, C. Wall, and P. Moin, *Partially reflecting and non-reflecting boundary conditions for simulation of compressible viscous flow*, J. Comput. Phys. 213 (2006), pp. 437–449. Available at https://dx.doi.org/10.1016/j.jcp.2005.08.016.
[45] L. Strobio Chen, S. Bomberg, and W. Polifke, *Propagation and generation of acoustic and entropy waves across a moving flame front*, Combust. Flame 166 (2016), pp. 170–180. Available at https://dx.doi.org/10.1016/j.combustame.2016.01.015.
[46] S. Föller and W. Polifke, *Advances in identification techniques for aero-acoustic scattering coefficients from large eddy simulation*, in *18th International Congress on Sound and Vibration (ICSV18)*, Vol. 4, Rio de Janeiro, Brazil, 2011, pp. 3122–3129.
[47] H. Akaike, *Modern development of statistical methods*, in *Trends and Progress in System Identification*, P. Eykhoff, ed., Pergamon Press, Oxford, UK, 1981, pp. 169–184. Available at https://doi.org/10.1016/B978-0-08-025683-2.50011-9.
[48] A.K. Tangirala, *Identification of dynamic models – concepts and principles*, in *Principles of System Identification: Theory and Practice*, CRC Press, Boca Raton, FL, 2014, pp. 479–518.
[49] A. Wills and B. Ninness, *On gradient-based search for multivariable system estimates*, IEEE Trans. Autom. Control 53 (2008), pp. 298–306. Available at https://dx.doi.org/10.1109/TAC.2007.914953.
[50] G. Pillonetto, F. Dinuzzo, T. Chen, G.D. Nicolao, and L. Ljung, *Kernel methods in system identification, machine learning and function estimation: A survey*, Automatica 50 (2014), pp. 657–682. Available at https://dx.doi.org/10.1016/j.automatica.2014.01.001.
[51] T. Chen, H. Ohlsson, and L. Ljung, *On the estimation of transfer functions, regularizations and Gaussian processes – Revisited*, Automatica 48 (2012), pp. 1525–1535. Available at https://dx.doi.org/10.1016/j.automatica.2012.05.026.
[52] L.L.T. Chen, *What can regularization offer for estimation of dynamical systems?* IFAC Proc. Vol. 46 (2013), pp. 1–8. Available at https://doi.org/10.3182/20130703-3-FR-4038.00155.
[53] T. Emmert, S. Jaensch, C. Sovardi, and W. Polifke, *taX – a flexible tool for low-order duct acoustic simulation in time and frequency domain*, 7th Forum Acusticum, Kraków, Poland, 7–12 September 2014, DEGA Workshop Fahrzeugakustik/Strömungsakustik, Stuttgart, Germany, 7–8 October 2014.
[54] T. Poinsot and S.K. Lelef, *Boundary conditions for direct simulation of compressible viscous flows*, J. Comput. Phys. 101 (1992), pp. 104–129. Available at https://dx.doi.org/10.1016/0021-9991(92)90046-2.

This is the authors accepted manuscript of an article published as the version of record in Combustion Theory and Modelling © Taylor & Francis `https://doi.org/10.1080/13647830.2018.1443517`

Journal of Sound and Vibration 422 (2018) 432–452

Contents lists available at ScienceDirect

Journal of Sound and Vibration

journal homepage: www.elsevier.com/locate/jsvi

Simultaneous identification of transfer functions and combustion noise of a turbulent flame

M. Merk *, S. Jaensch, C. Silva, W. Polifke

Fakultät für Maschinenwesen, Technische Universität München, Boltzmannstr. 15, 85747, Garching, Germany

ARTICLE INFO

Article history:
Received 18 August 2017
Revised 14 February 2018
Accepted 19 February 2018
Available online XXX

Keywords:
Thermoacoustics
Combustion noise
System identification
Low-order modeling

ABSTRACT

The Large Eddy Simulation/System Identification (LES/SI) approach allows to deduce a flame transfer function (FTF) from LES of turbulent reacting flow: Time series of fluctuations of reference velocity and global heat release rate resulting from broad-band excitation of a simulated turbulent flame are post-processed via SI techniques to derive a low order model of the flame dynamics, from which the FTF is readily deduced. The current work investigates an extension of the established LES/SI approach: In addition to estimation of the FTF, a low order model for the combustion noise source is deduced from the same time series data. By incorporating such a noise model into a linear thermoacoustic model, it is possible to predict the overall level as well as the spectral distribution of sound pressure in confined combustion systems that do not exhibit self-excited thermoacoustic instability. A variety of model structures for estimation of a noise model are tested in the present study. The suitability and quality of these model structures are compared against each other, their sensitivity regarding certain time series properties is studied. The influence of time series length, signal-to-noise ratio as well as acoustic reflection coefficient of the boundary conditions on the identification are examined. It is shown that the Box-Jenkins model structure is superior to simpler approaches for the simultaneous identification of models that describe the FTF as well as the combustion noise source. Subsequent to the question of the most adequate model structure, the choice of optimal model order is addressed, as in particular the optimal parametrization of the noise model is not obvious. Akaike's Information Criterion and a model residual analysis are applied to draw qualitative and quantitative conclusions on the most suitable model order. All investigations are based on a surrogate data model, which allows a Monte Carlo study across a large parameter space with modest computationally effort. The conducted study constitutes a solid basis for the application of advanced SI techniques to actual LES data.

© 2018 Elsevier Ltd. All rights reserved.

1. Introduction

In various industrial applications, e.g. gas turbines for power generation or propulsion, combustion noise is an undesirable, but unavoidable by-product of turbulent combustion. In aeronautical engines combustion noise may dominate the sound emissions within a certain frequency range [1]. Besides being harmful for those continuously exposed to noise emissions, elevated combustion noise levels may even trigger thermoacoustic instabilities [2], which should be avoided at any cost. Consequently, combustion noise is a subject of past as well as on-going research.

* Corresponding author.
E-mail address: merk@tfd.mw.tum.de (M. Merk).

https://doi.org/10.1016/j.jsv.2018.02.040
0022-460X/© 2018 Elsevier Ltd. All rights reserved.

With permission from M. Merk, S. Jaensch, C.Silva, and W. Polifke. Simultaneous identification of transfer functions and combustion noise of a turbulent flame. *Journal of Sound and Vibration, 422*, Elsevier, 2018.

Nomenclature

Latin letters

a_i, b_i, c_i, d_i, f_i	model coefficients
A, B, C, D, F	polynomial filters
$\mathbf{A}, \mathbf{B}, \mathbf{C}, \mathbf{D}$	state-space matrices
c	speed of sound
f	char. wave downstream
g	char. wave upstream
G	plant model
H	noise model
J	cost function
$\mathbf{K}$	correlation vector
l	length scale
n_a, n_b, n_c, n_d, n_f	polynomial model order
N	number of time series samples
p'	acoustic pressure fluctuation
P_{xx}	power spectral density
q	time shift operator
$\dot{Q}'$	heat release rate fluctuation
R	reflection coefficient
$\mathbf{R}$	weighting matrix
Δt	sampling interval
t	time
u'	acoustic velocity fluctuation
$\mathbf{x}$	state vector

Greek letters

α	cross-section ratio
$\gamma_{\epsilon\epsilon}$	auto-correlation of ϵ
$\gamma_{\epsilon u}$	cross-correlation of ϵ with input
Δ	noise model error
ϵ	model residual
$\boldsymbol{\theta}$	parameter vector
Θ	temperature ratio
λ	regularization parameter
ξ	specific acoustic impedance
ρ	density
τ	impulse response length
ω	angular frequency

Abbreviations

AIC	Akaike's Information Criterion
ARX	Autoregressive Exogenous Model
BJ	Box-Jenkins
FIR	Finite Impulse Response
FTF	Flame Transfer Function
LES	Large Eddy Simulation
nAIC	norm. Akaike's Information Criterion
PEM	Prediction Error Method
SNR	Signal-to-Noise Ratio
WHI	Wiener-Hopf Inversion

In any effort to reduce or limit sound emissions from turbulent combustion devices, two aspects are highly relevant: Firstly, a detailed understanding and characterization of the combustion noise source is essential. Secondly, an accurate and flexible prediction tool for estimating the spectral sound pressure distribution is needed in order to develop and assess suitable countermeasures. In this context 'flexible' means that changes in the geometry and acoustic reflection conditions of the setup, as well as changes in the noise source itself are quickly realizable. If this is the case, predictions of the spectral sound pressure distribution are possible across a large parameter space.

Over the last decades a multitude of studies were conducted to develop a deeper understanding of the generation of combustion noise and the noise source characteristics of a turbulent flame. Bragg [3] stated that a turbulent flame behaves like a set of monopole sources. Refining Bragg's theory and making use of Lighthill's analogy [4], Strahle [5] derived a formulation of the far field pressure for a region that encompasses a turbulent flame. This formulation related the fluctuations of acoustic pressure in the far field to those of unsteady heat release within the flame region. More recent work on the determination of the combustion noise source and its spectral distribution was conducted by Clavin and Siggia [6], who analytically predicted a spectral decay of combustion noise scaling as $f^{-2.5}$. Hirsch *et al.* [7] and Wäsle *et al.* [8] provided a quantitative closure for the spectral distribution of heat release in turbulent premixed combustion that is based on local, time-mean values of heat release rate, turbulent kinetic energy and turbulence lengthscale. The closure proposed by Hirsch *et al.* [7] and Wäsle *et al.* [8] was confirmed by Rajaram and Lieuwen [9], who measured the noise source spectra emitted from a turbulent open jet flame for a variety of operating conditions.

Once the noise source is characterized, the next step is to predict the spectral distribution of sound pressure levels. In this context, there is an essential difference between open and confined configurations. For open configurations the influence of the flame on the acoustics is strong, but not *vice versa*. In this scenario of '*one-way coupling*', the spectral distribution of sound pressure is strongly correlated to that of the combustion noise source. Only open configurations with pronounced intrinsic thermoacoustic feedback may reveal distinct peaks in their sound pressure spectrum [10].

For confined configurations, on the other hand, acoustic reflections at the confinement boundary can establish a '*two-way coupling*' between flame and acoustics [11–13]. The acoustic field of the enclosing cavity is excited by the broad-band combustion noise source and resonances at the acoustic eigenfrequencies may develop. This results in a spectral distribution of sound pressure that depends strongly on the acoustic properties of the enclosing cavity and may differ distinctly from the combustion noise source spectrum. Therefore, a correct description of the flame and the combustion noise source is not enough to predict the resulting spectral sound pressure distribution for confined configurations. An accurate acoustic characterization of the confinement cavity is crucially needed as well.

As almost every combustion device of applied interest is confined, the corresponding possible prediction approaches shall be further examined. Experimental measurements of a certain configuration represent the most straightforward approach. How-

With permission from M. Merk, S. Jaensch, C.Silva, and W. Polifke. Simultaneous identification of transfer functions and combustion noise of a turbulent flame. *Journal of Sound and Vibration, 422*, Elsevier, 2018.

ever, experimental measurements are laborious and rather inflexible if it comes to changes in the acoustic boundaries or the confinement geometry. Numerically, Large Eddy Simulation (LES) has shown to be capable in resolving the combustion noise generation, as it captures all physically relevant mechanisms. Silva *et al.* [14] and Kings *et al.* [15] predicted qualitatively correct the sound pressure spectra in confined combustion setups, whereas Merk *et al.* [16] achieved quantitatively agreement with experimentally measured sound pressure spectra. Although LES allows quick changes in the characteristics of the acoustic boundaries or the surrounding confinement, it is computationally expensive. A study across a large parameter space is hardly affordable.

Another very flexible and computationally more efficient prediction approach is based on the use of a linear acoustic models such as linear network models [10,12,17] or more complex formulations that describe the acoustic wave propagation within complex geometries [14,17–20]. Compared to the use of a compressible LES, which resolves the noise generation as well as the acoustic propagation directly, the key idea of using linear acoustic models is to decouple the noise source from the acoustic propagation. By providing a model for the noise source, linear acoustic models are then capable of predicting qualitatively and quantitatively correct sound pressure spectra e.g. of a confined turbulent swirl combustor [10,12,14,17]. However, Silva *et al.* [10] showed that due to a two-way coupling between flame and acoustics there are situations, in which the mere incorporation of a noise source is not enough to predict the sound pressure spectra correctly. In addition, a model for the flame dynamics, i.e. the flame transfer function (FTF), is needed for correct sound pressure predictions.

The attractiveness of the linear acoustic model approach consists mainly in its flexibility as well as in its computational efficiency. Changes in the geometry of the setup or its acoustic boundaries can be realized quickly by changing the properties of the respective element in the linear acoustic model. Changes in the source characteristics or the flame dynamics can be implemented by replacing the respective model. This allows parameter studies across a large parameter space with reasonable effort and provides thus a suitable tool for predicting sound pressure levels in confined setups.

2. Objectives and scope of the work

As explained in the previous section, the FTF and a respective noise model are the key features of a linear acoustic model that is used for sound pressure level predictions. These models rely on the assumption that the total heat release rate fluctuation $\dot{Q}'_{\text{sum}}$, which is responsible for the sound generation across a turbulent flame [5], can be distinguished into two contributions, see Fig. 1. 1) A deterministic part $\dot{Q}'_c$ described by the FTF. For premixed flames this part relates incoming acoustic velocity fluctuations u'_{ac} to the deterministic heat release rate fluctuations $\dot{Q}'_c$ [21]. 2) A stochastic contribution $\dot{Q}'_s$ representing the stochastic heat release rate fluctuations that are caused by turbulent velocity fluctuations impinging on the flame front. This contribution should be, by definition, uncorrelated to any acoustic forcing. It can be described by a noise model, which filters a Gaussian white noise signal and outputs a colored noise signal that match the noise source characteristics of the flame, see Fig. 1. The summation of these two contributions $\dot{Q}'_{\text{sum}}$ is fed into the linear network model, where it is related to the generated acoustic pressure fluctuations. So essential for a correct estimation of the sound pressure spectrum by a linear acoustic model are accurate models for the FTF and the respective noise model [12,13]. Therefore, the focus of the current work is not yet laid on the prediction of sound pressure spectra based on linear acoustic models, but one step before: The accurate determination of FTF and noise model.

Polifke and co-workers [22] introduced a method to extract a FTF by combining LES with System Identification (SI) techniques [23,24]. In LES the flame is excited by an acoustic velocity fluctuation u'_{ac} with a broad-band spectral distribution. The resulting total heat release rate fluctuation $\dot{Q}'_{\text{sum}}$ is measured. From this discrete input-output time series the FTF can be modeled as a Finite Impulse Response (FIR) model structure by correlation analysis and SI methods. In the current work the proposed LES/SI approach shall be extended by further pursuing the identification techniques and model structures introduced into the field of thermo- and aero-acoustics by Jaensch *et al.* [25] and Sovardi *et al.* [26], respectively. Instead of only identifying a FTF, advanced SI techniques allow the simultaneous estimation of a combustion noise model from the same discrete broad-band input-output time series. The simultaneous identification of a noise model does not only improve the estimation of the FTF [25]. It also

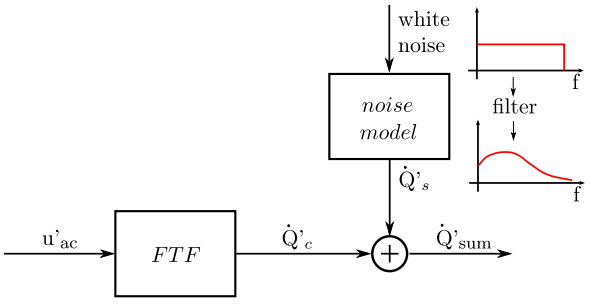

Fig. 1. Deterministic and stochastic contribution to the total heat release rate fluctuation.

With permission from M. Merk, S. Jaensch, C.Silva, and W. Polifke. Simultaneous identification of transfer functions and combustion noise of a turbulent flame. *Journal of Sound and Vibration, 422*, Elsevier, 2018.

provides valuable and necessary conclusions regarding the noise source strength and its spectral distribution, which are needed for the linear acoustic network model to predict the resulting sound pressure level. By extending the LES/SI approach, additional information is extracted from the generated time series data.

The overall goal of the current work is to investigate identifiability and quality assessment of model structures that allow the description of the deterministic part $\dot{Q}_c'$ and the stochastic part $\dot{Q}_s'$. Attention is paid particularly to the estimated noise models as the identification of the FTF received already notice [25]. However, it is emphasized that the noise model estimation always comes with a simultaneous identification of a FTF and cannot be isolated. It is then studied how the noise model quality of different model structures depends on certain properties of the used input-output time series, such as time series length and signal-to-noise ratio. Since a surrogate data model is used in this study to generate the time series, the reference FTF and noise model are known *a priori*. This offers a straightforward assessment of the identified model quality by comparing it against the reference model, which represents the *true* solution. As the *true* solution is normally not known when models are identified on the basis of LES data, an additional objective is to provide concepts allowing to draw conclusions on the identified model quality. Especially the determination of the most suitable model order is of high relevance for the application of SI methods on LES generated input-output time series.

The organization of the paper is as follows: In Section 3 the necessary SI theory is covered and the investigated model structures are introduced. In Section 4 the surrogate data model structure is explained along with its advantages regarding the current study, whereas the criteria of model quality assessment are shown in Section 5. Results of the respective identification for different model structures are presented in Section 6.1. Model order and quality is assessed in Section 6.2.

3. System identification

SI can be summarized as a combination of different theories, such as estimation theory, signal processing and systems theory. Keesman [27] describes the overall objective of SI as 'the construction of mathematical models of the system under study based on noisy time series'. The mathematical models, usually referred to as transfer functions, should correctly describe the observed input-output behavior of the system and thus its dynamics. In the herein considered framework of thermoacoustics, the FTF is a transfer function that treats acoustic velocity fluctuations u' as input signal and relates it to heat release rate fluctuations $\dot{Q}'$ as output signal. Therefore, the notation of u' as input and $\dot{Q}'$ as output signal is kept throughout the following sections. A single-input single-output system is generally described by

$$\dot{Q}'(t) = G \cdot u'(t) + H \cdot e(t) \tag{1}$$

here G refers to a polynomial transfer function of the 'plant' model that describes the deterministic part of the model. It establishes a causal relation between the input $u'(t)$ and the output $\dot{Q}'(t)$. H is a polynomial transfer function relating a white noise term $e(t)$ to the output $\dot{Q}'(t)$ and modeling thus the stochastic part of the model output. However, in the framework of thermoacoustics H would correspond to a noise model that mimics the contribution of turbulent combustion noise on the overall output $\dot{Q}'(t)$ and should not be mistaken as a sort of measurement noise that corrupts the measured output signal. H provides the contribution $\dot{Q}_s'$, which is physically related to combustion noise generated by turbulent velocity fluctuations. Note that incoming turbulent velocity fluctuations that impinge on a flame front and cause stochastic heat release rate fluctuations $\dot{Q}_s'$ are generally colored and not white. Yet, the noise model H uses by definition a white noise input term, from which every desired spectral distribution of $\dot{Q}_s'$ can be directly obtained by filtering the generic white noise input term $e(t)$ through the noise model H. So the noise model H mimics the effect of colored velocity fluctuations that cause a certain spectral distribution of $\dot{Q}_s'$, by shaping the same stochastic contribution from a generic white noise input. It contains thus physical information of the system. Recalling Fig. 1, the plant model G can be assigned to the FTF providing $\dot{Q}_c'$ whereas the polynomial transfer function H corresponds to the noise model with its output $\dot{Q}_s'$.

The SI procedure can be generally summarized in three steps. First, a broad-band time series with $u'(t)$ as input and $\dot{Q}'(t)$ as output is generated. Next, a specific model structure for G and H is chosen, suitable for describing the physics of the system under study. Last, depending on the model structure selected, the model coefficients of G and H are estimated within an optimization problem. The generation of input-output time series by means of a surrogate data model is explained in Section 4. The last two steps constitute the core of the SI procedure and are covered within the remainder of this section. Possible model structures and their characteristics are addressed in the following subsection 3.1. The estimation of the polynomial model coefficients is described in subsection 3.2.

3.1. Model structure

The most general structure of a rational polynomial model reads as

$$A(q,\boldsymbol{\theta})\dot{Q}'(t,\boldsymbol{\theta}) = \frac{B(q,\boldsymbol{\theta})}{F(q,\boldsymbol{\theta})}u'(t) + \frac{C(q,\boldsymbol{\theta})}{D(q,\boldsymbol{\theta})}e(t) \tag{2}$$

From this general formulation specific model structures may be derived by including or excluding the respective polynomial filters A, B, C, D and F. Accordingly, the different models vary in flexibility and modeling level of the deterministic and noise characteristics. The ones used in the current study are addressed in subsections 3.1.1–3.1.3. But first some remarks are made on

With permission from M. Merk, S. Jaensch, C.Silva, and W. Polifke. Simultaneous identification of transfer functions and combustion noise of a turbulent flame. *Journal of Sound and Vibration, 422*, Elsevier, 2018.

the general model structure and the physical interpretation of the respective polynomial filters. Compared to Eq. (1) and Fig. 1 it becomes evident that the polynomial filters $B(q,\boldsymbol{\theta})/F(q,\boldsymbol{\theta})$ describe the plant model G whereas $C(q,\boldsymbol{\theta})/D(q,\boldsymbol{\theta})$ specify the noise model H. The polynomial filters herein are expressed in terms of the time shift operator q^{-i} defined as

$$q^{-i}u'(t) = u'(t - i\Delta t) \tag{3}$$

yielding for the polynomial filters A, B, C, D and F

$$A(q) = 1 + a_1 q^{-1} + a_2 q^{-2} \ \dots a_{n_a} q^{-n_a}$$

$$B(q) = b_0 + b_1 q^{-1} + b_2 q^{-2} \ \dots b_{n_b} q^{-n_b}$$

$$C(q) = 1 + c_1 q^{-1} + c_2 q^{-2} \ \dots c_{n_c} q^{-n_c}$$

$$D(q) = 1 + d_1 q^{-1} + d_2 q^{-2} \ \dots d_{n_d} q^{-n_d}$$

$$F(q) = 1 + f_1 q^{-1} + f_2 q^{-2} \ \dots f_{n_f} q^{-n_f}$$

The polynomial model coefficients are summarized in the parameter vector $\boldsymbol{\theta}$

$$\boldsymbol{\theta} = \{a_1 \ \dots a_{n_a}, b_0 \ \dots b_{n_b}, c_1 \ \dots c_{n_c}, d_1 \ \dots d_{n_d}, f_1 \ \dots f_{n_f}\},$$

which is later estimated during the model coefficient estimation process described in Section 3.2. So inserting the polynomial filters into Eq. (2) the output $\dot{Q}'(t,\boldsymbol{\theta})$ results from a convolution of the respective polynomial model coefficients contained in $\boldsymbol{\theta}$ with present and past inputs or white noise disturbances. The values $\{n_a, n_b, n_c, n_d, n_f\}$ specify the polynomial model order and define how much prior input samples and stochastic disturbance samples are taken into account by the respective polynomial filter for the convolution. Explicitly modeling the stochastic disturbances by treating them as an output of a linear system driven by white noise, does not only provide valuable information on the noise source itself. It also improves the identification of the plant model, if the identification process relies on noisy data [25].

Whereas the polynomial filters B and C relate prior inputs $q^{-i}u'(t)$ and prior disturbances $q^{-i}e(t)$ to the current output $\dot{Q}'(t)$, respectively, the polynomial filters A, D and F relate former outputs $q^{-i}\dot{Q}'(t)$ to the current output $\dot{Q}'(t)$. A, D and F describe thus auto-regressive characteristics in the dynamics of the system. Prior outputs have an impact on the current one, hence an internal feedback mechanism is established. The difference between the polynomial filter A on the one hand and the two filters $\{F, D\}$ on the other hand is that A specifies poles that are shared by both the plant model as well as the noise model. This modeling approach is physics-wise reasonable when the disturbances enter the system already at the input and exhibit therefore the same dynamics as the plant model. In turn the polynomial filters F and D are independent and describe poles that are unique to the plant model and the noise model, respectively. From a practical point of view either a common polynomial filter A for the plant model $G(q,\boldsymbol{\theta})$ and the noise model $H(q,\boldsymbol{\theta})$ is used or two unique polynomial filters F and D.

Generally, the least complex model structure that is able to sufficiently describe the system's dynamics is regarded as the most suitable one. However, in the LES/SI approach for thermoacoustics, the choice of the most suitable model structure depends on the specific application and is still topic of ongoing research. Is a noise model needed? Should auto-regressive feedback be taken into account? If the model structure is too simple, a biased estimate results from the identification process. *Bias* means that a *systematic* error is made, since the selected model structure is not able to capture all relevant dynamics of the system under study. A second unknown in the SI procedure is the correct order of the polynomial filters. Assuming the model structure is chosen correctly, a model having a very small order may not be flexible enough to describe the system's behavior with a certain *accuracy*. Increasing the model order often increases its flexibility, meaning that the model error made decreases. Yet, if more model coefficients need to be estimated due to an increased model order, the model coefficient variance is also increasing. A large *variance* decreases the model's robustness. It yields excellent results on the training data set, which is the data set used for the identification. However, the prediction of the output based on a new data set, the so-called test data set, would fail. This behavior is known as *over-fitting* and is explained in more detail in Section 5.

To investigate the mentioned uncertainties in the SI procedure, three different model structures of varying complexity are investigated in detail and tested in regard to their suitability in the presence of noise. The model structure complexity ranges from the most simple FIR model (subsection 3.1.1) over an intermediately complex Auto-regressive Exogenous (ARX) model (subsection 3.1.2) to the rather complex Box-Jenkins (BJ) model structure (subsection 3.1.3). The choice of these tested model structures is related to the work of Jaensch *et al.* [25], who investigated only the FTF model quality for different model structures in the presence of noise and internal feedback. Yet, in the current study the focus is laid on the noise model quality and its general identifiability, a topic that has not received much attention so far.

3.1.1. *Finite Impulse Response + power spectral density (FIR + PSD)*

The FIR is a simple and widely used model in thermoacoustics [28–33]. It can be derived from the general polynomial model structure shown in Eq. (2) by setting the polynomial filters A, C, D and F equal to unity

$$\dot{Q}'(t,\boldsymbol{\theta}) = B(q,\boldsymbol{\theta})u'(t) + e(t) \tag{4}$$

With permission from M. Merk, S. Jaensch, C.Silva, and W. Polifke. Simultaneous identification of transfer functions and combustion noise of a turbulent flame. *Journal of Sound and Vibration, 422*, Elsevier, 2018.

The output of the model $\dot{Q}'(t,\boldsymbol{\theta})$ is computed by relating only prior inputs $u'(t)$ to the current output via the polynomial filter $B(q,\boldsymbol{\theta})$. The parameter vector $\boldsymbol{\theta}$ contains the model coefficients

$$\boldsymbol{\theta} = \{b_0, \quad b_2, \ \dots, b_{n_b}\}$$

wherein n_b specifies the number of model coefficients used and therefore the model order. The larger n_b the more prior inputs are taken into account and consequently more complex system responses can be modeled. Note that auto-regressive behavior cannot be taken into account in an FIR model since no former outputs $q^{-1}\dot{Q}'(t)$ are used for the computation of $\dot{Q}'(t)$. Regarding the noise treatment, it is emphasized that the FIR model structure does not come with any noise model estimates. The polynomial filters $C(q,\boldsymbol{\theta})$ and $D(q,\boldsymbol{\theta})$ are equal to unity and the FIR model assumes the noise to be Gaussian white noise with unity variance. Yet, as shown by Silva *et al.* [10] a rough estimation of the noise term is possible *after* the identification of the FIR model and can be seen as an additional post-processing step. The contribution of a colored noise term is consequently not taken into account *during* the identification process. Recalling the aforementioned assumption from Fig. 1 saying

$$\dot{Q}'_{\mathrm{sum}}(t,\boldsymbol{\theta}) = \dot{Q}'_c(t,\boldsymbol{\theta}) + \dot{Q}'_s \tag{5}$$

the term $\dot{Q}'_c(t,\boldsymbol{\theta})$ can be replaced by $B(q,\boldsymbol{\theta})u'(t)$ *after* the identification. The noise contribution of $\dot{Q}'_{\mathrm{sum}}$ can then be expressed as the unexplained portion between measured output $\dot{Q}'_{\mathrm{sum}}$ and the model output $\dot{Q}'_c$ as

$$\dot{Q}'_s = \dot{Q}'_{\mathrm{sum}} - B(q,\boldsymbol{\theta})u'(t). \tag{6}$$

By taking the power spectral density (PSD) of the noise term $\dot{Q}'_s$, here denoted as P_{QQ}

$$P_{QQ}(\omega) = \frac{2\Delta t}{N}\left|\sum_{n=0}^{N-1}\dot{Q}'_s \mathrm{e}^{-i\omega n\Delta t}\right|^2 \tag{7}$$

the normalized spectral distribution of the noise term can be computed by

$$\widehat{Q}_s(\omega) = \sqrt{\frac{P_{QQ}(\omega)}{2\Delta t}} \quad . \tag{8}$$

herein ω and N stand for the angular frequency and the total sample number of the time discrete input-output series, respectively. For the estimation of the spectral noise distribution no SI techniques are involved.

Note that the simple subtraction made in Eq. (6) is strictly seen only valid under open loop conditions. For closed loop conditions, a bias error is introduced, which is proportional to the cross-correlation matrix between input and noise signal [25]. Due to the flame inherent intrinsic thermoacoustic feedback the flame system is always a closed loop system and this bias error is thus unavoidable. Yet, as the magnitude of the introduced bias error is unclear and the FIR model structure is widely used in the field of thermoacoustics, the performance of this rather simple estimation approach will be tested against model structures that include a noise model estimation.

3.1.2. Autoregressive Exogenous Model (ARX)

The ARX model structure can be derived from the general polynomial model structure of Eq. (2) by setting the polynomial filters $C(q,\boldsymbol{\theta})$, $D(q,\boldsymbol{\theta})$ and $F(q,\boldsymbol{\theta})$ equal to unity. Compared to the FIR model described in the previous subsection, the ARX model structure additionally includes the polynomial filter $A(q,\boldsymbol{\theta})$ and reads as

$$A(q,\boldsymbol{\theta})\dot{Q}'(t,\boldsymbol{\theta}) = B(q,\boldsymbol{\theta})u'(t) + e(t) \tag{9}$$

The polynomial filter $A(q,\boldsymbol{\theta})$ here takes also prior outputs $q^{-i}\dot{Q}'(t)$ into account and allows thus the description of auto-regressive behavior. If an internal feedback mechanism is present in the system, the ARX model structure requires less model parameters than the FIR model to describe the in theory *infinite* response of the system to a given input. This yields a better estimate of the unknown model parameters contained in $\boldsymbol{\theta}$ as their variance is decreased [23]. By reformulating Eq. (9) to

$$\dot{Q}'(q,\boldsymbol{\theta}) = \frac{B(q,\boldsymbol{\theta})}{A(q,\boldsymbol{\theta})}u'(t) + \frac{1}{A(q,\boldsymbol{\theta})}e(t) \tag{10}$$

it gets evident that the ARX model structure also provides a noise model with $1/A(q,\boldsymbol{\theta})$. However, from Eq. (10) it can be seen that both the plant model $G(q,\boldsymbol{\theta}) = B(q,\boldsymbol{\theta})/A(q,\boldsymbol{\theta})$ and the noise model $H(q,\boldsymbol{\theta}) = 1/A(q,\boldsymbol{\theta})$ share the same polynomial filter $A(q,\boldsymbol{\theta})$. This implies that plant and noise model share the same poles and consequently the same dynamics. An independent modeling of plant and noise dynamics is not possible with an ARX model structure.

With permission from M. Merk, S. Jaensch, C.Silva, and W. Polifke. Simultaneous identification of transfer functions and combustion noise of a turbulent flame. *Journal of Sound and Vibration, 422*, Elsevier, 2018.

3.1.3. Box-Jenkins (BJ)

The BJ model structure represents the most general and thus most flexible model structure that can be derived from Eq. (2) and reads as

$$\dot{Q}'(t,\boldsymbol{\theta}) = \frac{B(q,\boldsymbol{\theta})}{F(q,\boldsymbol{\theta})}u'(t) + \frac{C(q,\boldsymbol{\theta})}{D(q,\boldsymbol{\theta})}e(t) \tag{11}$$

It contains the polynomial fractions $B(q,\boldsymbol{\theta})/F(q,\boldsymbol{\theta})$ and $C(q,\boldsymbol{\theta})/D(q,\boldsymbol{\theta})$ describing the plant model dynamics and the noise model dynamics, respectively. Regarding the previously described ARX model structure, the BJ model structure allows an independent characterization of plant and noise model and is therefore also consistent for closed loop systems [25]. Yet, as four independent polynomial filters have to be estimated, the number of model coefficients that need to be determined is higher than for an FIR model or an ARX model. This in turn yields usually higher model coefficient variances or requires more training data.

3.2. Model coefficient estimation

Once a certain model structure is chosen, the next step in the SI procedure is the determination of the respective model coefficients contained in the parameter vector $\boldsymbol{\theta}$. Accordingly, a least squares optimization problem can be formulated as

$$\min_{\boldsymbol{\theta}} J(\boldsymbol{\theta}) \equiv \min_{\boldsymbol{\theta}} \frac{1}{N}\sum_{i=0}^{N-1}\left(\dot{Q}'(i\Delta t,\boldsymbol{\theta}) - \dot{\mathcal{Q}}'(i\Delta t)\right)^2, \tag{12}$$

where the cost function $J(\boldsymbol{\theta})$ is minimized. The cost function $J(\boldsymbol{\theta})$ depends on the estimated model parameter vector $\boldsymbol{\theta}$ and is herein defined as the squared error between the *modeled* output $\dot{Q}'(i\Delta t,\boldsymbol{\theta})$ and the *real* output of the time discrete input-output time series $\dot{\mathcal{Q}}'(i\Delta t)$.

Depending on the model structure chosen, the least squares optimization problem in Eq. (12) has to be solved differently. This distinction arises from how the model structure relates the unpredictable white noise term $e(t)$ to the model output $\dot{Q}'(t,\boldsymbol{\theta})$. If an FIR model structure is used, no noise model $H(q,\boldsymbol{\theta})$ is taken into account. The predicted model output $\dot{Q}'(t,\boldsymbol{\theta})$ only depends on the input signal $u'(t)$. The least squares optimization problem becomes linear and can be solved for example via the so-called Wiener-Hopf inversion (WHI) [23–25]. A good estimate of $\boldsymbol{\theta}$ from the WHI requires uncorrelated input and noise signals, as shown in Ref. [25], otherwise a biased estimate results from the WHI. If a model structure is chosen that explicitly applies a noise model $H(q,\boldsymbol{\theta})$, the model's output $\dot{Q}'(t,\boldsymbol{\theta})$ depends at each instant on the current contribution of the noise term $e(t)$. But as aforementioned, the current contribution of the noise term $e(t)$ is by definition unpredictable. Therefore, Eq. (1) has to be cast into the so-called one-step ahead prediction form. First Eq. (1) is rewritten as

$$\dot{Q}'(t,\boldsymbol{\theta}) = G(q,\boldsymbol{\theta})u'(t) + H(q,\boldsymbol{\theta})e(t) = G(q,\boldsymbol{\theta})\ u'(t) + v(t), \tag{13}$$

wherein

$$v(t) = H(q,\boldsymbol{\theta})e(t) \longrightarrow e(t) = H(q,\boldsymbol{\theta})^{-1}v(t) \tag{14}$$

describes the colored noise contribution. As the noise contribution $e(t)$ is unknown at the current time step the best possible prediction of $v(t)$ can be achieved by taking all contributions of $e(t)$ except the current one into account. This results in

$$v(t|t-1,\boldsymbol{\theta}) = (H(q,\boldsymbol{\theta}) - 1)\, e(t) \tag{15}$$

The notation $v(t|t-1,\boldsymbol{\theta})$ indicates the one-step ahead prediction of the colored noise term. It is computed by a convolution of the noise model with all prior noise contributions of $e(t)$. Next, by combining Eq. (14) and Eq. (15) the relation between the one-step ahead prediction $v(t|t-1)$ and the actual colored noise term $v(t)$ adds up to

$$v(t|t-1,\boldsymbol{\theta}) = (1 - H(q,\boldsymbol{\theta})^{-1})v(t) \tag{16}$$

Next, inserting the one-step ahead prediction of the colored noise term into Eq. (13) results in an expression for the one-step ahead predicted output $Q'(t|t-1,\boldsymbol{\theta})$ according to

$$\dot{Q}'(t|t-1,\boldsymbol{\theta}) = G(q,\boldsymbol{\theta})u'(t) + (1 - H(q,\boldsymbol{\theta})^{-1})v(t) \tag{17}$$

herein the colored noise contribution $v(t)$ can be replaced by the subtraction of the real output $\dot{Q}'(t)$ from the plant model output

$$v(t) = \dot{Q}'(t) - G(q,\boldsymbol{\theta})u'(t) \tag{18}$$

yielding the final form of the one-step ahead prediction

$$\dot{Q}'(t|t-1,\boldsymbol{\theta}) = G(q,\boldsymbol{\theta})u'(t) + (1 - H(q,\boldsymbol{\theta})^{-1})(\dot{Q}'(t) - G(q,\boldsymbol{\theta})u'(t)) \tag{19}$$

It is emphasized that the predicted model output in Eq. (19) is now dependent on the discrete output time series $\dot{Q}'(t)$. This means that for the prediction of the model output $\dot{Q}'(t|t-1,\boldsymbol{\theta})$ not only all inputs, but also all outputs up to the current time

With permission from M. Merk, S. Jaensch, C.Silva, and W. Polifke. Simultaneous identification of transfer functions and combustion noise of a turbulent flame. *Journal of Sound and Vibration, 422*, Elsevier, 2018.

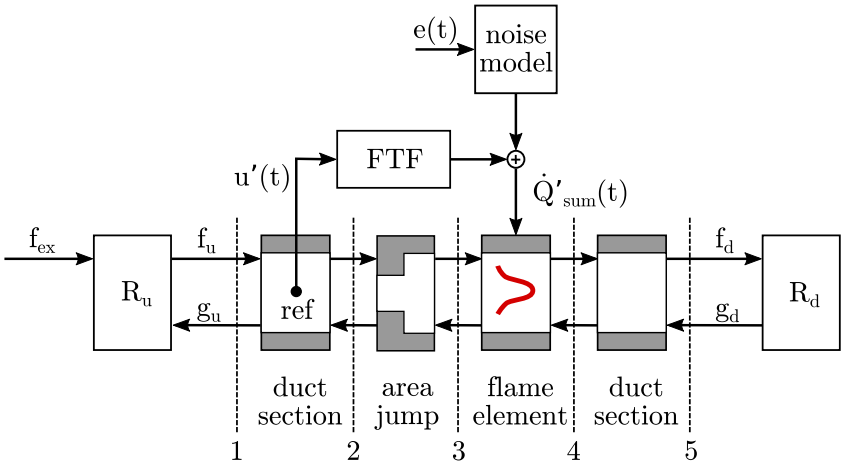

Fig. 2. Linear acoustic network model used for surrogate data generation.

step are used. The method of predicting the model outputs by using all information available up to the current time step is known as Prediction Error Method (PEM). For further details on PEM the reader is referred to [23,24].

In the present framework the PEM is needed for model structures which explicitly apply a noise model $H(q, \boldsymbol{\theta}) \neq 1$ such as ARX or BJ. The model parameter estimation based on PEM yields a non-linear least squares optimization of the form

$$\min_{\boldsymbol{\theta}} J(\boldsymbol{\theta})_{\mathrm{PEM}} \equiv \min_{b} \frac{1}{N} \sum_{i=0}^{N-1} \left(\dot{Q}'(i\Delta t|(i-1)\Delta t, \boldsymbol{\theta}) - \dot{Q}'(i\Delta t) \right)^2 \tag{20}$$

here the WHI is no longer applicable and numerical techniques like e.g. the Maximum Likelihood Estimation are necessary to solve the optimization problem. For further details the reader is again referred to [23,24].

3.3. Regularization of identification

The key idea of regularization is to constrain the model's flexibility in order to decrease the variance of the estimated model coefficients. It allows thus to control the trade-off between the model's accuracy and its variance. Hence, the cost function shown in Eq. (12) is extended in order to penalize the model's flexibility

$$J(\boldsymbol{\theta})_{\mathrm{reg}} = J(\boldsymbol{\theta}) + \lambda \boldsymbol{\theta}^T \mathbf{R} \boldsymbol{\theta} \tag{21}$$

herein λ defines a constant scalar regularization parameter that determines the trade-off between accuracy and variance. The larger the regularization parameter λ, the lower the accuracy of the model but also the variance of the estimated model coefficients in $\boldsymbol{\theta}$ is decreased. The positive definite matrix $\mathbf{R}$ allows a weighting of the respective model coefficients. A more detailed interpretation of the regularization parameters is given by Chen *et al.* [34]. If only short input-output time series are available, which is often the case for computationally expensive LES computations, regularization might help to limit the variance of the estimated model parameters. The effect and benefit of regularization on the identification of the *plant* model was already investigated [25,35,36]. However, the effect of regularization on the identified noise model is yet unclear and shall be investigated in the present study. The regularization technique will be applied on the ARX model structure.

4. Generation of surrogate data

As mentioned in Section 2 the goal of the present study is to investigate the identifiability of noise models and assess their quality. Testing different time series properties on LES generated data would be computationally very expensive. A surrogate data model is used instead in the present study. The surrogate data model consists of a linear acoustic network model that is solved in the time domain in order to generate a discrete input-output time series needed for the subsequent identification process. Acoustics within the network model are treated as linear and described by plane waves. The plane wave assumption holds as long as the cross-section of the geometry is much smaller than the acoustic wavelength of interest. For the given setup this condition is fulfilled as only frequencies below 1000 Hz are considered: Flames typically exhibit a low-pass behavior and combustion noise is known to be active in the low frequency region below 1000 Hz [37]. Plane acoustic waves are described via the characteristic wave amplitudes f and g defined as:

With permission from M. Merk, S. Jaensch, C.Silva, and W. Polifke. Simultaneous identification of transfer functions and combustion noise of a turbulent flame. *Journal of Sound and Vibration, 422*, Elsevier, 2018.

Table 1
Reference model structure and respective polynomial order.

Structure	na	nb	nc	nd	nf
BJ	–	30	5	5	1

$$f = \frac{1}{2}\left(\frac{p'}{\overline{\rho}\,\overline{c}} + u'\right) \tag{22}$$

$$g = \frac{1}{2}\left(\frac{p'}{\overline{\rho}\,\overline{c}} - u'\right) \tag{23}$$

A sketch of the linear network model used is shown in Fig. 2. It connects different elements, i.e duct sections, area jumps, reflective ends and a flame element. Across each element the characteristic waves can be mutually related. The duct sections shown in Fig. 2 are assumed to be much shorter than the minimal investigated wave length. Accordingly they are treated as acoustically compact meaning they do not introduce any phase lags due to wave propagation within the duct. Across an area jump the characteristic waves are related as

$$\begin{bmatrix} g_2 \\ f_3 \end{bmatrix} = \begin{bmatrix} \frac{\alpha-1}{\alpha+1} & \frac{2}{\alpha+1} \\ \frac{2\alpha}{\alpha+1} & \frac{\alpha-1}{\alpha+1} \end{bmatrix} \begin{bmatrix} f_2 \\ g_3 \end{bmatrix} \tag{24}$$

wherein α describes the area ratio between upstream to downstream cross-section area $\alpha = A_2/A_3 = 0.13$. The flame element couples the flame dynamics to the respective acoustic fluctuations at a given reference position via the linear Rankine-Hugoniot jump equations

$$\begin{bmatrix} g_3 \\ f_4 \end{bmatrix} = \frac{1}{\xi+1} \begin{bmatrix} 1-\xi & 2 & \Theta\bar{u}_3 \\ 2\xi & \xi-1 & \xi\Theta\bar{u}_3 \end{bmatrix} \begin{bmatrix} f_3 \\ g_4 \\ \dot{Q}' \end{bmatrix}, \tag{25}$$

herein ξ describes the specific acoustic impedance $\xi = \overline{\rho}_3\overline{c}_3/\overline{\rho}_4\overline{c}_4 = 2.57$ and the temperature ratio $\Theta = \overline{T}_4/\overline{T}_3 - 1 = 5.59$ across the compact flame element. The heat release rate fluctuation $\dot{Q}'$ is described by its two contributions $\dot{Q}'_c$ and $\dot{Q}'_s$, which are modeled via the plant model and the noise model, respectively. It is emphasized that the plant model and the noise model used in the surrogate data model, will serve as *reference* models for the estimated models of the SI procedure. As the reference models are used to generate the surrogate data, accurately identified models should be as close as possible to the reference models. In principle the reference models are a matter of choice. However, note that in the present study, the reference models (structure and order) should correspond to a model typically found in a thermoacoustic system. Otherwise the input-output time series properties found for an accurate identification of FTF and noise model, do not agree with those of the LES/SI approach applied on a real combustor. For example a reference model in the surrogate data approach with a very high model order would require overly long time series for an accurate identification.

To ensure a fairly realistic reference model in the surrogate data approach, a LES generated input-output time series of a turbulent swirl combustor [30] is used for the identification of the reference models. As reference model structure the most general BJ formulation is chosen with the polynomial filter orders $n_b = 30, n_c = 5, n_d = 5$ and $n_f = 1$, see also Table 1.

The choice of the BJ structure as a reference model is physically motivated. First, as shown by Silva *et al.* [38], the impulse response function of premixed flames is finite. Therefore, the reference model structure does not include an auto-regressive polynomial $F(q, \boldsymbol{\theta})$. Second, combustion noise is known to be colored [9,37,39], meaning that it is not equally distributed over the whole frequency range. This requires an explicit modeling of the noise term, since the white noise assumption as done e.g. in the FIR model structure, does not hold. Yet, the exact combustion noise dynamics are still unclear from a systems theory point of view. Hence the BJ model structure is the most convenient choice because it does not impose any restrictions on the noise term and does not result in a loss of generality. The resulting models are shown in Fig. 3 and Fig. 4. The reference FTF exhibits reasonable agreement with the experimentally measured FTF of Komarek and Polifke [40] and it can be concluded that the reference FTF is accurate enough to represent all relevant features of the turbulent swirl combustor. Its model order is sufficient.

After the reference models are determined and the geometrical elements are adapted to the combustor geometry described in Ref. [40], the network elements described can be formulated in state-space form and lumped together. This yields one state-space model describing the entire network model

$$\dot{x}(\mathbf{t}) = \mathbf{A}\mathbf{x} + \mathbf{B}\begin{bmatrix} f_{ex}(t) \\ e(t) \end{bmatrix} \tag{26}$$

$$\begin{bmatrix} u'(t) \\ \dot{Q}'(t) \end{bmatrix} = \mathbf{C}\mathbf{x} + \mathbf{D}\begin{bmatrix} f_{ex}(t) \\ e(t) \end{bmatrix} \tag{27}$$

With permission from M. Merk, S. Jaensch, C.Silva, and W. Polifke. Simultaneous identification of transfer functions and combustion noise of a turbulent flame. *Journal of Sound and Vibration, 422*, Elsevier, 2018.

Using the thermoacoustic network tool taX [41], the state-space model can be simulated in time to generate the surrogate input-output time series needed for the following identification process. Note that $f_{ex}(t)$ in Eq. (26) is a broad-band forcing signal imposed at the inlet of the system, as shown in Fig. 2. In accordance to typical LES values and if not specified otherwise, the length of the generated time series is equal to 350 ms and the forcing amplitude amounts to 10% of the mean flow velocity. The second input signal $e(t)$ in Eq. (26) describes a random Gaussian distributed white noise signal with zero mean and unity variance. After being filtered by the noise model it represents the stochastic contribution to the output caused by combustion noise. Because this contribution changes randomly during every simulation of the network model, different output time series are obtained for every realization. This is in line with the LES/SI approach. For unchanged working conditions but randomly different initial fields, the stochastic contribution of turbulent combustion noise manifests itself in varying output time series for each LES run. Consequently, the identified model may vary in accuracy. To take this uncertainty into account a Monte-Carlo approach is used in the present study. Every system with a certain test combination of parameters is evaluated 100 times. Due to the stochastic contribution $e(t)$ each input-output time series is unique and yields consequently different models for $G(q, \boldsymbol{\theta})$ and $H(q, \boldsymbol{\theta})$. From the data set for every test combination of parameters the mean model error (see Section 5.1) and its standard deviation can be computed.

Compared to the direct use of LES data, using a surrogate data approach to investigate the simultaneous identifiability of FTF and combustion noise model has two advantages. First, the chosen surrogate data approach is computationally efficient. This allows to quickly generate multiple realizations of input-output time series data with varying time series length, excitation amplitude or reflection conditions. Second, in a surrogate data approach the *true* FTF and the *true* noise model are known *a priori*, which would not be the case for a LES generated time series. The knowledge of the *true* models that are used to generate the data in the first place allows the calculation of the error made by the identified model against the *true* model. Of course, the ultimate aim is to apply the methodology on actual LES data, which is ongoing work, however, the surrogate data approach helps to obtain first a better understanding of the method itself.

5. Model quality assessment

An important aspect within the LES/SI approach is the model's quality assessment. The quality of the identified model usually depends on two general aspects: The chosen model structure and the respective polynomial model order. The model structure has to reflect the physics of the studied system. It should incorporate an auto-regressive part if a feedback loop is present in the original system or include a noise model if the stochastic perturbations are not white. An inadequate model structure usually yield a biased estimate of the identified model. Again, biased here means that a systematic error is introduced impeding the identified model to converge towards the *true* solution, even in the limit of infinitely long time series data. The bias introduced by different model structures into the FTF was already examined in Ref. [25]. However, how the noise model part $H(q, \boldsymbol{\theta})$ depends on the chosen model structure is yet unclear and is addressed in the current

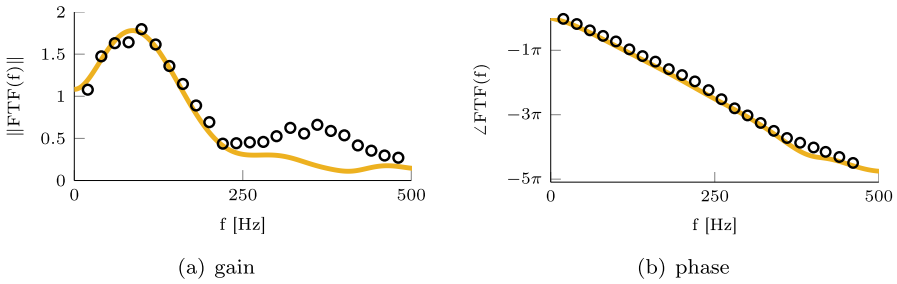

Fig. 3. FTF used in the surrogate data model: reference BJ model structure (solid), experimentally measured FTF [40] (circles).

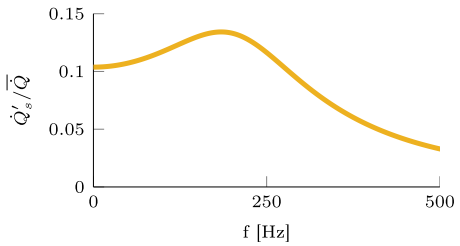

Fig. 4. Noise model used in the surrogate data model: reference BJ noise model (solid).

With permission from M. Merk, S. Jaensch, C.Silva, and W. Polifke. Simultaneous identification of transfer functions and combustion noise of a turbulent flame. *Journal of Sound and Vibration, 422*, Elsevier, 2018.

study.

To compare the error made by different model structures the *a priori* knowledge of the reference model is exploited. Details on the model error calculation are given in subsection 5.1. After a certain model structure is selected, the next step in the LES/SI approach consists in choosing a polynomial model order, i.e. choosing the number of polynomial model coefficients $\{n_a, n_b, n_c, n_d, n_f\}$. This is an important step because accuracy and variance of the identified model depend crucially on the polynomial order. If the polynomial model order is chosen too small, the identified models are said to be *under-resolved* and are not able to fully mimic the system's input-output behavior. Inaccurate models result from the identification. *Over-fitting* refers to the case, in which the polynomial model order is chosen higher than necessary. If the polynomial model order of the FTF is too high, it starts to describe stochastic processes in the particular realization of the training data set and *vice versa* if the noise model order is higher than adequate. The fitting of the noise realization implies high variances of the model coefficients. Even though the over-fitted model is able to describe the training data set with a high accuracy, the identified model coefficients come with a significant uncertainty. The over-fitted model is thus not general, but is tailored to the specific input-output time series. It would fail on a test data set, as the stochastic contribution would be different. The choice of the model structure and its model order is thus always a trade-off between generality and accuracy. An optimal model uses as few model coefficients as possible to describe the system's dynamics with acceptable accuracy. This is also known as the *principle of parsimony* [23,24]. The most suitable model order is not known beforehand. For an FIR model the number of coefficients necessary can be roughly estimated by number of relevant time lags that need to be captured [22]. If a more complex model structure is chosen such as ARX or BJ, the best model order of the auto-regressive part or the noise model is not evident. To find a suitable model order for these model structures Akaike's Information Criterion (AIC) (subsection 5.2) and a residual analysis (subsection 5.3) will be used. Besides their robustness these methods have the advantage that conclusions on the identified model quality can be drawn even without the knowledge of the *true* models, which is usually the case in the LES/SI approach.

5.1. Calculation of noise model error

The agreement between the reference noise model $H_{\mathrm{ref}}(j\omega)$ and the identified model from surrogate data can be expressed via the noise model error Δ as

$$\Delta \equiv \frac{\left\| H_{\mathrm{ref}}(j\omega) - H(j\omega, \boldsymbol{\theta}) \right\|_{\mathcal{H}_2}}{\left\| H(j\omega, \boldsymbol{\theta}) \right\|_{\mathcal{H}_2}} \tag{28}$$

wherein $\|\cdot\|_{\mathcal{H}_2}$ denotes the $\mathcal{H}_2$-norm given as

$$\left\| H(j\omega) \right\|_{\mathcal{H}_2} = \sqrt{\frac{1}{2\pi} \int_{-\pi}^{\pi} H(j\omega)^H H(j\omega)\, d\omega} \tag{29}$$

The error term is evaluated in the frequency domain and across all defined frequencies. No weighting of certain frequencies is applied. The noise model error Δ allows a quantitative comparison between the reference model and the estimated one. Thus conclusions on the accuracy and suitability of different model structures can be drawn.

5.2. Akaike's Information Criterion

Akaike's Information Criterion [42] can be used to determine the best model order for a certain model structure. Best refers here to the trade-off between the models accuracy and its variance. In its normalized from the AIC reads as

$$\mathrm{nAIC} \equiv \log\left(\det\left(\frac{1}{N} \sum_{i=0}^{N-1} \epsilon(i\Delta t, \boldsymbol{\theta}) (\epsilon(i\Delta t, \boldsymbol{\theta}))^T \right) \right) + \frac{2 n_p}{N} \tag{30}$$

herein $\epsilon(i\Delta t, \boldsymbol{\theta})$ describes the model residual, and n_p is the total number of estimated coefficients. The model residual is described similar to Eq. (20) as the difference between the real output and the predicted one. It represents the portion of the real output time series, which is not explained by the identified model and is defined as

$$\epsilon(i\Delta t, \boldsymbol{\theta}) = \dot{Q}'(i\Delta t) - \dot{Q}'(i\Delta t | (i-1)\Delta t, \boldsymbol{\theta}) \tag{31}$$

The first term of the nAIC in Eq. (30) increases if the model residuals $\epsilon(i\Delta t, \boldsymbol{\theta})$ increase, as it would be the case for an inaccurate model. The second term in Eq. (30) grows with the number of used polynomial coefficients and grows thus with the model order. According to Akaike's theory, the lower the AIC the better the selected model order. Consequently the AIC provides a quality metric that judges the mentioned trade-off between model accuracy and its variance as it penalizes both, model inaccuracies as well as high model orders. Results of the AIC are shown in Section 6.2.

With permission from M. Merk, S. Jaensch, C.Silva, and W. Polifke. Simultaneous identification of transfer functions and combustion noise of a turbulent flame. *Journal of Sound and Vibration, 422*, Elsevier, 2018.

5.3. Residual analysis

A second method helping to determine a suitable model order is based on a correlation analysis of the model residuals $\epsilon(i\Delta t, \boldsymbol{\theta})$. The residual analysis consist of two different tests: The *Independence Test* and the *Whiteness Test*.

The Independence Test is based on the cross-correlation between the model residuals ϵ and priors inputs u defined as

$$\gamma_{\epsilon u}(k, \boldsymbol{\theta}) = \frac{1}{\sqrt{\mathbf{K}_{uu}(0, \boldsymbol{\theta})\mathbf{K}_{\epsilon\epsilon}(0, \boldsymbol{\theta})}} \frac{1}{N-k} \sum_{i=1}^{N-k} \left(\left(\epsilon(i\Delta t, \boldsymbol{\theta}) - \overline{\epsilon} \right) \left(u\left((i+k)\Delta t\right) - \overline{u} \right) \right) \tag{32}$$

herein $\mathbf{K}_{uu}(0, \boldsymbol{\theta})$ and $\mathbf{K}_{\epsilon\epsilon}(0, \boldsymbol{\theta})$ are the first elements of the auto-correlation vector of the model inputs and the model residuals, respectively. According to the Independence Test the residuals should be uncorrelated to prior inputs, which is fulfilled if the cross-correlation values $\gamma_{\epsilon u}(k, \boldsymbol{\theta})$ are statistically insignificant. Statistical insignificance can be assumed if all values of $\gamma_{\epsilon u}(k, \boldsymbol{\theta})$ are within a certain confidence region, e.g. the 99% confidence region defined as $2.58/\sqrt{N}$. A significant correlation between residuals and input means that the identified plant model $G(t, \boldsymbol{\theta})$ describes the system's dynamics insufficiently. A value of $\gamma_{\epsilon u}(k, \boldsymbol{\theta})$ outside the confidence region at a certain time lag k implies that the output $\dot{Q}'(i\Delta t, \boldsymbol{\theta})$ that originates from the input at time $u\left((i-k)\Delta t\right)$ is not correctly described by the model because the residual contains input information. So the Independence Test allows primarily an estimation of the plant model order that should be chosen high enough to pass the Independence Test, but not higher in order to avoid over-fitting.

The Whiteness Test ensures that the residuals are an unpredictable random process. This is given if the auto-correlation values of the model residuals

$$\gamma_{\epsilon\epsilon}(k, \boldsymbol{\theta}) = \frac{1}{\mathbf{K}_{\epsilon\epsilon}(0, \boldsymbol{\theta})} \frac{1}{N-k} \sum_{i=1}^{N-k} \left(\left(\epsilon(i\Delta t, \boldsymbol{\theta}) - \overline{\epsilon} \right) \left(\epsilon\left((i+k)\Delta t\right) - \overline{\epsilon} \right) \right) \tag{33}$$

are always within a certain confidence region. A significant auto-correlation of the model residuals exhibits the possibility of predicting the residual dynamics that are not related to the input signal. These residual dynamics may e.g. correspond to a colored noise contribution. Especially in the framework of thermoacoustics this is of high relevance as combustion noise is known to be colored and only active in a certain frequency range [37,39]. Hence, the model order of the stochastic model can be estimated by means of the Whiteness Test. Again, the stochastic model order should be selected high enough to pass the Whiteness Test, but not unnecessarily higher. Results of the Independence Test and the Whiteness Test for surrogate data time series are shown in Section 6.2.

6. Results

The following result section is divided into two parts. Section 6.1 deals with the question of how different models structures (FIR+PSD, regularized ARX, BJ) generally perform regarding different time series and system properties, namely the excitation amplitude, the reflection conditions and the time series length. After the investigation of different model structures Section 6.2 focuses on the estimation of the model order, assuming that the *true* model order is unknown. The model identification and data processing is realized by using the system identification toolbox of Matlab 2016b.

6.1. Model structure

In this first subsection advantage is taken of the fact that the *true* FTF and noise model are known in the chosen surrogate data approach. This allows the computation of the noise model error Δ made by the identified noise models compared to the reference model, see Section 5.1. The 95% confidence interval of the noise model error Δ can be computed from the 100 Monte Carlo Samples of each realization.

A similar study was already performed [25]. However, therein only the evolution of the plant model error was investigated. Even for model structures as ARX or BJ the noise model part of the identified models was not further taken into account. But since also the noise model part contains valuable information on the physics of the system, especially in the framework of thermoacoustics, the focus within the current section is laid on the noise model estimates. Consequently only the errors made for the noise model estimation are shown in the following sections. For the respective behavior of the FTF model error the reader is referred to [25].

This section aims to carve out the differences between the model structures and not yet the influence of the respective model order. Accordingly, the respective model orders are set constantly equal to the reference model, described in Section 4. The used FIR models have a model order of $n_b = 30$ whereas the ARX models have an additional polynomial filter of order $n_{a_{\text{arx}}} = n_{c_{\text{BJ}}} = n_{d_{\text{BJ}}} = 5$.

6.1.1. Influence of excitation amplitude

First the influence of the signal-to-noise ratio (SNR) on the quality of the identified models is investigated. To get a behavior comparable to a real LES/SI application, the time series length is limited to 350 ms, which is a typically affordable length

With permission from M. Merk, S. Jaensch, C.Silva, and W. Polifke. Simultaneous identification of transfer functions and combustion noise of a turbulent flame. *Journal of Sound and Vibration, 422*, Elsevier, 2018.

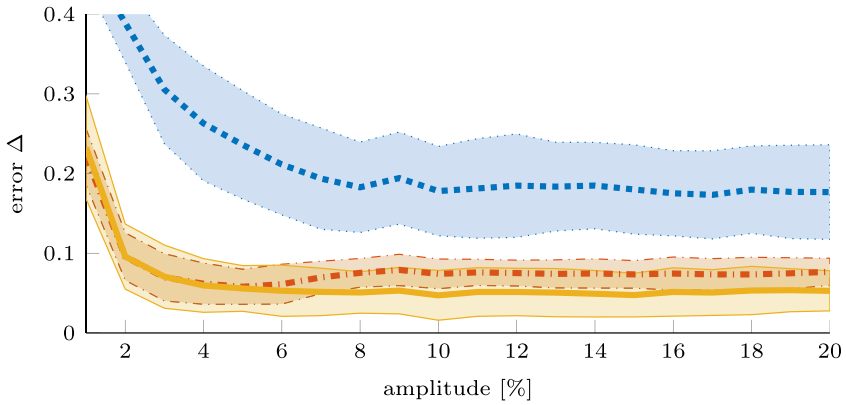

Fig. 5. Evolution of the noise model error Δ and its respective 95% confidence interval depending on the excitation amplitude: FIR+PSD (dotted), regularized ARX (dash-dotted), BJ (solid).

for a LES generated input-output time series. Non-reflective boundary conditions are applied with $R_u = R_d = 0$. The amplitude of the excitation signal f_{ex} in the surrogate data model is varied between $1\% - 20\%$ of the mean flow velocity in order to realize different SNR. Note that in a LES/SI application the forcing amplitude is limited. If the forcing amplitude is chosen too high, the flame response may become non-linear, which makes a linear identification impossible. In the surrogate data approach, however, the system responds linearly by definition, thus also the behavior in the limit of large SNR may be investigated.

The evolution of the noise model error Δ with increasing excitation is shown in Fig. 5. By first focusing on the FIR+PSD model, it can be observed that it is inferior to the other two model structures over the entire amplitude range. It does not only result in larger mean noise model errors (dotted line in Fig. 5) but also provides the largest confidence intervals (shaded area). As demonstrated in Ref. [25] for thermoacoustic applications, an FIR model for the FTF yields biased plant model estimates if the noise contribution is not white or the system exhibits a feedback mechanism that causes a correlation between input signal and noise term. Due to the simplistic computation of the noise contribution in the FIR+PSD approach, the plant model and the noise model are not independent, see Eq. (6). The simple subtraction in Eq. (6) is responsible for the fact that errors in the plant model directly propagate into the noise model part resulting in poor estimates of the noise model. In the range of small excitation amplitudes ($1\% - 6\%$), the small SNR yields poor plant model estimations. This in turn results in noise model estimates of poor accuracy. Above a certain excitation amplitude the noise model error Δ remains at a constant level.

Comparing the two remaining model structures, it can be observed that the noise model estimates of the regularized ARX model provide similar noise model errors Δ as the BJ model structure for small excitation amplitudes. Due to the regularization of the ARX model the confidence intervals remain relatively narrow even for small forcing amplitudes. The non-regularized BJ model structure shows here significantly wider confidence intervals. However, if the forcing amplitude is increased, the BJ model structure yield smaller noise model errors Δ compared to the regularized ARX model. The narrower confidence intervals of the regularized ARX model are bought by a slightly larger noise model error Δ.

6.1.2. Influence of acoustic reflection conditions

In many applications the flame is exposed to acoustic waves that are reflected at the acoustic boundaries of the system and subsequently fed back into the flame. Besides the already present flame inherent feedback mechanism [21,38], these acoustic reflections at the domain boundaries introduce an additional feedback mechanism. The strength of this feedback loop can be quantified e.g. by the outlet reflection coefficient R_d defined as the fraction of incoming to outgoing acoustic wave

$$R_d = \frac{g_d}{f_d} \tag{34}$$

Depending on the values of the reflection coefficient R_d, the system's stability may change from stable to unstable working conditions, in which self-sustained thermo-acoustic oscillations arise [43,44].

Fig. 6 represents the influence of the downstream reflection coefficient (see Fig. 2) on the identified noise model. The time series data for all Monte Carlo realizations have a length of 350 ms with a forcing amplitude of 10%. Again the FIR+PSD model structure exhibits the largest noise model error Δ throughout the parameter space examined. Moreover, only the FIR+PSD model structure shows a dependency of the noise model error on the downstream reflection coefficient R_d. This can be explained by the lack of any auto-regressive terms in the FIR model structure. The larger the outlet reflection coefficient R_d becomes, the stronger the feedback loop across the acoustic boundaries gets and consequently the larger the error made by an FIR model structure. Again, the error of the plant model propagates then directly into the noise model part. The regularized ARX and the BJ model structure include an auto-regressive part and hence do not show a dependency of the noise model error on the outlet reflection coefficient.

With permission from M. Merk, S. Jaensch, C.Silva, and W. Polifke. Simultaneous identification of transfer functions and combustion noise of a turbulent flame. *Journal of Sound and Vibration, 422*, Elsevier, 2018.

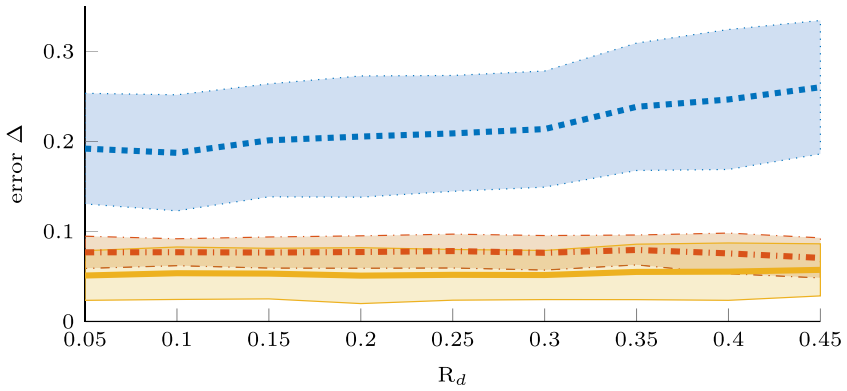

Fig. 6. Evolution of the noise model error Δ and its respective 95% confidence interval depending on the downstream reflection coefficient: FIR+PSD (dotted), regularized ARX (dash-dotted), BJ (solid).

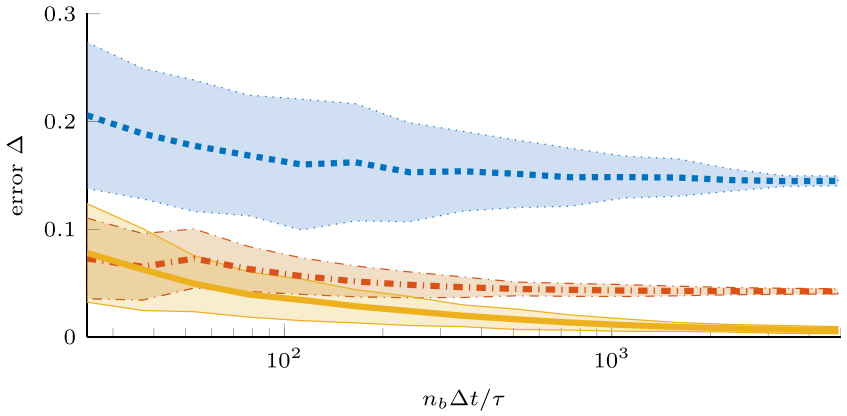

Fig. 7. Evolution of the noise model error Δ and its respective 95% confidence interval depending on the time series length used for the identification: FIR+PSD (dotted), regularized ARX (dash-dotted), BJ (solid).

For the LES/SI approach this implies an extension of the validity range. As long as the system remains linearly stable, completely non-reflective boundary conditions are not needed in the LES for a proper noise model identification. Only a model structure has to be chosen that includes auto-regressive terms, such as ARX or BJ. The FIR+PSD approach still provides reasonable estimates for reflecting boundary conditions, however, a stronger increase of the noise model error with increasing reflection is observable.

6.1.3. Behavior in the limit of infinite long time series

In this section the influence of the time series length on the noise model identification is examined. Whereas in experiments the measurement of relatively long time series is generally affordable, the time series length in LES is limited by the large computational effort. A study of the dependence of the model error on the time series length is thus important for the application of the LES/SI approach. Fig. 7 plots the noise model error over the length of the input-output time series used for the identification. The excitation amplitude amounts 10% of the mean flow velocity, non-reflective boundary conditions are applied. The time series length is normalized by the impulse response length τ, which depends on the flame length and a convective velocity close to the mean flow velocity [22]. An usually affordable LES generated time series of 350 ms, as it was used in the two previous sections, corresponds approximately to 30 τ.

In accordance with [25], the noise model should converge towards the reference model in the limit of infinitely long time series if a proper model structure is applied. Correspondingly, the BJ model in Fig. 7 converges towards a noise model error Δ equal to zero. The respective confidence intervals decrease with longer time series. However, the other two model structures yield biased estimates of the noise model even for very long time series, although their confidence intervals decrease for longer timer series. Since the ARX model structure comes up at least with a noise model estimation (the common $A(q, \boldsymbol{\theta})$ polynomial of FTF and noise model) its bias is smaller than for the FIR+PSD model structure in the limit of long time series. Yet, the constraint of the common polynomial $A(q, \boldsymbol{\theta})$ forces the plant model and the noise model to undergo the same dynamics, which is not

With permission from M. Merk, S. Jaensch, C.Silva, and W. Polifke. Simultaneous identification of transfer functions and combustion noise of a turbulent flame. *Journal of Sound and Vibration, 422*, Elsevier, 2018.

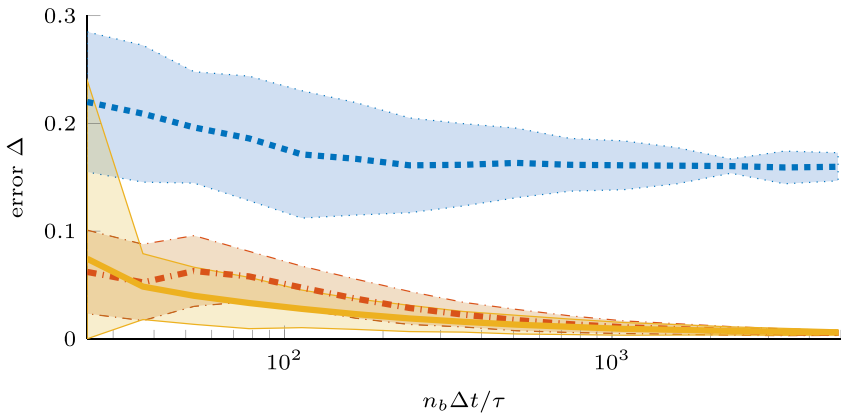

Fig. 8. Evolution of the noise model error Δ and its respective 95% confidence interval depending on the time series length used for the identification. An ARX model structure is used as reference model: FIR+PSD (dotted), regularized ARX (dash-dotted), BJ (solid).

the case for the reference BJ model structure. Thus a bias for the regularized ARX model structure results compared to the BJ reference model.

To underline the potential and the flexibility of the BJ model structure, the reference model is now replaced by an ARX reference model with $n_b = 30$ and $n_a = 5$. The same study as in Fig. 7 is carried out. Fig. 8 shows that also the ARX model structure is converging now towards the reference model for long timer series. This is not surprising as it agrees with the reference model structure in this case. But also the BJ models converge towards the correct solution, although the reference model has an ARX structure. This is possible as the BJ model structure is more flexible than the ARX model structure. With its independent polynomials $D(q, \boldsymbol{\theta})$ and $F(q, \boldsymbol{\theta})$ it allows to cover also the case of shared dynamics between plant and noise model. In this case $D(q, \boldsymbol{\theta}) \approx F(q, \boldsymbol{\theta})$ holds. However, in the range of short time series it exhibits slightly larger errors than the ARX model structure since more polynomial filters ($F(q, \boldsymbol{\theta})$ and $D(q, \boldsymbol{\theta})$ instead of only $A(q, \boldsymbol{\theta})$) and consequently more model coefficients have to be estimated. As already observable in Fig. 7, the FIR+PSD model structure does not converge towards the correct solution in the limit of infinitely long time series.

In the framework of the LES/SI approach this means that the BJ model structure is the most flexible one and has thus the largest range of validity. As especially the combustion noise dynamics are still unclear from a systems theory point of view, the BJ model structure is the most convenient choice. It provides unbiased estimates for independent plant and noise model dynamics as well as for a common dynamic behavior.

6.2. Model order

Note that in the previous section, the model order for all experiments and Monte Carlo realizations has been the same as the reference model order. This was only possible as the reference model and its model order were known *a priori*. In a usual LES/SI application this is not the case. Therefore, the focus of the following section is laid on the estimation and determination of the most suitable model order of FTF and noise model. Two different methods will be used in combination to estimate the most suitable model order: Akaike's Information Criterion (Section 5.2) and a model residual analysis (Section 5.3). It is emphasized that both methods may be used without the knowledge of the *true* reference model and are thus applicable in the LES/SI approach.

To investigate the different model orders, the BJ reference model is used to generate a data set of 100 time series with a time series length of 350 ms each. Subsequently, from this data set of time series BJ models with varying polynomial order are identified. In a first step, the model order of the plant model $G(q, \boldsymbol{\theta})$ is studied in more detail, see Section 6.2.1. The identification is evaluated for a range of different polynomial filter orders of the plant model, namely the order n_b of the polynomial filter $B(q, \boldsymbol{\theta})$ and n_c of the polynomial filter $C(q, \boldsymbol{\theta})$ is varied. For every combination of polynomial filter orders a Monte Carlo set of 100 samples is obtained.

Consequently in Section 6.2.2, the model order of the noise model $H(q, \boldsymbol{\theta})$ is further investigated. The plant model order of $G(q, \boldsymbol{\theta})$ is set to $n_b = 30$ according to the reference model. Again, 100 Monte Carlo samples are generated for every combination of the polynomial model orders n_c and n_d.

6.2.1. Plant model order

As described already in Section 5.2, the AIC judges the trade-off between the model's accuracy and its variance, depending on the chosen model order: The lower the AIC value, the better the trade-off. The shading in Fig. 9 corresponds to the mean nAIC value of the Monte Carlo data set. For an improved readability the global absolute minimum value of all combinations is used as an offset. The most favorable combination of polynomial model orders corresponds thus to a nAIC value of zero. Additionally to

With permission from M. Merk, S. Jaensch, C.Silva, and W. Polifke. Simultaneous identification of transfer functions and combustion noise of a turbulent flame. *Journal of Sound and Vibration, 422*, Elsevier, 2018.

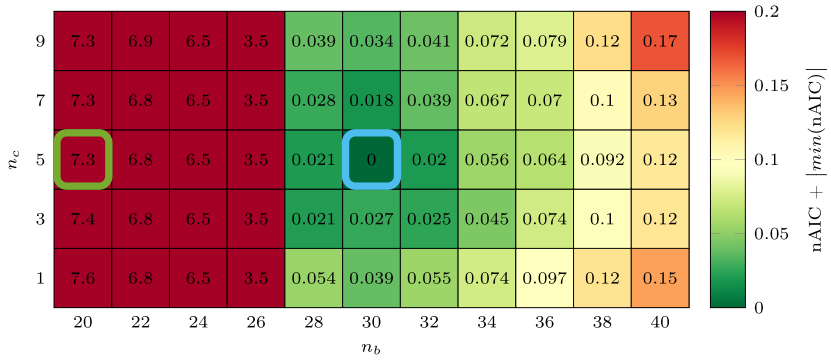

Fig. 9. nAIC for different combinations of polynomial filter orders n_b and n_c. The mean values are computed from 100 Monte Carlo samples per combination. Due to the chosen normalization, the overall best combination has a value equal to zero.

the shading the respective numeric mean value per combination is given in Fig. 9.

The optimal nAIC value appears for $n_b = 30$ and $n_c = 5$, which is equal to the reference model order. For smaller values of n_b the AIC values steeply increase. In this region the identified plant models are under-resolved and are not able to mimic the systems dynamics. The first term on the right-hand side of Eq. (30), which penalizes large model residuals, is dominant. The nAIC values also increase again towards higher model orders of the studied parameter space. Although the first term in Eq. (30) becomes eventually smaller for higher model orders as the accuracy further increases, the second term on the right hand side of Eq. (30) becomes dominant. The large amount of model parameters is penalized causing the nAIC to rise.

It is shown that the AIC converges towards the reference model order if enough data sets are evaluated. However, in the LES/SI approach usually only a few or even one time series is available. The AIC is thus rather a qualitative criterion for the chosen polynomial order since there are variations in the identified model quality within each combination of polynomial orders. Consequently, if the AIC is applied only on one data set, it does not stringently provide the correct reference model order. So to ascertain the AIC predictions of the most suitable model order, a residual analysis may be used to judge whether the model captures all relevant dynamics. The residual analysis allows to detect model parts that are not properly parametrized, e.g. which are under-resolved. To avoid over-fitting the model order should be chosen as small as possible to still pass the residual tests.

Moreover, the AIC does not allow conclusions on the absolute error made against a reference model. Hence, in the following mean values and confidence intervals of the identified models within a data set as well as a residual analysis for selected models are shown to underline the characteristics of certain combinations of polynomial model orders. Fig. 10(a) demonstrates the statistics for the data set with $n_b = 30$ and $n_c = 5$, represented by a square in Fig. 9. This combination corresponds to the polynomial model order of the reference model. The mean value of the identified FTF and noise models agree well with the reference model. The model errors are small. For models with a higher model order than the reference model (not shown here) this would also be true, yet, these models would exhibit larger variance and consequently a wider confidence interval.

Fig. 10(b) depicts the residual analysis of the example model shown in Fig. 10(a) (dotted line). The cross-correlation values between the input $u'(i\Delta t)$ and the model residuals $\epsilon(i\Delta t, \boldsymbol{\theta})$ do not exhibit any significance. All values fall into the 99% confidence region, indicating that there is no remaining correlation between the input and the model residuals. So all relevant deterministic processes are captured by the plant model and the Independence Test is passed.

Also all auto-correlation values of the residual $\epsilon(i\Delta t, \boldsymbol{\theta})$ lie within the shaded area of the 99% confidence region, except the one at time lag zero, which is equal to unity due to the normalization of the auto-correlation values. This implies that there is no significant auto-correlation within the model residuals and that the noise model thus captures all relevant dynamics contained in the process noise, e.g. a colored noise contribution. The chosen noise model order is high enough, the Whiteness Test is successful. If the Whiteness Test as well as the Independence Test are passed by an identified model, the model order can be assumed to be adequate. Again, an over-fitted model would also pass the residual test. Therefore, the smallest possible model order, which still passes both tests, should be chosen to avoid over-fitting.

In Fig. 11 the order of the FTF is reduced to $n_b = 20$, the noise model order is kept equal to the reference model order with $n_c = n_d = 5$. This case is also represented in Fig. 9 by a square. From the statistics of the identified FTF, shown on top in Fig. 11(a), it can be observed that the confidence intervals are slightly smaller than the ones of the case with $n_b = 30$, but the mean value (solid line) shows a discrepancy to the reference model (dashed line). The FTF is under-resolved and thus not capable of capturing all deterministic processes of the reference system. This is also observable in the Independence test in Fig. 11(b). The cross-correlation values for larger time lags fall outside the 99% confidence region. This can be interpreted as follows: The output of $\dot{Q}'(i\Delta t)$ that originates e.g. from the input $u'((i-n)\Delta t)$ is not correctly described by the model. This yields a significant cross-correlation of the input signal and the model residual for time lags larger than n. This indicates that a higher model order for the plant model should be chosen.

With permission from M. Merk, S. Jaensch, C.Silva, and W. Polifke. Simultaneous identification of transfer functions and combustion noise of a turbulent flame. *Journal of Sound and Vibration, 422*, Elsevier, 2018.

The noise model order is still equal to the reference model order. Accordingly, the mean values of the identified models, shown in Fig. 11(a), match the reference model and no significant auto-correlation is observable in the model residuals, see bottom of Fig. 11(b). This example illustrates how the prediction of the AIC criterion regarding the plant model order may be assured by the residual analysis.

6.2.2. Noise model order

In a next step the noise model order shall be studied in detail. The polynomial model order n_b of the plant model $G(q, \boldsymbol{\theta})$ is held constant and set equal to the reference model order. The model orders n_c and n_d of the noise model $H(q, \boldsymbol{\theta})$ are varied. In Fig. 12 it is confirmed, that the AIC statistically converges to the reference model order. For the LES/SI approach this makes the AIC criterion a valuable qualitative metric as it serves as a quick screening of the parameter space and allows

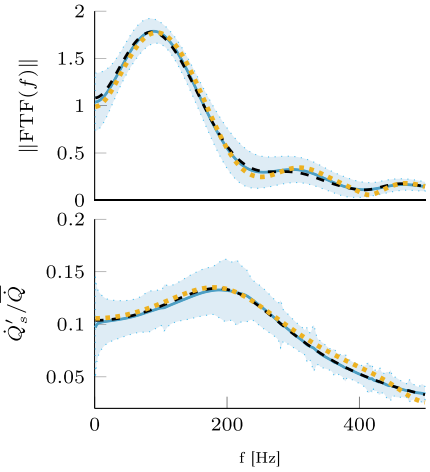

(a) Mean value (solid) and respective 99% confidence interval of identified models compared to the reference model (dashed) and an example of one identified model within the data set (dotted).

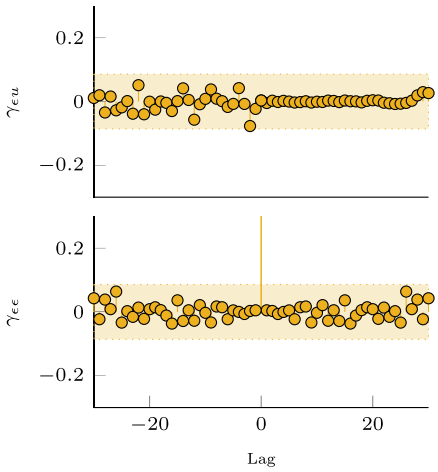

(b) Residual analysis of the example model shown in sub-figure (a) (dotted). The shaded area represents the 99% confidence interval.

Fig. 10. Statistics of identified data set with $n_b = 30$ and $n_c = 5$ (a) and residual analysis of example model within the data set (b).

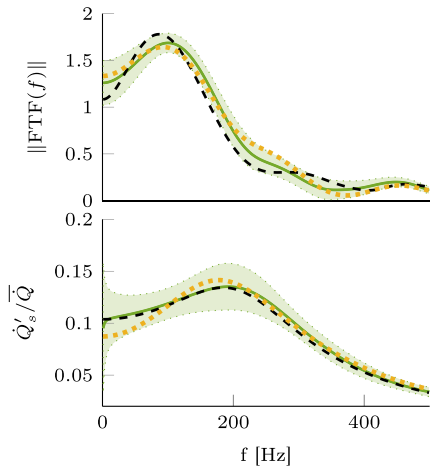

(a) Mean value (solid) and respective 99% confidence interval of identified models compared to the reference model (dashed) and an example of one identified model within the data set (dotted).

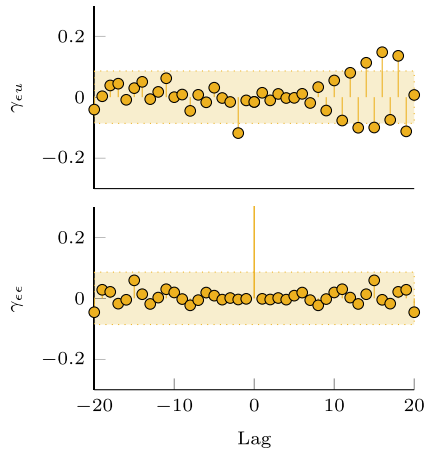

(b) Residual analysis of the example model shown in sub-figure (a) (dotted). The shaded area represents the 99% confidence interval.

Fig. 11. Statistics of identified data set with $n_b = 20$ and $n_c = 5$ (a) and residual analysis of example model within the data set (b).

With permission from M. Merk, S. Jaensch, C.Silva, and W. Polifke. Simultaneous identification of transfer functions and combustion noise of a turbulent flame. *Journal of Sound and Vibration, 422*, Elsevier, 2018.

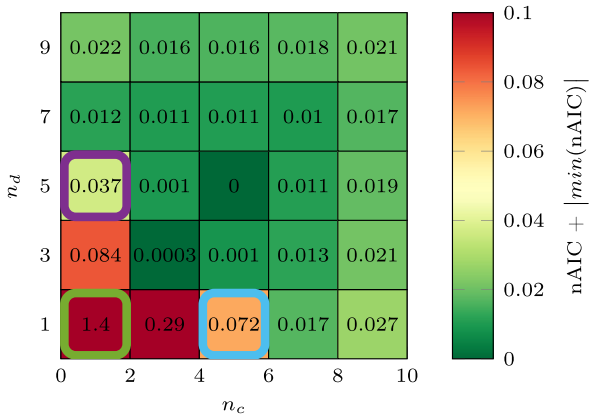

Fig. 12. nAIC for different combinations of polynomial filter orders n_c and n_d. The mean values are computed from 100 Monte Carlo samples per combination. Due to the chosen normalization, the overall best combination has a value equal to zero.

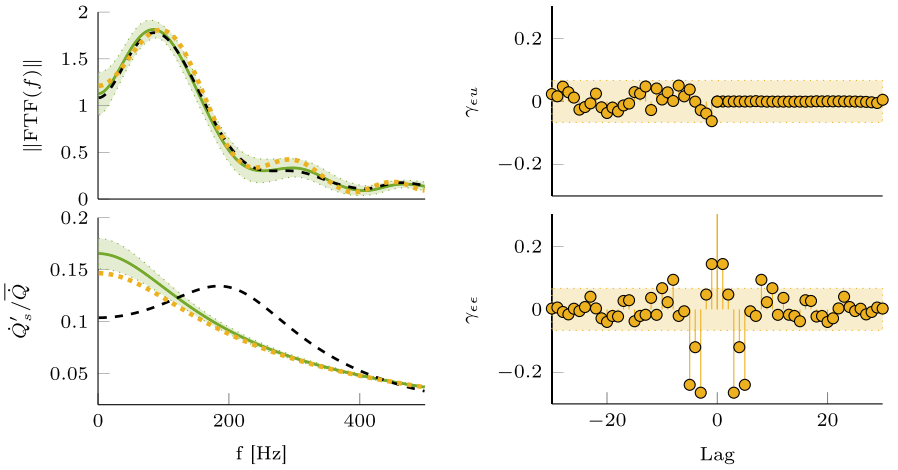

(a) Mean value (solid) and respective 99% confidence interval of identified models compared to the reference model (dashed) and an example of one identified model within the data set (dotted).

(b) Residual analysis of the example model shown in sub-figure (a) (dotted). The shaded area represents the 99% confidence interval.

Fig. 13. Statistics of identified data set with $n_c = 1$ and $n_d = 1$ (a) and residual analysis of example model within the data set (b).

conclusion on regions of suitable model orders. Especially for the noise model, for which a sophisticated guess of the best model order is difficult beforehand, the AIC can serve as a qualitative indicator. Again, certain model order combinations in Fig. 12 are investigated in more detail by means of their statistics and a residual analysis in order to get a more quantitative insight on the identified models. Fig. 13(a) represents the statistics of the FTFs and noise models with a polynomial order of $n_c = n_d = 1$. The estimates of the FTF is still in good agreement with the reference model as the plant model order is equal to reference model order with $n_b = 30$. The Independence Test is consequently passed by the chosen example model (see Fig. 13(b)). However, very poor estimates of the noise model are obtained. This can also be observed in the failed Whiteness Test. The strong auto-correlation indicate that the model residuals are not following an unpredictable random process but contain certain predictable dynamics. This is always the case if the noise contribution is colored. The noise model order should be increased to capture the dynamics contained in the noise contribution. Fig. 14 shows the results for a polynomial noise model order of $n_c = 1$ and $n_d = 5$. Even though the polynomial $C(q, \boldsymbol{\theta})$ is under-resolved the mean value of the noise model predictions is in very good agreement with the reference model, see Fig. 14(a). Hence both residual tests are passed. If the overall noise model order is kept constant, but the model order of the auto-regressive noise model part is decreased, the situation is different. For a parametrization of the noise model equal to $n_c = 5$ and $n_d = 1$ the mean value of the noise model estimates differ stronger from the reference model, see Fig. 15(a). The insufficiently parametrized auto-regressive part of the noise model can also be observed in the Independence Test. A significant cross-correlation of the input signal and the

With permission from M. Merk, S. Jaensch, C.Silva, and W. Polifke. Simultaneous identification of transfer functions and combustion noise of a turbulent flame. *Journal of Sound and Vibration, 422*, Elsevier, 2018.

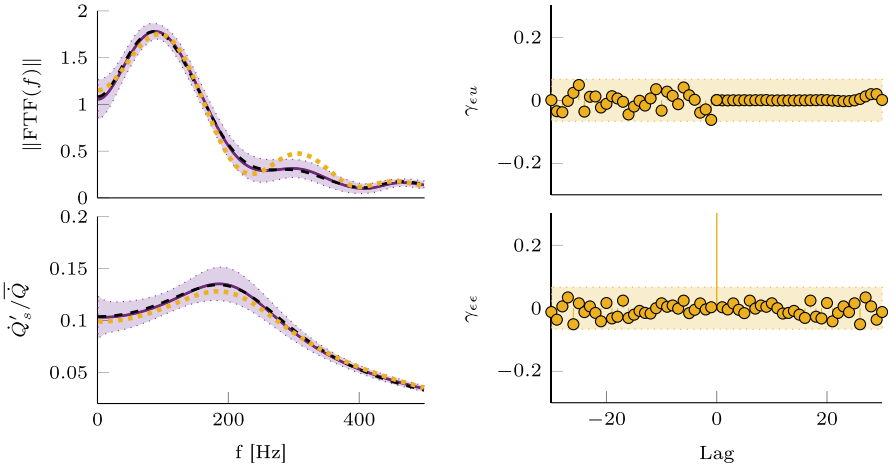

(a) Mean value (solid) and respective 99% confidence interval of identified models compared to the reference model (dashed) and an example of one identified model within the data set (dotted).

(b) Residual analysis of the example model shown in sub-figure (a) (dotted). The shaded area represents the 99% confidence interval.

Fig. 14. Statistics of identified data set with $n_c = 1$ and $n_d = 5$ (a) and residual analysis of example model within the data set (b).

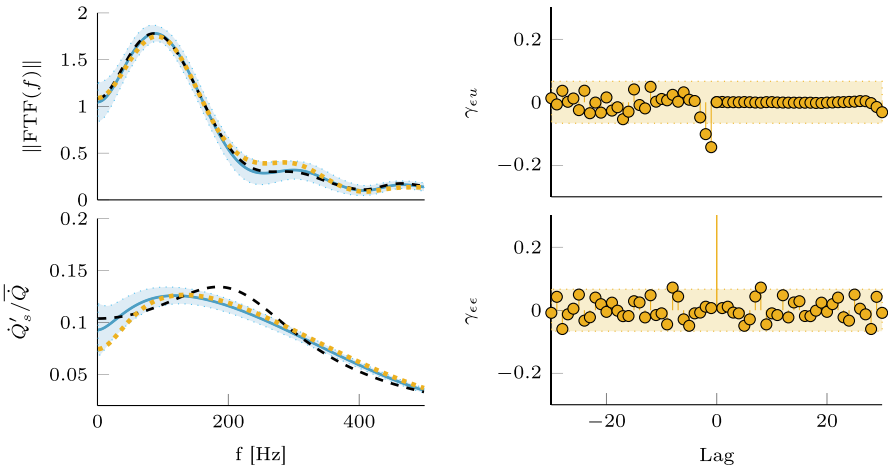

(a) Mean value (solid) and respective 99% confidence interval of identified models compared to the reference model (dashed) and an example of one identified model within the data set (dotted).

(b) Residual analysis of the example model shown in sub-figure (a) (dotted). The shaded area represents the 99% confidence interval.

Fig. 15. Statistics of identified data set with $n_c = 5$ and $n_d = 1$ (a) and residual analysis of example model within the data set (b).

model residuals for negative time lags indicates an unresolved auto-regressive model part [23]. So from comparing the results of Figs. 14 and 15 it can be concluded that especially a correct parametrization of the auto-regressive noise model part is important.

Summarizing this section, the demonstrated combination of AIC criterion and residual analysis provides a closed framework that allows to estimate a suitable model order in the LES/SI approach. Both methods may be used without the knowledge of the *true* reference models. Whereas the AIC criterion identifies qualitatively regions of suitable model orders, the residual analysis may be used to check the parametrization of an identified model in detail.

With permission from M. Merk, S. Jaensch, C.Silva, and W. Polifke. Simultaneous identification of transfer functions and combustion noise of a turbulent flame. *Journal of Sound and Vibration, 422*, Elsevier, 2018.

7. Conclusion

Based on a surrogate data model, the Large Eddy Simulation/System Identification (LES/SI) approach is extended to allow the additional identification of a noise model. The identifiability of the noise model is systematically examined and the influence of different time series properties, such as time series length and signal-to-noise ratio is studied. It could be shown that the Box-Jenkins model structure is superior to simpler model structures, especially if the identified system contains an independent colored noise contribution. This is expected in the case of identifying a turbulent flame, which makes the Box-Jenkins model structure the most promising modeling approach for the simultaneous identification of a flame transfer function (FTF) and a respective noise model of a turbulent flame. Even if the system is simpler and could be described by a model that exhibits shared dynamics of plant and noise model (Autoregressive Exogenous Model, ARX), the Box-Jenkins model structure converges towards the *true* solution in the limit of infinitive long time series. Moreover, it is demonstrated that the noise model of the Box-Jenkins model is not corrupted if reflecting boundary conditions are applied during the generation of the time series that are consequently used for the identification. As long as the system studied remains linearly stable no dependency of the noise model error on the reflection coefficient is observed. This increases the applicability of the LES/SI approach, since it can be used even if perfectly non-reflective boundaries are not available in the LES. The identifiability of the noise model in setups featuring a strong intrinsic thermoacoustic feedback is yet unclear and remains topic of on-going research.

Furthermore, two robust methods are demonstrated that allow the estimation of an adequate model order, which is especially for the noise model not evident beforehand. Akaike's Information criterion provides qualitative information on the model order of plant and noise model and judges the trade-off between a model's accuracy and its variance. The subsequent residual analysis yields a more detailed view on the respective parametrization of FTF and noise model.

The conducted study represents a solid basis for the application of advanced System Identification techniques on real LES data.

Acknowledgments

The authors acknowledge financial support by the German Research Foundation DFG, project PO 710/16-1 and by the Research Association for Combustion Engines (Forschungsvereinigung Verbrennung e.V - FVV, project number: 6011150).

References

[1] A.P. Dowling, Y. Mahmoudi, Combustion noise, Proc. Combust. Inst. 35 (1) (2015) 65–100, https://doi.org/10.1016/j.proci.2014.08.016.
[2] V.S. Burnley, F.E. Culick, Influence of random excitations on acoustic instabilities in combustion chambers, AIAA J. 38 (8) (2000) 1403–1410, https://doi.org/10.2514/2.1116.
[3] S.L. Bragg, Combustion noise, J. Inst. Fuel 36 (1963) 12–16.
[4] M.J. Lighthill, The bakerian lecture, 1961. Sound generated aerodynamically, Proc. R. Soc. Math. Phys. Eng. Sci. 267 (1329) (1962) 147–182, https://doi.org/10.1098/rspa.1962.0090.
[5] W.C. Strahle, On combustion generated noise, J. Fluid Mech. 49 (2) (1971) 399–414, https://doi.org/10.1017/S0022112071002167.
[6] P. Clavin, E.D. Siggia, Turbulent premixed flames and sound generation, Combust. Sci. Technol. 78 (1–3) (1991) 147–155, https://doi.org/10.1080/00102209108951745.
[7] C. Hirsch, J. Wäsle, A. Winkler, T. Sattelmayer, A spectral model for the sound pressure from turbulent premixed combustion, Proc. Combust. Inst. 31 (1) (2007) 1435–1441, https://doi.org/10.1016/j.proci.2006.07.154.
[8] J. Wäsle, A. Winkler, F. Weyermann, C. Hirsch, T. Sattelmayer, A model for turbulent combustion noise, Acta Acust. United Acust 95 (3) (2009) 391–401, https://doi.org/10.3813/AAA.918163.
[9] R. Rajaram, T. Lieuwen, Acoustic radiation from turbulent premixed flames, J. Fluid Mech. 637 (2009) 357–385, https://doi.org/10.1017/S0022112009990681.
[10] C.F. Silva, M. Merk, T. Komarek, W. Polifke, The contribution of intrinsic thermoacoustic feedback to combustion noise and resonances of a confined turbulent premixed flame, Combust. Flame 182 (2017) 269–278, https://doi.org/10.1016/j.combustflame.2017.04.015.
[11] B.B.H. Schuermans, W. Polifke, C.O. Paschereit, Modeling transfer matrices of premixed flames and comparison with experimental results, in: ASME 1999 International Gas Turbine and Aeroengine Congress and Exhibition, ASME 99-GT-132, ASME, Indianapolis, Indiana, USA, 1999, https://doi.org/10.1115/99-GT-132.
[12] F. Weyermann, C. Hirsch, T. Sattelmayer, Influence of boundary conditions on the noise emission of turbulent premixed swirl flames, in: J. Janicka, A. Schwarz (Eds.), Combustion Noise, Springer Verlag, 2009, pp. 161–188. ISBN-13: 978-3642020377.
[13] C.F. Silva, W. Polifke, J. O'Brien, M. Ihme, Towards concurrent identification of flame dynamics and combustion noise of enclosed flames, in: Proceedings of the Summer Program, Center for Turbulence Research, Stanford University, Stanford, USA, 2014, p. 179.
[14] C.F. Silva, M. Leyko, F. Nicoud, S. Moreau, Assessment of combustion noise in a premixed swirled combustor via Large-Eddy Simulation, Comput. Fluids 78 (2013) 1–9, https://doi.org/10.1016/j.compfluid.2010.09.034.
[15] N. Kings, W. Tao, P. Scouflaire, F. Richecoeur, S. Ducruix, Experimental, Numerical, Investigation of direct and indirect combustion noise contributions in a lean premixed laboratory swirled combustor, in: ASME Turbo Expo 2016: Turbomachinery Technical Conference and Exposition, GT2016–57848, ASME, Seoul, South Korea, 2016, https://doi.org/10.1115/GT2016-57848.
[16] M. Merk, R. Gaudron, M. Gatti, C. Mirat, T. Schuller, W. Polifke, Measurement and simulation of combustion noise and dynamics of a confined swirl flame, AIAA J. (2018) 1–13, https://doi.org/10.2514/1.J056502.
[17] W.C. Ullrich, Y. Mahmoudi, K. Lackhove, A. Fischer, C. Hirsch, T. Sattelmayer, A.P. Dowling, N. Swaminathan, A. Sadiki, M. Staufer, Prediction of combustion noise in a model combustor using a network model and a LNSE Approach, J. Eng. Gas Turbines Power 140 (4) (2017) 041501, https://doi.org/10.1115/1.4038026.
[18] T. Bui, W. Schröder, M. Meinke, Numerical analysis of the acoustic field of reacting flows via acoustic perturbation equations, Comput. Fluids 37 (9) (2008) 1157–1169, https://doi.org/10.1016/j.compfluid.2007.10.014.
[19] F. Flemming, A. Sadiki, J. Janicka, Investigation of combustion noise using a LES/CAA hybrid approach, Proc. Combust. Inst. 31 (2) (2007) 3189–3196, https://doi.org/10.1016/j.proci.2006.07.060.
[20] F. Grimm, R. Ewert, J. Dierke, G. Reichling, B. Noll, M. Aigner, Efficient combustion noise simulation of a gas turbine model combustor based on stochastic sound sources, in: ASME Turbo Expo 2016: Turbomachinery Technical Conference and Exposition, GT2015–42390, ASME, Montreal, Quebec, Canada, 2015, https://doi.org/10.1115/GT2015-42390.

With permission from M. Merk, S. Jaensch, C.Silva, and W. Polifke. Simultaneous identification of transfer functions and combustion noise of a turbulent flame. *Journal of Sound and Vibration, 422*, Elsevier, 2018.

[21] S. Bomberg, T. Emmert, W. Polifke, Thermal versus acoustic response of velocity sensitive premixed flames, Proc. Combust. Inst. 26 (3) (2015) 3185–3192, https://doi.org/10.1016/j.proci.2014.07.032.
[22] W. Polifke, Black-box system identification for reduced order model construction, Ann. Nucl. Energy 67C (2014) 109–128, https://doi.org/10.1016/j.anucene.2013.10.037.
[23] L. Ljung, System identification, in: J.J. Benedetto, A. Procházka, J. Uhlíř, P.W.J. Rayner, N.G. Kingsbury (Eds.), Signal Analysis and Prediction, Birkhäuser Boston, Boston, MA, 1998, pp. 163–173, https://doi.org/10.1007/978-1-4612-1768-8_11.
[24] A.K. Tangirala, Identification of dynamic models - concepts and principles, in: Principles of System Identification: Theory and Practice, CRC Press, Boca Raton, FL, 2014, pp. 479–518.
[25] S. Jaensch, M. Merk, T. Emmert, W. Polifke, Identification of flame transfer functions in the presence of intrinsic thermoacoustic feedback and noise, Combust. Theor. Model. (YY) (2018), https://doi.org/10.1080/13647830.2018.1443517.
[26] C. Sovardi, S. Jaensch, W. Polifke, Concurrent identification of aero-acoustic scattering and noise sources at a flow duct singularity in low mach number flow, J. Sound Vib. 377 (2016) 90–105, https://doi.org/10.1016/j.jsv.2016.05.025.
[27] K.J. Keesman, Time-invariant system identification, in: System Identification, Advanced Textbooks in Control and Signal Processing, Springer London, London, 2011, pp. 59–167.
[28] A. Gentemann, C. Hirsch, K. Kunze, F. Kiesewetter, T. Sattelmayer, W. Polifke, Validation of flame transfer function reconstruction for perfectly premixed swirl flames, in: ASME Turbo Expo 2004: Power for Land, Sea, and Air, GT2004–53776, ASME, Vienna, Austria, 2004, https://doi.org/10.1115/GT2004-53776.
[29] A. Giauque, T. Poinsot, F. Nicoud, Validation of a flame transfer function reconstruction method for complex turbulent configurations, in: 14th AIAA/CEAS Aeroacoustics Conference (29th AIAA Aeroacoustics Conference), AIAA/CEAS, Vancouver, Canada, 2008, https://doi.org/10.2514/6.2008-2943.
[30] L. Tay-Wo-Chong, S. Bomberg, A. Ulhaq, T. Komarek, W. Polifke, Comparative validation study on identification of premixed flame transfer function, J. Eng. Gas Turbines Power 134 (2) (2012), https://doi.org/10.1115/1.4004183, 021502–1–8.
[31] L. Tay-Wo-Chong, W. Polifke, Large Eddy simulation-based study of the influence of thermal boundary condition and combustor confinement on premix flame transfer functions, J. Eng. Gas Turbines Power 135 (2013) 021502, https://doi.org/10.1115/1.4007734.
[32] A. Innocenti, A. Andreini, B. Facchini, Numerical identification of a premixed flame transfer function and stability analysis of a lean burn combustor, Energy Procedia 82 (2015) 358–365, https://doi.org/10.1016/j.egypro.2015.11.803.
[33] Y. Yang, N. Noiray, A. Scarpato, O. Schulz, K.M. Düsing, M. Bothien, Numerical analysis of the dynamic flame response in alstom reheat combustion systems, in: ASME Turbo Expo 2015: Turbine Technical Conference and Exposition, GT2015–42622, ASME, Montreal, Quebec, Canada, 2015, https://doi.org/10.1115/GT2015-42622.
[34] T. Chen, H. Ohlsson, L. Ljung, On the estimation of transfer functions, regularizations and Gaussian processes—Revisited, Automatica 48 (8) (2012) 1525–1535, https://doi.org/10.1016/j.automatica.2012.05.026.
[35] S. Föller, W. Polifke, Advances in identification techniques for aero-acoustic scattering coefficients from large Eddy simulation, in: 18th International Congress on Sound and Vibration (ICSV18), vol. 4, 2011, pp. 3122–3129. Rio de Janeiro, Brazil.
[36] Y. Li, X. Wang, S. Mak, S.-T. Yeh, L.-H. Lin, C.-F.J. Wu, V. Yang, A two-stage transfer function identification methodology and its applications to Bi-swirl injectors, in: 53rd AIAA/SAE/ASEE Joint Propulsion Conference, AIAA Propulsion and Energy Forum, American Institute of Aeronautics and Astronautics, Atlanta, GA, U.S.A., 2017, https://doi.org/10.2514/6.2017-4933.
[37] H.A. Hassan, Scaling of combustion-generated noise, J. Fluid Mech. 66 (03) (1974) 445, https://doi.org/10.1017/S0022112074000292.
[38] C.F. Silva, S. Jaensch, T. Emmert, W. Polifke, On the autoregressive behavior of the intrinsic thermoacoustic feedback loop observed in premixed flames, in: 22nd International Congress on Sound and Vibration (ICSV22), Florence, Italy, 2015.
[39] S. Kotake, K. Takamoto, Combustion noise: effects of the shape and size of burner nozzle, J. Sound Vib. 112 (2) (1987) 345–354, https://doi.org/10.1016/S0022-460X(87)80201-8.
[40] T. Komarek, W. Polifke, Impact of swirl fluctuations on the flame response of a perfectly premixed swirl burner, J. Eng. Gas Turbines Power 132(6) (2010) 061503, https://doi.org/10.1115/1.4000127.
[41] T. Emmert, S. Jaensch, C. Sovardi, W. Polifke, taX - a flexible tool for low-order duct acoustic simulation in time and frequency domain, in: 7th Forum Acusticum, DEGA, Krakow, 2014.
[42] H. Akaike, Modern development of statistical methods, in: Trends and Progress in System Identification, Elsevier, 1981, pp. 169–184, https://doi.org/10.1016/B978-0-08-025683-2.50011-9.
[43] T. Poinsot, D. Veynante, Flame-acoustics interactions, in: Theoretical and Numerical Combustion, second ed., R.T. Edwards, Inc., Philadelphia, PA, 2012, pp. 375–431.
[44] S. Jaensch, M. Merk, E. Gopalakrishnan, S. Bomberg, T. Emmert, R. Sujith, W. Polifke, Hybrid CFD/low-order modeling of nonlinear thermoacoustic oscillations, Proc. Combust. Inst. 36 (3) (2017) 3827–3834, https://doi.org/10.1016/j.proci.2016.08.006.

With permission from M. Merk, S. Jaensch, C.Silva, and W. Polifke. Simultaneous identification of transfer functions and combustion noise of a turbulent flame. *Journal of Sound and Vibration, 422*, Elsevier, 2018.

With permission from M. Merk, S. Jaensch, C.Silva, and W. Polifke. Simultaneous identification of transfer functions and combustion noise of a turbulent flame. *Journal of Sound and Vibration, 422*, Elsevier, 2018.

Malte Merk[1]
Fakultät für Maschinenwesen,
Technische Universität München,
Garching 85747, Germany
e-mail: merk@tfd.mw.tum.de

Camilo Silva
Fakultät für Maschinenwesen,
Technische Universität München,
Garching 85747, Germany

Wolfgang Polifke
Fakultät für Maschinenwesen,
Technische Universität München,
Garching 85747, Germany

Renaud Gaudron
Laboratoire EM2C, CNRS,
CentraleSupélec,
Université Paris Saclay,
3, rue Joliot Curie,
Gif-sur-Yvette cedex 91192, France

Marco Gatti
Laboratoire EM2C, CNRS,
CentraleSupélec,
Université Paris Saclay,
3, rue Joliot Curie,
Gif-sur-Yvette cedex 91192, France

Clément Mirat
Laboratoire EM2C, CNRS,
CentraleSupélec,
Université Paris Saclay,
3, rue Joliot Curie,
Gif-sur-Yvette cedex 91192, France

Thierry Schuller
Institut de Mécanique des
Fluides Toulouse (IMFT),
Université de Toulouse,
CNRS, INPT, UPS,
Toulouse 31062, France

Direct Assessment of the Acoustic Scattering Matrix of a Turbulent Swirl Combustor by Combining System Identification, Large Eddy Simulation and Analytical Approaches

This study assesses and compares two alternative approaches to determine the acoustic scattering matrix of a premixed turbulent swirl combustor: (1) The acoustic scattering matrix coefficients are obtained directly from a compressible large eddy simulation (LES). Specifically, the incoming and outgoing characteristic waves f *and* g *extracted from the LES are used to determine the respective transmission and reflection coefficients via System Identification (SI) techniques. (2) The flame transfer function (FTF) is identified from LES time series data of upstream velocity and heat release rate. The transfer matrix of the reactive combustor is then derived by combining the FTF with the Rankine–Hugoniot (RH) relations across a compact heat source and a transfer matrix of the cold combustor, which is deduced from a linear network model. Linear algebraic transformation of the transfer matrix consequently yields the combustor scattering matrix. In a cross-comparison study that includes comprehensive experimental data, it is shown that both approaches successfully predict the scattering matrix of the reactive turbulent swirl combustor.* [DOI: 10.1115/1.4040731]

Introduction

Increasing environmental awareness and stringent emission regulations drive gas turbine manufacturers toward lean combustion technology [1]. This technology comes with lower emissions of nitrogen oxides or unburnt hydrocarbons. Unfortunately, lean combustion systems are also susceptible to self-excited thermoacoustic instabilities, which may generate pressure fluctuations of intolerable amplitude, causing severe damage to an engine.

For thermoacoustic stability analysis, a combustion system may conveniently be regarded as an assembly of elements, see Fig. 1. The acoustic properties of individual combustor elements may be described in terms of the respective *transfer matrix* or alternatively the *scattering matrix*. Transfer and scattering matrices are interchangeable inasmuch as one may be transformed into the other by straightforward algebraic manipulation. However, as we shall elaborate below, these two descriptions of acoustic behavior are not fully equivalent to each other and there are situations where it is advantageous to use one instead of the other.

The idea of describing individual elements of a complex acoustic system by two-port matrices was introduced by Munjal [2]. This approach has the advantage that the transfer behavior is independent of upstream and downstream impedance, which would not be true for a one-port element. For simple element types such as duct sections or area jumps, matrix coefficients may be derived approximately by analytical methods. Coefficient values for the geometrically more complex parts found in a combustor typically

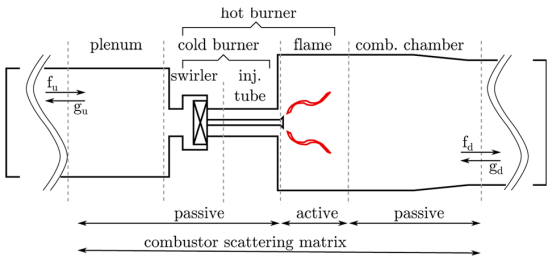

Fig. 1 Example of fragmenting a combustor into its acoustic elements

[1]Corresponding author.

Manuscript received June 22, 2018; final manuscript received June 29, 2018; published online November 14, 2018. Editor: Jerzy T. Sawicki.

Copyright © 2019 by ASME

M. Merk, R. Gaudron, C.Silva, M. Gatti, C. Mirat, T. Schuller, and W. Polifke. Direct assessment of the acoustic scattering matrix of a turbulent swirl combustor by combining system identification, large eddy simulation and analytical approaches. In *Journal of Engineering for Gas Turbines and Power, 2018*. Reprinted with permission from ASME.

have to be determined experimentally or numerically. Indeed, several studies deduced matrix coefficients for acoustically passive combustor parts of varying complexity, e.g., a single orifice [3], a tandem orifice [4], multiperforated liner plates [5], or a premixed nozzle [6]. The acoustic transfer behavior of swirl generators, which are an unavoidable part in swirl stabilized combustion systems, was numerically determined by Gikadi et al. [7] and Ni et al. [8]. A system of algebraic equations may be constructed from the collection of transfer (or scattering) matrices of the combustor elements. After closing this system with upstream and downstream boundary conditions, an "acoustic network model" or reduced order model (ROM) of the combustion system is obtained, which may be used, e.g., for linear stability analysis [9–11]. Experience has shown that this kind of analysis provides not only quantitative data on stability limits and dynamics of a combustion system but also important physical insight [9,11–16]. Several previous studies have concentrated on the transfer or scattering matrices of individual combustor elements such as a flame, a burner, a swirl nozzle, or a dissipative element [3–6,8,9,11,13,14,17–19]. The present study concerns in an integrated fashion a *combustor scattering matrix* that includes swirler, injection tube, and flame as well as parts of the combustion chamber, see Fig. 1.

In the absence of a flame, the passive parts of the combustor such as, e.g., swirler, area changes, or duct sections result in a certain acoustic transmission and reflection behavior of the combustor, described by the nonreactive or *cold* combustor scattering matrix. Under reacting conditions, the flame is an *active* element that introduces an additional degree of complexity. This applies in particular to swirl flames. Because of the swirling flow, the complex geometries involved, and the intricacies of flame dynamics with interaction of various physical processes [20], the assessed acoustic transfer relations will in general not be straightforward. The transfer matrix of a lean premixed gas turbine burner in a reactive or *hot* configuration was studied experimentally by Paschereit et al. [17,18]. Transfer matrix coefficients were measured by successive monofrequent excitation of the combustor flow with a two-source scheme. However, such *direct* measurement of a hot transfer matrix is very challenging and can be tedious. A careful calibration of the diagnostics is required for precise measurements of the acoustic variables and the downstream conditions in the reacting case are not conducive for precise measurements [14].

Therefore, alternative methods for determining the transfer matrix of a burner or combustor under hot conditions are desirable. One possibility is the use of large eddy simulation (LES) to *directly* deduce the combustor transfer or scattering matrix [13,19,21] from simulations with acoustic forcing, where a prescribed acoustic signal is imposed at the inlet or outlet of the LES domain. Considering that successive monofrequent excitation in LES entails very significant computational costs, the LES/system identification (SI) is the method of choice here. This approach is computationally efficient, as it allows to identify transfer functions or matrices over a range of frequencies from a single simulation with broadband acoustic forcing [22].

An indirect approach for determining a hot burner transfer matrix from a flame transfer function (FTF), which relates upstream velocity fluctuations to resulting heat release rate fluctuations, is proposed by Keller [9] and Polifke et al. [11]. Specifically, the hot burner transfer matrix is computed as the product of the transfer matrix of the cold burner and the transfer matrix of the flame, which is deduced from the Rankine–Hugoniot (RH) equations that describe the conservation of mass, momentum, and energy across an acoustically compact zone of heat release [9]. This *composition* method for the reactive configuration has been applied successfully in several studies [13–15] and is also employed in the present study: the FTF is coupled via the RH relations into a ROM of the full cold combustor, which is built from simpler acoustic elements (ducts, area jumps, flame element, …, see Fig. 1), in order to determine the hot combustor transfer matrix.

The *direct* as well as the *composed* approach come with certain advantages, but also limitations. The composed combustor scattering matrix is valid only for systems that respect the modeling assumptions of the RH+FTF coupling, such as, e.g., acoustic compactness of the flame and a dominant sensitivity of the flame to upstream velocity perturbations. The latter is not always the case for technically premixed flames. Moreover, simplifications due to the one-dimensional (1D) acoustics assumption are made in the composed approach. All these limitations are nonexistent in the direct approach, as all relevant effects are fully described within the LES. This means that, e.g., for noncompact or technically premixed flames, only the direct approach is applicable. On the other hand, if the composed approach is applicable, it requires significantly less computational effort than the direct approach. Even though both approaches require a computationally demanding LES in the first place, the identification of *four* frequency-dependent scattering matrix coefficients requires longer LES time series data for accurate estimation than *one* FTF model. More important though, as long as changes in the combustor geometry do not have an impact on the FTF, they may be easily taken into account in the respective element of the network model. So, once the FTF is identified, scattering matrices for a wide parameter space may be derived by a simple re-evaluation of the adapted ROM. In the direct approach, new LES runs need to be carried out if the geometry within the computational domain is changed.

The current work aims for a one-to-one comparison between the two different numerical methods of determining the scattering matrix of a turbulent swirl combustor in reacting conditions. This comparison provides valuable insight to which extent results of the two methods coincide for a case where the composed approach is applicable. Modeling results are also validated against and compared to experimental measurements of the FTF and the combustor scattering matrix. Note that a direct computation of a turbulent combustor scattering matrix with LES/SI constitutes a novelty and that a one-to-one comparison between the aforementioned methods is still lacking in literature for turbulent combustors.

Transfer and Scattering Matrices

Formally, the transfer matrix representation and the scattering matrix counterpart are mutually interchangeable. The transfer matrix defines the dynamic relation of the acoustic fields upstream and downstream of an element and is expressed in terms of primitive acoustic variables, i.e., the fluctuation of pressure p' and velocity u'

$$\begin{bmatrix} \frac{p'_d}{\overline{\rho c}} \\ u'_d \end{bmatrix} = \begin{bmatrix} T_{11} & T_{12} \\ T_{21} & T_{22} \end{bmatrix} \begin{bmatrix} \frac{p'_u}{\overline{\rho c}} \\ u'_u \end{bmatrix} \tag{1}$$

On the other hand, the scattering matrix is defined in terms of the characteristic waves or Riemann invariants

$$f = \frac{1}{2}\left(\frac{p'}{\overline{\rho c}} + u'\right) \tag{2a}$$

$$g = \frac{1}{2}\left(\frac{p'}{\overline{\rho c}} - u'\right) \tag{2b}$$

and relates the outgoing characteristic waves (f_d, g_u) to the incoming counterparts (f_u, g_d)

$$\underbrace{\begin{bmatrix} f_d \\ g_u \end{bmatrix}}_{\text{response}} = \begin{bmatrix} S_{11} & S_{12} \\ S_{21} & S_{22} \end{bmatrix} \underbrace{\begin{bmatrix} f_u \\ g_d \end{bmatrix}}_{\text{signal}} \tag{3}$$

As both representations are interchangeable, the scattering matrix coefficients can be computed from the transfer matrix coefficients by a simple algebraic transformation

M. Merk, R. Gaudron, C.Silva, M. Gatti, C. Mirat, T. Schuller, and W. Polifke. Direct assessment of the acoustic scattering matrix of a turbulent swirl combustor by combining system identification, large eddy simulation and analytical approaches. In *Journal of Engineering for Gas Turbines and Power, 2018*. Reprinted with permission from ASME.

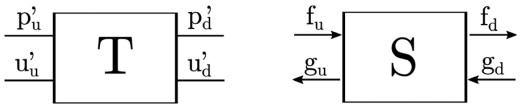

Fig. 2 Representation in terms of transfer matrix (left) and scattering matrix (right)

$$S_{11} = 2(T_{11}T_{22} - T_{12}T_{21})/D \tag{4a}$$

$$S_{12} = (T_{11} - T_{12} + T_{21} - T_{22})/D \tag{4b}$$

$$S_{21} = (-T_{11} - T_{12} + T_{21} + T_{22})/D \tag{4c}$$

$$S_{22} = 2/D \tag{4d}$$

with $D = T_{11} - T_{12} - T_{21} + T_{22}$.

As shown in Eq. (3) and Fig. 2, the scattering matrix coefficients S_{11} and S_{22} describe the transmission from upstream to downstream and *vice versa*. The scattering matrix coefficients S_{12} and S_{21} define the reflection of characteristic waves impinging from downstream and upstream, respectively. Compared to the transfer matrix representation, the scattering matrix representation respects the causality of the system. The characteristic waves f and g have a distinct propagation direction, which in turn allows to establish a causal relation between the input *signal* and the system's *response*, see Eq. (3). A certain input signal causes a certain response of the system. This in turn means that the present output of the system only depends on the present and previous inputs. Even though the transfer matrix is related to the scattering matrix by simple algebraic relations, see Eqs. (4*a*)–(4*d*), it does not respect causality since the primitive acoustic variables, in which the transfer matrix is expressed, do not have a distinct propagation direction. Thus, a strict separation between input *signal* and system's *response* is no longer possible. For further details on the causality of the respective representations, the reader is referred to Ref. [22].

Although only the scattering matrix respects causality, both representation exhibit certain advantages and disadvantages—so it makes sense to use both. On the one hand, the transfer matrix representation allows a fluid dynamical interpretation of its coefficients in terms of inertia and losses. The T_{22} coefficient, which relates upstream to downstream velocity perturbations, mainly characterizes the thermoacoustic interaction [14]. On the other hand, the scattering matrix allows to set up an acoustic energy balance determining the amplification or damping across the scattering object [15,19]. Based on that, the system's stability may be judged or possible feedback mechanism may be revealed [19]. The scattering matrix representation is also helpful when it comes to the definition of a combustion noise source vector, as shown by Paschereit et al. [18].

In regard to the costs of determination, both representations are comparable. In experiments, often the transfer matrix is measured [12,14,17,18,23] since the primitive acoustic variables p' and u' can be assessed directly. In the LES/SI approach, the scattering matrix is easier to identify as it respects causality and allows thus to apply a causal finite impulse response (FIR) model [19]. In the current work, the comparison between experimental and numerical results is presented in terms of the scattering matrix representation, since it provides a straight forward interpretation of the acoustic processes involved compared to the one given by the transfer matrix. Hence, the experimentally measured transfer matrices are transformed into the scattering matrix representation via Eqs. (4*a*)–(4*d*).

Experimental Setup

The investigated swirl combustor, shown in Fig. 3, is located at EM2C laboratory, Paris. A mixture of methane and air is injected

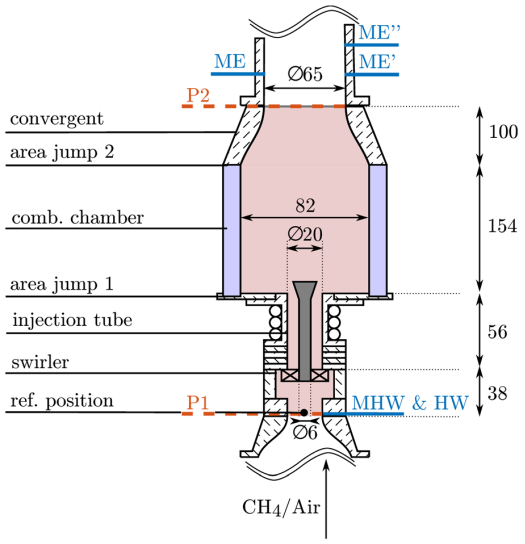

Fig. 3 Sketch of the EM2C turbulent swirl combustor. Dimensions are given in millimeter.

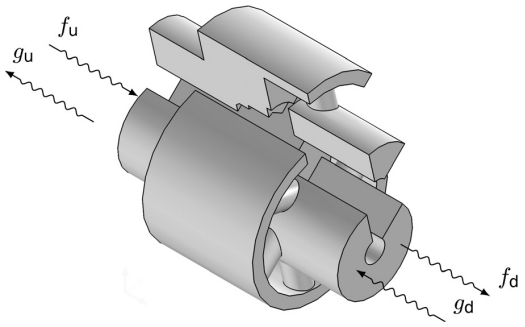

Fig. 4 Radial swirler geometry

in a tranquilization box (not shown in Fig. 3). A loudspeaker (Monacor SP-6/108PRO - 100 W RMS) is added at the bottom of the tranquilization box and generates the acoustic forcing corresponding to 10% of the mean inlet velocity. A plenum followed by a converging nozzle (contraction ratio: 8.73) generates a laminar flow with a top-hat velocity profile in the reference plane where a hot-wire probe HW (Dantec Dynamics Mini-CTA 54T30 with a 55P16 probe) is used to measure the velocity signal u'_u (in the top-hat region of the profile). At the same location, a microphone MHW (Bruel & Kjaer 4938) is used to measure the acoustic pressure fluctuations p'_u. A swirler (see Fig. 4) comprising six off-centered radial vanes of radius $R = 3$ mm (contraction ratio: 7.41) produces a flow with a swirl number $S = 0.8$ that was measured by Laser Doppler Velocimetry in the confinement chamber, just after the injector tube exit. A bluff body of conical shape is used to stabilize the flame inside the confinement chamber. A second convergent (contraction ratio: 2.03) is placed at the top of the combustion chamber, followed by an exhaust tube. The flame investigated in this study is a perfectly premixed methane/air flame with an equivalence ratio $\phi = 0.82$ and a thermal power of 5.5 kW. The associated bulk velocity at the hot-wire location is $u_b = 5.4$ m/s in a tube of diameter $D = 22$ mm, yielding a Reynolds number of approximately Re ≈ 7000.

Three microphones (Bruel & Kjaer 4938) are mounted on water-cooled waveguides in the hot gases region. The small

M. Merk, R. Gaudron, C.Silva, M. Gatti, C. Mirat, T. Schuller, and W. Polifke. Direct assessment of the acoustic scattering matrix of a turbulent swirl combustor by combining system identification, large eddy simulation and analytical approaches. In *Journal of Engineering for Gas Turbines and Power, 2018*. Reprinted with permission from ASME.

distortions induced by these waveguides while propagating the acoustic waves are corrected through the use of their transfer function that was determined previously. The first two microphones, ME and ME′ in Fig. 3, are located directly opposed in the exhaust tube, 35 mm downstream of the second convergent. A third microphone, ME″ in Fig. 3, is located 85 mm downstream the second convergent. In addition to the acoustic pressure fluctuations p'_d measured by ME″ in the downstream region, the three-microphone method [24] is used to reconstruct the acoustic velocity fluctuations u'_d at the same axial position. In order to improve the signal-to-noise ratio, all experiments are made twice: one in the original configuration presented in Fig. 3 and another one with the microphones ME′ and ME″ switched. Moreover, coherence functions are also adopted when reconstructing u'_d [24].

Equation system (1) contains four unknowns T_{11}, T_{12}, T_{21}, T_{22} but only two equations, which explains why two independent acoustic states are needed. In most experiments, the two source method is used [14,17,18,23]. Here, the two loads method is retained [25]. Both methods are based on the same physical process, namely a modification of one or more acoustic boundary conditions. For reactive conditions, the two loads used in this study consist of an exhaust tube of length $L = 220$ mm and the same exhaust tube with a perforated plate added at the top of it. For nonreactive conditions, the first load consists again of an exhaust tube of length $L = 220$ mm, whereas the second load makes use of two exhaust tubes with a total length of $L = 440$ mm. The configurations used in both cases are independent for all frequencies of interest.

Large Eddy Simulation/System Identification Approaches

Two different approaches are applied to obtain the scattering matrix for cold and hot conditions. First, in the direct approach, the scattering matrix is directly computed from the LES time series. Second, only the FTF is identified from LES generated time series data. The identified FTF is then coupled via the RH jump equations into a ROM of the passive combustor. The hot combustor scattering matrix is consequently obtained from the composed model. Before the individual approaches are described in detail, the LES setup and the SI method as used in both approaches are introduced.

Large Eddy Simulation/System Identification Methodology. Compared to the studies of Polifke and coworkers [19,21], which were based on unsteady Reynolds-averaged Navier–Stokes (RANS) simulation, a compressible LES is used in the present study. Giauque et al. [26] showed that LES provides a better estimation of the time lag between heat release fluctuations and upstream velocity fluctuations than a RANS computation. Similarly, Tay-Wo-Chong et al. [27] stated that LES yields more accurate estimates of the FTF than unsteady RANS.

The LES is performed with the solver AVBP [28]. The fully compressible Navier–Stokes equations are solved on an unstructured grid consisting of approximately 19 million cells with a maximum cell size of 0.6 mm in the flame region. The shaded area in Fig. 3 indicates the domain resolved by the LES. The rather complex geometry of the swirler shown in Fig. 4 is fully resolved by the LES. No geometrical simplifications are applied. The six off-centered radial swirler vanes, which have a diameter of 6 mm, are resolved by approximately 18 cells in the diameter that are refined toward the walls. In total, the section containing the swirler is resolved by about 4 million cells.

For handling subgrid scales in the LES, the WALE model is applied [29] due to its capacity to recover turbulent subscale statistics in near wall regions. Turbulence–flame interaction is taken into account by the dynamically thickened flame [30] model with seven cells resolving the laminar flame thickness. The chemistry of the perfectly premixed methane/air flame is described by a

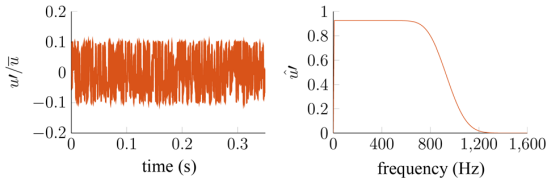

Fig. 5 Forcing signal: time series (left) and spectral distributions (right)

global two-step scheme. Nonreflecting boundary conditions are applied at the inlet and outlet by using plane wave masking [31]. For further details and a proper validation of the LES setup, the reader is referred to Ref. [32].

Instead of computing discrete values of the scattering matrix or the FTF by forcing the flow monofrequently and repeatedly over a certain frequency range, the flow is forced with an acoustic broadband signal. As forcing signal, a wavelet type signal is used, see Fig. 5. The forcing amplitude is set to 10% of the mean inlet velocity and the signal has a constant power spectral density and a low auto-correlation up to the cut-off frequency of approximately 800 Hz. Having no peak values in the broadband forcing signal above 10% of the mean inlet velocity ensures that the flame response remains in the linear regime. Two independent data sets with a respective time series length of 350 ms are created. The chosen time series length of 350 ms represents a compromise. Generally, longer time series yield a more accurate identification but are also computationally more expensive. A value of 350 ms results thus from best practice as it allows a proper and robust identification with reasonable computational effort. For the first data set, the acoustic forcing signal is applied at the inlet (f_u) and the resulting signals are extracted from the measurement planes P1 (g_u) and P2 (f_d). The second data set is generated analogously by applying a downstream forcing (g_d) and measuring the time series (g_u, f_d).

From the generated time series data, models can be identified that relate respective inputs and outputs. Depending on the choice of input and output signals, the four scattering matrix coefficients or the FTF can be identified. In both cases, every transfer expression is modeled by a causal FIR, which relates present outputs to prior inputs [27,33,34]. Note that for a noncausal system representation, as, e.g., the transfer matrix, a noncausal FIR model needs to be applied that requires both prior and future inputs in order to estimate the model output [13]. The causal FIR model reads as

$$y(t) = \sum_{i=0}^{n_b} b_i\, x(t - i\Delta t) + e(t) \tag{5}$$

Herein, the model output $y(t)$ is computed by convoluting the prior inputs $x(t - i\Delta t)$ and the FIR coefficients b_i. The number of prior input samples that are taken into account via the impulse coefficients b_i and thus the length of the FIR are specified by the model order n_b. Conversely, this means that the model order n_b determines how many model FIR coefficients b_i have to be estimated from the time series data. The higher the chosen model order n_b, the longer the time series needed for an accurate and robust identification of the respective FIR coefficients b_i. The term $e(t)$ represents a white noise perturbation on the output $y(t)$.

Direct Approach for Scattering Matrix. In the direct approach, the characteristic waves f and g are extracted from the LES measurement planes P1 and P2, see Fig. 3. These two measurement planes coincide with the inlet and the outlet of the LES domain and contain all combustor parts shown in Fig. 3 in between them. Note that the location of the downstream measurement ME″ does not coincide with the measurement plane P2 in the LES domain. This discrepancy stems from the fact that the

M. Merk, R. Gaudron, C.Silva, M. Gatti, C. Mirat, T. Schuller, and W. Polifke. Direct assessment of the acoustic scattering matrix of a turbulent swirl combustor by combining system identification, large eddy simulation and analytical approaches. In *Journal of Engineering for Gas Turbines and Power, 2018*. Reprinted with permission from ASME.

same LES setup is used as in Ref. [32], for which the LES was validated. However, the need in the current study of properly measuring the acoustic fluctuations downstream requires the test rig to be equipped with an additional pipe that contains the mounted microphones ME, ME′, and ME″ (see Fig. 3). Since the additional pipe has a constant cross section area, its only effect on the measured acoustic waves is the introduction of an additional time lag compared to the plane P2. To take this into account and to guarantee a proper comparison between measurements and numerical results, the numerically extracted time series in the direct approach are shifted by the aforementioned time lag in a first postprocessing step. This has an influence on the phase of the computed scattering matrix coefficients from the direct approach. The time lag Δt can be computed via the distance between the numerical measurement plane P2 and the microphone ME″ $\Delta x = 0.085$ m and the respective speed of sound c_c (nonreactive case) or c_h (reactive case). In order to separate acoustic from turbulent fluctuations, a characteristics-based filter [35] is applied, which improves the quality of the SI. Flame dynamics, flame-acoustic interactions, as well as acoustic propagation in the complex combustor geometry are directly resolved by the LES. From the upstream forced data set, the scattering matrix coefficients S_{11} and S_{21}, which describe the reflection and transmission of characteristic waves impinging from upstream, are directly identified via the SI procedure. Analogously, the coefficients S_{12} and S_{22} are estimated from the data set with downstream forcing applied.

In theory, it is also possible to get the four scattering matrix coefficients from one single data set, in which independent upstream and downstream forcing is applied simultaneously. Although this technique yielded accurate results for cold conditions, unsatisfactory results were obtained in the reactive case for a time series length of 350 ms. One possible reason might be that the generated time series was too short in the reactive case for the simultaneously identification of all four scattering matrix coefficients. Moreover, other than in the nonreactive case, combustion noise corrupts the time series data. This means that acoustic fluctuations, generated by turbulent velocity perturbations impinging on the flame front, overlay the forced flame response resulting from the acoustic broadband forcing. It is emphasized that this issue applies not only for a broadband forcing method but also in cases of a monofrequent forcing of the flow. The totally recorded acoustic fluctuations may thus be distinguished into two contributions: First, a contribution that results from the acoustic forcing and second, a contribution that stems from turbulent combustion noise. Note, the second contribution is by definition *uncorrelated* to the deterministic flame response and hinders thus the identification in hot conditions [16]. For consistency, two independent data sets (upstream and downstream forcing) are thus used in the current study for both reactive and nonreactive conditions.

Flame Transfer Function + Reduced Order Model Approach. The ROM is based on a linear acoustic network model as it was used, e.g., in Refs. [36] and [37]. It describes the main elements of the combustor and is implemented in the open-source acoustic network tool taX [38]. The model is depicted in Fig. 6. The geometrical and thermodynamical parameters of the ROM are summarized in Table 1.

Every element of the linear network model is defined by a 2×2 transfer matrix that relates the upstream characteristic waves f_u and g_u to the characteristic waves f_d and g_d downstream of the element. Note that instead of using a network model based on transfer matrices, the respective elements could also be described equivalently by their scattering matrix. The connection of two elements would then be either realized by using the Redheffer Star-Product [39], which combines two scattering matrices to form an overall scattering matrix through simple algebraic combination of the respective subelements, or by converting the scattering matrices into a transfer matrix representation before connecting them by simple concatenation.

Duct sections like the injection tube or the convergent part downstream of the combustion chamber only introduce a time lag between the upstream and the downstream characteristic waves and are described as

$$\begin{bmatrix} f_d \\ g_d \end{bmatrix} = \begin{bmatrix} e^{-\mathrm{i}\omega l/\bar{c}} & 0 \\ 0 & e^{\mathrm{i}\omega l/\bar{c}} \end{bmatrix} \begin{bmatrix} f_u \\ g_u \end{bmatrix} \tag{6}$$

with ω as angular frequency, l as respective duct length, and $\bar{c}$ as the mean speed of sound in the respective duct section. The area jumps within the network model are described in a simplistic manner

$$\begin{bmatrix} f_d \\ g_d \end{bmatrix} = \begin{bmatrix} 1 + A_u/A_d & 1 - A_u/A_d \\ 1 - A_u/A_d & 1 + A_u/A_d \end{bmatrix} \begin{bmatrix} f_u \\ g_u \end{bmatrix} \tag{7}$$

wherein A_u/A_d describes the area ratio from upstream to downstream section. The area jumps are assumed to be loss free and have no end correction.

Since the complex radial swirler geometry is only insufficiently approximated by simple duct and area jump elements, it is replaced by a 2×2 scattering matrix that is converted into a transfer matrix representation. The swirler scattering matrix is

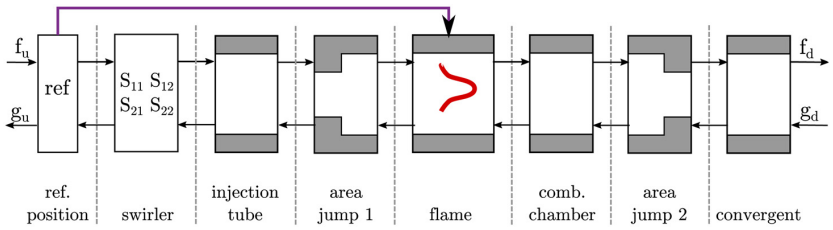

Fig. 6 Reduced order model: the swirler is replaced by an identified scattering matrix

Table 1 Summary of the geometrical and thermodynamical parameters used in the ROM

Injection tube	Flame	Comb. chamber	Convergent
$l_{\mathrm{inj}} = 0.034$ m $A_{\mathrm{inj}} = 3.52 \times 10^{-4}$ m^2 $u_{\mathrm{inj}} = 7.1$ m/s	$T_c = 293$ K $T_h = 1550$ K $\rho_c = 1.205$ kg/m^3 $\rho_h = 0.235$ kg/m^3	$l_{cc} = 0.154$ m $A_{cc} = 6.73 \times 10^{-3}$ m^2	$l_{\mathrm{conv}} = 0.185$ m $A_{\mathrm{conv}} = 3.32 \times 10^{-4}$ m^2

M. Merk, R. Gaudron, C.Silva, M. Gatti, C. Mirat, T. Schuller, and W. Polifke. Direct assessment of the acoustic scattering matrix of a turbulent swirl combustor by combining system identification, large eddy simulation and analytical approaches. In *Journal of Engineering for Gas Turbines and Power, 2018*. Reprinted with permission from ASME.

identified similarly to the direct approach: the flow in a LES, whose domain comprises only the swirler geometry, is simultaneously forced from upstream and downstream by a broadband acoustic signal. From the generated time series, the scattering matrix is determined via SI techniques. For brevity, the resulting swirler scattering matrix is not explicitly shown here.

The FTF is identified from a time series of velocity fluctuations at the reference position u'_{ref}, which coincides with the experimental reference position as shown in Fig. 3, and total heat release rate fluctuations $\dot{Q}'$, both extracted from the upstream forced data set

$$F(\omega) = \frac{\dot{Q}'/\bar{\dot{Q}}}{u'_{\text{ref}}/\bar{u}} \tag{8}$$

The comparison between the experimentally measured FTF and the one deduced from the LES/SI approach is depicted in Fig. 7. The error bars for the measured FTF are deduced from three experimental data sets for the same operating conditions and represent the maximum error in reproducibility of the experiment. The model order of the identified FTF is equal to $n_b = 30$.

In the following step, the identified FTF is coupled into the ROM via the linearized RH equations that describe the jump conditions across a thin zone of heat release at low Mach number

$$p'_d = p'_u \tag{9a}$$

$$u'_d = u'_u + \frac{(\gamma-1)}{\gamma \bar{p} A}\dot{Q}' \tag{9b}$$

where γ represents the heat capacity ratio and A the cross section area of the flame region. By inserting Eqs. (2*a*) and (2*b*) into the RH jump equations (9*a*) and (9*b*), the transfer matrix across the thin reaction zone is obtained as

$$\begin{bmatrix} f_d \\ g_d \end{bmatrix} = \frac{1}{2}\begin{bmatrix} \xi+1 & \xi-1 \\ \xi-1 & \xi+1 \end{bmatrix}\begin{bmatrix} f_u \\ g_u \end{bmatrix} + \frac{1}{2}\frac{A_u}{A_d}\theta F(\omega)\begin{bmatrix} 1 & -1 \\ -1 & 1 \end{bmatrix}\begin{bmatrix} f_{\text{ref}} \\ g_{\text{ref}} \end{bmatrix} \tag{10}$$

with ξ denoting the specific acoustic impedance between burnt and unburnt gases $\xi = (\rho_c c_c)/(\rho_h c_h)$ and θ specifying the temperature ratio $\theta = T_h/T_c - 1$.

The coupling of the FTF into the ROM is indicated by the additional arrow in Fig. 6. Note that this coupling approach only holds if certain constraints are respected: (1) The flame is assumed to be compact with respect to the acoustic wavelength considered. (2) Influence of pressure fluctuations on the flame response is insignificant. For the given working conditions, the flame length is about $l_f \approx 0.04$ m. The scattering matrices are evaluated in the low frequency region up to a frequency of 400 Hz resulting in a maximum Helmholtz number of He < 0.05. The Helmholtz number is thus much smaller than unity, implying that the flame may be assumed to be acoustically compact. As mentioned in the experimental description, methane and air are already premixed before their injection into the plenum. For perfectly premixed flames, velocity sensitivity is a valid assumption [40]. From these considerations, it is concluded that the FTF+ROM approach should provide valid predictions for the scattering matrix coefficients in the hot configuration.

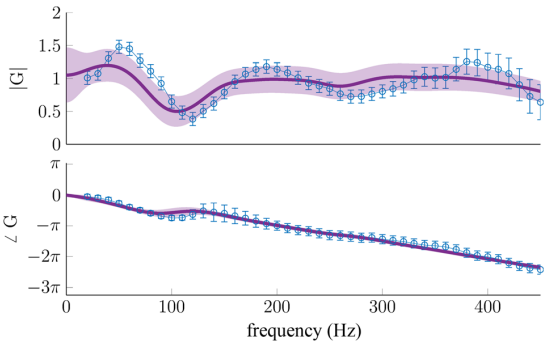

Fig. 7 Comparison between measured FTF (○) with respective error bars and FTF from LES/SI (——). The shaded area represents the 95% confidence interval of the identified FTF.

Results

First, the combustor scattering matrix from experiment, the direct approach, and the ROM prediction are compared for the cold case. This validates the LES/SI procedure and the ROM of the cold combustor to a certain extent and derives the results of the reactive case on a solid basis. In a second step, the hot configuration is investigated.

Nonreactive Case. Figure 8 depicts the four scattering matrix coefficients deduced from experiment (○), the direct LES approach without combustion (——), and the ROM prediction for the cold configuration (——). In the ROM, the downstream temperature T_h is set equal to the upstream temperature T_c resulting in $\theta = 0$. The second term on the r.h.s in Eq. (10) thus vanishes: the flame does not have any influence. In the direct approach, the model order for each of the four scattering matrix coefficients is set to $n_b = 10$. The confidence intervals for the direct approach that come from the SI procedure are not shown in Fig. 8. Due to the low model order of $n_b = 10$ and the high signal-to-noise ratio, the 95%

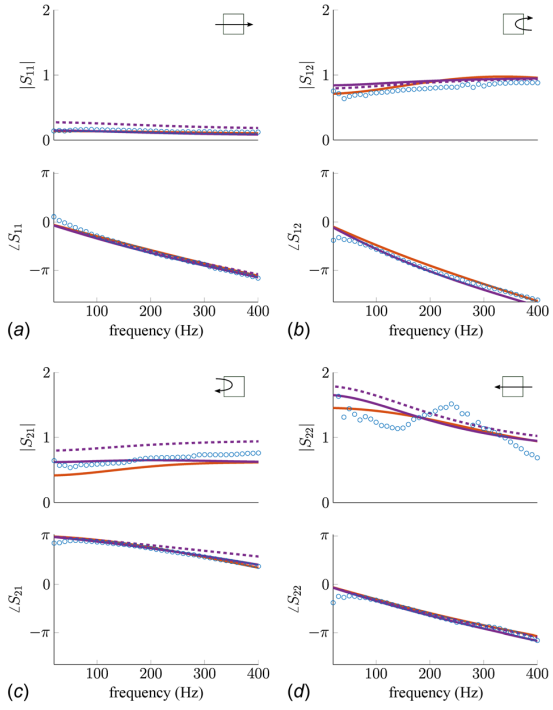

Fig. 8 Combustor scattering matrix for cold conditions. Experiment (○), direct LES approach (——), passive ROM (——) and passive ROM without swirler (- - -). (*a*) S_{11}, (*b*) S_{12}, (*c*) S_{21}, and (*d*) S_{22}.

M. Merk, R. Gaudron, C.Silva, M. Gatti, C. Mirat, T. Schuller, and W. Polifke. Direct assessment of the acoustic scattering matrix of a turbulent swirl combustor by combining system identification, large eddy simulation and analytical approaches. In *Journal of Engineering for Gas Turbines and Power, 2018*. Reprinted with permission from ASME.

confidence intervals of the estimated scattering coefficients are very small and could hardly be recognized in Fig. 8.

Considering the two reflection coefficients S_{12} and S_{21} as well as S_{11}, i.e., the transmission coefficients from upstream to downstream all three methods are in fairly good agreement. In particular, the phase matches excellently. On the other hand, the absolute values exhibit subtle differences. In contrast to the ROM, the direct LES approach takes acoustic losses into account. Therefore, the coefficients' magnitudes obtained by the direct LES approach are slightly smaller than the ones from the ROM. It can be observed that the magnitude of the transmission coefficient from downstream to upstream S_{22} exceeds unity for low frequencies. This results from the cross section area ratio between downstream measurement plane P2 and the upstream measurement plane P1 that is also above unity, see Fig. 3. Due to mass conservation, the ratio g_u/g_d, which is exactly described by the S_{22} coefficient, becomes larger than unity. For the same reason, the transmission coefficient S_{11} is distinctively below unity. The magnitude of the reflection coefficients S_{12} and S_{21} is of order unity. This strong reflection within the combustor geometry is caused by the large area jump between the injection tube and the combustion chamber, denoted as "area jump 1" in Fig. 6. An evaluation of its scattering behavior, see Eq. (7), shows that the largest parts of the incoming waves are reflected, whereas only a small part is transmitted across the area jump. Even though the phase of all three methods matches well for the transmission coefficient S_{22}, the variations measured in the absolute value are observed neither by the direct LES approach nor by the ROM. This discrepancy might be caused by inaccuracies in describing the acoustic transmission from the combustion chamber into the injection tube. However, the general trend and the magnitude of $|S_{22}|$ are in fairly good agreement for all three methods.

To show the effect of the swirler scattering matrix within the ROM, it was replaced by a simple duct element having the same length as the swirler element, see (- - -) in Fig. 8. Compared to the ROM containing the swirler scattering matrix (——), a larger deviation to experimental results and to the direct approach is observable. It can be concluded that the use of a nontrivial swirler scattering matrix increases the accuracy of the ROM.

Overall, several conclusion may be drawn from the results of the cold configuration: (1) The compressible LES correctly describes the acoustic propagation within the complex combustor geometry, allowing the LES/SI procedure to extract all four scattering matrix coefficients from the broadband time series data over a range of frequencies. (2) The ROM based on a linear network model is able to correctly reproduce the main features of the cold scattering matrix. This means that the passive combustor parts are modeled by the ROM with sufficient accuracy, despite the simplifications made such as 1D acoustics or the simplified geometry. (3) The area jump between injection tube and combustion chamber reflects most of the incoming waves. (4) The swirler is acoustically not completely transparent. (5) The direct LES approach and the ROM correctly capture the time lag between ingoing and outgoing characteristic waves as the phase is in excellent agreement with experimental measurements. This in turn means that the time lag correction due to the differing measurement locations in experiment and direct approach is valid and yields satisfying results.

Conclusions (1) to (5) put the following study of the hot configuration on a solid basis and allow to exclude some reasons for any discrepancies between the methods in the reactive configuration.

Reactive Case. Figure 9 shows the scattering matrix coefficients for the reactive configuration obtained by experiment (○), the direct LES approach with combustion (——), the FTF+ROM approach (——), and a ROM with *passive flame* (- - -). In the last case, the temperature increase across the flame is taken into account, but the unsteady heat release as represented by the FTF is not, i.e., the flame is inactive. For the direct approach, the FIR model order is now increased to $n_b = 30$ for each of the four

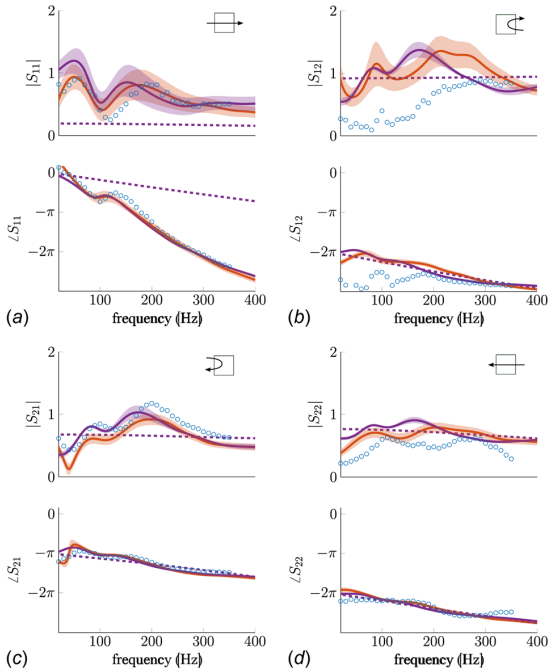

Fig. 9 Combustor scattering matrix for hot conditions. Experiment (○), direct LES approach (——) and FTF+ROM (——) and ROM with passive flame (- - -). The shaded areas describe the 95% confidence interval of the respective numerical approach. (*a*) S_{11}, (*b*) S_{12}, (*c*) S_{21}, and (*d*) S_{22}.

scattering matrix coefficients, as the presence of the flame results in a more complex scattering behavior and the flame time lag is quite large compared to acoustic scales.

The direct and the FTF+ROM approaches yield results for the four scattering matrix coefficients that are largely consistent with each other and show overall satisfactory agreement with measurements. However, the downstream reflection coefficient S_{12} (top-right subplot) exhibits pronounced discrepancies between the numerical results and experiment, especially in the low-frequency region. A possible explanation for the discrepancy might be that the acoustic signals in experiment as well as in LES are overlaid by combustion noise emitted from the turbulent flame, which is known to be active predominantly in the low-frequency region. One should expect that combustion noise is most detrimental for determination of the S_{12} coefficient, since it describes reflection of a wave g_d coming from downstream into a wave f_d propagating in the downstream direction. For the determination of this coefficient, both signals are extracted downstream of the flame in the combustion chamber, where combustion noise amplitudes higher than in the plenum must be expected.[2] Consistently, the measurement variation observed is largest in the S_{12} coefficient.

Note that forcing amplitudes should not be increased arbitrarily, in order to avoid a nonlinear flame response. A decrease in the signal-to-noise is thus unavoidable, which worsens the reliability of the SI results. Indeed, the confidence intervals of the scattering coefficient S_{12} estimated with the direct approach are quite wide, see Fig. 9(*b*). However, the confidence intervals are not wide enough to account for the discrepancies between simulation and experiment. One should also consider that in the experiments, the acquisition time per frequency measurement was fixed. Thus, measurements for higher frequencies are statistically more

[2]In the cold configuration, the only physical noise source is aero-acoustic noise, which is rather small for low Mach numbers. The signal-to-noise ratio is thus favorable in this case, yielding reliable results also for S_{12}.

M. Merk, R. Gaudron, C.Silva, M. Gatti, C. Mirat, T. Schuller, and W. Polifke. Direct assessment of the acoustic scattering matrix of a turbulent swirl combustor by combining system identification, large eddy simulation and analytical approaches. In *Journal of Engineering for Gas Turbines and Power, 2018*. Reprinted with permission from ASME.

reliable, as more forcing cycles are recorded and the stochastic noise contribution becomes less significant. Indeed, the agreement between numerical predictions and measurements improves with frequency. Conversely, with decreasing forcing frequency, fewer and fewer cycles were recorded and agreement deteriorates. Differences in measurement principle—two-source with broad-band forcing and nonreflection boundary conditions in LES/SI versus two-load with monofrequent forcing and partial reflection in experiment—may also contribute to the discrepancies.

The 95% confidence intervals shown for the FTF+ROM approach are determined by propagating the uncertainties in FTF magnitude (see Fig. 7) through the ROM. By comparing the width of confidence intervals obtained with the FTF+ROM approach, it becomes evident that in particular the upstream transmission coefficient S_{11} exhibits significant uncertainties. The interpretation of this behavior is the following: If the flow is forced upstream, significant velocity perturbations are generated at the reference position, see Fig. 6. Via the FTF and the RH coupling, these fluctuations cause acoustic waves at the flame position, see Eq. (10). On the other hand, due to the aforementioned reflective area jump in between the injection tube and the combustion chamber (area jump 1 in Fig. 6), only a small part of the initial forcing signal reaches the outlet of the combustor. It follows that the signal at the outlet should be dominated by the acoustic waves generated at the flame position caused by velocity perturbations at the reference position. These arguments are corroborated by the following observations: (1) S_{11} as predicted by the ROM with passive flame (- - -) differs strongly from the prediction with active flame, (2) the magnitude of S_{11} shows a similar succession of local maxima and minima as the FTF at corresponding frequencies, (3) the phase of S_{11} is dominated by the flame time lag and not by the acoustic scales (as it is the case for the ROM with passive flame). Consequently, uncertainties in FTF identification impact noticeably the prediction of the S_{11} transmission coefficient.

The impact of the flame dynamics on the remaining scattering coefficients is weaker. The coefficients are closer in magnitude to the predictions of the ROM with passive flame (- - -) while the phase is dominated by acoustic time scales and matches thus the phase of the ROM with passive flame. This can be explained again through the reflective area jump between the injection tube and the combustion chamber. If the flow is forced from downstream, only a small portion of the acoustic forcing signal reaches the reference position upstream, since the largest part of the signal is reflected at the area jump. Accordingly, the contribution of the flame generated acoustic waves remains relatively small. The impact of the flame on the scattering coefficients S_{12} and S_{22} is only moderate. The same holds for the upstream reflection coefficient S_{21}. Even though the flame response is considerable—the upstream acoustic forcing directly causes velocity perturbations at the reference position—only a small part of the upstream traveling acoustic waves generated at the flame position reach again the upstream end of the combustor.

To conclude, uncertainties in the determination of the scattering coefficients in the FTF+ROM approach are largest, where the flame modulates the passive scattering matrix the most.

Summary and Conclusions

The aim of this paper is a one-to-one comparison between two alternative numerical approaches for deducing the scattering matrix of a turbulent swirl combustor under nonreactive as well as reactive conditions. The respective approaches combine LES, SI and ROM. Numerical results for the *cold* and *hot* combustor scattering matrix are compared against each other and against experiment. The first approach identifies scattering matrix coefficients directly from broadband time series data that are generated by a compressible LES with broadband forcing. The second approach identifies only the FTF from the compressible LES, which is then coupled into a ROM of the combustor acoustics via the RH equations in order to compose the scattering matrix.

The results for the nonreactive scattering matrix show excellent agreement between simulation and experiment. This suggests that the 1D acoustic assumption made in the ROM is justified. Moreover, it becomes evident that the radial swirler is acoustically not completely transparent. Consequently, the use of nontrivial swirler scattering matrix further increases the accuracy of the ROM.

The scattering matrices for the reactive setup also exhibit satisfactory agreement, even though the downstream reflection coefficient S_{12} shows a distinct discrepancy between the numerical predictions—which coincide with each other—and the measurements. Possible reasons for the discrepancies are the small signal-to-noise ratio of the time series data extracted in the burnt gas region and the finite time series length available. In the direct approach, a finite time series length introduces uncertainties in the identification process in particular at low frequencies, in experiment fewer cycles can be recorded for low forcing frequencies due to the fixed acquisition time. Nonetheless, considering the good agreement between the two quite different numerical approaches and the overall good agreement with the measurements of the nonreactive and the reactive scattering matrix, it is principally shown that both numerical approaches are capable of determining the scattering matrix of a complex combustor. Moreover, the comparison to the ROM with a passive flame highlights the impact of the flame on the acoustic scattering matrix of the combustor. It is shown that the transmission coefficient from upstream to downstream S_{11} is dominated by the flame dynamics, i.e., the FTF.

The composed approach yields accurate results, as long as the constraints of the coupling between FTF and ROM via the Rankine–Hugoniot equations are respected. The perfectly premixed flame investigated in this study is indeed predominantly velocity sensitive and acoustically compact. One may conclude that the other simplifications implied by the composed approach, such as 1D acoustics or a constant temperature distribution in the hot gas region, do not introduce significant errors. The applicability of the composed approach in this case would allow the computationally efficient determination of the combustor scattering matrix for a wide parameter space, as changes could be easily implemented in the ROM. However, there are situations in which the constraints of the composed approach are no longer respected. The mixture might be technically premixed introducing a pressure sensitivity of the flame or the flame might be no longer acoustically compact. In these situations, the more general direct LES approach would be necessary to accurately predict the reactive scattering matrix, as it allows to drop the constraints of the composed approach. All relevant mechanisms are directly resolved within the compressible LES.

The comparisons and analysis carried out in this study thus provide valuable insight to which extent both numerical methods yield coinciding results for a configuration, where the composed approach is applicable.

Funding Data

- The authors acknowledge financial support by the German Research Foundation DFG, project PO 710/16-1 and by the Agence Nationale de la Recherche, NOISEDYN project (ANR-14-CE35-0025-01). This project also has received funding from the European Union's Horizon 2020 research and innovation programme under the Marie Sklodowska-Curie grant agreement No 643134. Moreover, the author gratefully acknowledges the Gauss Centre for Supercomputing e.V. for funding this project by providing computing time on the GCS Supercomputer SuperMUC at Leibniz Supercomputing Centre.

References

[1] Lefebvre, A. H., 1999, *Gas Turbine Combustion*, 2nd ed., Taylor & Francis, Philadelphia, PA.
[2] Munjal, M. L., 2014, *Acoustics of Ducts and Mufflers*, 2nd ed., Wiley, Chichester, UK.
[3] Su, J., Rupp, J., Garmory, A., and Carrotte, J., 2015, "Measurements and Computational Fluid Dynamics Predictions of the Acoustic Impedance of Orifices," J. Sound Vib., **352**, pp. 174–191.

M. Merk, R. Gaudron, C.Silva, M. Gatti, C. Mirat, T. Schuller, and W. Polifke. Direct assessment of the acoustic scattering matrix of a turbulent swirl combustor by combining system identification, large eddy simulation and analytical approaches. In *Journal of Engineering for Gas Turbines and Power, 2018*. Reprinted with permission from ASME.

[4] Sovardi, C., Aurégan, Y., and Polifke, W., 2016, "Parametric LES/SI Based Aeroacoustic Characterization of Tandem Orifices in Low Mach Number Flows," Acta Acust. Acust., **102**(5), pp. 793–803.
[5] Andreini, A., Bianchini, C., Facchini, B., Peschiulli, A., and Vitale, I., 2012, "LES for the Evaluation of Acoustic Damping of Effusion Plates," ASME Paper No. GT2012-68792.
[6] Yoon, C., Graham, O., Han, F., Kim, K., Maxted, K., Caley, T., and Lee, J. G., 2017, "LES-Based Scattering Matrix Method for Low-Order Acoustic Network Models," ASME Paper No. GT2017-65123.
[7] Gikadi, J., Ullrich, W. C., Sattelmayer, T., and Turrini, F., 2013, "Prediction of the Acoustic Losses of a Swirl Atomizer Nozzle Under Non-Reactive Conditions," ASME Paper No. GT2013-95449.
[8] Ni, F., Miguel-Brebion, M., Nicoud, F., and Poinsot, T., 2017, "Accounting for Acoustic Damping in a Helmholtz Solver," AIAA J., **55**(4), pp. 1205–1220.
[9] Keller, J. J., 1995, "Thermoacoustic Oscillations in Combustion Chambers of Gas Turbines," AIAA J., **33**(12), pp. 2280–2287.
[10] Dowling, A. P., 1995, "The Calculation of Thermoacoustic Oscillation," J. Sound Vib., **180**(4), pp. 557–581.
[11] Polifke, W., Paschereit, C. O., and Döbbeling, K., 2001, "Constructive and Destructive Interference of Acoustic and Entropy Waves in a Premixed Combustor With a Choked Exit," Int. J. Acoust. Vib., **6**(3), pp. 135–146.
[12] Schuermans, B., Bellucci, V., Guethe, F., Meili, F., Flohr, P., and Paschereit, O., 2004, "A Detailed Analysis of Thermoacoustic Interaction Mechanisms in a Turbulent Premixed Flame," ASME Paper No. GT2004-53831.
[13] Bothien, M., Lauper, D., Yang, Y., and Scarpato, A., 2017, "Reconstruction and Analysis of the Acoustic Transfer Matrix of a Reheat Flame From Large-Eddy Simulations," ASME Paper No. GT2017-64188.
[14] Alemela, P. R., Fanaca, D., Ettner, F., Hirsch, C., Sattelmayer, T., and Schuermans, B., 2008, "Flame Transfer Matrices of a Premixed Flame and a Global Check With Modelling and Experiments," ASME Paper No. GT2008-50111.
[15] Laera, D., Gentile, A., Camporeale, S. M., Bertolotto, E., Rofi, L., and Bonzani, F., 2015, "Numerical and Experimental Investigation of Thermo–Acoustic Combustion Instability in a Longitudinal Combustion Chamber: Influence of the Geometry of the Plenum," ASME Paper No. GT2015-42322.
[16] Silva, C. F., Merk, M., Komarek, T., and Polifke, W., 2017, "The Contribution of Intrinsic Thermoacoustic Feedback to Combustion Noise and Resonances of a Confined Turbulent Premixed Flame," Combust. Flame, **182**, pp. 269–278.
[17] Paschereit, C. O., and Polifke, W., 1998, "Investigation of the Thermo-Acoustic Characteristics of a Lean Premixed Gas Turbine Burner," ASME Paper No. 98-GT-582.
[18] Paschereit, C. O., Schuermans, B. B. H., Polifke, W., and Mattson, O., 2002, "Measurement of Transfer Matrices and Source Terms of Premixed Flames," ASME J. Eng. Gas Turbines Power, **124**(2), pp. 239–247.
[19] Gentemann, A., and Polifke, W., 2007, "Scattering and Generation of Acoustic Energy by a Premix Swirl Burner," ASME Paper No. GT2007-27238.
[20] Candel, S., Durox, D., Schuller, T., Bourgouin, J. F., and Moeck, J. P., 2014, "Dynamics of Swirling Flames," Annu. Rev. Fluid Mech., **46**(1), pp. 147–173.
[21] Polifke, W., Poncet, A., Paschereit, C. O., and Döbbeling, K., 2001, "Reconstruction of Acoustic Transfer Matrices by Instationary Computational Fluid Dynamics," J. Sound Vib., **245**(3), pp. 483–510.
[22] Polifke, W., 2014, "Black-Box System Identification for Reduced Order Model Construction," Ann. Nucl. Energy, **67C**, pp. 109–128.
[23] Fischer, A., Hirsch, C., and Sattelmayer, T., 2006, "Comparison of Multi-Microphone Transfer Matrix Measurements With Acoustic Network Models of Swirl Burners," J. Sound Vib., **298**(1–2), pp. 73–83.
[24] Chung, J. Y., and Blaser, D. A., 1980, "Transfer Function Method of Measuring In-Duct Acoustic Properties—II: Experiment," J. Acoust. Soc. Am., **68**(3), pp. 914–921.
[25] Guedra, M., Penelet, G., Lotton, P., and Dalmont, J., 2011, "Theoretical Prediction of the Onset of Thermoacoustic Instability From the Experimental Transfer Matrix of a Thermoacoustic Core," J. Acoust. Soc. Am., **130**(1), pp. 145–152.
[26] Giauque, A., Selle, L., Gicquel, L., Poinsot, T., Buechner, H., Kaufmann, P., and Krebs, W., 2005, "System Identification of a Large-Scale Swirled Partially Premixed Combustor Using LES and Measurements," J. Turbul., **6**, pp. 1–21.
[27] Tay-Wo-Chong, L., Bomberg, S., Ulhaq, A., Komarek, T., and Polifke, W., 2012, "Comparative Validation Study on Identification of Premixed Flame Transfer Function," ASME J. Eng. Gas Turbines Power, **134**(2), p. 021502.
[28] CERFACS and IMFT, 2008, "The AVBP HandBook," Cerfacs, Toulouse, France, accessed Oct. 10, 2017, http://www.cerfacs.fr/avbp6x/
[29] Nicoud, F., and Ducros, F., 1999, "Subgrid-Scale Stress Modelling Based on the Square of the Velocity Gradient Tensor," Flow Turbul. Combust., **62**(3), pp. 183–200.
[30] Colin, O., Ducros, F., Veynante, D., and Poinsot, T., 2000, "A Thickened Flame Model for Large Eddy Simulation of Turbulent Premixed Combustion," Phys. Fluids, **12**(7), pp. 1843–1863.
[31] Polifke, W., Wall, C., and Moin, P., 2006, "Partially Reflecting and Non-Reflecting Boundary Conditions for Simulation of Compressible Viscous Flow," J. Comput. Phys., **213**(1), pp. 437–449.
[32] Merk, M., Gaudron, R., Gatti, M., Mirat, C., Schuller, T., and Polifke, W., 2018, "Measurement and Simulation of Combustion Noise and Dynamics of a Confined Swirl Flame," AIAA J., **56**(5), pp. 1930–1942.
[33] Yang, Y., Noiray, N., Scarpato, A., Schulz, O., Düsing, K. M., and Bothien, M., 2015, "Numerical Analysis of the Dynamic Flame Response in Alstom Reheat Combustion Systems," ASME Paper No. GT2015-42622.
[34] Innocenti, A., Andreini, A., and Facchini, B., 2015, "Numerical Identification of a Premixed Flame Transfer Function and Stability Analysis of a Lean Burn Combustor," Energy Procedia, **82**, pp. 358–365.
[35] Kopitz, J., Bröcker, E., and Polifke, W., 2005, "Characteristics-Based Filter for Identification of Planar Acoustic Waves in Numerical Simulation of Turbulent Compressible Flow," 12th International Congress on Sound and Vibration (ICSV12), Lisbon, Portugal, July 11–14.
[36] Dowling, A. P., and Stow, S. R., 2003, "Acoustic Analysis of Gas Turbine Combustors," J. Propul. Power, **19**(5), pp. 751–764.
[37] Li, J., and Morgans, A. S., 2015, "Time Domain Simulations of Nonlinear Thermoacoustic Behaviour in a Simple Combustor Using a Wave-Based Approach," J. Sound Vib., **346**, pp. 345–360.
[38] Emmert, T., Jaensch, S., Sovardi, C., and Polifke, W., 2014, "TaX—A Flexible Tool for Low-Order Duct Acoustic Simulation in Time and Frequency Domain," 7th Forum Acusticum, Krakow, Poland, Sept., pp. 7–12.
[39] Bothien, M., Moeck, J., Lacarelle, A., and Paschereit, C. O., 2007, "Time Domain Modelling and Stability Analysis of Complex Thermoacoustic Systems," Proc. Inst. Mech. Eng., Part A, **221**(5), pp. 657–668.
[40] Lieuwen, T. C., 2012, *Unsteady Combustor Physics*, Cambridge University Press, New York.

M. Merk, R. Gaudron, C.Silva, M. Gatti, C. Mirat, T. Schuller, and W. Polifke. Direct assessment of the acoustic scattering matrix of a turbulent swirl combustor by combining system identification, large eddy simulation and analytical approaches. In *Journal of Engineering for Gas Turbines and Power, 2018*. Reprinted with permission from ASME.

M. Merk, R. Gaudron, C.Silva, M. Gatti, C. Mirat, T. Schuller, and W. Polifke. Direct assessment of the acoustic scattering matrix of a turbulent swirl combustor by combining system identification, large eddy simulation and analytical approaches. In *Journal of Engineering for Gas Turbines and Power, 2018*. Reprinted with permission from ASME.

Combustion and Flame 182 (2017) 269–278

Contents lists available at ScienceDirect

Combustion and Flame

journal homepage: www.elsevier.com/locate/combustflame

The contribution of intrinsic thermoacoustic feedback to combustion noise and resonances of a confined turbulent premixed flame

Camilo F. Silva*, Malte Merk, Thomas Komarek, Wolfgang Polifke

Technische Universität München, Fakultät für Maschinenwesen, Garching D-85747, Germany

ARTICLE INFO

Article history:
Received 30 June 2016
Revised 19 September 2016
Accepted 12 April 2017
Available online 8 May 2017

Keywords:
Intrinsic thermoacoustic feedback
Combustion noise
Combustion resonance
LES
System identification
Low-order model

ABSTRACT

The influence of Intrinsic Thermoacoustic (ITA) feedback on the combustion noise spectrum produced by a confined, turbulent, premixed, swirl flame is investigated. The analysis is based on the understanding that sound is generated by unsteady heat release resulting from turbulent fluctuations on the one hand, and from the response of the flame to incoming acoustic perturbations on the other. The former effect is described by a source term for combustion noise, i.e. a spectral distribution of unsteady heat release rate, the latter by the flame transfer function. Both quantities are identified from time series data for fluctuating velocity and heat release rate, generated with large eddy simulation of premix swirl burner. The combustion noise source term and the flame transfer function are then introduced in an acoustic network model of the test rig in order to compute the spectral distribution of the sound pressure level at a certain location in the combustion chamber. Results for the noise spectrum are in good agreement with experiment, showing a broadband component and well-defined peaks. The frequencies of the peaks correspond to either acoustic cavity or ITA resonances. The acoustic network model is used for parametric studies, where the acoustic reflection coefficient at the combustor exit is varied. Remarkably, it is found that the magnitude of the ITA peak increases with decreasing values of the acoustic reflection coefficient, and vice versa. Furthermore, the influence of combustion chamber length on resonance frequencies is explored. It is observed that the frequency of the ITA resonance is insensitive to combustor length. This behaviour is observed qualitatively also in experiments.

© 2017 The Combustion Institute. Published by Elsevier Inc. All rights reserved.

1. Introduction

Combustion noise results from unsteady volumetric expansion generated by fluctuations of the heat release rate [1]. A turbulent flame should be considered as a broad-band source of combustion noise, with a spectral distribution that is governed by the length and time scales of the turbulent reacting flow field [2]. In the case of enclosed flames, it is well understood that resonances with acoustic eigenmodes of the enclosure will lead to peaks in the spectral distribution of pressure fluctuations [3–5]. Moreover, it is to be expected that acoustic waves generated by unsteady heat release are reflected at the acoustic boundaries, such that they subsequently perturb the flame. It is not always appreciated that this feedback from the acoustics to the flame generates a two-way coupling, which may modify the strength of resonance peaks, or give rise to additional resonances between the source of combustion noise and the combustor acoustics [6–11].

Intrinsic thermoacoustic (ITA) feedback has only recently been identified as a flow-flame-acoustic interaction mechanism that can give rise to important and sometimes paradoxical effects in combustion dynamics. The structure of the ITA feedback loop was explained by Bomberg et al. [12] as follows: fluctuations of the heat release rate radiate acoustic waves in both the downstream and upstream directions. The upstream traveling wave perturbs the velocity field upstream of the flame, which subsequently will influence the heat release produced by the flame, especially so for premixed flames, which are velocity sensitive. The acoustic fields in combustion chamber and plenum are not part of this feedback loop.

Intrinsic thermoacoustic feedback adds corresponding ITA modes to the spectrum of thermoacoustic eigenmodes, which need not lock on to acoustic eigenmodes of a combustor [13,14]. Remarkably, simple low-order models suggest that ITA modes may be unstable even in anechoic configurations [15–17]. Such instabilities have been observed in numerical simulations of laminar flames [18,19], corroborated by experiment on laminar and turbulent flames [12–14]. Furthermore ITA feedback can cause pronounced peaks in the acoustic response and the instability potentiality of premixed flames [12,17].

* Corresponding author.
E-mail addresses: camilo.f.silva.g@gmail.com, silva@tfd.mw.tum.de (C.F. Silva), merk@tfd.mw.tum.de (M. Merk), thomas.a.k@gmx.de (T. Komarek), polifke@tfd.mw.tum.de (W. Polifke).

http://dx.doi.org/10.1016/j.combustflame.2017.04.015
0010-2180/© 2017 The Combustion Institute. Published by Elsevier Inc. All rights reserved.

With permission from C. Silva, M. Merk, T. Komarek, and W. Polifke. The contribution of intrinsic thermoacoustic feedback to combustion noise and resonances of a confined turbulent premixed flame. *Combustion and Flame, 182*, Elsevier, 2017.

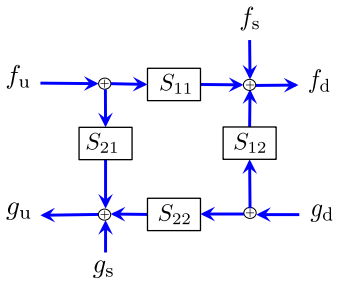

Fig. 1. Schematic representation of Eq. (1). A turbulent flame is considered as an element that transmits and reflects incoming acoustic waves f_u, g_d and in addition generates acoustic waves f_s, g_s. Overall, the outgoing waves f_d, g_u result from scattering, i.e. transmission and reflection, plus generation of sound.

The present paper investigates the contribution of ITA feedback to the spectral distribution of combustion noise generated by an enclosed, turbulent flame. It is found that resonance peaks in the combustion noise spectrum of a confined, turbulent, premixed, swirl flame can be related to either acoustic cavity modes, or the ITA feedback loop. The analysis is based on the understanding that turbulent fluctuations will perturb the heat release rate of a flame and thereby give rise to a combustion noise source term and a corresponding acoustic source vector. The former is quantified in terms of the spectral distribution of fluctuations of overall heat release rate, the latter in terms of the strength of acoustic waves that travel away from the flame in the down- and upstream directions, respectively. In order to capture the two-way coupling described above, the response of the flame to upstream velocity perturbations is described in terms of the flame transfer function. Moreover, the acoustic properties of the combustor – speed of sound, length of plenum, burner and combustion chamber, reflection coefficients, etc. – shape the spectral distribution of pressure fluctuations and must also be taken into account in order to predict combustion noise.

This paper is organized as follows: The next section explains how a turbulent flame may be characterized acoustically by a combustion noise source term, as introduced above, plus the flame transfer function. The third section describes the combustion system under investigation, while the fourth section exposes a methodology, previously suggested by Silva et al. [11], to obtain both the combustion noise source term and the flame transfer function from time series data generated by Large Eddy Simulation (LES) of combustion, with broad-band acoustic excitation and non-reflecting boundary conditions. Subsequently in the fifth and sixth section, an acoustic network model with combustion noise source term is presented and the proper interpretation of the solutions of this model is discussed. Finally, the sound pressure level spectrum of combustion noise produced at a location close to the outlet of the combustor under investigation is estimated. This is achieved by implementing the acoustic network model of the combustion test rig under study, including the previously obtained flame response and noise source. A careful analysis shows that one of the resonance peaks exhibited by the noise spectrum results from ITA feedback. Its frequency is independent of both the combustion chamber length of the system and its acoustic boundary conditions. Results are satisfactorily compared against experiment.

2. Acoustic characterization of a turbulent flame

As discussed above, the acoustic characteristics of a turbulent flame can be described by coefficients of transmission and reflection of incoming acoustic waves on the one hand, and a source term for combustion noise on the other, as illustrated in Fig. 1. Schuermans et al. [6] and Paschereit et al. [8] express this concept mathematically as follows:

$$\begin{bmatrix} f_d \\ g_u \end{bmatrix} = \underbrace{\begin{bmatrix} S_{11} & S_{12} \\ S_{21} & S_{22} \end{bmatrix}}_{\text{Acoustic Scattering}} \begin{bmatrix} f_u \\ g_d \end{bmatrix} + \underbrace{\begin{bmatrix} f_s \\ g_s \end{bmatrix}}_{\text{Acoustic source vector}}, \tag{1}$$

where f and g denote acoustic waves traveling in the down- and upstream directions, respectively. The indices d, u and s stand for 'downstream of the flame', 'upstream of the flame', and 'acoustic source', i.e. acoustic waves produced by unsteady heat release driven by turbulent fluctuations. The coefficients S_{ij} of the scattering matrix, as observed in Fig. 1, may be interpreted as coefficients of transmission and reflection of incoming acoustic waves f_u, g_d. For an acoustically compact flame, the scattering matrix coefficients S_{ij} depend on mean flow properties such as temperature, density and speed of sound up- and downstream of the flame, respectively, and on the response of the flame to flow perturbations, which may be expressed in terms of the flame transfer function (FTF).

The fundamental premise of the model expressed in Eq. (1) is that the acoustic source vector manifested by the acoustic waves f_s, g_s is uncorrelated with the incoming acoustic waves f_u and g_d. This assumption is reasonable, because the source of combustion noise can be considered as random process driven by the stochastic activity of the turbulent flow, resulting in corresponding turbulent unsteadiness of heat release [2,8,20]. The description of the flame acoustics given by Eq. (1) can be introduced in an acoustic network model to evaluate the acoustic pressure at given locations of the system [6,7], provided that both the scattering matrix coefficients S_{ij} and the acoustic source vector f_s and g_s are known. Lavrentjev et al. [21] and Paschereit et al. [8] discuss techniques to obtain these quantities experimentally by using two or three independent acoustic states.

In keeping with the concept expressed in Fig. 1 and Eq. (1), the present study distinguishes between two contributions to the global unsteady heat release rate $\dot{Q}'$: firstly a term $\dot{Q}'_c$, which results from incoming acoustic waves and can be related to upstream velocity perturbations u'_{ref} by the FTF $\mathcal{F}(\omega)$, and secondly a term $\dot{Q}'_s$ that is uncorrelated with incoming acoustic perturbations. Assuming harmonic oscillations, with $[\ ]' = [\hat{\ }]e^{i\omega t}$, we express $\hat{\dot{Q}}(\omega)$ as

$$\frac{\hat{\dot{Q}}(\omega)}{\bar{\dot{Q}}} = \underbrace{\overbrace{\mathcal{F}(\omega)\frac{\hat{u}_{ref}}{\bar{u}_{ref}}}^{\hat{\dot{Q}}_c(\omega)/\bar{\dot{Q}}}}_{\text{Flame response}} + \underbrace{\frac{\hat{\dot{Q}}_s(\omega)}{\bar{\dot{Q}}}}_{\text{Comb. noise source}} \tag{2}$$

where $[\bar{\ }]$ represents the temporal average of a quantity, and u_{ref} stands for the velocity at a reference position upstream of the flame.

Note that there may be cases where the global heat release rate $\hat{\dot{Q}}$ is not strongly influenced by the incoming acoustic waves, such that $\hat{\dot{Q}} \approx \hat{\dot{Q}}_s$, see e.g. [22]. It will be shown, however, that it is mandatory to account for the complete description of $\hat{\dot{Q}}$ according to Eq. (2) in order to capture the resonance associated with two-way coupling and ITA feedback.

3. Combustion test rig with BRS burner

A schematic of the swirl-stabilized combustor investigated in this study is shown in Fig. 2. The setup consists of the 'BRS' swirl burner placed between an upstream plenum of length $l_1 = 0.17$ m with circular cross section of diameter 200 mm and a downstream

With permission from C. Silva, M. Merk, T. Komarek, and W. Polifke. The contribution of intrinsic thermoacoustic feedback to combustion noise and resonances of a confined turbulent premixed flame. *Combustion and Flame, 182*, Elsevier, 2017.

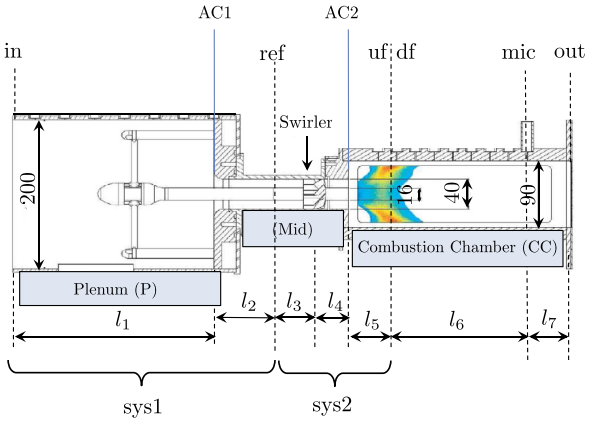

Fig. 2. Schematic of combustion test rig with BRS premix swirl burner.

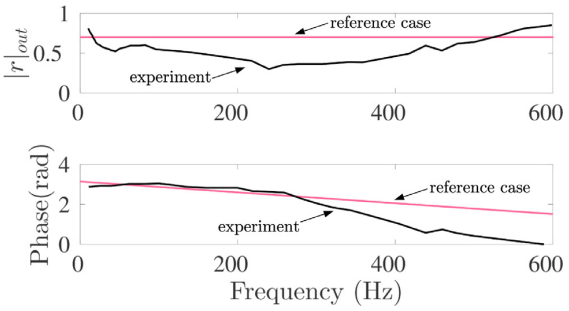

Fig. 3. Reflection coefficient r_{out}. —— Experimental data retrieved from Weyermann [24]. —— Fitted data used in the network model.

combustion chamber of variable length with quadratic cross section of 90 mm × 90 mm. The BRS burner itself is simply an annular flow passage formed by a bluff body with an outer diameter of 16 mm, and a duct with an inner diameter of 40 mm. An axial swirler with eight vanes and characterized by a swirl number equal to 0.74 is mounted on the bluff body, see Fig. 2. The flame is stabilized predominantly by the central recirculation zone downstream of the bluff body, which is strong thanks to the swirl imposed on the flow.

This test-rig was investigated experimentally by Komarek and Polifke [23], who studied and modeled the response of a premixed swirl flame to swirl fluctuations. The burner was operated under perfectly premixed conditions of methane and air with an equivalence ratio $\phi = 0.77$ and a range of thermal power between 30 kW and 70 kW. For different swirler positions the flame transfer function $\mathcal{F}(\omega)$ and the respective noise spectra were measured. The experimental validation data used in the present work always refer to operating conditions of 30 kW thermal power, with the swirler mounted at a position $l_4 = 45$ mm upstream of the burner mouth.

The combustor outlet is equipped with a perforated plate, which reduces the magnitude of the downstream acoustic reflection coefficient r_{out} below unity, see Fig. 3. Unfortunately, the measured values of the reflection coefficient exhibit considerable uncertainty. Consequently, in this study we define a 'reference' case with constant absolute value of the reflection coefficient $|r_{\text{out}}|$ equal to 0.7 (red line in Fig. 3). The phase is approximated by a linear dependence on frequency, with a slope that fits measurement values quite well in the range of frequencies of interest.

LES of the BRS burner at the aforementioned operating conditions was performed by Tay-Wo-Chong et al. [25] using the numerical solver AVBP, which solves the fully compressible Navier Stokes equations with second order accuracy in space and time. The interaction between turbulence and combustion were modeled by the dynamically thickened flame model [26]. The walls were considered non-adiabatic, whereas the inlet and outlet boundaries were made to be acoustically non-reflecting. For that purpose Navier Stokes characteristic boundary conditions with characteristic based filtering and plane wave masking [27] were accounted for. Besides mean velocity and mean heat release distributions, the FTF $\mathcal{F}(\omega)$ was identified and compared to experimental measurements.

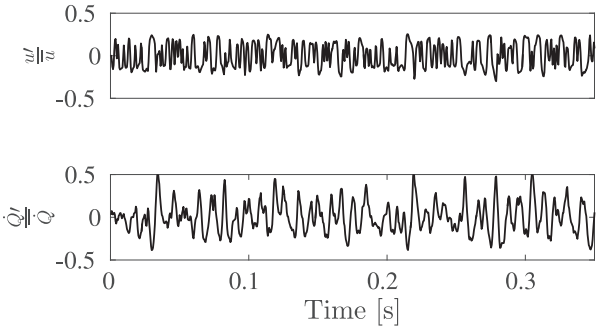

Fig. 4. Normalized velocity u' at a reference position (top) and global heat release rate (bottom) $\dot{Q}'$.

4. System identification

Time series data of $u' = [u'_0, \ldots, u'_N]$ at the reference position 'ref' (see Fig. 2) and of the global heat release rate $\dot{Q}' = [\dot{Q}'_0, \ldots, \dot{Q}'_N]$ were generated with LES over a time intervall of 0.35 s at a sampling rate of 800 kHZ by Tay-Wo-Chong et al. [25]. The present study makes use of this LES data. In view of System Identification, these signals, displayed in Fig. 4, are down-sampled to a rate of 2200 Hz. It should be remarked that u' is obtained after applying Characteristic Based Filtering [27] to velocity fields at four adjacent, transversal planes in order to remove perturbations that are not of acoustic nature.

In the following, we will summarize how Tay-Wo-Chong et al. [25] obtained the flame transfer function $\mathcal{F}(\omega)$ by correlation analysis of this data. Furthermore, we will show how the combustion noise source term $\hat{\dot{Q}}_s(\omega)$ over the entire frequency range of interest can be also estimated from the same data set.

4.1. Identification of flame transfer function $\mathcal{F}(\omega)$

The linear flame response to incoming acoustic perturbations can be modeled either by the FTF in frequency domain (see first term on the right hand side of Eq. (2)) or by a Finite Impulse Response (FIR) model in the time domain [28]. Both methods are fundamentally equivalent. In the FIR model, the input signal u' is convoluted with the *impulse response* $\boldsymbol{h}$ to create the output $\dot{Q}'_c$. If any (uncorrelated) noise $\dot{Q}'_s$ is present, it is added to the flame response, such that for a discrete times $t = n\Delta t$

$$\frac{\dot{Q}'_n}{\bar{\dot{Q}}} = \frac{1}{\bar{u}}\left(h_0 u'_n + h_1 u'_{n-1} + \cdots + h_{n_h} u'_{n-n_h}\right) + \frac{\dot{Q}'_{s,n}}{\bar{\dot{Q}}}, \tag{3}$$

where h_k denotes the coefficients of the impulse response $\boldsymbol{h}$. Note that the subscript 'ref' in the signal u' has been dropped to ease readability. In compact form one writes

$$\frac{\dot{Q}'_n}{\bar{\dot{Q}}} = \frac{1}{\bar{u}} \sum_{k=0}^{n_h} h_k u'_{n-k} + \frac{\dot{Q}'_{s,n}}{\bar{\dot{Q}}}, \qquad n = n_h, \ldots, N \tag{4}$$

With permission from C. Silva, M. Merk, T. Komarek, and W. Polifke. The contribution of intrinsic thermoacoustic feedback to combustion noise and resonances of a confined turbulent premixed flame. *Combustion and Flame, 182*, Elsevier, 2017.

The impulse response $\boldsymbol{h} = [h_0, \ldots, h_{n_h}]^\intercal$ may be estimated from time series data $[u'], [\dot{Q}']$ by a suitable optimization technique. In the case of a FIR structure, a minimum-least-square method yields

$$\boldsymbol{h} = \boldsymbol{\Gamma}^{-1}\boldsymbol{c}, \tag{5}$$

where auto-correlation matrix $\boldsymbol{\Gamma}$ and cross-correlation vector $\boldsymbol{c}$ are defined as

$$\Gamma_{kl} \equiv \sum_{n=n_h}^{N} u'_{n-k}u'_{n-l} \qquad k, l = 0, \ldots, n_h, \tag{6}$$

$$c_k \equiv \sum_{n=n_h}^{N} u'_{n-k}Q'_n \qquad k = 0, \ldots, n_h. \tag{7}$$

Details are given by Polifke [28] and references cited therein.

In statistics and system identification, the bias (or bias error) of an estimate is the difference between the true value and the *expected value* – i.e. the value that one obtains in the limit of an infinitely long time series – of the parameter being estimated. Eq. (5) is guaranteed to give an unbiased estimate of the impulse response $\boldsymbol{h}$ only if any stochastic contributions to the output are white noise [29]. Combustion noise is in general colored noise, with a power spectral distribution related to turbulent statistics [2]. Nevertheless, we argue that in the present case Eq. (5) gives a sufficiently accurate estimate of the impulse response with a minor bias.

This argument is developed as follows: Recall first that the source of combustion noise is described as a sum of correlated and stochastic contributions to unsteady heat release rate, $\dot{Q}' = \dot{Q}'_c + \dot{Q}'_s$. Then consider that the LES of Tay-Wo-Chong et al. [25] employed non-reflecting boundary conditions, and thus the acoustic waves impinging upon the flame were dominated by the imposed excitation signal. Furthermore, a fairly strong excitation with a signal-to-noise ratio larger than 10 was imposed (while maintaining linear flame dynamics). These circumstances ensure firstly that the source of noise $\dot{Q}'_s$ is not strongly correlated with the upstream velocity u', and secondly that $\dot{Q}'_s < \dot{Q}'_c$. Rewriting Eq. (7) as

$$c_k = \sum_{n=n_h}^{N} u'_{n-k}Q'_{c,n} + \sum_{n=n_b}^{N} u'_{n-k}Q'_{s,n}, \tag{8}$$

it follows that in the present case the estimate of the cross-correlation vector $\boldsymbol{c}$, cannot be strongly influenced by the noise source term $\dot{Q}'_s$, because the second term on the r.h.s. of the above equation is small.

The impulse response is converted to the FTF $\mathcal{F}(\omega)$ by the z-transform,

$$\mathcal{F}(\omega) = \sum_{k=0}^{n_h} h_k e^{-\mathbf{i}\omega k\Delta t}, \quad \text{where} \quad \omega \in \mathbb{C}. \tag{9}$$

The frequency response of the flame – i.e. the flame transfer function $\mathcal{F}(\omega)$ evaluated for real-valued frequencies $\omega \in \mathbb{R}$ – is shown in Fig. 5. The agreement with experimental measurements, which employed harmonic forcing and did not rely on system identification [23,25], is very good – in particular at frequencies below 250 Hz, where the gain of the frequency response is significant. This confirms that in the present case the non-white character of the noise does not lead to a significant bias in the estimation of the impulse response $\boldsymbol{h}$ and the source of noise $\dot{Q}'_s$.

In closing this section it is remarked that there are model structures such as the Box–Jenkins model [29,30], which model both the impulse response $\boldsymbol{h}$ and the noise source $\dot{Q}'_s$. The application of such advanced methods to the acoustic characterization of turbulent flames with colored combustion noise is beyond the scope of the present study.

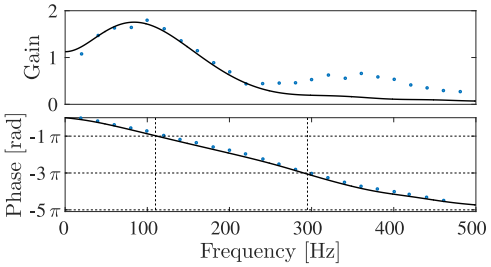

Fig. 5. Flame frequency response of the BRS burner identified from LES data (——) and measured in experiment (●).

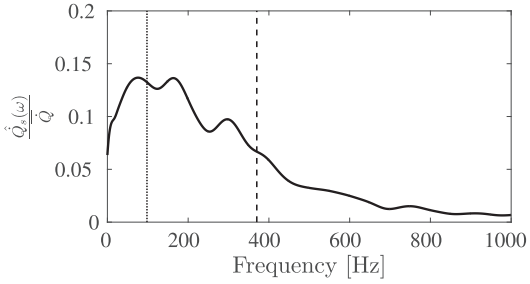

Fig. 6. Spectral content of the combustion noise source $\hat{Q}_s(\omega)/\bar{Q}$. Dashed lines indicate the frequencies where sound pressure level in the combustor peaks, see Figs. 9 and 10.

4.2. Estimate of noise source $\hat{Q}_s(\omega)$

If an FIR model is used to estimate the impulse response $\boldsymbol{h}$ of the flame – see Eq. (5) – the source of combustion noise $\dot{Q}'_s$ may be estimated as the residual

$$\frac{\dot{Q}'_{s,n}}{\bar{\dot{Q}}} = \frac{\dot{Q}'_n}{\bar{\dot{Q}}} - \frac{1}{\bar{u}}\sum_{k=0}^{n_h} h_k u'_{n-k} \qquad t = n_h, \ldots, N. \tag{10}$$

This simple estimate is justified by the premise that the combustion noise source term $\dot{Q}'_s$ results from turbulent fluctuations, which are uncorrelated with the acoustic excitation signal. Furthermore, in LES there are no other significant sources of (measurement) noise, which could contribute to fluctuations not represented by the FIR model.

The Power Spectral Density (PSD) of the noise source $\dot{Q}'_s$, here denoted S_{QQ} and defined as

$$S_{QQ}(\omega) = \frac{2\Delta t}{N}\left|\sum_{n=0}^{N-1}\dot{Q}'_{s,n}e^{-\mathbf{i}\omega n\Delta t}\right|^2, \tag{11}$$

is then obtained by using Welch's method with 16 Hamming Windows. The magnitude of the unitary discrete Fourier transform, obtained by means of LES data and shown in Fig. 6, is finally computed from S_{QQ} as

$$\hat{Q}_s(\omega) = \sqrt{\frac{S_{QQ}(\omega)}{2\Delta t}}. \tag{12}$$

5. Acoustic network model

In this section we formulate a linear acoustic network model of the combustion test rig under investigation, with the objective of predicting the noise levels at a given location of the confined system. Let us first define the downstream traveling acoustic wave

With permission from C. Silva, M. Merk, T. Komarek, and W. Polifke. The contribution of intrinsic thermoacoustic feedback to combustion noise and resonances of a confined turbulent premixed flame. *Combustion and Flame, 182*, Elsevier, 2017.

f and upstream traveling acoustic wave g by

$$f = \frac{1}{2}\left(\frac{\hat{p}}{\bar{\rho}\bar{c}} + \hat{u}\right) \quad \text{and} \quad g = \frac{1}{2}\left(\frac{\hat{p}}{\bar{\rho}\bar{c}} - \hat{u}\right). \tag{13}$$

The quantities p, u, ρ and c stand for pressure, velocity, density and sound speed, respectively. Let us also define a 2×2 transfer matrix T, which relates the acoustic waves f and g at a downstream location 'd' with respect to those at an upstream location 'u' as

$$\begin{bmatrix} f_\mathrm{d} \\ g_\mathrm{d} \end{bmatrix} = T \begin{bmatrix} f_\mathrm{u} \\ g_\mathrm{u} \end{bmatrix}. \tag{14}$$

Note that instead of using a network model based on scattering matrices (as the one given by Eq. (1)), we use here a network model based on transfer matrices, because it allows the assembly of multiple system elements by simple concatenation. We can acoustically describe the elements of the swirled burner (see indices in Fig. 2) by the corresponding acoustic transfer matrices T. The ducts 'D' are described by

$$T^{D}_{\mathrm{x},j} = \begin{bmatrix} e^{-i\omega l_j/\bar{c}_\mathrm{x}} & 0 \\ 0 & e^{i\omega l_j/\bar{c}_\mathrm{x}} \end{bmatrix}, \tag{15}$$

where 'x' can take either a cold 'c' or a hot 'h' value, whereas the first and second cross changes ('AC1' and 'AC2') are characterized by

$$T^{\mathrm{AC1}} = \frac{1}{2}\begin{bmatrix} 1+\alpha_1-\bar{\mathcal{M}}_\mathrm{in}\zeta & 1-\alpha_1+\bar{\mathcal{M}}_\mathrm{in}\zeta \\ 1-\alpha_1-\bar{\mathcal{M}}_\mathrm{in}\zeta & 1+\alpha_1+\bar{\mathcal{M}}_\mathrm{in}\zeta \end{bmatrix} \tag{16}$$

$$T^{\mathrm{AC2}} = \frac{1}{2}\begin{bmatrix} 1+\alpha_2 & 1-\alpha_2 \\ 1-\alpha_2 & 1+\alpha_2 \end{bmatrix} \tag{17}$$

where $\alpha_1 = A_\mathrm{P}/A_\mathrm{Mid}$ and $\alpha_2 = A_\mathrm{Mid}/A_\mathrm{CC}$ represent the area changes '1' and '2', respectively. The quantity $\bar{\mathcal{M}}$ stands for the Mach number and ζ denotes a loss coefficient. In a similar way, the swirler is acoustically described by

$$T^{\mathrm{S}} = \frac{1}{2}\begin{bmatrix} 2-\bar{\mathcal{M}}_\mathrm{mid}\zeta_\mathrm{S} & \bar{\mathcal{M}}_\mathrm{mid}\zeta_\mathrm{S} \\ -\bar{\mathcal{M}}_\mathrm{mid}\zeta_\mathrm{S} & 2+\bar{\mathcal{M}}_\mathrm{mid}\zeta_\mathrm{S} \end{bmatrix}. \tag{18}$$

The acoustic reflection at the inlet and outlet of the system are characterized, respectively, by

$$R_\mathrm{in} = \begin{bmatrix} 1 & -r_\mathrm{in}(\omega) \\ 0 & 0 \end{bmatrix} \quad \text{and} \quad R_\mathrm{out} = \begin{bmatrix} 0 & 0 \\ -r_\mathrm{out}(\omega) & 1 \end{bmatrix}, \tag{19}$$

where $r_\mathrm{in}(\omega)$ and $r_\mathrm{out}(\omega)$ represent the frequency depending reflection coefficient. Note that we keep terms $\bar{\mathcal{M}}\zeta$ for aero-acoustic losses, because they are of first order in mean flow Mach number $\bar{\mathcal{M}}$, while we have neglected the contributions of non-zero Mach number on acoustic wave propagation in Eq. (15), because their effect on the eigenfrequencies is only second order in Mach number.

The plenum of the test rig is closed on the upstream side by a porous plate with high pressure loss, thus the inlet reflection coefficient r_in may be considered equal to unity for the entire range of frequencies. For the combustor exit coefficient r_out the 'reference' case from Fig. 3 is used.

Let us now introduce the Rankine–Hugoniot jump conditions across the flame, which up to second order in Mach number read

$$\hat{p}_\mathrm{df} = \hat{p}_\mathrm{uf}, \tag{20}$$

$$\hat{u}_\mathrm{df} = \hat{u}_\mathrm{uf} + \frac{(\gamma-1)}{\gamma\bar{p}A_\mathrm{CC}}\hat{Q}(\omega), \tag{21}$$

where γ stands for the heat capacity ratio, and 'uf' and 'df' represents a location immediately 'upstream' or 'downstream' of the flame, respectively. Inserting now the definition of f and g of Eq. (13) in Eq. (20) and Eq. (21), and recalling that $\hat{Q}(\omega) = \hat{Q}_\mathrm{c}(\omega) + \hat{Q}_\mathrm{s}(\omega)$, we obtain

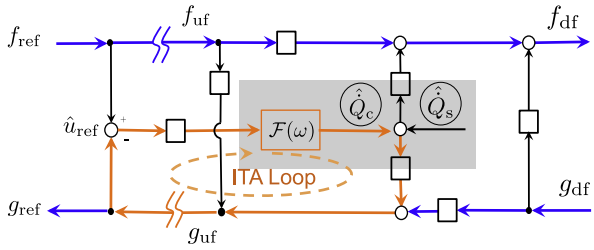

Fig. 7. Schematic representation of Eq. (22). The ITA feedback loop is illustrated in orange, whereas acoustic waves are displayed in blue. The shaded region features the Flame as $\hat{Q}(\omega) = \hat{Q}_\mathrm{c}(\omega) + \hat{Q}_\mathrm{s}(\omega)$. Empty blocks represent constant multiplicators. (For interpretation of the references to color in this figure legend, the reader is referred to the web version of this article).

$$\begin{bmatrix} f_\mathrm{df} \\ g_\mathrm{df} \end{bmatrix} = \underbrace{\frac{1}{2}\begin{bmatrix} \xi+1 & \xi-1 \\ \xi-1 & \xi+1 \end{bmatrix}}_{T^{\mathrm{PF}}} \begin{bmatrix} f_\mathrm{uf} \\ g_\mathrm{uf} \end{bmatrix} + \underbrace{\alpha_2\theta\mathcal{F}(\omega)\frac{1}{2}\begin{bmatrix} 1 & -1 \\ -1 & 1 \end{bmatrix}}_{T^{\mathrm{AF}}} \begin{bmatrix} f_\mathrm{ref} \\ g_\mathrm{ref} \end{bmatrix} - \mathbb{S}, \tag{22}$$

where we have introduced the sources $\mathbb{S}$ as

$$\mathbb{S} \equiv \frac{1}{2}\frac{(\gamma-1)}{\gamma\bar{p}A_\mathrm{CC}}\hat{Q}_\mathrm{s}(\omega)\begin{bmatrix} -1 \\ 1 \end{bmatrix}. \tag{23}$$

Furthermore, $\xi = \rho_\mathrm{c}c_\mathrm{c}/\rho_\mathrm{h}c_\mathrm{h}$ and $\theta = (T_\mathrm{df}/T_\mathrm{uf} - 1)$ denote the specific acoustic impedance and the relative temperature increment, respectively. T^{PF} stands for the transfer matrix of the "passive flame", i.e. the temperature discontinuity across the flame, while T^{AF} denotes the "active flame" transfer matrix, i.e. the effect of unsteady flame heat release in response to flow perturbations. A schematic representation of Eq. (22) is given by Fig. 7. Note that in Eq. (22) the flame transfer function is defined with respect to the reference position 'ref' and not with respect to 'uf'.

We define now, considering the illustration of the system in Fig. 2, the transfer matrices 'sys1', 'sys2' and 'SYS'

$$T^{\mathrm{sys1}} \equiv T^{\mathrm{D}}_{\mathrm{c},2}\ T^{\mathrm{AC1}}\ T^{\mathrm{D}}_{\mathrm{c},1}, \tag{24}$$

$$T^{\mathrm{sys2}} \equiv T^{\mathrm{D}}_{\mathrm{c},5}\ T^{\mathrm{AC2}}\ T^{\mathrm{D}}_{\mathrm{c},4},\ T^{\mathrm{S}}\ T^{\mathrm{D}}_{\mathrm{c},3} \tag{25}$$

$$T^{\mathrm{SYS}} \equiv \left(T^{\mathrm{PF}}T^{\mathrm{sys2}} + T^{\mathrm{AF}}\right)T^{\mathrm{sys1}}, \tag{26}$$

and wave vectors

$$\mathbb{W}_n \equiv \begin{bmatrix} f_n \\ g_n \end{bmatrix}, \tag{27}$$

so that Eq. (22) may be written in compact form

$$\mathbb{W}_\mathrm{df} = T^{\mathrm{SYS}}\mathbb{W}_\mathrm{in} - \mathbb{S}. \tag{28}$$

Finally, system element transfer matrices, reflection coefficients and the source $\mathbb{S}$ are assembled to form an inhomogeneous system of equations,

$$\underbrace{\begin{bmatrix} R_\mathrm{in} & & & & R_\mathrm{out} \\ T^{\mathrm{SYS}} & -I & & & \\ & T^{\mathrm{D}}_{\mathrm{d},6} & -I & & \\ & & T^{\mathrm{D}}_{\mathrm{d},7} & -I & \end{bmatrix}}_{M} \underbrace{\begin{bmatrix} \mathbb{W}_\mathrm{in} \\ \mathbb{W}_\mathrm{df} \\ \mathbb{W}_\mathrm{mic} \\ \mathbb{W}_\mathrm{out} \end{bmatrix}}_{x} = \underbrace{\begin{bmatrix} \mathbb{S} \end{bmatrix}}_{b}, \tag{29}$$

With permission from C. Silva, M. Merk, T. Komarek, and W. Polifke. The contribution of intrinsic thermoacoustic feedback to combustion noise and resonances of a confined turbulent premixed flame. *Combustion and Flame, 182*, Elsevier, 2017.

Table 1
Geometrical and thermodynamic parameters obtained from LES and used in the acoustic network model. Indices are graphically represented in Fig. 2. The loss coefficients ζ and ζ_S were obtained numerically by Weyermann [24].

Length (m)
$l_1 = 0.17,\ l_2 = 0.11,\ l_3 = 0.025,\ l_4 = 0.045,\ l_5 = 0.045$
$l_6 = 0.255,\ l_7 = \{0.0, 0.4\} + l_{\text{eff}},\ \ l_{\text{eff}} = 0.036$
Mean velocity at 'Mid' section (m.s^{-1})
$\bar{u}_{\text{mid}} = 11.3$
Cross section area (m^2)
$A_{\text{P}} = \frac{\pi}{4}0.2^2,\ A_{\text{mid}} = \frac{\pi}{4}(0.04^2 - 0.016^2),\ A_{\text{CC}} = 0.09^2$
Density (kg.m^{-3})
$\rho_c = 1.205\ ,\ \rho_h = 0.183$
Temperatures (K)
$T_c = 293\ ,\ T_h = 1930$
Loss coefficient
$\zeta = 0.8\ ,\ \zeta_S = 1.7$
Reflection coefficient at inlet
$R_{\text{in}} = 1$

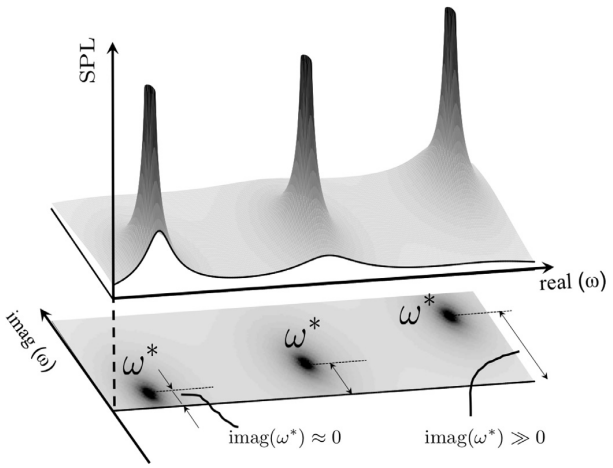

Fig. 8. Association of resonant peaks in the SPL spectrum with the eigenfrequencies ω^* of the homogeneous system model. A source $\mathbb{S}$ with a PSD that is uniform in frequency is assumed.

where I denotes a 2×2 identity matrix. Once the linear system given by Eq. (29) is solved, the acoustic pressure at the microphone located in the combustion chamber – see Fig. 2 – is computed as $\hat{p}_{\text{mic}} = \bar{\rho}_h \bar{c}_h (f_{\text{mic}} + g_{\text{mic}})$. The network model here presented was built and solved with the in-house numerical tool taX [31]. Table 1 lists values of model parameters that describe the combustor test rig under study. In finishing this section is useful to remark that the acoustic source vector (see Eq. (1)) is related to $\mathbb{S}$ by

$$\begin{bmatrix} f_s \\ g_s \end{bmatrix} = \frac{2}{1+\xi} \begin{bmatrix} -\xi & 0 \\ 0 & 1 \end{bmatrix} \mathbb{S}. \tag{30}$$

6. Interpretation of solutions of the network model

The inhomogeneous system of equations (29) may be written as

$$M(\omega)\, x = b(\omega) \quad \text{for} \quad \omega \in \mathbb{R}. \tag{31}$$

The restriction to real-valued frequencies results from the combustion noise source term $\hat{Q}_s(\omega)$ contained in the vector b, which is defined only for $\omega \in \mathbb{R}$. The vector of unknowns x – i.e. the characteristic wave amplitudes f_n, g_n at the network nodes – may be determined as $x(\omega) = M^{-1}(\omega) b(\omega)$, provided that the matrix $M(\omega)$ at frequency ω is non-singular. The system (31) behaves in many aspects analogously to a forced oscillator, but some peculiarities result from the facts that the combustion noise source term is broad-band in nature; that thermo-acoustic system may develop self-excited instabilities due to feedback; and that nonlinear effects will become significant at large oscillation amplitudes. Ramifications for the proper interpretation of peaks in the spectral distribution of pressure fluctuations predicted by the model (31) result, which are discussed in this section.

Consider first that the inhomogeneous system of equations (31) will be ill-defined with singular matrix $M(\omega)$ for specific frequencies ω^*,

$$\det(M(\omega^*)) = 0 \quad \text{with} \quad \omega^* \in \mathbb{C}. \tag{32}$$

These frequencies are associated with eigenmodes[1] of the corresponding homogeneous system $Mx = 0$, with non-trivial eigenvectors $x^* \neq 0$. As discussed by Emmert et al. [13], the complete set of eigenvectors of a thermoacoustic system M should be interpreted as the sum of cavity acoustic and ITA eigenmodes. If the imaginary part of an eigenfrequency is positive, $\text{imag}(\omega^*) > 0$, the amplitude of that mode will decay $\sim \exp\{-\text{imag}(\omega^*)t\}$, and the mode is considered stable. This is analogous to an oscillator without driving, where oscillation amplitude will decay due to friction. If the imaginary part of *all* eigenfrequencies is positive, the system M is judged to be linearly stable. Conversely, if $\text{imag}(\omega^*) < 0$ for one (or several) of the eigenmodes, the mode is thermoacoustically unstable and amplitudes will grow exponentially until nonlinear effects – such as saturation of flame response, or increases losses – lead to an asymptotic state, e.g. a limit cycle. These considerations apply to both cavity acoustic and ITA modes. The case of exact marginal stability with $\text{imag}(\omega^*) = 0$ is very unlikely and not considered further.

Now let us discuss under which circumstances the model (31) will produce peaks in the spectral distribution of the Sound Pressure Level (SPL) in the combustor. The first possibility is that the spectral distribution of the combustion noise source term $\hat{Q}_s$ and accordingly the acoustic source vector itself exhibit a peak at a certain frequency. For a linear system, enhanced forcing results in increased amplitudes, such that the SPL spectra should exhibit a corresponding peak at the same frequency. However, the spectral distribution of the combustion noise source term $\hat{Q}_s$ is related to turbulent statistics [2], which in general will not generate pronounced peaks.

A more relevant mechanism is resonant driving of a stable eigenmode. This scenario is straightforward to understand, in obvious analogy to a forced oscillator with damping, where for given forcing amplitude the amplitude of oscillation will increase as the forcing frequency approaches the oscillator eigenfrequency. Thus even with a broad-band source of combustion noise without any peaks, the model (31) will generate peaks in the SPL spectra at frequencies $\text{real}(\omega^*)$, where the ω^*'s are the eigenfrequencies of the homogeneous system $Mx = 0$. As sketched in Fig. 8, we should expect a pronounced peak if the imaginary part of an eigenfrequency $\text{imag}(\omega^*)$ is small, because in that case the determinant $\det(M(\omega))$ will be close to zero. This behaviour is quite intuitive: persistent forcing of a mildly damped mode can result in large oscillation amplitudes. On the contrary, a strongly damped mode with $\text{imag}(\omega^*) \gg 0$ will only exhibit a mild peak, as depicted in Fig. 8 for the modes at higher frequencies. The reader should appreciate that for a *stable* eigenmode, the inhomogeneous linear system model (31) will in principle afford a quantitative prediction of the sound

[1] Note that this is not a standard linear algebra eigenvalue problem, because in general some of the coefficients of the matrix M depend on frequency ω.

With permission from C. Silva, M. Merk, T. Komarek, and W. Polifke. The contribution of intrinsic thermoacoustic feedback to combustion noise and resonances of a confined turbulent premixed flame. *Combustion and Flame, 182*, Elsevier, 2017.

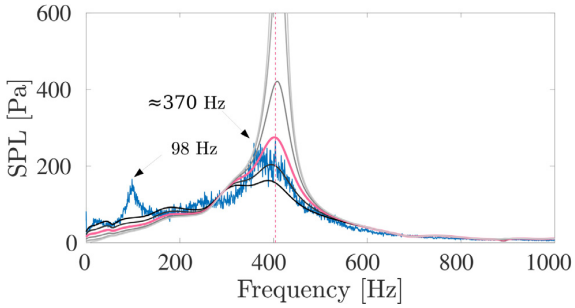

Fig. 9. OWC case: Noise spectrum at position 'mic' predicted by the network model with one-way-coupling for varying values of $|r_{out}|$: —— 0.5, —— 0.6, —— 0.7, —— 0.8, —— 0.9, —— 1.0, —— experimental results.

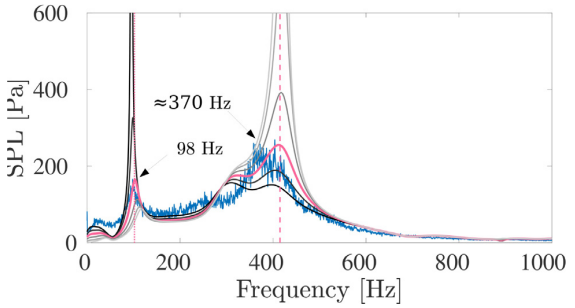

Fig. 10. TWC case: Noise spectrum at position 'mic' predicted by the network model with two-way-coupling and varying values of $|r_{out}|$: —— 0.5, —— 0.6, —— 0.7, —— 0.8, —— 0.9, —— 1.0, —— experimental results.

pressure level, provided that oscillation amplitudes remain at a level where nonlinear effects are not yet significant.

What to expect if one of the eigenmodes is *unstable*? In this case, combustion noise or some other kind of initial perturbation triggers oscillations, which subsequently grow (without the need of a driver) until nonlinear effects lead to saturation. The magnitude of the combustion noise source term is most likely irrelevant for the limit cycle oscillation amplitudes. Furthermore, a linear model is not capable of predicting sound pressure levels in the limit cycle, and it might seem that the model (31) provides no useful information whatsoever about unstable modes. However, growth rates of thermoacoustic instabilities are in general not very large – realistic values correspond to cycle increments of a few percent. This implies that the imaginary part of the eigenfrequency ω^* of unstable modes will be small, i.e. the modes are located close to the real axis Fig. 8, and the inhomogeneous model (31) will produce a pronounced resonance peak at the frequency real(ω^*) and thereby indicate the presence of an unstable mode. This justifies the use of the inhomogeneous model (31) for thermoacoustic stability analysis [7,32]. However, the magnitude of the resonance peak should not be equated with the oscillation amplitude in the limit cycle.

The discussion in this section may be summarized as follows: the linear, inhomogeneous model $Mx = b$ can identify frequencies, where one should expect large oscillation amplitudes. If one determines in addition the eigenfrequencies ω^* of the homogeneous model $Mx = 0$, one is able to distinguish between peaks in the SPL spectra that result from resonant driving of a stable mode, and those that result from self-excited instability. For the former, amplitude levels predicted by the liner model may be quantitatively accurate, for the latter a nonlinear model is required to predict limit cycle amplitudes.

7. Results

According to elementary considerations, the fundamental ITA mode should occur close to a frequency where the phase of $\mathcal{F}(\omega)$ equals $-\pi$, as argued by Hoeijmakers et al. [16], Emmert et al. [17], and Courtine et al. [19]. By inspection of the phase plot in Fig. 5, one estimates this frequency to be near 100 Hz. Indeed, the sound pressure level measured at the combustor exit shows a distinct peak at a frequency of 98 Hz (see Fig. 9 and/or Fig. 10). The proximity in frequency suggests that this peak may be associated with the first mode of the ITA feedback loop. However, the agreement in frequency by itself does not rule out the possibility that by coincidence we have encountered a cavity acoustic mode of the test rig.

In the following, we shall present results of parametric studies carried out with the network model presented in the previous section and considering the flame transfer function $\mathcal{F}(\omega)$ and combustion noise source $\hat{Q}_s(\omega)$ estimated with LES data (Figs. 5 and 6). We shall explore how frequency and strength of resonance peaks, but also frequency and growth rate of eigenmodes of the system matrix M (see Eq. (29)) vary due to the inclusion of two-way-coupling, and due to changes in exit reflection coefficient r_{out} and combustor length l_{cc}. This will allow us to ascertain that indeed the resonance peak at 98 Hz is due to the ITA feedback loop. A second pronounced peak in sound pressure level is observed at 370 Hz. The network model study will confirm that this peak is related to an acoustic cavity mode (see below).

Note that a narrow, low-frequency (130 Hz) peak in the combustion noise spectrum of the BRS burner was previously observed and discussed by Weyermann [24] at different operating conditions. Unfortunately, at that time the concept of ITA feedback was not yet known. Thus a proper interpretation of this observation and further implications were not developed.

7.1. SPL spectra with one- and two-way coupling

In this section we compare the spectral distribution of sound pressure level (SPL) measured in experiment with the results of the network model Eq. (29), for the case in which the combustion chamber length $l_{CC} = l_5 + l_6 + l_7$ (see Fig. 2) is equal to 0.3 m. In addition we study the influence of the reflection coefficient $r_{out}(\omega)$ on the results, which also impacts the complex eigenfrequencies ω^* of the system matrix M of Eq. (29). The SPL spectrum observed in experiment at the location 'mic' (see Fig. 2), which is shown in blue in Fig. 9 and also in Fig. 10, exhibits two prominent peaks around 98 Hz and around 370 Hz.[2]

For the low-order network model, let us first consider a model variant in which the influence of the acoustic waves on the unsteady heat release rate of the flame is neglected by setting $T^{AF} = [0 \;\; 0; 0 \;\; 0]$ in Eq. (26). Recalling the discussion in the introduction, we label this case as OWC for 'One-Way-Coupling'. In Fig. 9 we show in shades of gray the curves that represent the acoustic pressure estimated by the network model, for the range $0.5 < |r(\omega)| < 1.0$. Results of the case where $|r(\omega)| = 0.7$, which correspond to the 'reference' value of $|r_{out}|$ illustrated in Fig. 3, are plotted in red.

Remarkably, the peak observed in experiment at 98 Hz is not predicted *at all* by the network model with OWC. On the other hand, the physically motivated model of 'Two-Way-Coupling' (TWC), where the response of the flame to acoustic perturbations

[2] In order to avoid confusion, the reader should be aware that these measurements are performed on the same experimental setup (see measurements of $\mathcal{F}(\omega)$ in Fig. 5), but considering no external acoustic forcing.

With permission from C. Silva, M. Merk, T. Komarek, and W. Polifke. The contribution of intrinsic thermoacoustic feedback to combustion noise and resonances of a confined turbulent premixed flame. *Combustion and Flame, 182*, Elsevier, 2017.

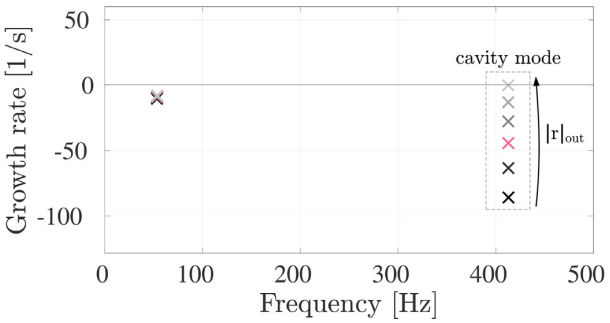

Fig. 11. OWC case: Pole map of the system matrix M with one-way-coupling for varying values of $|r_{out}|$: **x** 0.5, **x** 0.6, **x** 0.7, **x** 0.8, **x** 0.9, **x** 1.0.

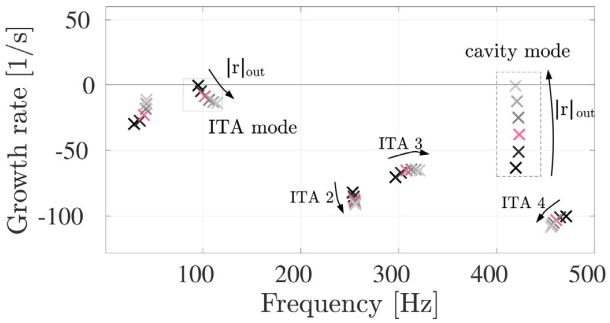

Fig. 12. TWC case: Pole map of the system matrix M with two-way-coupling for values of $|r_{out}|$: **x** 0.5, **x** 0.6, **x** 0.7, **x** 0.8, **x** 0.9, **x** 1.0.

is duly taken into account with T^{AF} in Eq. (22), recovers a peak near 98 Hz, see Fig. 10.

These results indicate unequivocally that the peak at 98 Hz results not from coupling to a cavity acoustic mode, but from ITA feedback. Let as assume, for the sake of the argument, that a cavity acoustic mode exists at 98 Hz. Both OWC and TWC account for the combustion noise source term $\dot{Q}'_s$ as the driving mechanism, thus *both* models would produce a peak in the SPL as the result of resonance of the noise source term $\dot{Q}'_s$, which is quite strong in this frequency range (see Fig. 6), with the acoustic mode. However, the OWC result does not exhibit a peak in this frequency range, while the TWC result does. Let as assume the alternative, i.e. that an ITA mode exists at 98 Hz. In the OWC model, the ITA feedback loop is broken, because the link between upstream velocity fluctuations u'_{ref} and unsteady heat release rate $\dot{Q}'_c$ is severed. Thus the combustion noise source term $\dot{Q}'_s$ cannot produce a peak due to resonance with an ITA mode in the OWC model. On the other hand, the TWC model retains the link between u'_{ref} and $\dot{Q}'_c$ and consequently, the combustion noise source term $\dot{Q}'_s$ can go in resonance with the ITA feedback loop. We conclude with confidence that the presence of the peak in the TWC model, and its absence in the OWC model, supports the hypothesis that this peak results from ITA feedback.

A second peak around 400 Hz is associated with the quarter-wave mode of the combustion chamber and corresponds well with the peak at 370 Hz observed in experiment. Note that the mismatch of 30 Hz is likely due to an overestimation of the hot gas temperature ($T_h = 1930$ K) obtained by LES and used in the acoustic network model. The strength of the peak increases with increasing magnitude of the exit reflection coefficient, as one would expect for a forced oscillation at resonance when acoustic losses decrease. Conversely, the strength of the peak at 98 Hz related to ITA feedback *decreases* with an increase of the magnitude of the exit reflection coefficient. This will be discussed further in the following.

In closing this section we note that the maxima in the spectral distribution of the combustion noise source $\hat{Q}_s(\omega)$ – see Fig. 6 – do not correspond with the peaks in the SPL spectrum in the combustor. This lends further support to our argument that in confined systems resonant coupling between the noise source term and the acoustic environment as well as the ITA feedback loop shape the spectral distribution of combustion noise in a decisive manner.

7.2. Relation between SPL spectra and the poles of M – stable case

In order to further analyze the nature of the resonances near 100 Hz and 400 Hz, Figs. 11 and 12 show pole maps of the system matrix M of the network model (see Eq. (29)), obtained by solving the characteristic equation $\det(M(\omega^*)) = 0$, where $\omega^* \in \mathbb{C}$, for the eigenfrequencies ω^* of the homogeneous system (without driving by combustion noise). As mentioned in Section 6, real(ω^*) is associated to the resonance frequency whereas -imag(ω^*) defines the growth rate of the mode under investigation.

The pole map Fig. 11 of the OWC case shows eigenfrequencies around 50 Hz and 400 Hz. The 50 Hz mode corresponds to a Helmholtz mode, where the plenum acts as the resonator 'volume', and the burner annulus as the 'neck' of a Helmholtz resonator. The 400 Hz mode can be identified as a quarter wave mode of the combustion chamber. The pole map shows clearly that the growth rate of this mode increases as the outlet reflection coefficient $|r_{out}|$ increases. This is expected for a cavity acoustic mode, since for larger values of $|r_{out}|$, the loss of acoustic energy at the outlet boundary decreases. This corresponds to the observation that with larger $|r_{out}|$, the amplitude of the resonance peak at 400 Hz increases, see Figs. 9 and 10.

Results for the TWC case, where feedback from the acoustics on the flame is taken into account, are shown in Fig. 12. Additional poles around 100 Hz, 250 Hz, 300 Hz and 450 Hz are observed. In this work, we exclusively concentrate on the mode at 100 Hz, because this is the one with larger growth rate (although still negative) and, therefore, the one that dominates the noise spectrum. A more comprehensive analysis of the nature of the various modes is given by Emmert et al. [13]. Again it is very interesting to see the influence of the magnitude of the reflection coefficient $|r_{out}|$ on the eigenfrequencies. The growth rate of the 100 Hz mode *increases* as $|r_{out}|$ decreases, as seen in Fig. 12. This behavior might seem counter-intuitive at first sight, but it does correspond with the decrease in strength of the SPL peak in Fig. 10. In contrast to acoustic cavity modes, the growth rate of an ITA mode may increase when the acoustic reflection at the boundaries is reduced, as already observed by Hoeijmakers et al. [16]. Specific flame/burner properties determine whether the growth rate of an ITA mode increases or decreases when lowering acoustic reflection at the boundaries.

In order to further understand the nature of the resonance at 100 Hz, we will consider a system where no cavity acoustic modes are possible. This is achieved by setting $r_{in}, r_{out} = 0$ and by disregarding the plenum from the system by setting $T^{sys1} = I$. In order to fully simplify the resulting expression we consider all lengths l of the system equal to zero. The eigenfrequencies ω^* of the simplified system are now easily obtained from the solution of the characteristic equation

$$\det(M(\omega^*)) = \xi + \alpha_2 + \alpha_2\theta\mathcal{F}(\omega^*) = 0, \quad \text{where } \omega^* \in \mathbb{C}. \tag{33}$$

For the fundamental mode, we obtain a frequency real(ω^*) = 2π (106) s^{-1} and a growth rate $-$imag(ω^*) = -18 s^{-1}. We can consider the frequency 106 Hz to be close enough to the one predicted by the complete network model (case TWC) at 100 Hz and observed in experiments at 98 Hz. We conclude, therefore, that the peak at 100 Hz is of ITA nature. Following a similar analysis,

With permission from C. Silva, M. Merk, T. Komarek, and W. Polifke. The contribution of intrinsic thermoacoustic feedback to combustion noise and resonances of a confined turbulent premixed flame. *Combustion and Flame, 182*, Elsevier, 2017.

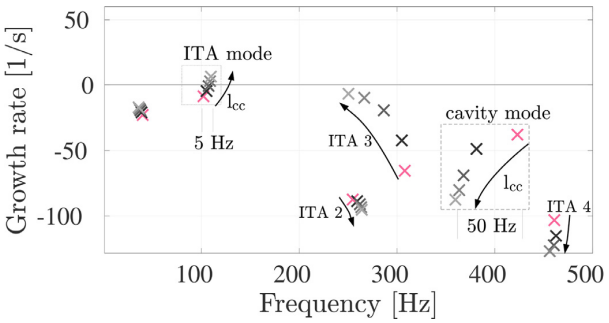

Fig. 13. Pole map of systems with varying combustion chamber length l_{cc}: X 0.3 m, X 0.4 m, X 0.5 m, X 0.6 m, X 0.7 m.

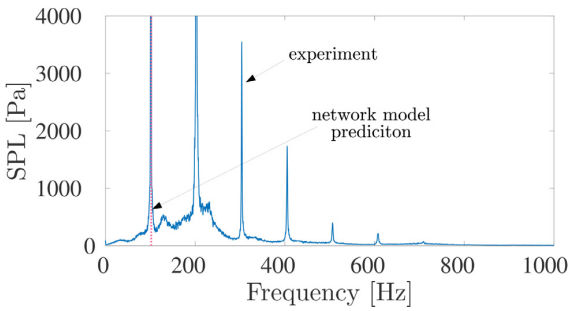

Fig. 14. Experimentally measured noise spectrum for a combustion chamber length of $l_{cc} = 0.7$ m.

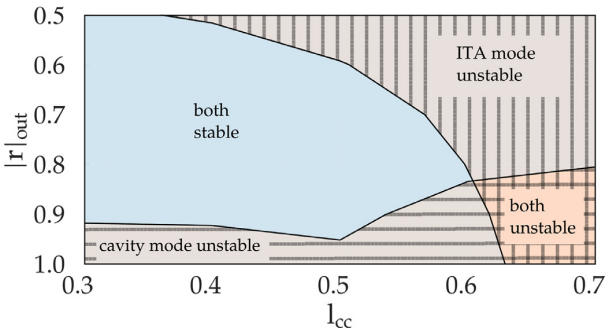

Fig. 15. Stability map of the system that simultaneously depicts the influence of a variation of $|r_{out}|$ and l_{cc} on the overall stability. Unstable regions are further separated in unstable cavity modes and an unstable ITA mode.

we recognized the poles around 250 Hz, 300 Hz and 450 Hz of the complete system M to be also of ITA nature[3]. They are labeled 'ITA2', 'ITA3', 'ITA4' in Figs. 12 and 13. It should be remarked that in order to obtain valid solutions of Eq. (33), the flame transfer function $\mathcal{F}(\omega)$ must be well-defined for $\omega \in \mathbb{C}$. This is guaranteed by computing $\mathcal{F}(\omega)$ as the z-transform of the impulse response, see Eq. (9).

7.3. Relation between the SPL spectra and the poles of M – unstable case

In the previous section, we have recognized the presence of the ITA feedback loop in the SPL spectrum of noise. In addition, we have analyzed the influence of the magnitude of the reflection coefficient $|r_{out}|$ both on the strength of the peaks of the noise spectrum and on the growth rate of the two main acoustic modes (of cavity resonance and ITA nature, respectively). We study now the influence of the combustion chamber length l_{CC} on the eigenfrequencies ω^* of these two acoustic modes.

Figure 13 shows the trajectories of the eigenfrequencies on the complex plane when varying l_{CC}. The eigenfrequencies that correspond to the case $l_{CC} = 0.3$ m where $|r| = 0.7$ are displayed in red. We observe that an increment of l_{CC} in the range 0.3 m$< l_{CC} <$ 0.7 m changes the resonance frequency of the cavity mode by 50 Hz. This is naturally expected, because a longer combustion chamber can be associated with a longer wavelength of the corresponding cavity mode. In contrast, the frequency of the ITA resonance is only shifted by 5 Hz (see Fig. 13) by this change in combustion chamber length. The increment of l_{CC} influences significantly also the growth rate of the modes under investigation: Whereas the cavity resonance mode exhibits a reduced growth rate for larger values of l_{CC}, the growth of the ITA mode increases as l_{CC} gets larger. The network model predicts that for $l_{CC} > 0.6$ the system becomes unstable due to the positive growth rate of the ITA mode.

This trend corresponds well with experiment: Fig. 14 shows measurements of the SPL for the case $l_{CC} = 0.7$. We observe a large peak of the fundamental mode at 100 Hz, with corresponding harmonics at multiples of the fundamental frequency. Since this case is recognized as unstable, the amplitude of the peaks caused by the combustion instability correspond to the amplitude of the associated limit cycle. Because the model given by Eq. (29) is based on linear acoustics and linear flame dynamics, it cannot predict the amplitude of this limit cycle. Nevertheless, the results of the network model can give a good estimate of the frequency of the limit cycle. We observe that the peak measured in experiments corresponds well to the frequency of the unstable ITA mode near 100 Hz.

The parametric study is completed by presenting in Fig. 15 the influence of both reflection coefficient $|r_{out}|$ and combustor length l_{CC} on the growth rates of the acoustic modes. We observe that for values of $|r_{out}|$ close to unity the mode corresponding to acoustic cavity resonance is triggered, whereas for lower values of $|r_{out}|$ the ITA mode is predominant.

8. Conclusions and outlook

We have studied numerically and experimentally the combustion noise produced by a turbulent flame. Peaks in the spectral distribution of sound pressure level were found to result not from corresponding peaks in the spectral distribution of the combustion noise source term, but from resonances with acoustic cavity modes or intrinsic thermoacoustic (ITA) modes. This observation holds for stable as well as unstable configurations, although peaks in SPL spectra are much more pronounced if thermoacoustic instability occurs. It is concluded that in order to predict combustion noise and resonances of confined turbulent flames, acoustic models must in general account for the two-way-coupling between the sources of noise and the surrounding acoustic field. Further implications result for sound radiated by open turbulent flames, where acoustic cavity modes cannot exist due to the anechoic environment. Nevertheless, ITA feedback will be present in general, and the spectrum of noise may be determined by both the broadband nature of the noise source term of the flames, as well as by resonance peaks that correspond to ITA feedback.

[3] For small values of |imag(ω)| it can be demonstrated that $\mathcal{F}(\omega) = \mathcal{F}(\text{real}(\omega), \text{imag}(\omega))$ is a dilated (or contracted) version of $\mathcal{F}(\text{real}(\omega), 0)$. On the contrary, for large values of |imag(ω)|, the function $\mathcal{F}(\text{real}(\omega), \text{imag}(\omega))$ cannot be easily mapped from $\mathcal{F}(\text{real}(\omega), 0)$. In the system under investigation |imag(ω^*)| is small for the fundamental ITA mode and is large for the modes ITA2, ITA3 and ITA4. Consequently, the value of $\mathcal{F}(\text{real}(\omega^*), \text{imag}(\omega^*))$ cannot be easily presumed from $\mathcal{F}(\text{real}(\omega^*), 0)$. A further consequence is that the intrinsic eigenfrequencies ω^*, labelled ITA2, ITA3 and ITA4 are *not* found at $\angle\mathcal{F}(\text{real}(\omega), 0) = -3\pi, -5\pi, -7\pi$.

With permission from C. Silva, M. Merk, T. Komarek, and W. Polifke. The contribution of intrinsic thermoacoustic feedback to combustion noise and resonances of a confined turbulent premixed flame. *Combustion and Flame, 182*, Elsevier, 2017.

Furthermore, our results show that ITA modes do not necessarily lock on to cavity acoustic modes, as already observed in the studies of Hoeijmakers et al. [14] and Emmert et al. [13]. Instead, modes of different nature coexist in the test rig investigated in this study, one associated with cavity resonance and another associated with ITA resonance. In this study, these two types of modes are influenced by acoustic boundaries in a rather different way: While the growth rate of the cavity mode becomes larger with increasing magnitude of the downstream reflection coefficient $|r_{out}|$, the growth rate of the ITA mode *decreases*. Similarly, a change in the length of the combustion chamber l_{CC} – which can be also seen as a change in the argument of r_{out} – causes a large shift in the frequency of the cavity mode, whereas it has almost no impact on the frequency of the ITA mode. These findings are quite important for passive control of thermoacoustic instabilities, because it is classically believed that changes in magnitude or the phase of acoustic boundaries of a combustion system should imply a corresponding shift in the growth rate or resonance frequency of the associated acoustic mode. We have shown that the latter is not always the case if the acoustic mode is of ITA nature. A more in-depth and comprehensive analysis of the nature and the interactions of cavity vs. ITA modes was presented by Emmert et al. [13].

In this study we have for the first time deduced concurrently the flame transfer function and the combustion noise source term of a turbulent flame from LES time series data with system identification. The application of advanced system identification techniques for this task is the topic of ongoing work.

Acknowledgments

The authors acknowledge financial support by the German Research Foundation DFG, project PO 710/16-1.

References

[1] W.C. Strahle, On combustion generated noise, J. Fluid Mech. 49 (1971) 399–414.
[2] C. Hirsch, J. Wäsle, A. Winkler, T. Sattelmayer, A spectral model for the sound pressure from turbulent premixed combustion, Proc. Combust. Inst. 31 (1) (2007) 1435–1441.
[3] W.C. Strahle, Combustion Noise, Prog. Energy Combust. Sci. 4 (1978) 157–176.
[4] U. Hedge, D. Reuter, B.T. Zinn, Sound generation by ducted flames, AIAA J. 26 (1987) 532–537.
[5] S.R. Chakravarthy, O.J. Shreenivasan, B. Boehm, A. Dreizler, J. Janicka, Experimental characterization of onset of acoustic instability in a nonpremixed half–dump combustor, J. Acoust. Soc. Am. 122 (1) (2007) 120–127.
[6] B.B.H. Schuermans, W. Polifke, C.O. Paschereit, J.H. van der Linden, Prediction of acoustic pressure spectra in combustion systems using swirl stabilized gas turbine burners, International gas turbine and aeroengine congress & exhibition, no. ASME 2000-GT-105 (2000). (Munich, Bavaria, Germany).
[7] W. Polifke, C.O. Paschereit, K. Döbbeling, Constructive and destructive interference of acoustic and entropy waves in a premixed combustor with a choked exit, Int. J. Acoust. Vib. 6 (3) (2001) 135–146.
[8] C.O. Paschereit, B. Schuermans, W. Polifke, O. Mattson, Measurement of transfer matrices and source terms of premixed flames, J. Eng. Gas Turb. Power 124 (2002) 239–247.
[9] F. Weyermann, C. Hirsch, T. Sattelmayer, Influence of boundary conditions on the noise emission of turbulent premixed swirl flames, in: J. Janicka, A. Schwarz (Eds.), Combustion Noise, Springer Verlag (2009), pp. 161–188. No. ISBN-13: 978–3642020377, ch. 6.
[10] N. Noiray, B. Schuermans, Theoretical and experimental investigations on damper performance for suppression of thermoacoustic oscillations, J. Sound Vib. 331 (2012) 2753–2763.
[11] C.F. Silva, W. Polifke, J. O'Brien, M. Ihme, Towards concurrent identification of flame dynamics and combustion noise of enclosed flames, Proceedings of the summer program, Center for Turbulence Research, Stanford University/NASA Ames, USA (2014).
[12] S. Bomberg, T. Emmert, W. Polifke, Thermal versus acoustic response of velocity sensitive premixed flames, Proc. Combust. Inst. 35 (3) (2015) 3185–3192.
[13] T. Emmert, S. Bomberg, S. Jaensch, W. Polifke, Acoustic and intrinsic thermoacoustic modes of a premixed combustor, Proc. Combust. Inst. 36 (3) (2017) 3835–3842.
[14] M. Hoeijmakers, V. Kornilov, I.L. Arteaga, P. de Goey, H. Nijmeijer, Flame dominated thermoacoustic instabilities in a system with high acoustic losses, Combust. Flame 169 (2016) 209–215.
[15] M. Hoeijmakers, I.L. Arteaga, V. Kornilov, H. Nijmeijer, P. de Goey, Experimental investigation of intrinsic flame stability, Proceedings of the European Combustion Meeting (2013). Lund, Sweden.
[16] M. Hoeijmakers, V. Kornilov, I. Lopez Arteaga, H. Nijmeijer, Intrinsic instability of flame-acoustic coupling, Combust. Flame 161 (11) (2014) 2860–2867.
[17] T. Emmert, S. Bomberg, W. Polifke, Intrinsic thermoacoustic instability of premixed flames, Combust. Flame 162 (1) (2015) 75–85.
[18] C.F. Silva, T. Emmert, S. Jaensch, W. Polifke, Numerical study on intrinsic thermoacoustic instability of a laminar premixed flame, Combust. Flame 162 (2015) 3370–3378.
[19] E. Courtine, L. Selle, T. Poinsot, DNS of Intrinsic thermoacoustic modes in laminar premixed flames, Combust. Flame 162 (11) (2015) 4331–4341.
[20] J. Wäsle, A. Winkler, F. Weyermann, C. Hirsch, T. Sattelmayer, A model for turbulent combustion noise, Acta Acust. United Acust. 95 (3) (2009) 391–401.
[21] J. Lavrentjev, M. Åbom, H. Bodén, A measurement method for determining the source data of acoustic two-port sources, J. Sound Vib. 183 (3) (1995) 517–531.
[22] C.F. Silva, M. Leyko, F. Nicoud, S. Moreau, Assessment of combustion noise in a premixed swirled combustor via large-eddy simulation, Comput. Fluids 78 (2013) 1–9.
[23] T. Komarek, W. Polifke, Impact of swirl fluctuations on the flame response of a perfectly premixed swirl burner, J. Eng. Gas Turbines Power 132 (2010). 061503–1,7.
[24] F. Weyermann, Numerische Berechnung der Emission verbrennungsinduzierten Lärms automobiler Zusatzheizungen Phd thesis, Technische Universität München, 2010.
[25] L. Tay-Wo-Chong, S. Bomberg, A. Ulhaq, T. Komarek, W. Polifke, Comparative validation study on identification of premixed flame transfer function, J. Eng. Gas Turb. Power 134 (2) (2012). 021502–1–8.
[26] O. Colin, F. Ducros, D. Veynante, T. Poinsot, A thickened flame model for large eddy simulations of turbulent premixed combustion, Phys. Fluids 12 (7) (2000) 1843–1863.
[27] W. Polifke, C. Wall, P. Moin, Partially reflecting and non-reflecting boundary conditions for simulation of compressible viscous flow, J. Comput. Phys. 213 (1) (2006) 437–449.
[28] W. Polifke, Black-box system identification for reduced order model construction, Ann. Nucl. Energy 67 (2014) 109–128.
[29] L. Ljung, System identification - theory for the user, 2nd, Prentice Hall, 1999.
[30] C. Sovardi, S. Jaensch, W. Polifke, Concurrent identification of aero-acoustic scattering and noise sources at a flow duct singularity in low mach number flow, J. Sound Vib. 377 (2016) 90–105.
[31] T. Emmert, S. Jaensch, C. Sovardi, W. Polifke, taX - a flexible tool for low-order duct acoustic simulation in time and frequency domain, 7th Forum Acusticum (2014). (Krakow), DEGA, bibtex: EmmerJaens14.
[32] J.J. Keller, Thermoacoustic oscillations in combustion chambers of gas turbines, AIAA J. 33 (12) (1995) 2280–2287.

With permission from C. Silva, M. Merk, T. Komarek, and W. Polifke. The contribution of intrinsic thermoacoustic feedback to combustion noise and resonances of a confined turbulent premixed flame. *Combustion and Flame, 182*, Elsevier, 2017.

ARTICLE IN PRESS
JID: PROCI [m;June 23, 2018;0:7]

Available online at www.sciencedirect.com

ScienceDirect

Proceedings of the Combustion Institute 000 (2018) 1–8

Proceedings of the Combustion Institute

www.elsevier.com/locate/proci

Prediction of combustion noise of an enclosed flame by simultaneous identification of noise source and flame dynamics

M. Merk [a,*], R. Gaudron [b], C. Silva [a], M. Gatti [b], C. Mirat [b], T. Schuller [b,c], W. Polifke [a]

[a] *Fakultät für Maschinenwesen, Technische Universität München, Boltzmannstr. 15, Garching D-85747, Germany*
[b] *Laboratoire EM2C, CNRS, CentraleSupélec, Université Paris-Saclay, 3, rue Joliot Curie, Gif-sur-Yvette cedex 91192, France*
[c] *Institut de Mécanique des Fluides de Toulouse, IMFT, Université de Toulouse, CNRS, Toulouse, France*

Received 30 November 2017; accepted 31 May 2018
Available online xxx

Abstract

Large-Eddy Simulation (LES) is combined with advanced System Identification (SI) to simultaneously infer models for the source of combustion noise and the dynamic response to velocity fluctuations of a turbulent premixed flame. A Box-Jenkins model structure allows SI of both the noise source and the flame dynamics from time series data generated with single LES. The models that result from this 'black-box' SI approach are purely data-driven and do not rely on estimates of characteristic flow or flame parameters, such as turbulence intensity or flame length. In confined combustion systems the spectral distribution of combustion noise is strongly modulated by the cavity acoustics and the flame dynamics. By incorporating the identified models into a network model for the combustor acoustics, a linear Reduced Order Model (ROM) is built to predict the spectral distribution of sound pressure within the combustor for two different outlet reflection conditions. The identified flame transfer function as well as the ROM-based predictions of the pressure spectra in the combustor are compared with satisfactory qualitative and quantitative agreement against measurements. An interpretation of the pressure spectra based on eigenmode analysis elucidates the interplay between combustion noise generation, flame dynamics and cavity resonances.
© 2018 The Combustion Institute. Published by Elsevier Inc. All rights reserved.

Keywords: Combustion noise; Large-Eddy Simulation; System identification; Linear acoustic network model

1. Introduction

Combustion noise is an unavoidable by-product of turbulent combustion. For aeronautical engines it constitutes a significant contribution to the overall noise emissions [1]. Combustion noise re-

* Corresponding author.
E-mail address: merk@tfd.mw.tum.de (M. Merk).
URL: http://www.tfd.mw.tum.de (M. Merk)

https://doi.org/10.1016/j.proci.2018.05.124
1540-7489 © 2018 The Combustion Institute. Published by Elsevier Inc. All rights reserved.

Please cite this article as: M. Merk et al., Prediction of combustion noise of an enclosed flame by simultaneous identification of noise source and flame dynamics, Proceedings of the Combustion Institute (2018), https://doi.org/10.1016/j.proci.2018.05.124

With permission from M. Merk, R. Gaudron, C. Silva, M. Gatti, C. Mirat, T. Schuller and W. Polifke. Prediction of combustion noise of an enclosed flame by simultaneous identification of noise source and flame dynamics. *Proceedings of the Combustion Institute*, Elsevier, 2018.

ARTICLE IN PRESS
JID: PROCI [m;June 23, 2018;0:7]

sults from unsteady heat release by the flame [2]. The fluctuations of heat release rate may be seen as the sum of two contributions

$$\dot{Q}' = \dot{Q}'_c + \dot{Q}'_s \,. \tag{1}$$

Following the nomenclature of [3], $\dot{Q}'_c$ denotes perturbations of heat release rate that result from acoustic velocity fluctuations upstream of the flame. This flame dynamic response may be taken into account via a Flame Transfer Function (FTF). Flame dynamics play a key role in self-excited thermoacoustic instability – which is not discussed further in the present paper – but can also shape the spectrum of combustion noise, as will be shown in the following. The second term $\dot{Q}'_s$ describes a broadband *source of combustion noise*, which results from stochastic activity of the turbulent flow field and is understood to be uncorrelated with incoming acoustic perturbations.

Regarding the spectral distribution of noise generated by turbulent flames, one should distinguish between unconfined and enclosed configurations. In unconfined configurations, the sound pressure spectrum strongly correlates with $\dot{Q}'_s$ and is thus of broadband nature. Nevertheless, even in this case $\dot{Q}'_c$ cannot be neglected: flame intrinsic thermoacoustic (ITA) feedback may establish a two-way coupling between flame and acoustics [3,4], where the acoustic field generated by the flame causes velocity fluctuations upstream of the flame. These fluctuations in turn perturb the flame, causing a contribution $\dot{Q}'_c$ to the fluctuations of heat release rate that may go in constructive or destructive interference with the noise source term $\dot{Q}'_s$. Consequently, the sound pressure spectrum is modulated. In case of an enclosed flame, acoustic reflections at the system boundaries constitute an additional feedback loop, which may modulate the shape of the sound pressure spectrum in a distinctive manner. The noise source $\dot{Q}'_s$ may excite an acoustic cavity mode, causing resonance peaks in the pressure spectrum [3,4]. Hence, the sound pressure level and its spectral distribution depend in general strongly on the acoustic boundaries of the combustion system [5,6].

To reduce the overall sound pressure level in applied confined systems and to better understand the nature of the sound spectrum, accurate, reliable and flexible prediction methods are necessary, which take all relevant thermo-acoustic mechanisms into account. 'Flexible' here means that it should be possible to assess in a convenient and affordable manner the effect of changes in the acoustic boundary conditions, say, or the combustor geometry on the pressure spectrum.

Obviously, sound pressure levels in a combustion system may be determined by measurement [6–8]. However, experiments are rather laborious and inflexible in regard to changes in the acoustic boundaries. Reactive compressible Large-Eddy Simulation (LES) resolves directly the combustion noise generation as well as the acoustic propagation and reflection within the cavity and has proven itself to be capable of reproducing accurately the sound pressure spectra in confined systems [8–10]. Even though changes in the acoustic boundaries are feasible to implement, the computational effort of LES is considerable, and the investigation of a wide range of parameters, say, is prohibitively expensive.

Linear acoustic network models, on the other hand, are computationally much less demanding. Acoustic propagation, reflection and dissipation are described by network elements that relate the acoustic field up- and downstream of each element. In combination with an FTF, which describes the flame dynamics, and a model for the generation of combustion noise, a Reduced Order Model (ROM) can be formulated that should allow quantitative estimation of the sound pressure level for thermoacoustically stable configurations [3,4]. Whereas acoustic propagation, damping and reflection within the network model are rather straightforward to describe, the determination of the FTF and the noise source is more challenging.

A combustion noise source vector in terms of emitted characteristic wave amplitudes may be extracted experimentally [4,11], but the experimental assessment of the combustion noise source is difficult and laborious. An alternative approach relies on a Strouhal number scaling for the noise source [12–14]. These models predict an increase of the combustion noise source strength towards a peak frequency, with a subsequent roll-off to higher frequencies. These estimations rely on various assumptions that depend on the flame type and require detailed information about the flow field and the flame shape as model input.

The reader is reminded at this point that according to Eq. (1) the determination of only the noise source $\dot{Q}'_s$ is not sufficient for an accurate prediction of combustion generated sound via a ROM. The possibility of two-way coupling requires to take into account also the flame response to acoustic fluctuations $\dot{Q}'_c$, i.e. to incorporate also the FTF into the ROM [3,4].

In the current work the FTF as well as a noise source model are derived from a LES / System Identification (LES/SI) approach [15]. Instead of the widely used Finite Impulse Response (FIR) identification [16,17], which only estimates the FTF from broadband LES time series data, a Box-Jenkins (BJ) model identification is applied [18]. In addition to a deterministic part, the BJ model includes also the estimation of a stochastic process. This model structure corresponds directly to the two contributions of the heat release fluctuations shown in Eq. (1) and makes possible the simultaneous identification of the FTF *and* the noise source from

Please cite this article as: M. Merk et al., Prediction of combustion noise of an enclosed flame by simultaneous identification of noise source and flame dynamics, Proceedings of the Combustion Institute (2018), https://doi.org/10.1016/j.proci.2018.05.124

With permission from M. Merk, R. Gaudron, C. Silva, M. Gatti, C. Mirat, T. Schuller and W. Polifke. Prediction of combustion noise of an enclosed flame by simultaneous identification of noise source and flame dynamics. *Proceedings of the Combustion Institute*, Elsevier, 2018.

ARTICLE IN PRESS
JID: PROCI [m;June 23, 2018;0:7]
M. Merk et al. / Proceedings of the Combustion Institute 000 (2018) 1–8

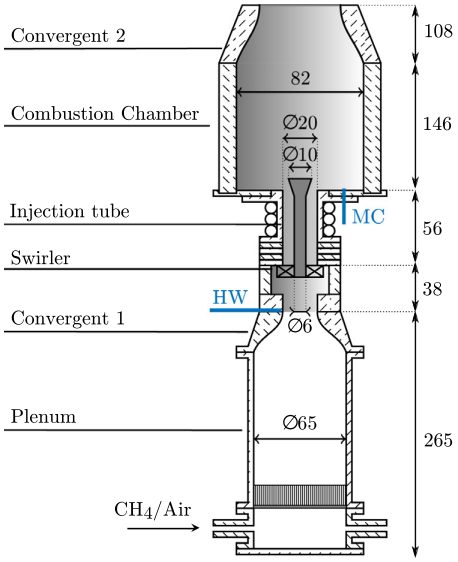

Fig. 1. Experimental setup of the turbulent swirl combustor. The shaded area represents the part of the test rig resolved within the LES. Dimensions are given in mm.

a single broadband LES time series data set. The black-box identification provides a purely data-driven noise model.

Application of BJ identification in the field of thermoacoustics was explored by Silva et al. [19] in a numerical study of a laminar flame, where stochastic combustion noise was mimicked by imposed equivalence ratio fluctuations. Merk et al. [18] investigated on the basis of surrogate data the general applicability of BJ identification to thermoacoustic systems, with emphasis on optimal model order, error margins and confidence levels. The present study is the first to apply BJ identification to actual LES time series data of a turbulent combustor and to juxtapose the subsequent ROM-based predictions of sound pressure spectra with a unique set of experimental results, where the flame dynamics (i.e. the FTF), the spectral distribution of sound pressure and the acoustic boundary conditions were measured with quantitative accuracy.

2. Experimental configuration

The turbulent swirl combustor shown in Fig. 1 was developed at EM2C laboratory, Paris. A methane and air mixture of equivalence ratio equal to $\phi = 0.82$ is injected at the bottom of the plenum. After flowing through the upstream plenum, a first convergent (contraction ratio: 8.73), a radial swirler and an injection tube, the mixture enters the combustion chamber. In the injection tube of diameter $D = 20$ mm, which has a reduced cross section due

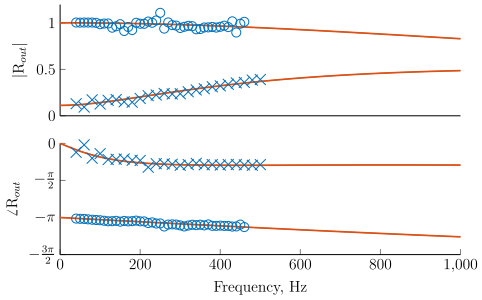

Fig. 2. Measured modulus (top) and phase (bottom) of the outlet reflection coefficients for an open end (○) and a perforated plate (×). Solid lines (—) show the fitted transfer functions used in the ROM.

to the central bluff body, a bulk flow velocity of $u_b = 7.1$ m/s is reached yielding a Reynolds number of $\mathrm{Re} = u_b D/\nu \approx 7000$ at $p = 1$ atm and T=20°C. In the combustion chamber a swirl stabilized V-shaped flame develops with a thermal power of $P_{th} = 5.5$ kW. The burnt gases leave the combustion chamber through a small convergent exhaust (contraction ratio: 2.03) without indirect combustion noise production.

In order to measure the FTF, acoustic forcing is applied with a loudspeaker (Monacor SP-6/108PRO - 100 W RMS) mounted at the plenum bottom. At the reference position "HW" in Fig. 1, the resulting velocity fluctuations u'_{ref} are measured by a hot-wire probe (Dantec Dynamics Mini-CTA 54T30 with a 55P16 probe). Combustion chamber walls made of quartz glass provide optical access to the flame. A photomultiplier mounted with an interferometric filter centered on 310 ± 10 nm records the OH^* chemiluminescence signal of the flame, which is assumed to be proportional to the heat release rate. The FTF is deduced from the photomultiplier and hot-wire signals by sweeping the excitation frequency while maintaining a perturbation level of 10% of the mean flow speed at the hot wire probe.

The acoustic pressure within the combustion chamber is measured by the microphone "MC" in Fig. 1. It is mounted on a water-cooled waveguide, which is connected to the backplate of the combustion chamber. A fully reflecting rigid wall terminates the upstream end of the combustor. On the downstream side the combustor is either open-ended or equipped with a perforated plate having the same outer diameter as the convergent exhaust and a square pattern of 12 holes of radius $R = 2.5$ mm with an inter-hole spacing $d = 20$ mm. For both conditions, the reflection coefficient is measured with the three-microphone method [20]. Results are shown in Fig. 2. Uncertainties in the measurement of the pressure fluctuation (and thus in the measurement of the reflection coefficient) arise

Please cite this article as: M. Merk et al., Prediction of combustion noise of an enclosed flame by simultaneous identification of noise source and flame dynamics, Proceedings of the Combustion Institute (2018), https://doi.org/10.1016/j.proci.2018.05.124

With permission from M. Merk, R. Gaudron, C. Silva, M. Gatti, C. Mirat, T. Schuller and W. Polifke. Prediction of combustion noise of an enclosed flame by simultaneous identification of noise source and flame dynamics. *Proceedings of the Combustion Institute*, Elsevier, 2018.

ARTICLE IN PRESS
JID: PROCI [m;June 23, 2018;0:7]

in the vicinity of pressure nodes. These uncertainties are reduced using a switching method during data acquisition and coherence functions during data post-processing.

3. Simultaneous identification of Flame Transfer Function and noise model from LES

To determine the FTF and the noise source numerically, the time series data of a compressible LES is post-processed via advanced SI techniques. Flame dynamics, noise generation and acoustic propagation are all accounted for in the compressible LES by means of the solver AVBP [21]. The LES domain, represented by the shaded area in Fig. 1, fully resolves the radial swirler and the combustor geometry without geometric simplifications. An unstructured mesh with approximately 19 million tetrahedral cells exhibits a maximum cell size of 0.6 mm in the flame region and 1.5 mm the burnt gas region, respectively. A dynamically thickened flame model [22] resolves the flame thickness with at least 7 cells. A global 2-step chemical reaction mechanism optimized for premixed methane/air mixture is used [23]. Non-reflective boundary conditions using a wave masking technique [24] are applied. The upstream plenum is not part of the LES domain. From experiments, however, it is known that the flow after the first convergent is laminar. Thus, a laminar velocity profile is imposed at the inlet. For further details and validation of the LES setup, the reader is referred to [8].

Instead of deducing laboriously the flame response at discrete frequencies from repeated LES runs with harmonic flow forcing, a broadband excitation signal is applied at the LES inlet. The wavelet type excitation signal used has a constant power spectral density up to a cut-off frequency of 1000 Hz. As in experiment the forcing amplitude corresponds to 10% of the mean inlet velocity. Note that a trade-off has to be made, regarding the forcing amplitude. A small forcing amplitude yields a low signal-to-noise ratio with possibly unsatisfactory results of the identification procedure [18]. A large forcing amplitude may trigger a non-linear flame response, which can not be adequately described by the linear identification techniques used. Time series data of the acoustic velocity fluctuations at the reference position $u'_{\mathrm{ref}}(t)$ (input) and of the total heat release rate fluctuations $\dot{Q}'(t)$ (output) are extracted from the LES. The length of the generated input-output time series amounts to 350 ms, which is down sampled to a cut-off frequency of 1000 Hz for the subsequent BJ identification.

As shown in Eq. (1) the key concept is to separate the fluctuations of total heat release rate into two contributions: a part resulting from the acoustic excitation $\dot{Q}'_c$, and a second term $\dot{Q}'_s$ that is uncorrelated to the acoustic forcing, but instead accounts for the contribution of combustion noise. By definition, a BJ model is composed of a deterministic sub-model plus a sub-model for stochastic noise – a structure that corresponds exactly to the modeling approach implied by Eq. (1). Formally, one writes

$$\dot{Q}'(t,\theta) = \underbrace{\frac{B(q,\theta)}{F(q,\theta)}}_{G} u'_{\mathrm{ref}}(t) + \underbrace{\frac{C(q,\theta)}{D(q,\theta)}}_{H} e(t). \tag{2}$$

The deterministic model G represents the FTF and establishes a causal relation between the input $u'_{\mathrm{ref}}(t)$ and the deterministic part of the output $\dot{Q}'(t,\theta)$. Conversely, the noise model H filters a Gaussian White Noise input signal $e(t)$, which is *uncorrelated* to the input signal.

The filters $B(q,\theta)$, $F(q,\theta)$ and $C(q,\theta)$, $D(q,\theta)$ that appear in the above equation are polynomials in the time shift operator q, defined as $q^{-i}u'_{\mathrm{ref}}(t) \equiv u'_{\mathrm{ref}}(t - i\Delta t)$. The filters B and C relate prior inputs to the current output $\dot{Q}'(t,\theta)$. F and D can describe possible auto-regressive behavior, as they relate prior *outputs* $q^{-i}\dot{Q}'(t)$ to the current output. The vector of polynomial coefficients $\theta = \{b_0 \dots b_{n_b}, f_0, \dots, d_{n_d}\}$ weighs the relations between present as well as prior input and output signals. The number of prior samples taken into account is determined by the polynomial filter orders $\{n_b, n_c, n_d, n_f\}$. This becomes apparent when rewriting the above equation as follows

$$\dot{Q}'(t,\theta) = \underbrace{\frac{\sum_{i=0}^{n_b} b_i q^{-i}}{\sum_{i=0}^{n_f} f_i q^{-i}} u'_{\mathrm{ref}}(t)}_{\dot{Q}'_c} + \underbrace{\frac{\sum_{i=0}^{n_c} c_i q^{-i}}{\sum_{i=0}^{n_d} d_i q^{-i}} e(t)}_{\dot{Q}'_s}. \tag{3}$$

This equation also makes explicit the structural equivalence of the BJ model to Eq. (1). During identification of a BJ model, the vector of polynomial model coefficients θ is estimated by a non-linear least-squares problem that minimizes the error between estimated and actual output [18].

To summarize, the model output $\dot{Q}'(t,\theta)$ results from a convolution of the respective polynomial filters with prior input and output samples, see Eq. (3). Note that if the polynomial filters F, C and D are set to unity, the widely used FIR model structure [16,17] is recovered. The FIR describes the combustion noise problem in a less comprehensive manner than the BJ model structure. Although combustion noise is known to be colored [25], the FIR approach does not identify a noise model, but instead treats the noise contribution as a white noise disturbance. The BJ identification, however, drops the white noise assumption by explicitly filtering a generic Gaussian White Noise signal $e(t)$ through the estimated noise filter H resulting in a

Please cite this article as: M. Merk et al., Prediction of combustion noise of an enclosed flame by simultaneous identification of noise source and flame dynamics, Proceedings of the Combustion Institute (2018), https://doi.org/10.1016/j.proci.2018.05.124

With permission from M. Merk, R. Gaudron, C. Silva, M. Gatti, C. Mirat, T. Schuller and W. Polifke. Prediction of combustion noise of an enclosed flame by simultaneous identification of noise source and flame dynamics. *Proceedings of the Combustion Institute*, Elsevier, 2018.

ARTICLE IN PRESS
JID: PROCI [m;June 23, 2018;0:7]

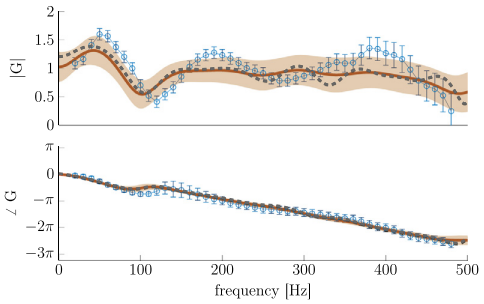

Fig. 3. Measured FTF values (○) with respective error bars. FTF identified via BJ identification (——) and via FIR identification (- - -). The shaded areas represent the 95% confidence interval of the FTF from the BJ model identification.

colored noise sub-model for $\dot{Q}'_s(t,\theta)$. This contribution mimics directly the effect of colored turbulent velocity fluctuations that would cause a certain spectral distribution of heat release rate fluctuations, by shaping the same stochastic contribution from the generic Gaussian White Noise signal. Further details on the BJ model and its implications in the field of thermoacoustics can be found in [18].

By applying the BJ identification on the LES time series, the FTF (G) and the noise model (H) are identified simultaneously. Auto-regressive behavior within the FTF is not expected, thus n_f is set equal to $n_f = 1$. The remaining polynomial orders are set to $n_b = 30$, $n_c = 6$, $n_d = 6$. The data processing and the model identification are realized via MATLAB 2016b.

In Fig. 3 the identified FTF (——) is shown and compared against measured values (○). Error bars for the measured FTF values stem from three experimental data sets for the same operating conditions and represent reproducibility of the experiment. For further comparison the FTF is also identified with the established FIR model structure (- - -), in which the model order is chosen as the sum of $n_b + n_c + n_d$. The number of estimated parameters is hence equal in both approaches. For the FTF gain both identified models yield similar values and describe the measured FTF values with slight deviations. The phase values of the identified models are in excellent agreement with the measured values. Comparable results between BJ and FIR identification suggest that deviations from experimental results stem not from the BJ identification procedure. Rather uncertainties in the experimental measurement itself (see increasing error bars for increasing frequencies in Fig. 3) or inadequacies in the LES for the flame dynamics description might be responsible for the deviations.

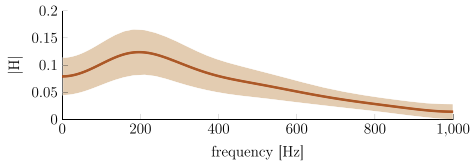

Fig. 4. Noise model identified via BJ identification (——) with 95% confidence interval represented by the shaded area.

Figure 4 depicts the identified noise model H. It shows that the noise source peaks slightly above 200 Hz. The amplitude of H has to be interpreted in terms of normalized heat release rate fluctuations, meaning that e.g. at 200 Hz, the noise source amplitude amounts to about 13% of the mean heat release rate. For the further usage of the noise model, the absolute level of noise fluctuations is consequently fixed by specifying the mean heat release rate.

As the BJ identification results in a data-driven model, a prerequisite for a reliable noise model identification is that the LES, from which the time series data is extracted, correctly reproduces the combustion noise generation. If the SI procedure is fed with erroneous data (e.g. if the LES generates spurious heat release rate fluctuations), erroneous noise models will result, independent of the chosen model structure. For the current study the validity of the LES with respect to the combustion noise generation was validated in [8] by comparing LES results against measured sound pressure spectra. Note that to a certain extent the combustion noise generation is independent from the flame dynamics. The generation of combustion noise strongly depends on the incoming turbulent velocity field, which in turn only plays a secondary role for the flame dynamics. This means that inaccuracies in the FTF identification are not directly transferable to the estimated noise model.

In closing this section it is remarked that the BJ identification could be applied to any signal in particular experimentally measured broadband data. However, since broadband forcing is not available in the test-rig facility, a one-to-one validation of the identified noise source model H for the combustion noise source is not possible. Nonetheless, the comparison presented below of measured and predicted sound pressure spectra, where the latter directly depends on the identified noise model H, corroborate the accuracy of the noise model H.

4. Reduced order model

The identified FTF and the noise model are incorporated into a linear acoustic network model of the combustor. The network model, which is

Please cite this article as: M. Merk et al., Prediction of combustion noise of an enclosed flame by simultaneous identification of noise source and flame dynamics, Proceedings of the Combustion Institute (2018), https://doi.org/10.1016/j.proci.2018.05.124

With permission from M. Merk, R. Gaudron, C. Silva, M. Gatti, C. Mirat, T. Schuller and W. Polifke. Prediction of combustion noise of an enclosed flame by simultaneous identification of noise source and flame dynamics. *Proceedings of the Combustion Institute*, Elsevier, 2018.

ARTICLE IN PRESS
JID: PROCI [m;June 23, 2018;0:7]

Table 1
Geometric and thermodynamic parameters of the ROM.

Plenum (p)	$R_{\text{in}} = 1,\ l_p = 0.265$ m, $A_p = 0.0033$ m^2 $T_c = 300$ K, $\rho_c = 1.205$ kg/m^3
swirler (sw) + inj. tube	$l_{sw} = 0.06$ m, $l_{\text{inj}} = 0.034$ m, $A_{\text{inj}} = 3.5 \times 10^{-4}$ m^2, $\bar{u}_{\text{inj}} = 7.1$ m/s
comb. chamber (cc)	$l_{cc} = 0.146$ m, $A_{cc} = 6.7e-04$ m^2, $\Theta = 5.82$, $T_h = 1500$ K, $\rho_h = 0.235$ kg/m^3
convergent (conv.)	$R_{\text{out}}(\omega) =$ see Fig. 2, $l_{\text{conv}} = 0.108$ m, $A_{\text{conv}} = 0.0033$ m^2

formulated in terms of the characteristic waves $f = 0.5 \cdot (p'/\bar{\rho}\bar{c} + u')$ and $g = 0.5 \cdot (p'/\bar{\rho}\bar{c} - u')$, is implemented in the open-source software taX [26]. The expressions for duct sections and area jumps, which are derived from linearized Euler equations, are written in terms of length and cross section ratio, respectively. No loss coefficients are introduced in order to avoid uncertain modeling parameters. For a detailed formulation of these elements the reader is referred to [3]. At the downstream end the reflection coefficient is taken into account by

$$\begin{bmatrix} f_d \\ g_d \end{bmatrix} = \begin{bmatrix} 0 & 0 \\ -R_{\text{out}}(\omega) & 1 \end{bmatrix} \begin{bmatrix} f_u \\ g_u \end{bmatrix} \tag{4}$$

Depending on the outlet condition studied, the outlet reflection coefficient R_{out} is adapted according to the polynomial fits shown in Fig. 2. At the combustor upstream end, the rigid plate is assumed to be fully reflecting with $R_{\text{in}} = 1$. The acoustic transfer behavior of the complex radial swirler geometry is represented by a 2×2 scattering matrix identified from LES on a domain that only comprises the swirler geometry. Note that the compressible LES takes acoustic losses across the swirler into account such that they are implicitly included in the identified scattering matrix of the radial swirler. Consequently, acoustic losses are only taken into account across the swirler element and at the downstream end via R_{out}. By means of the Rankine–Hugoniot jump conditions across a thin reaction zone [3,27], the identified FTF and the noise model are coupled into the linear network model across the flame element by

$$\begin{bmatrix} f_d \\ g_d \end{bmatrix} = \frac{1}{2}\begin{bmatrix} \xi+1 & \xi-1 \\ \xi-1 & \xi+1 \end{bmatrix}\begin{bmatrix} f_u \\ g_u \end{bmatrix} + \frac{1}{2}\frac{A_{\text{inj}}}{A_{cc}}\Theta\, G(\omega)\begin{bmatrix} 1 & -1 \\ -1 & 1 \end{bmatrix}\begin{bmatrix} f_{\text{ref}} \\ g_{\text{ref}} \end{bmatrix} - \mathbb{S}, \tag{5}$$

where the noise source $\mathbb{S}$ is introduced as

$$\mathbb{S} = \frac{1}{2}\frac{A_{\text{inj}}}{A_{cc}}\bar{u}_{\text{inj}}\,\Theta\, H(\omega) e \begin{bmatrix} -1 \\ 1 \end{bmatrix} \tag{6}$$

Furthermore, ξ denotes the specific acoustic impedance and Θ the temperature jump across the flame $\Theta = T_b/T_c - 1$. The transfer matrix of the passive flame, i.e. the temperature discontinuity across the flame, is taken into account by the first term on the rhs. of Eq. (5). The second term describes the active flame part and hence the effect of unsteady flame heat release in response to velocity perturbations at the reference position. The third term $\mathbb{S}$ accounts for the contribution from the combustion noise source term. Note that this formulation implicitly recovers the two-way coupling between noise source and flame dynamics [3]. All parameters used in the network model are given in Table 1.

The eigenfrequencies predicted by the network model (×) agree with measured eigenfrequencies for *non-reactive* conditions, see Fig. 6. The FTF is not taken into account here. Only the fourth eigenmode shows a slight discrepancy. Thus, it is concluded that the acoustic network model fairly well captures the eigenmodes of the combustor cavity, which is a prerequisite for the following sound pressure prediction of the reactive setup. Moreover, in Fig. 6 it gets evident that an increase of the mean temperature in the combustion chamber T_h mainly affects the second eigenmode. This eigenmode corresponds predominantly to a $\lambda/4$ wave mode within the combustion chamber. Hence, its frequency is strongly modulated by an increased combustion chamber temperature and the thereof resulting increase in the speed of sound. The first and third eigenmode are associated with the combustor Helmholtz mode and a $\lambda/2$ plenum mode, respectively. Both are predominantly active in the plenum and consequently hardly affected by the increase of T_h.

5. ROM based sound pressure predictions

The ROM, now including the identified FTF model $G(\omega)$ *and* the noise model $H(\omega)$, is evaluated in the frequency domain and the spectrum of the acoustic pressure fluctuations in the combustion chamber (p'_{MC} in Fig. 5) is compared with corresponding measurements. The 95% confidence interval is computed by propagating the uncertainties of the identified noise model through the network model. The influence of the uncertainties in the FTF identification on the sound pressure prediction are found to be small and are thus neglected.

Fig. 7 shows excellent agreement between the experimental spectrum (○○○) and the ROM prediction (—). Note that due to the cavity acoustics, the sound pressure spectrum differs markedly from the spectral distribution of the combustion

Please cite this article as: M. Merk et al., Prediction of combustion noise of an enclosed flame by simultaneous identification of noise source and flame dynamics, Proceedings of the Combustion Institute (2018), https://doi.org/10.1016/j.proci.2018.05.124

With permission from M. Merk, R. Gaudron, C. Silva, M. Gatti, C. Mirat, T. Schuller and W. Polifke. Prediction of combustion noise of an enclosed flame by simultaneous identification of noise source and flame dynamics. *Proceedings of the Combustion Institute*, Elsevier, 2018.

ARTICLE IN PRESS
JID: PROCI [m;June 23, 2018;0:7]
M. Merk et al. / Proceedings of the Combustion Institute 000 (2018) 1–8

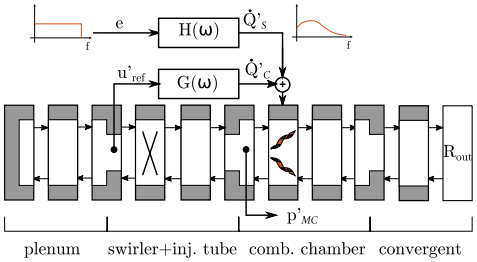

Fig. 5. Reduced order model used. The radial swirler part is replaced by a scattering matrix identified via LES/SI.

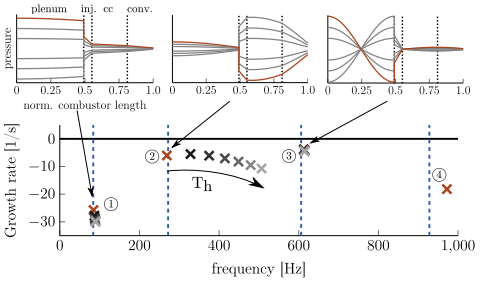

Fig. 6. Frequencies of the measured *cold* eigenmodes (- - -) and the *cold* eigenmodes predicted by the network model (×) for the open-ended configuration. Gray-scaled crosses represent the frequency shift if the mean temperature in the combustion chamber is increased up to $T_h = 1500$ K.

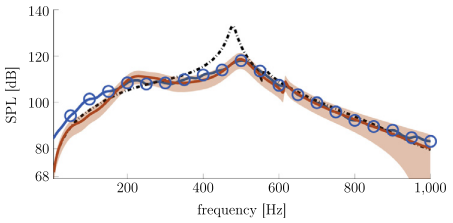

Fig. 7. Measured sound pressure spectrum (⊖⊖⊖) and ROM prediction for the open-ended configuration: two-way coupling (——) with confidence interval, one-way coupling (- . - . -).

noise source: the maximum in the combustion noise source spectrum near 200 Hz seen in Fig. 4 generates only a secondary peak in the sound pressure spectrum, which indeed has its maximum around 515 Hz. This peak arises from resonance with the second cavity mode – Fig. 6 shows that its eigenfrequency is somewhat above 500 Hz if the combustion chamber temperature T_h is increased.

The sound pressure spectrum predicted by the one-way coupling approach is also shown in Fig. 7 (- . - . -). The FTF is not taken into account

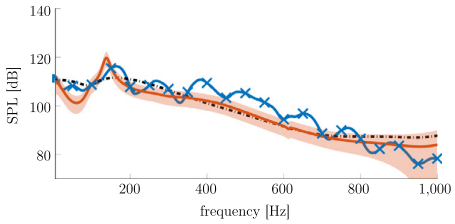

Fig. 8. Measured sound pressure spectrum (×××) and ROM prediction for the configuration equipped with a perforated plate: two-way coupling (——) with confidence interval, one-way coupling (- . - . -).

here, such that the cavity is only excited by the noise source. Hence, the feedback from the acoustic field onto the upstream velocity field and the thereof resulting heat release rate fluctuations are neglected. Overall, one-way coupling produces acceptable results, with the exception of amplitude and frequency of the spectral peak that results from acoustic resonance. Similar behavior is reported in [3]. Note that taking $\dot{Q}'_c$ into account, as it is done with two-way coupling (——), does not necessarily imply an increase in the sound pressure spectrum. The relative phase between $\dot{Q}'_s$ and $\dot{Q}'_c$ determines whether interference is constructive or destructive.

Figure 8 shows the sound pressure spectra that result if the downstream end of the combustor is equipped with the perforated plate. Note that jet noise generated by the flow crossing the perforated plate causes a less smooth experimental spectrum compared to the open-ended configuration shown in Fig. 7. From evaluating the mode shapes depicted in Fig. 6, it is evident that a change of the outlet reflection condition mainly affects the second cavity mode. Indeed, the sound pressure peak observed in the open-ended configuration vanishes when the combustor is terminated by the perforated plate. A decreased outlet reflection reduces acoustic reflections at the system boundary and consequently weakens the modulation of the sound pressure spectrum by the cavity acoustics. As a result the sound pressure spectrum follows more closely the spectral distribution of the combustion noise source shown in Fig. 4. Note that a change in the acoustic boundary of the combustor does neither modify the flame dynamics nor the combustion noise source. Thus, the same models for $G(\omega)$ and $H(\omega)$ are used and the experimental results can be reproduced with negligible computational cost by merely adjusting the cavity of the network model.

6. Conclusion

Models for the source of combustion noise and the flame dynamics are identified simultaneously from a single broadband LES time series by Box-Jenkins system identification. Compared to the

Please cite this article as: M. Merk et al., Prediction of combustion noise of an enclosed flame by simultaneous identification of noise source and flame dynamics, Proceedings of the Combustion Institute (2018), https://doi.org/10.1016/j.proci.2018.05.124

With permission from M. Merk, R. Gaudron, C. Silva, M. Gatti, C. Mirat, T. Schuller and W. Polifke. Prediction of combustion noise of an enclosed flame by simultaneous identification of noise source and flame dynamics. *Proceedings of the Combustion Institute*, Elsevier, 2018.

ARTICLE IN PRESS
JID: PROCI [m;June 23, 2018;0:7]

established finite impulse response, a Box-Jenkins structure estimates also a model for the noise characteristics, which constitutes a novelty in the field of thermoacoustics. The Box-Jenkins model does not assume white noise and allows thus the additional identification of a data-driven noise model, which provides insight into the amplitude and spectral distribution of the combustion noise source. Combined with a linear network model for the cavity acoustics of the combustor, a reduced order model is built to predict sound pressure spectra and their associated confidence intervals. Two different configurations are studied that differ by their respective outlet reflection coefficient. Since a change in the acoustic boundary does not affect the flame dynamics and the combustion noise source, only the outlet reflection coefficient of the reduced order model has to be adopted to represent the two configurations. Convincing agreement with measurements of flame transfer function and sound pressure spectra is found. Compared to stand-alone LES, the proposed methodology allows the evaluation of the sound pressure spectrum across a large parameter space with reduced computational effort. Even if the flame operating conditions change, only *one* additional LES computation is required to derive again models for the flame dynamics and the noise source. Although it would also be possible to directly extract the sound pressure level for *one* certain configuration from LES, the ROM approach provides additionally valuable insight into the interplay between generation of combustion noise, flame dynamics and cavity resonances. Hence, a computational efficient approach is retained that offers a comprehensive examination of the nature of sound pressure peaks and allows the optimization of the combustor in terms of combustion noise levels reached.

Acknowledgment

Financial support is acknowledged by the DFG (project PO 710/16-1), by the ANR (project ANR-14-CE35-0025-01) and by the European Union's Horizon 2020 research and innovation programme under the Marie Sklodowska-Curie grant agreement No 643134. Computing time on the GCS Supercomputer SuperMUC was provided by Gauss Centre for Supercomputing e.V.

References

[1] A.P. Dowling, Y. Mahmoudi, *Proc. Combust. Inst.* 35 (1) (2015) 65–100, doi:10.1016/j.proci.2014.08.016.
[2] W.C. Strahle, *Prog. Energy Combust. Sci.* 4 (1978) 157–176, doi:10.1016/0360-1285(78)90002-3.
[3] C.F. Silva, M. Merk, T. Komarek, W. Polifke, *Combust. Flame* 182 (2017) 269–278, doi:10.1016/j.combustflame.2017.04.015.
[4] B.B.H. Schuermans, W. Polifke, C.O. Paschereit, J.H. van der Linden, in: ASME 2000-GT-105, Munich, Germany, 2000.
[5] N. Tran, S. Ducruix, T. Schuller, *Proc. Combust. Inst.* 32 (2) (2009) 2917–2924, doi:10.1016/j.proci.2008.06.123.
[6] A. Lamraoui, F. Richecoeur, T. Schuller, S. Ducruix, *J. Eng. Gas Turbines Power* 133 (1) (2011) 011504, doi:10.1115/1.4001987.
[7] V. Bellucci, B. Schuermans, D. Nowak, P. Flohr, C.O. Paschereit, *J. Turbomach.* 127 (2) (2005) 372–379, doi:10.1115/1.1791284.
[8] M. Merk, R. Gaudron, M. Gatti, C. Mirat, T. Schuller, W. Polifke, *AIAA J.* (2018) 1–13, doi:10.2514/1.J056502.
[9] M. Huet, F. Vuillot, N. Bertier, M. Mazur, N. Kings, W. Tao, P. Scouflaire, F. Richecoeur, S. Ducruix, C. Lapeyre, T. Poinsot, *J. AerospaceLab* (11) (2016), doi:10.12762/2016.AL11-10.
[10] J.M. Lourier, M. Stöhr, B. Noll, S. Werner, A. Fiolitakis, *Combust. Flame* 183 (2017) 343–357, doi:10.1016/j.combustflame.2017.02.024.
[11] C.O. Paschereit, B.B.H. Schuermans, W. Polifke, O. Mattson, *J. Eng. Gas Turbines Power* 124 (2) (2002) 239–247, doi:10.1115/1.1383255.
[12] C. Hirsch, J. Wäsle, A. Winkler, T. Sattelmayer, *Proc. Combust. Inst.* 31 (1) (2007) 1435–1441, doi:10.1016/j.proci.2006.07.154.
[13] R. Rajaram, T. Lieuwen, *J. Fluid Mech.* 637 (2009) 357–385, doi:10.1017/S0022112009990681.
[14] Y. Liu, *J. Sound Vib.* 353 (2015) 119–134, doi:10.1016/j.jsv.2015.05.027.
[15] W. Polifke, *Ann. Nucl. Energy* 67C (2014) 109–128, doi:10.1016/j.anucene.2013.10.037.
[16] A. Giauque, T. Poinsot, F. Nicoud, in: Fourteenth AIAA/CEAS Aeroacoustics Conference (Twenty-Ninth AIAA Aeroacoustics Conference), AIAA/CEAS, Vancouver, Canada, 2008, doi:10.2514/6.2008-2943.
[17] A. Innocenti, A. Andreini, B. Facchini, *Energy Procedia* 82 (2015) 358–365, doi:10.1016/j.egypro.2015.11.803.
[18] M. Merk, S. Jaensch, C. Silva, W. Polifke, *J. Sound Vib.* 422 (2018) 432–452, doi:10.1016/j.jsv.2018.02.040.
[19] C.F. Silva, W. Polifke, J. O'Brien, M. Ihme, in: Summer Program, Center for Turbulence Research, Stanford University, Stanford, USA, 2014, p. 179.
[20] J.Y. Chung, D.A. Blaser, *J. Acoust. Soc. Am.* 68 (3) (1980) 914–921, doi:10.1121/1.384779.
[21] CERFACS, IMFT, The AVBP HandBook, http://www.cerfacs.fr/avbp6x/, 2008.
[22] O. Colin, F. Ducros, D. Veynante, T. Poinsot, *Phys. Fluids* 12 (7) (2000) 1843–1863, doi:10.1063/1.870436.
[23] B. Franzelli, E. Riber, M. Sanjosé, T. Poinsot, *Combust. Flame* 157 (7) (2010) 1364–1373, doi:10.1016/j.combustflame.2010.03.014.
[24] W. Polifke, C. Wall, P. Moin, *J. Comp. Phys.* 213 (2006) 437–449, doi:10.1016/j.jcp.2005.08.016.
[25] H.A. Hassan, *J. Fluid Mech.* 66 (03) (1974) 445, doi:10.1017/S0022112074000292.
[26] T. Emmert, S. Jaensch, C. Sovardi, W. Polifke, in: Seventh Forum Acusticum, DEGA, Krakow, 2014.
[27] J.J. Keller, *AIAA J.* 33 (12) (1995) 2280–2287, doi:10.2514/3.12980.

Please cite this article as: M. Merk et al., Prediction of combustion noise of an enclosed flame by simultaneous identification of noise source and flame dynamics, Proceedings of the Combustion Institute (2018), https://doi.org/10.1016/j.proci.2018.05.124

With permission from M. Merk, R. Gaudron, C. Silva, M. Gatti, C. Mirat, T. Schuller and W. Polifke. Prediction of combustion noise of an enclosed flame by simultaneous identification of noise source and flame dynamics. *Proceedings of the Combustion Institute*, Elsevier, 2018.